PILLAR[5]ARENE BASED SENSORS

RAGHURAM REDDY KOTHUR

A thesis submitted in partial fulfilment of the requirements of the University of Brighton for the degree of Doctor of Philosophy

September 2016

ABSTRACT

The aim of this project was to synthesise and characterise pillar[5]arenes, macrocycles comprised of 1,4-dialkoxybenzene moieties linked in the 1,5-positions by methylene bridges, and to incorporate them in a range of sensors. Pillar[5]arene-based ion-selective electrodes (ISEs) were used to detect protons, alkali metal cations and biogenic amines to investigate sensing properties resulting in the fabrication of a low pH sensor. Composite sensors incorporating 1,4-dimethoxypillar[5]arene were able to detect Na^+ concentrations in the physiological range, whereas K^+ concentrations were well above those encountered *in vivo*. The composite electrodes did not show significant differences in capacitance for biogenic amines making them suitable to detect Na^+ and K^+ over alkali metal ions and unaffected by the presence of biogenic amines. A novel thiolated copillar[4+1]arene was synthesised and attached to gold electrodes. It was tested against alkali metals and biogenic amines and was most selective to Li^+ over other alkali metal cations. Copillar[4+1]arene-capped gold nanoparticles were synthesised and assessed for biogenic amine selectivity. Complexation occurred strongly with spermidine and spermine compared to pentylamine and putrescine. Overall, the common purpose of the research presented in this thesis was to assess the pillar[5]arene macrocycle for its selectivity of small molecules and ions, specifically alkali metals and biogenic amines of biological importance. The difference in the nature of ion selectivity by the same macrocyclic binding motif appears to be due to its arrangement and conformational freedom in the different types of electrodes. In the ISE, the crystalline macrocycle integrates with polyvinyl chloride (PVC) which makes the upper and lower rim functional groups available for complex formation. In composite sensors, the alignment of the macrocycles is very rigid making complex formation reliant on the guest fitting into the rigid macrocyclic cavity. On gold electrodes, one of the aromatic rings is involved in surface attachment with the remaining four free to change their conformations and bind guest species.

CONTENTS

LIST OF COMPOUNDS

The compounds presented in the thesis are shown below.

1. Pillar[5]arene derivatives

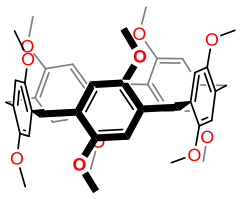

1*

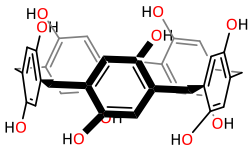

3

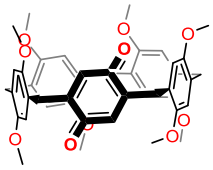

6

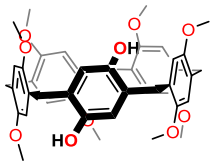

7

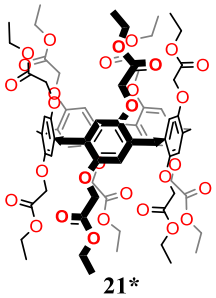

21*

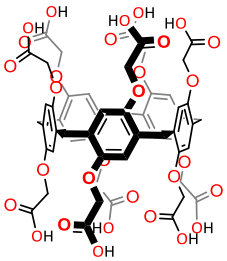

22

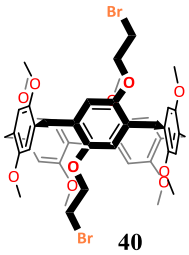

40

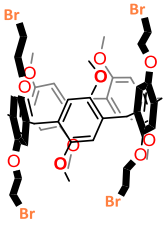

41

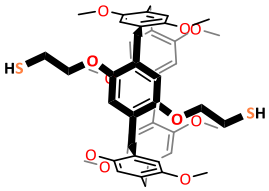

42*

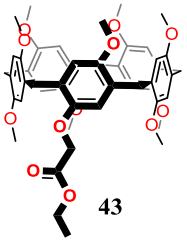

43

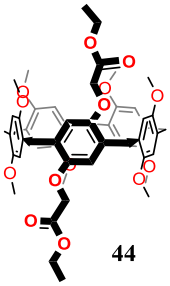

44

*** P[5]A derivaties used in sensor fabrication.**

1* Modified composite and ISE sensor
21* Modified ISE sensor
42* Modified Au sensor and AuNPs

2. Monomer units

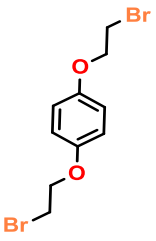

35

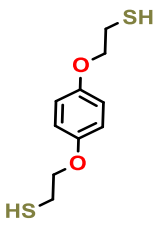

36

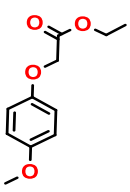

37

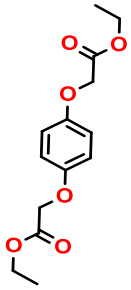

38

LIST OF TABLES

LIST OF FIGURES

LIST OF SCHEMES

ACRONYMS AND ABBREVIATIONS

AFM	atomic force microscopy
Ag|AgCl	silver/silver chloride
AgNPs	silver nanoparticles
$AlBr_3$	aluminium tribromide
AuNPs	gold nanoparticles
BA	biogenic amine
BBr_3	boron tribromide
$BF_3{\cdot}O(C_2H_5)_2$	boron trifluoride diethyl etherate
$CDCl_3$	deuterochloroform
CE	counter electrode
CH_3CN	acetonitrile
CPE	carbon paste electrode
CV	cyclic voltammetry/voltammogram
DCM	dichloromethane
DMF	*N*,*N*-dimethylformamide
EDX	energy-dispersive X-ray spectroscopy
EIS	electrochemical impedance spectroscopy
E_{pa}	anodic peak potential
E_{pc}	cathodic peak potential
F	Faraday constant
$FeCl_3$	iron(III) chloride
FTIR	Fourier transform infrared spectroscopy
GC	glassy carbon
$HAuCl_4{\cdot}3H_2O$	hydrogen tetrachloroaurate(III) trihydrate
HPLC	high performance liquid chromatography
HRMS	high-resolution mass spectrometry
IHP	inner Helmholtz plane
IL	ionic liquid
Ipa	anodic current
Ipc	cathodic current
ISE	ion-selective electrode

ISM	ion-selective membrane
ISM	ion-selective membrane
KCl	potassium chloride
$K_4[Fe(CN)_6]$	potassium ferrocyanide
MeOH	methanol
M	molar
mM	millimolar
mV	millivolt
$NaBH_4$	sodium borohydride
NaN_3	sodium azide
$(NH_4)_2[Ce(NO_3)_6]$	ceric ammonium nitrate (CAN)
NMR	nuclear magnetic resonance
OHP	outer Helmholtz plane
P[5]A	pillar[5]arene
P[6]A	pillar[6]arene
PA	pentylamine
PUT	putrescine
RE	reference electrode
SAM	self-assembled monolayer
SCE	saturated calomel electrode
SD	standard deviation
SEM	scanning electron microscopy
SHE	standard hydrogen electrode
SPD	spermidine
SPR	spermine
SPR	surface plasmon resonance
TEM	transmission electron microscopy
TFA	trifluoroacetic acid
THF	tetrahydrofuran
TOAB	tetraoctylammonium bromide
TMS	tetramethylsilane
V	volts
WE	working electrode

ACKNOWLEDGEMENTS

I take immense pleasure in thanking **Dr. Peter Cragg**, my academic supervisor, whose wisdom, inspiration, creativity and patience has been greatly valued. I have been lucky to learn a lot over the past three years, and have gained a lot of knowledge regarding scientific research and far more. I hope that I can take this forward with me. I wish to express my deep sense of gratitude to **Dr. Bhavik Patel**, my co-supervisor, for priceless help, guidance and support throughout my Ph.D. I would like to extend my cordial thanks to my co-supervisor **Dr. Ian Cooper**.

I wish to place on record my profound indebtedness to **Dr. Gareth Cave** at Nottingham Trent University, for assistance with collecting X-ray crystallography data and also **Dr. Ian Gass**, University of Brighton for solving the structures. I'd like to thank **Dr. Peter Cragg** for computational data. **Prof. Martyn Boutelle**, thank you for training and allowing sensor fabrication experiments to be performed at Imperial College London. My research would not have been possible without their help.

I would like to thank the School of Pharmacy and Biomolecular Sciences (PABS) and Doctoral College, University of Brighton not only for providing studentship which allowed me to undertake this research, but also for giving me the opportunity to attend conferences and meet so many interesting people.

My sincere thanks also goes to **Dr. Malla Reddy Chilla**, for offering me the internship opportunity in his group. A special thanks goes to **Dr. Flavia Fuccasi**, who was always willing to help and give her best suggestions. I would like to extend my cordial thanks for constant support to lab technicians, lab mates and all my friends.

Most importantly, none of this would have been possible without the love and patience of my family. My gratitude goes to my family; **Gopal Reddy**, **Narsamma**, **Geetha, Janardhan Reddy, Sreeja, Karun, Venkateshwar Reddy, Ramprasad, Bhavya, Shanker Rao, Vimala, Kavitha, Mamatha** for their infinite support. I want to thank my mother, **Balamani** and grandfather, **Thimma Reddy** – your

memory will be eternal. They are the most important people in my world and I dedicate this thesis to them.

Above all I would like to thank my wife, **Swetha Reddy Kothur** for her love and constant support, for all the late nights and early mornings, and for keeping me sane over the past few months.

Finally, I thank God for using this work to reveal my weakness to me and build me up. All glory to God for He makes the impossible become possible!

DECLARATION

I declare that the research contained in this thesis, unless otherwise formally indicated within the text, is the original work of the author. The thesis has not been previously submitted to this or any other university for a degree, and does not incorporate any material already submitted for a degree.

Signed: Raghuram Reddy Kothur

Dated: 13/09/2016

CHAPTER - I

1. Introduction

1.1 General overview and context of project

Molecular sensor design is one of the most active areas of supramolecular chemistry and is dependent on harnessing the forces involved in a complex formation to elicit a response to a chemical species that can be detected by the observer. IUPAC defines a chemical sensor as "a device that transforms chemical information, ranging from the concentration of a specific sample component to total composition analysis, into a useful analytical signal".[1] The objectives of pillar[5]arene (P[5]A) -based molecular sensor design come from analogous studies on the selective binding of alkali metal ions by natural and synthetic macrocyclic ligands such as valinomycin, crown ethers and cryptands. Molecular sensor design and development has always been a huge area of supramolecular chemistry and remains a complex and challenging field in the present day. Many researchers are involved in the development of systems designed to detect specific chemical and biological analytes.[2]

A chemical sensor has two main factors in order to function: molecular recognition and signal transduction. The molecular recognition portion of the sensor interacts with the target molecule whereas the transducer transforms the recognition process into a measurable signal. Chemical sensors represent an excellent choice for detecting small molecules over other methods due to a range of potential transduction mechanisms. Based on the type of transduction process, chemical sensors are classified into optical sensors, electrochemical sensors, mass sensitive sensors and magnetic sensors. Among these sensors, electrochemical sensors are widely used and are the most established.[2]

Electrochemical sensors have been manufactured and used in the research presented here as they offer detection with low limits, a broad continuous response range, excellent stability and reproducibility. Depending on the mechanism two methods are available: potentiometric and voltammetric electrochemical sensors which

measure potential and current, respectively. Despite many advantages of electrochemical modified sensors, such as their sensitivity, selectivity, non-destructive nature, rapidity and ease of use, there are still challenges in their use, particularly in the aspects of improving reproducibility, calibration and manufacturability.[2] There is widespread interest for modified electrochemical sensors within supramolecular chemistry due to their use in metal ion detection. Calixarenes, cyclodextrins and crown ethers have all been used as surface modifiers in fabrication of electrochemical sensors such as ion selective electrode (ISE), gold, and carbon composite electrodes.[3] These three macrocyclic electrode modifiers have generally been used for metal ion detection but in the work presented here P[5]As have been used as surface modifiers in ISE, gold and graphite composite electrodes for both alkali metal ion and biogenic amine detection. ISEs are well established as sensors for alkali metal ions and other analytes: to date at least 60 distinct ions have been assessed using ISEs.[3] The ISE response is achieved by selective complexation of the objective ion by ionophores dispersed in a matrix. Polymeric membrane ISEs serve as one of the best sensing methods due to their ability to select different compounds with respect to the charge and size of the desired ion in clinical and environmental measurements.[4] ISEs offer excellent method for ion determination because they are simple, cheap, and the extensible of using them for field investigations.[3]

Using surface modifiers to detect analytes has a long history most clearly found in the field of self-assembled monolayers (SAMs). The detection of various guests by SAMs occurs though their terminal functional groups. Electrochemically active metal ions can be detected by SAMs using cyclic voltammetry, while inactive metal ions can be detected by impedance spectroscopy.[5,6] Numerous SAMs have been fabricated with macrocyclic receptors on their surfaces such as calix[4]resorcinarenes[7,8] and cyclodextrins[9] with Bryce[10] and Reinhoudt[11] using crown-ether groups attached to SAMs for metal ion detection. In the work presented here, gold surfaces have been covered with SAMs to detect alkali metals and biogenic amines. SAMs attached to gold were first reported by Nuzzo and Allara[12] in 1983 but to be used as a sensing device they require two key properties: selective binding by explicit and reversible interaction between the target and the SAM and

the generation of an observable signal for detection as a result of guest and SAM binding.[13]

Functionalised crown ethers and calixarenes have been immobilised on substrates to form SAMs for alkali metal detection.[14] Echegoyen and his group reported that crown-1,2-tetrathiafulvalenes (TTFs), bis(thioctic ester) derivatives of crown ethers incorporating TTF, form a stable SAM on gold electrodes and can detect alkali metal ions by cyclic voltammetry.[15] The same group also demonstrated that crown ether-containing SAMs can detect K^+ in aqueous solutions.[16] The Reinhoudt group was the first to use impedance spectroscopy to confirm the binding properties of SAMs having non-redox active crown ethers as receptors for redox inactive alkali metal ions in aqueous solution. Later in 1998, the same group reported that the 2-[(6-mercaptohexyl)oxy]methyl-12-crown-4 SAMs could be used to selectively detect Na^+, even in a 100-fold excess of K^+, and a 2-[(6-mercaptohexyl)oxy]methyl-15-crown-5 SAM modified gold electrode was seen to selectively bind K^+ reversibly in aqueous solutions.[11] The Moyer group reported a SAM from a 1,3-alternate calix[4]crown-6 with excellent affinity and selectivity for ^{137}Cs ion extracted from radioactive waste.[17] SAMs based on 1,3-alternate *p*-tertbutylcalix[4]crown-6 can also selectively detect Cs^+ in aqueous media.[18]

1.1.1 Alkali metal ion detection

Alkali metal ions are essential elements in the human body and also are used in various clinical and biological processes.[19] For example, Na^+ and K^+ perform integral fluid balance functions and maintain blood pressure in the human body by playing a vital role in the Na^+/K^+ pump.[20,21]

Na^+ and K^+ are the most abundant alkali metal ions in the body and the most commonly analysed in clinical samples, usually in blood but occasionally in urine, saliva or sweat. Physiologically, Na^+ and K^+ are usually in the concentration range of 135 - 145 mM and 3.5 - 4.5 nm, respectively, in the human plasma. Reports on the *Streptomyces lividans* K^+-channel structure initiated renewed research to illuminate crucial structural and mechanistic features of ion channels *via* the development of

abiotic systems.[22-24] The recognition elements necessary for both biotic and abiotic ion channels are of direct relevance to the design of sensors for specific cations.

Lithium is another alkali metal which occurs naturally in the human blood. It is present in much lower concentrations with only 0.8 - 1.2 mM in the serum.[25] Li^+ is toxic in high concentration and over 5 mM in the blood may lead to death[26] so definitive assessment of Li^+ in the blood of patients taking lithium-related medication for bipolar disorders is essential for safe treatment.[4] Hence, it is very important for Li^+ sensors to operate in the 0.5 - 1.5 mM range. A main challenge in developing Li^+ sensors in the blood is the fact that it can contain 140 mM Na^+, or around 100 to 300 times the Li^+ concentration, which may interfere with the assay.[4]

Alkali metal ion complexation research devolved rapidly following discovery of valinomicin's mode of action. Valinomycin and other similar antibiotics transport K^+ through biological membranes effortlessly and selectively. Key features for the selective binding by macrocycles include the size and electrostatic complementarity between host and guest.[2,27] Later, Pedersen and Lehn reported the synthesis of crown ethers and cryptands possessing similar alkali metal ion binding properties based on complementarity between the ions and their hosts.[28, 29]

Current ISE sensors for alkali metal cations generally comprise a polymeric membrane and a small amount (ca. 1%) of an appropriate ionophore. The field was pioneered by a K^+ ISE incorporating valinomycin, with the first fully automated clinical sensor to detect Na^+ and K^+ by potentiometry appearing in 1972.[30,31] Later alternatives to valinomycin included bis(crown ether)s which are comparable to valinomycin in their affinity for K^+ but are more lipophilic and thus offer superior electrode lifetimes for clinical applications.[32,33] For Na^+-ISEs, the preferred, and most extensively used, ionophores are calix[4]arenes.[34,35] Reinhoudt reported that crown ether bridge calix[4]arenes have better selectivity towards Na^+ compared to bis(crown ether)s.[36] No suitable calixarene ionophore has been identified for Li^+, however, sterically hindered mono-14-crown-4 ethers are effective as ISE modifiers.[37,38]

1.2 Introduction and scope of supramolecular chemistry

1.2.1 Historical background of supramolecular chemistry

The underlying principles of supramolecular chemistry can be traced back to two aspects of molecular recognition, enzyme catalysis and non-covalent interactions between molecules. In 1894 Fisher proposed a 'lock and key' model to explain enzyme-substrate interactions. This model explains how selective recognition of the substrate by the enzyme is based on complementarily between their sizes and shapes.[39,40] This was expanded upon by Ehrlich in 1906 who discovered that molecules do not react if they do not bind to the substrate.[41,42] The effects of non-covalent interactions were claimed as the reason for the formation of carboxylic acid dimers in the gas phase by Wolf in 1937 and the concept of hydrogen-bonding was described by Pauling in 1939.[43]

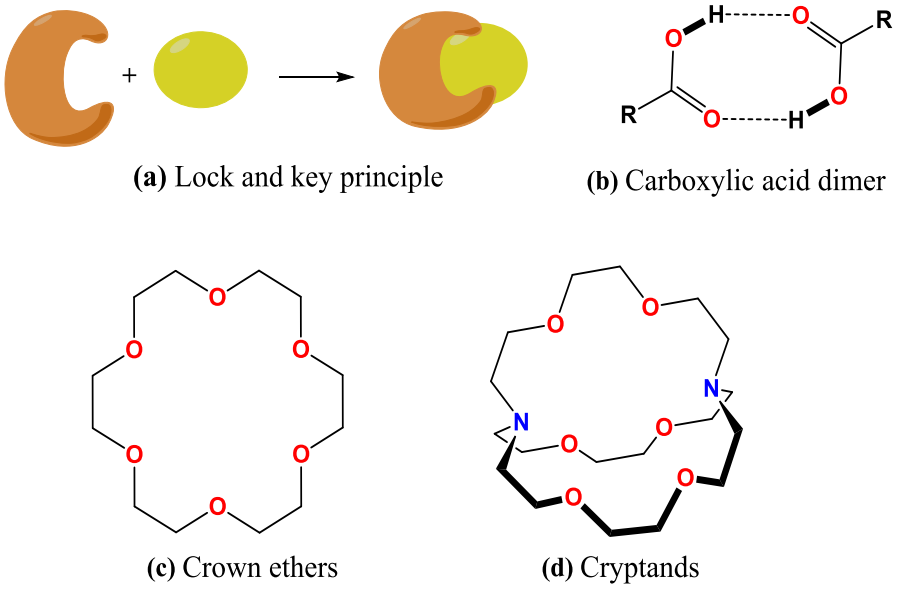

Figure 1. Representation of (a) the lock and key principle, (b) carboxylic acid dimer, (c) crown ethers and (d) cryptands.

The molecular recognition properties of crown ethers and cryptands were reported by Pedersen and Lehn in 1967, and those of cavitands by Cram in 1973, for which they shared the 1987 Nobel Prize for their contributions in supramolecular chemistry. Lehn described supramolecular chemistry as "chemistry beyond the molecule, the science of non-covalent, intermolecular interactions".[29, 44, 45]

1.2.2 Introduction to supramolecular chemistry

Supramolecular chemistry is the phenomenon leading to the formation of molecules or complexes through the association of two or more chemical entities and its concept was initially started in the context of biological structures.[46] Later extensive contributions in this field by Lehn describing supramolecular chemistry as "*chemistry beyond the molecule*" in his Nobel lecture.[29,46] It can be broadened to include concepts such as 'inclusion phenomena', 'host–guest chemistry' or 'molecular recognition' Supramolecular chemistry emerged through collaborations between various areas of research in chemistry, physics and biology which led to the strengthening of the supramolecular chemistry concept extending even to the study of life at a molecular level.[47] Understanding various molecular interactions is the essential factor in the study of biological concepts such as enzymatic reactions, the central dogma of cell transcription and the translation of the genetic code, the association of biomolecules and signal induction by neurotransmitters.[43] Designing devices to study molecular interactions starts from an understanding of substrate and ligand binding, leading to supramolecular assemblies, and finally resulting in organised assemblies of biomolecules or complexes which form the device itself.[47]

Supramolecular chemistry is a broad field which impinges upon various other disciplines, including organic and inorganic chemistry, essential in the synthesis of supermolecule precursors. Physical chemistry facilitates an understanding of the equilibria of supramolecular systems and computational modelling helps to discern complex supramolecular behaviour. In biological chemistry, understanding supramolecular concepts can help to explain various biological molecular interactions. Supramolecular concepts can be applied to the real world to improve nanotechnological applications.[43] A schematic of the molecular, supramolecular and organised assembly concept is shown in Figure 2.

Supramolecular chemistry may be further divided into two major groups based on different factors of size and shape: host–guest chemistry and self-assembly.[46]

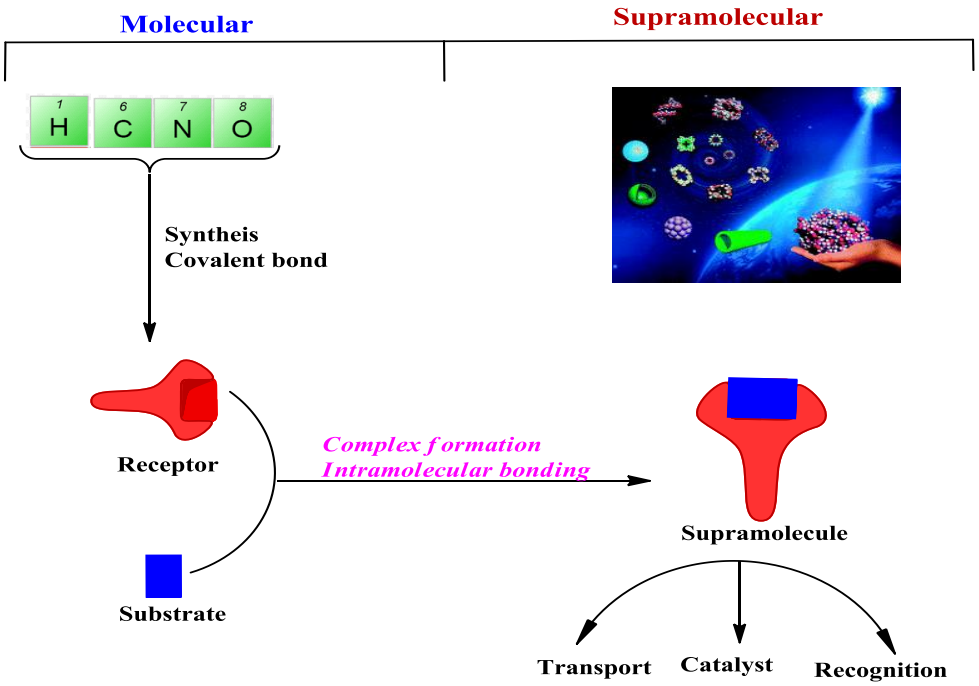

Figure 2. Schematic concept of molecular, supramolecular and to organised assemblies.

1.3 Host-guest chemistry

To form a supramolecule, complementary interactions are necessary. These can be achieved by manipulation of structure at molecular level such that the effects are reflected in its molecular shape. Thus the supramolecular interactions themselves are dependent on the complementarities of the shape. It is for this reason that the most important intermolecular interactions, such as ion-dipole, dipole-dipole and hydrogen-bonding, are directionally dependent. Additionally, the forces which support the stability of supramolecules, notably van der Waals and hydrophobic forces, depend on the close proximity of interacting groups. The best example of complementarity in nature is enzymes as identified by Fischer and Koshland.[39,43] Cram defined their non-biological equivalents as the 'host', an ion or organic molecule with convergent binding sites, in whose binding site the complex was assembled, and the 'guest' as the ion or molecule, with divergent binding sites, bound by the host. The binding site is where the host and guest molecules interact due to their complementary sizes, geometries or general chemical natures.[29,46,48] A simple model to explain host-guest is shown in Figure 3 where four binding sites in the host bind a guest in the centre.

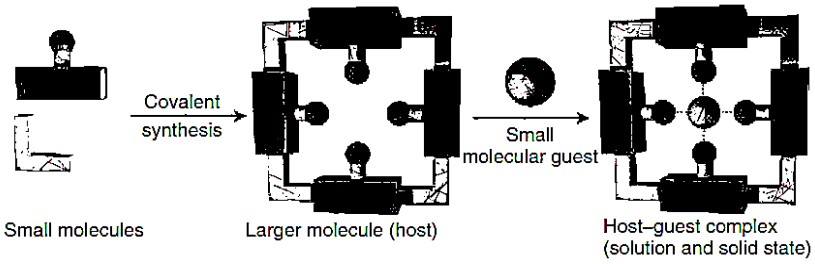

Figure 3. Schematic concept of the host-guest complex formation from the molecular to the supramolecular scale.[46]

1.4 Self-assembly

The natural association of two or more molecules or ions to generate a larger, aggregated molecular species through the generation of reversible interactions is known as self-assembly. Intrinsically simple molecules interact with one another through reciprocal functionalities under suitable conditions to form supramolecular species which interact through non-covalent interactions.[46]

A simple example of self-assembly is the DNA double-helix, where two complementary single strands of DNA are entwined through hydrogen-bonds and π-stacking in a self-assembly process as shown in Figure 4.[49] The single strands recognise each other to form a thermodynamically stable DNA complex. Other biomolecular examples of self-assembly include protein folding and viral assembly[46]

Figure 4. A simple example of self-assembly: the DNA double-helix.

1.5 Supramolecular interactions

Chemists working in supramolecular science attempt to control and regulate the pattern of intermolecular bonds which Lehn described, in order to create materials with unique structures and properties. The intermolecular bonds may take several forms which are employed to construct supramolecular species with specific functionality.[43, 46]

Supramolecular complexes are held together by non-covalent interactions. Covalent single bond energy values, which range from 150 kJ mol^{-1} to 450 kJ mol^{-1}, are considerably greater than weaker non-covalent energies where dispersion forces range from 2 kJ mol^{-1} and up to 300 kJ mol^{-1} for interionic interactions.[50] A stable supramolecular complex can be formed by these interactions in a concerted manner. Non-covalent bonds include dipole and ionic interactions, inter- and intra-molecular interactions, hydrogen-bonds, cation-π, van der Waals and hydrophobic interactions.

1.5.1 Dipole and ionic interactions

Resulting from coulombic attraction between opposite charges, dipole and ionic interactions are further divided into ion–ion, ion–dipole and dipole–dipole interactions. Ion–ion interactions are the strongest; their energies are equivalent to those of stronger covalent bonds. These interactions can occur in any orientation as they are non-directional in nature.[50] Ion–dipole and dipole–dipole interactions require at least two functional group or molecules to be parallel such that the interactions are in the most favourable orientation. Thus ion–dipole and dipole–dipole interactions are directional, the mutually attractive molecular species are able to form aggregates because of the associative rigidity of numerous weak interactions (Figure 5).

Non-directional interactions in ion–dipole and dipole–dipole stabilise a broad range of molecular pairings. The energy value of ion–dipole interactions ranges from 50-200 kJ $mole^{-1}$. Dipole–dipole interaction energy values range from 5–50 kJ mol^{-1}. Ion–dipole interactions have a higher charge density than simple dipoles and hence a higher energy than dipole–dipole interactions.[46] Ionic interactions play a key role in understanding aspects that impact high binding affinities, especially in enzyme-

substrate interactions. The folding and unfolding of these biological systems involves charge–charge interactions as well as hydrogen-bond rearrangements.[46, 50]

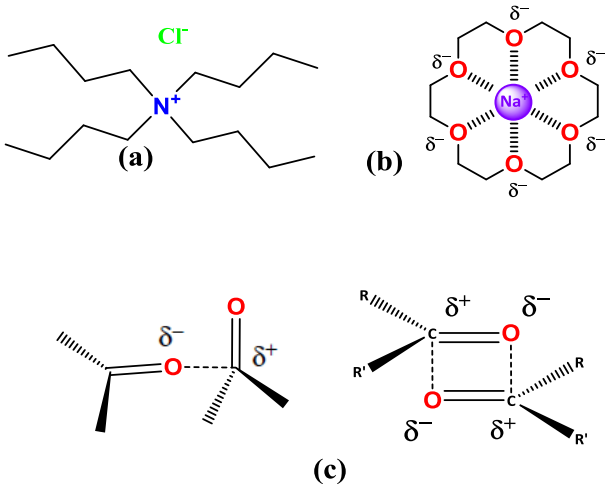

Figure 5. Examples of dipole and ionic interactions.

1.5.2 Inter- and intra-molecular interactions

The design and control of intermolecular bonds is important to produce materials possessing novel structures and properties. Lehn wrote that intermolecular bonds have the ability to take several relevent different forms during the construction of various functional supramolecular molecules. The molecular structures and bulk functions of many supramolecules are defined by the type of interactions in these complexes.[46]

1.5.3 Hydrogen-bonds

The inter- or intramolecular interaction between a hydrogen atom and an electronegative atom is known as a hydrogen-bond. The heteroatomic interaction thus formed through hydrogen-bonding occurs as a result. Hydrogen-bonds can have a wide variety of bond strengths, from 4 – 120 kJ mol^{-1}, which in neutral molecules is proportional to the distance between the two interacting atoms, usually in the range of 1.2 Å to 3.2 Å.

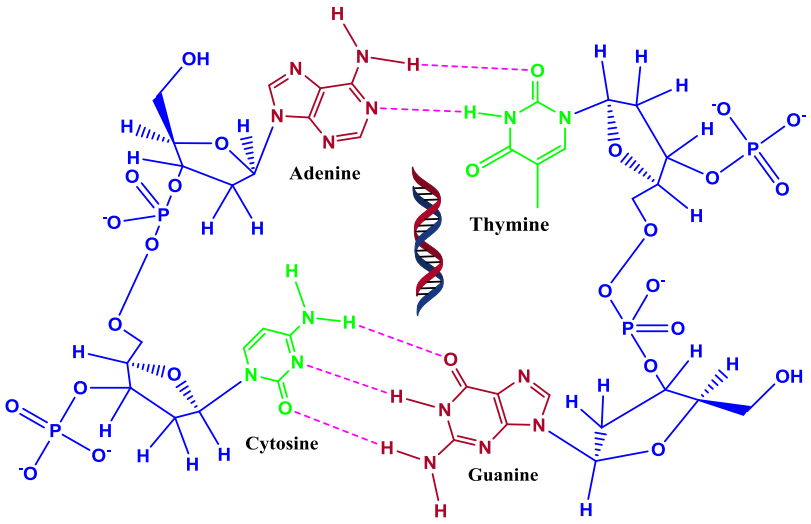

Figure 6. A visual representation of H-bonding with DNA base pairs.

Hydrogen-bonds are directionally dependent, which means that the strongest hydrogen-bonds are formed between atoms arranged at 180° to each other. From the strongest to the weakest, hydrogen-bonds can have a range of bond angles from 180° to 90°. The deformation of hydrogen-bonds is entropically favoured and compromises between the angle formed and other packing forces are often reached.[46]

1.5.4 Cation-π interactions

Among non-covalent intermolecular interactions, cation-π interactions of aromatic system are strong, falling in the range of 60-160 $kJmol^{-1}$. Models explaining electrostatic arrangement on the both sides of the plane of aromatic ring in cation-π interactions have been investigated through cation binding studies with cyclophane hosts.[51]

1.5.5 van der Waals interactions

van der Waals interactions occur because of the non-permanent polarisation of electron clouds and are non-directional.[52] The electron cloud close to the surrounding non-polar atoms or groups gives the polarisation effect. When the van der Waals interacting atoms are close, their fluctuations may become aligned and produce an attractive force. Thus the force produced is strongly dependent on inter- and intramolecular distances. The strength of the interaction decreases inversely as a function of r^6 where r is the internuclear distance.[50] The main interactions between alkyl chains in a variety of isomers are van der Waals interactions. If the carbon

atom numbers are even, then the interactions in the chain disrupts because the alkyl groups in the chains are unable to come close enough proximity to create a van der Waals interacting environment.[53] Disruption of these interactions, in case of the long alkyl chain substituents, leads to the development of an odd-even effect in calamitic liquid crystals. The van der Waals interactions result in mesogenic phase disruption.

1.5.6 The hydrophobic effect

The entropically-related phenomenon which causes aggregation of non-polar groups together in aqueous solution is an example of the hydrophobic effect. During the process of aggregation, water, which would otherwise be associated firmly around non-polar groups, is liberated and results in an increase in entropy. Furthermore, the increase in entropy formed due to the liberation of water is caused by decreasing surface when non-polar atoms or groups associates together.[46]

1.5.7 Macrocyclic compounds

Macrocyclic compounds play a key role in supramolecular chemistry due to their defined shape, nanoscale size, and molecular selectivity.[54] Simple starting materials like alkyl ethers, phenols, pyrroles, glycolurils or glucose can be reacted to yield crown ethers, calixarenes, porphyrins, cucurbiturils and cyclodextrins (Figure 7).[55] These macrocyclic molecules display distinctive shapes and properties.[56] Many supramolecules have been synthesised from these macrocycles and investigated as artificial biomolecules with biomimetic structures and functions.[57]

Crown ethers, novel macrocyclic with interesting binding characteristics, were reported in 1967 by Pederson,[45] following on from the discovery of phthalocyanines in the 1920's by Dandridge.[58] Cucurbiturils were first synthesised in 1905[59], metacyclophanes were observed by Pellagrin in 1899 and cyclodextrins by Villers in 1891. In the 1870's and 1880's research on phenol-formaldehyde chemistry by Baeyer revealed the macrocyclic calixarenes, resorcinarenes and calixpyrroles.[57]

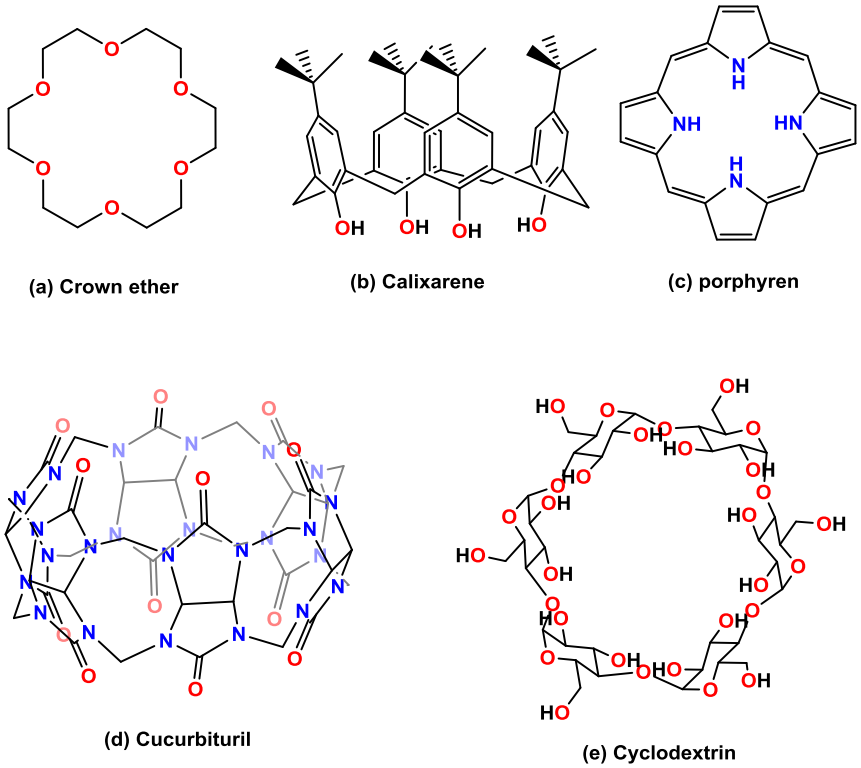

Figure 7. Macrocyclic compounds- (a) crown ether, (b) calixarene, (c) porphyrin, (d) cucurbituril and (e) cyclodextrin**.**

The function of supramolecular compounds is dependent on the shape and properties of macrocyclic hosts. For example, cyclodextrins are natural, water-soluble, non-toxic and available commercially, and have been used as supramolecular hosts for biomedical purposes. Hydroxyl groups are reactive species and are present on both rims of these macrocycles. An example of a supramolecular material from cyclodextrins is a gel formed by the hydroxyl crosslinking groups which lead to the formation of polyrotaxanes.[60]

1.6 Pillar[*n*]arene chemistry

Numerous macrocyclic compounds have been reported but their synthesis often involves multi-step processes, low yields and purification difficulties.[61] Pillar[*n*]arene chemistry has become a chemical focus following its first reported by Ogoshi in 2008. The current nomenclature involves the general name pillar[*n*]arene where [*n*] indicates the number of aromatic rings in the macrocycle. P[5]As are conformationally stable 5-membered macrocycles and are part of the paracyclophane family of macrocycles due to linkage between the 2-5 positons of the aromatic rings.

In comparison to other macrocycles, P[5]A have several advantages: they can be synthesised using cheap reagents, are easily re-crystallised and can be obtained in high yields.[61] P[5]As have a total of 10 substituents on their rims with the type of substituent contributing to their solubility. Over 300 papers on the synthesis and applications of pillar[*n*]arenes have been reported between 2008 and the end of 2015.

1.6.1 Characteristics of pillar[5]arenes

Characteristic properties of pillar[*n*]arenes are:

1. They have simple structure due to which they display excellent host-guest properties and planar chirality. They are made of the repeating 1,4-dialkoxybenzenes units which are linked by methylene bridges in the 2- and 5-positions.[62]
2. They are notably symmetrical structures and have pillar-shaped architectures. The cavity size of P[5]As is approximately 5.5 Å. Because of its cavity size is comparable with well-known α-cyclodextrin, its cavities will also fit the guests like linear alkanes and simple aromatic compounds.[63]
3. They have versatile functionality. P[5]As can accommodate 10 functional groups, so functionalisation of this compound can be achieved for selective positions by various organic synthetic approaches.[63]

1.6.2 Host-guest properties of pillar[5]arenes

P[5]As are excellent host molecules to study host-guest interactions because of their well-defined central cavity. The size of the cavity, 5.5 Å, is comparable to α-cyclodextrin, sufficiently large to incorporate the size of guest molecules, hence they can accommodate linear-shaped hydrocarbons and simple aromatic molecules. P[5]As can seize guest molecules by various physical interactions confide on the size of the cavity and the nature of the alkoxy substituents.[64] Surrounded by ten oxygen atoms, the central cavity is perfectly suited be involved in host-guest complexation with metal ions and ammonium salts. Most of P[5]A crystal structures show the inclusion of solvent or other small molecules either within the macrocycle or associated strongly with the oxygen atoms that surround the two openings.[65] It was reported that the P[5]A cavity was ideal for small, linear molecules such as acetonitrile,[66] 1,4-dicyanobutane,[67] and hexane.[68] The inner surface of the P[5]As

cavities is negative because alkoxy groups on the rims are electron-donating moieties. Compared with an open-ended calix[5]arene structure, their pillar-shaped structure contribute to enhance the π-electron density of their cavity.[63] Therefore, P[5]As are excellent hosts which can accommodate cationic molecules and molecules containing electron with-drawing groups, in their cavities. Several reports exist which demonstrate that P[5]As form complexes with aromatic compounds like pyridinium and viologen derivatives[69,70] and also with linear alkanes with electron-poor amine,[71] ammonium,[71] cyano,[67] and halogen[72] termini. In 2010, Stoddart[73] was the first to show that the cavity within P[5]As could be used as a receptor for linear alkylamines. We believed that these recognition properties could be exploited to generate P[5]A-based sensors and chose to target their potential electrochemical response to guest binding. The aim of this work is ultimately to use P[5]A-based sensors to investigate biogenic amines and alkali metal ion selectivities. In order to achieve this, the first step is to synthesise P[5]A-based receptors as focused in the Chapter 2.

1.6.3 Synthesis of pillar[*n*]arenes

Ogoshi synthesised 1,4-dimethoxypillar[5]arene for the first time by the condensation of 1,4 dimethoxybenzene and paraformaldehyde in the presence of the Lewis acid $BF_3{\cdot}O(C_2H_5)_2$.[62] The yield in this first reported synthesis was a modest 22%. Removal of the methoxy protecting groups by BBr_3 led to the isolation of perhydroxylated pillar[5]arene.[62,74] A variety of alkyl substituted P[5]As were synthesised in a similar fashion with functional groups in 1,4-positions including ethoxy, n-propoxy, n-butoxy, n-pentyloxy, n-hexyloxy and n-dodecanoxy derivatives. The yields of these P[5]As varied ranging from 7 to 28%.[75] Functionalisation of macrocyclic compounds is very important because it can change the solubility and physical properties of the macrocyclic compounds.[75] The synthesis of the P[5]As and functionalised co-P[5]A derivatives are detailed in Chapter 2.

1.6.4 Mechanism of pillar[5]arene formation

P[5]As are formed through the Friedel–Crafts reaction in which carbon addition onto an aromatic ring can be achieved. Nierengarten,[76] Yang[77] and Chupakhin groups[78] have suggested a mechanism of formation in which the first step is the acid catalysed

hydroxymethylation of 1,4-methoxybenzene with paraformaldehyde to give benzyl alcohol **A** as shown in Figure 8.

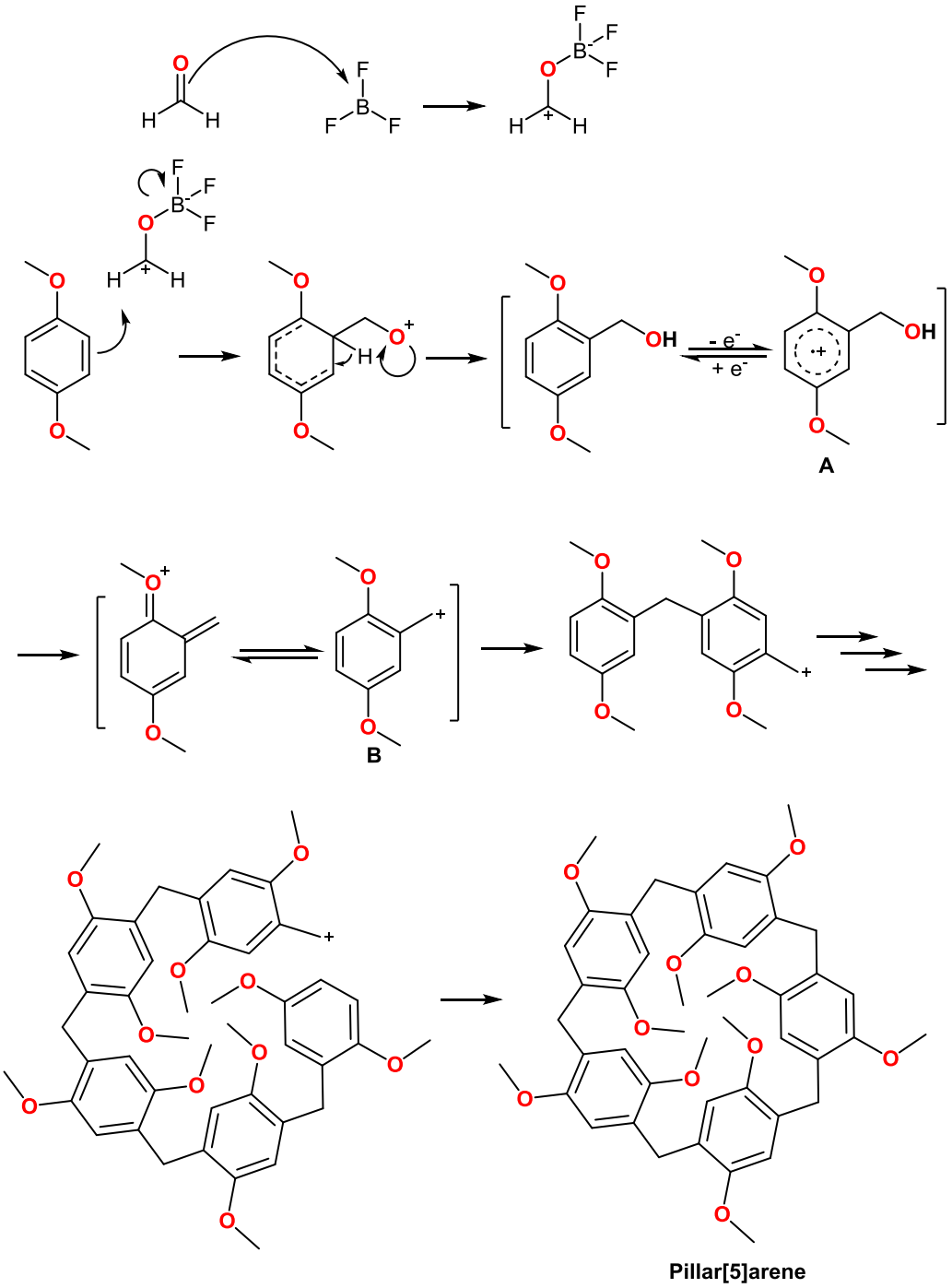

Figure 8. Proposed pathway for the preparation of P[5]As under Friedel–Crafts conditions.[77, 79]

Benzylic cation **B** is formed upon elimination of water from the benzyl alcohol. Under acidic conditions **B** will form another benzyl alcohol which reacts to give a dimeric benzylic cation. The reaction is repeated to yield oligomeric cations which

may cyclise upon formation of the pentamer to give the most stable pillar[*n*]arene. The cyclopentamer is stabilised because the internal methylene bond angles achieve 108° which is the closest to the ideal tetrahedral angle of 109.5°. This contrasts with 90° for the cyclotetramer, which has never been observed, and 120° for the cyclohexamer which is occasionally isolated as a by-product of P[5]A synthesis.

The Nierengarten group[76] reported that the cyclisation product is formed under thermodynamic control and that the distribution of cyclic products is dependent on the relative stabilities of the final products (Figure 9). Hence the P[5]A derivative should be the thermodynamic product. Nierengarten reported that crystallographic observations confirmed that the 1,4-dimethoxypillar[5]arene methylene bridge bond angle is 111.3^{o} which is close to the sp^{3} hybridised carbon value of 109.5^{o} and the theoretical 108^{o} internal bond angle for an unstrained pentagon. The reaction where solvents nitrobenzene and 1,2-dichloroethane leads to oligomer precipitation which explains why synthesis of P[5]A is not achieved using these solvents.

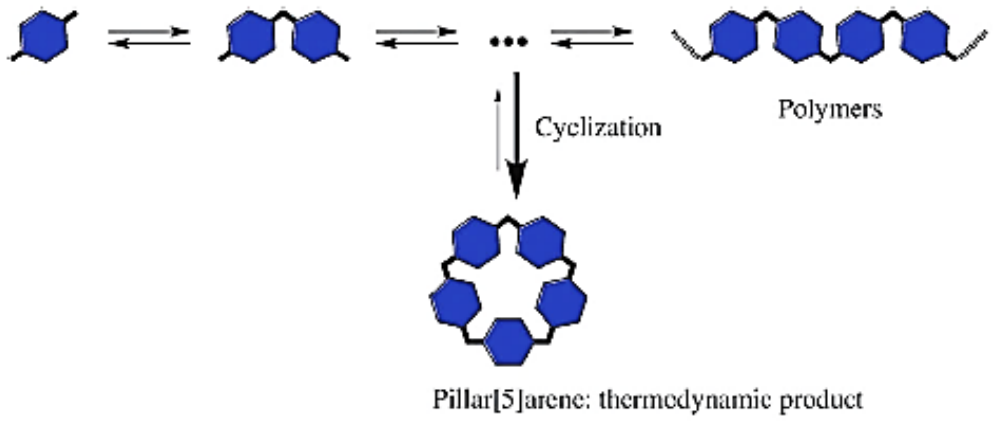

Figure 9. schematic representation of thermodynamic P[5]A product.[76]

1.6.5 Various pillar[5]arene synthetic methods.

Scheme 1 provides an outline of few of the important pillar[*n*]arene synthetic procedures reported. Ogoshi's original synthesis is shown in pathway A where R is a methyl group. Pathway A is thermodynamically favoured and involves the condensation of the pentamer, where an electrophile attacks electron-rich hydroquinone dimethyl ether generated by $BF_3{\cdot}O(C_2H_5)_2$ and paraformaldehyde. New methods involving an excess of paraformaldehyde[74] and the use of the catalyst

TFA[80] increased the yields to 71% to 81% respectively. Pathway B was reported by Meier in which 1,4-dialkoxy-2,5-bis(alkoxy-methyl)benzenes are the starting materials.[81] Cyclooligomers were formed though a Friedel-Crafts reaction and cleavage by *ipso*-substitution forms a new C-C bond to give **1** as shown in pathway C. **1** can also be synthesised by pathway D which was reported by Nierengarten in 2012.[76]

Pillar[5]quinone **2** is synthesised by cleaving the ether groups in **1** which in turn leads to perhydroxylated system **3**.[62, 81] Compound **2** was synthesised and shown to be a cyclic polyquinone.[81] Partial oxidisation of **1** was achieved by using Ce^{4+} to yield regioisomeric diquinones.[82] Subsequently, hypervalent iodine compounds were used to oxidise macrocycles containing more than five quinone units.[83, 84]

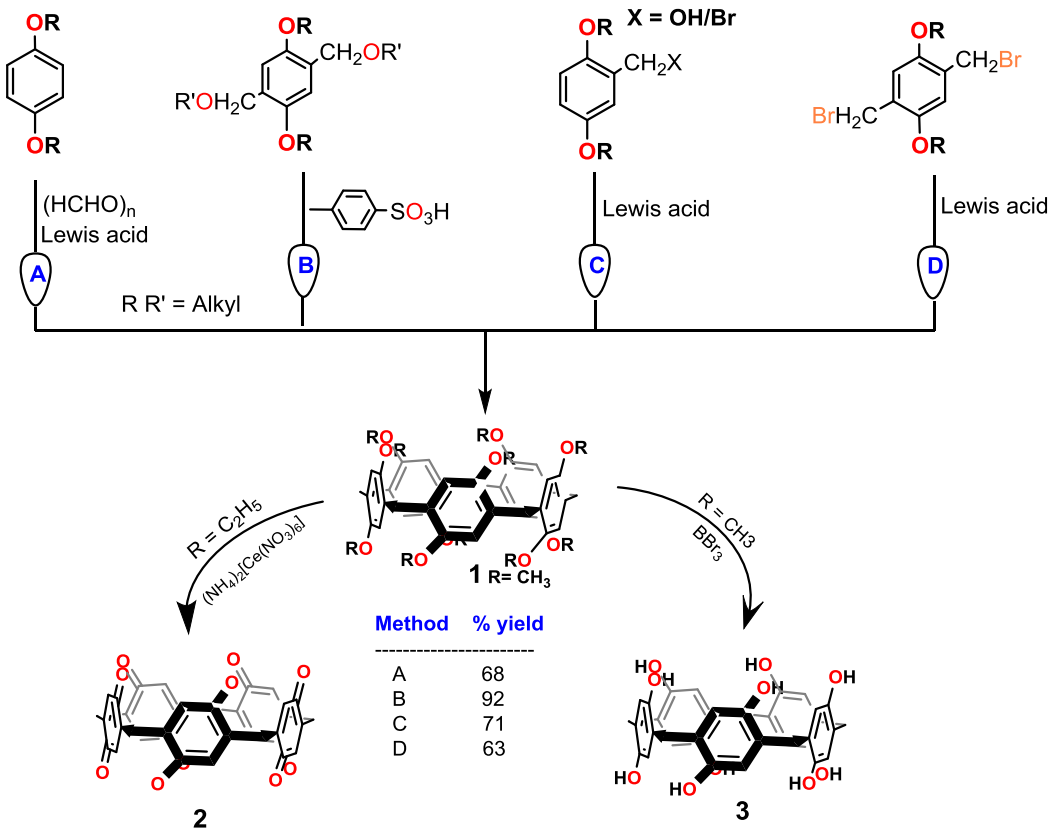

Scheme 1. Schematic representation of various methods for synthesis of P[5]As.

1.6.6 Mono- and dihydroxylated pillar[5]arenes

In 2009 Meier reported the oxidation of P[5]A using $(NH_4)_2[Ce(NO_3)_6]$ to synthesise pillar[5]quinone **2**.[81, 85] This was the first reported in literature detailing synthesis of

the cyclic quinone and it gave the target in 62% yield. Later in 2012, Hou reported perhydroxylated P[5]A[86] and pillar[6]arene (P[6]A)[87] through demethylation with BBr_3. Various per-functionalised pillar[*n*]arene derivatives are possible because of the nature of the highly reactive phenolic species.

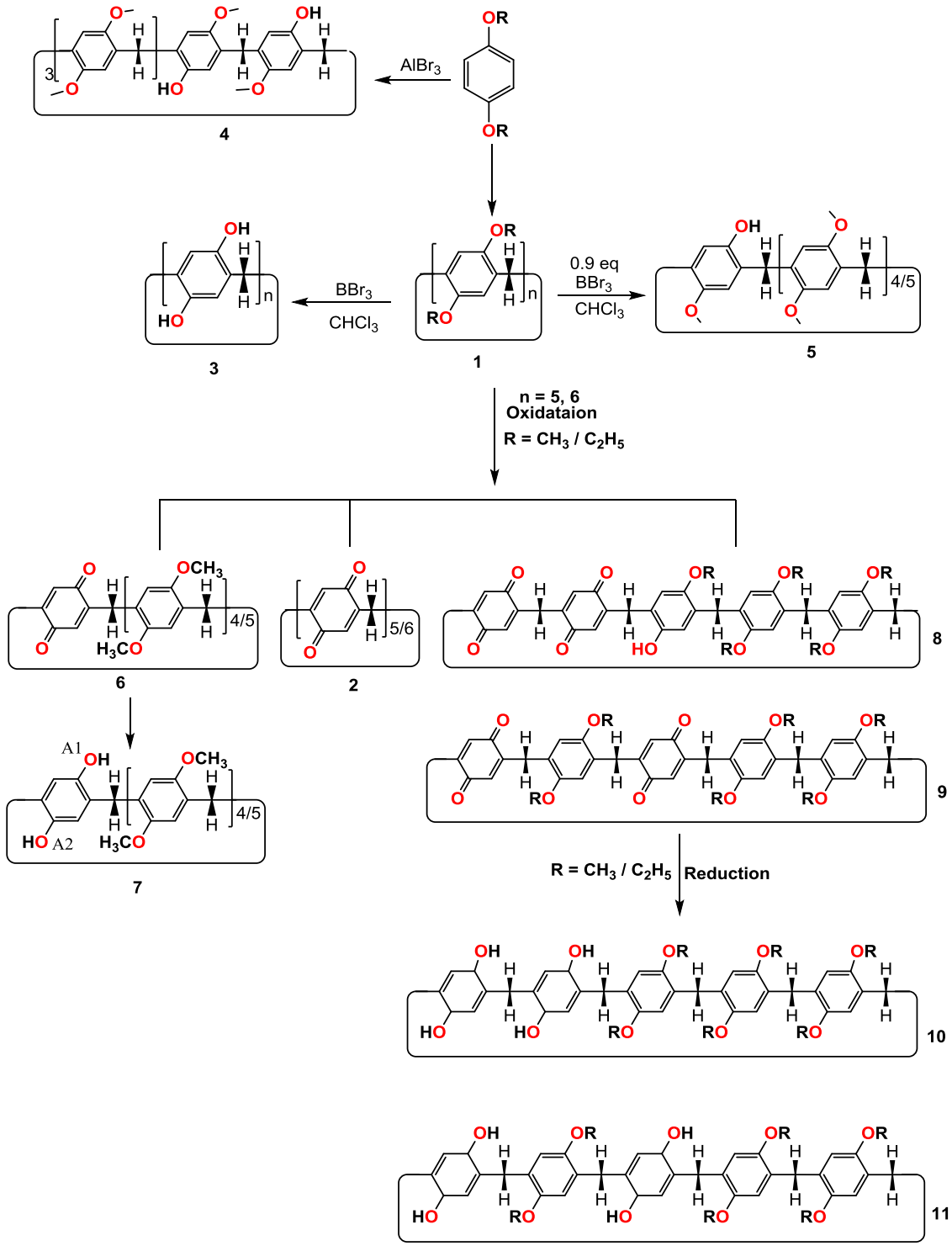

Scheme 2. Schematic representation of mono, di, tetra- hydroxyl pillar[*n*]arene synthesis.

Monohydroxylated pillar[*n*]arenes were prepared by optimising perhydroxylatation conditions, for example, 0.9 equivalents of BBr_3 were used in the reaction with P[5]A[86] and P[6]A[88] to give monohydroxylated P[5]A and P[6]A, respectively, reported by Yamaguschi in 2011 and 2012.[88, 89] Another method of synthesising P[5]A was reported in 2011 where $AlBr_3$ was used as a Lewis acid to synthesise **4**. In this method, the synthesis of P[5]A and cleavage of methoxy groups attained at the same time.[89] The cyclisation and cleavage of the methoxy groups in this reaction was achieved by using $AlBr_3$. In 2012 Ogoshi and Huang reported the oxidation of a single dialkoxybenzene to give a derivative possessing a single benzoquinone unit **6**.[90, 91] Another approach is to introduce one benzoquinone unit in P[6]A through hydroxylated P[5]A derivative A1/A2 (shown as **7** in Scheme 2), prepared by the reduction of benzoquinone units.[83]

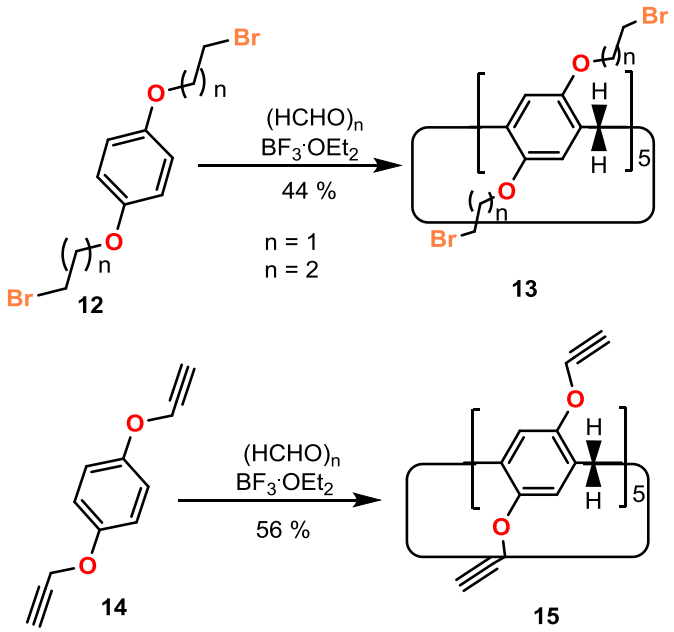

Scheme 3. Schematic representation of synthesis of **13** from **12** and **15** from **14** through condensation with paraformaldehyde and $BF_3{\cdot}O(C_2H_5)_2$. [71]

Conformational isomers of pillar[*n*]arenes can be formed through the partial reaction of these pillar[*n*]arenes possessing multiple substituents so a specific synthetic methodology is important to synthesise the desired products. Synthesis of A1/A2 difunctionalised P[5]As leads to minor products which are tetrafunctionalised under optimised reaction conditions. Ogoshi reported the oxidation/reduction of two diethoxybenzene entity of perethylated P[5]A **10** and **11** for the first time by a

method which gave the quadruply deprotected P[5]As.[82] Two hydroquinone units at the A, B or the A, C units were isolated following chromatography. These were subsequently tetrahydroxylated by reducing the benzoquinone units. A 1,4-bis(bromoalkoxy)pillar[5]arene was synthesised by condensation of monomer **12** (n = 2 or 3) in 44% yield and condensation of 1,4-bis(prop-2-yn-1-yloxy)benzene **13** with paraformaldehyde and $BF_3 \cdot O(C_2H_5)_2$ gave the desired product in 56% yield (Scheme 3).[71]

1.6.7 Copillar[5]arene synthesis

Copillar[5]arenes describe P[5]As comprising different aromatic moieties, for example those with 1,4-dimethoxy and 1,4-diethylester substituents. For this project the synthesis of copillar[5]arenes with high yields and selectivity was very important. Yields where R_1 and R_2 are bulky were reportedly low, whereas higher yields were achieved when synthesised for the corresponding homopillar[5]arenes under the same experimental conditions (Scheme 4).[92,93]

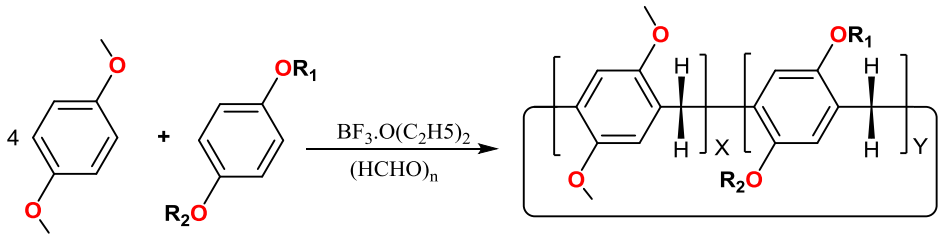

R_1	R_2	X	Y	Catalyst	% Yield
n-C_4H_9	*n*-C_4H_9	4	1	$BF_3.O(C_2H_5)_2$	16
n-C_4H_9	*n*-C_4H_9	1	4	$BF_3.O(C_2H_5)_2$	9
CH_3	*n*-C_3H_7	4	1	$FeCl_3$	50

Scheme 4. Schematic representation of copillar[5]arenes synthesis by $BF_3.O(C_2H_5)_2$ and $FeCl_3$[91,94]

The third example in Scheme 5 illustrates an extension of the scope of copillar[5]arenes by a cyclococondensation reaction to introduce different alkyl groups. The yield was comparatively much higher than the other examples which may be due to $FeCl_3$ being used as the catalyst.

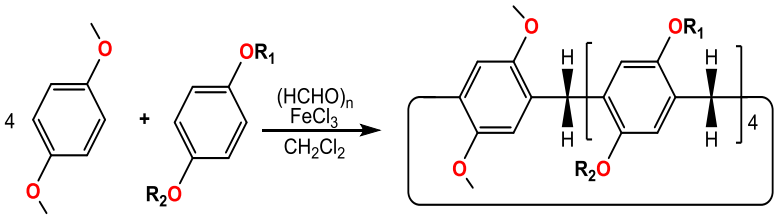

R_1	R_2	Yield %
CH_3	$(CH_2)_2Br$	55
CH_3	$(CH_2)_4Br$	78
CH_3	$(CH_2)_6Br$	85
CH_3	$(CH_2)_{10}Br$	45
$(CH_2)_6Br$	$(CH_2)_6Br$	71

Scheme 5. Schematic representation of an efficient synthesis of copillar[5]arenes using $FeCl_3$.[94]

A reproducible approach for the high yield synthesis of copillar[5]arenes was achieved using $FeCl_3$ as the catalyst shown in Scheme 5; combinations of various dialkoxybenzenes and paraformaldehyde gave yields ranging from 50–85%.[95] A range of catalysts, solvents and mixtures in different ratios of the corresponding 1,4-dialkoxybenzenes were screened and it was finally recognised that $FeCl_3$ in CH_2Cl_2 provided the best catalytic conditions (Scheme 6).[95]

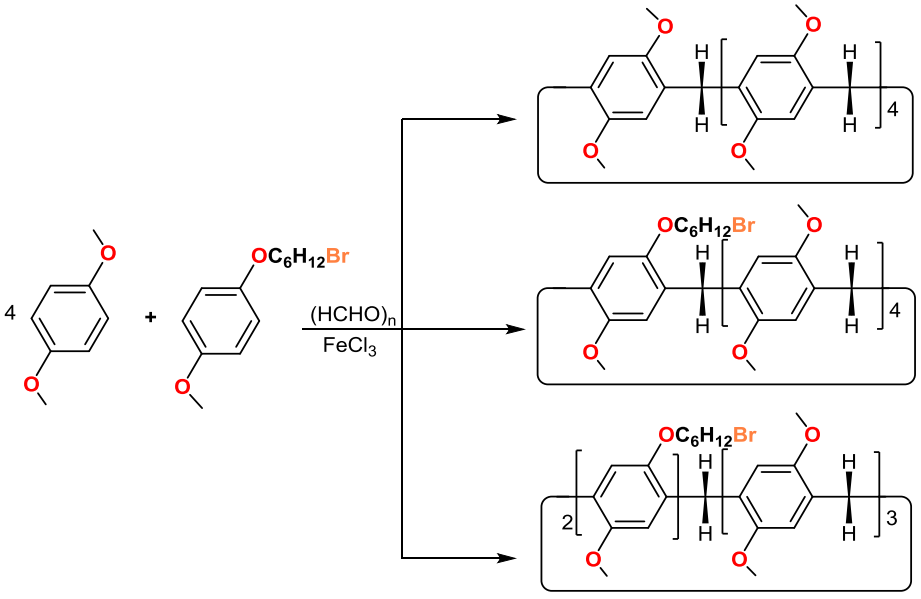

Scheme 6. A schematic showing formation of the paraformaldehyde, 1,4-dimethoxybenzene and 1-(6-bromohexyloxy)-4-methoxybenzene is shown. Three types of products result.[75]

1.6.8 Pillar[6]arene and pillar[7-10]arenes

P[6]As were prepared a year after the P[5]A synthesis was first reported.[81] The higher pillar[*n*]arenes (n > 6) were usually obtained as by-products in the synthesis

of P[5]As as minor products with low yields because of the thermodynamically favoured formation of P[5]As (Scheme 7).[81] The synthesis of P[6]As as the major product in better yields was enhanced by using catalytic $FeCl_3$ in chloroform. The first pillar[7]arene was synthesised by Cao and Meier[80] followed by larger pillar[*n*]arenes, where n = 8-10 which were synthesised by Hu (Scheme 8). However, it is expected that pillar[*n*]arenes of larger size may have different conformations due to the relatively rigid tetrahedron bonding feature of the methylene bridge.[86]

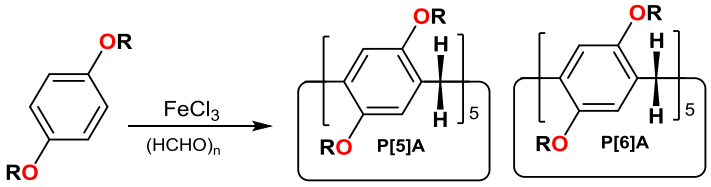

R	P[5]A yield %	P[5]A yield %	Ratio (P[6]A/[5]A)
CH_3	29	--	--
C_2H_5	30	34	1.1
n-C_3H_7	28	35	1.2
i-C_3H_7	31	30	1.0
n-C_4H_9	30	43	1.4
n-C_6H_{13}	28	45	1.6
n-C_6H_{17}	22	45	2.0

Scheme 7. Schematic representation of P[5]A and P[6]A synthesis with their R groups, yields and P6A/P5A ratios.

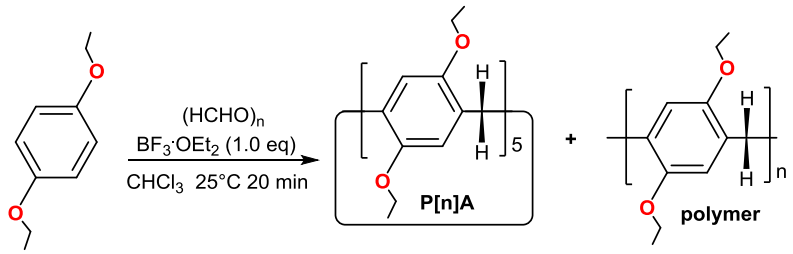

P[n]A	n	(%) Yield
P[5]A	5	20
P[6]A	6	15
P[7]A	7	3
P[8]A	8	1
P[9]A	9	2
P[10]A	10	2

Scheme 8. Schematic representation of pillar[*n*]arene (n=5/6/7/8/9 and 10) synthesis and yields.[86]

1.7 X-Ray structures of pillar[*n*]arenes

Host-guest binding properties are dependent on the structural features of the constituent molecules, therefore it is very important to examine the structural characteristics of the novel host molecules.

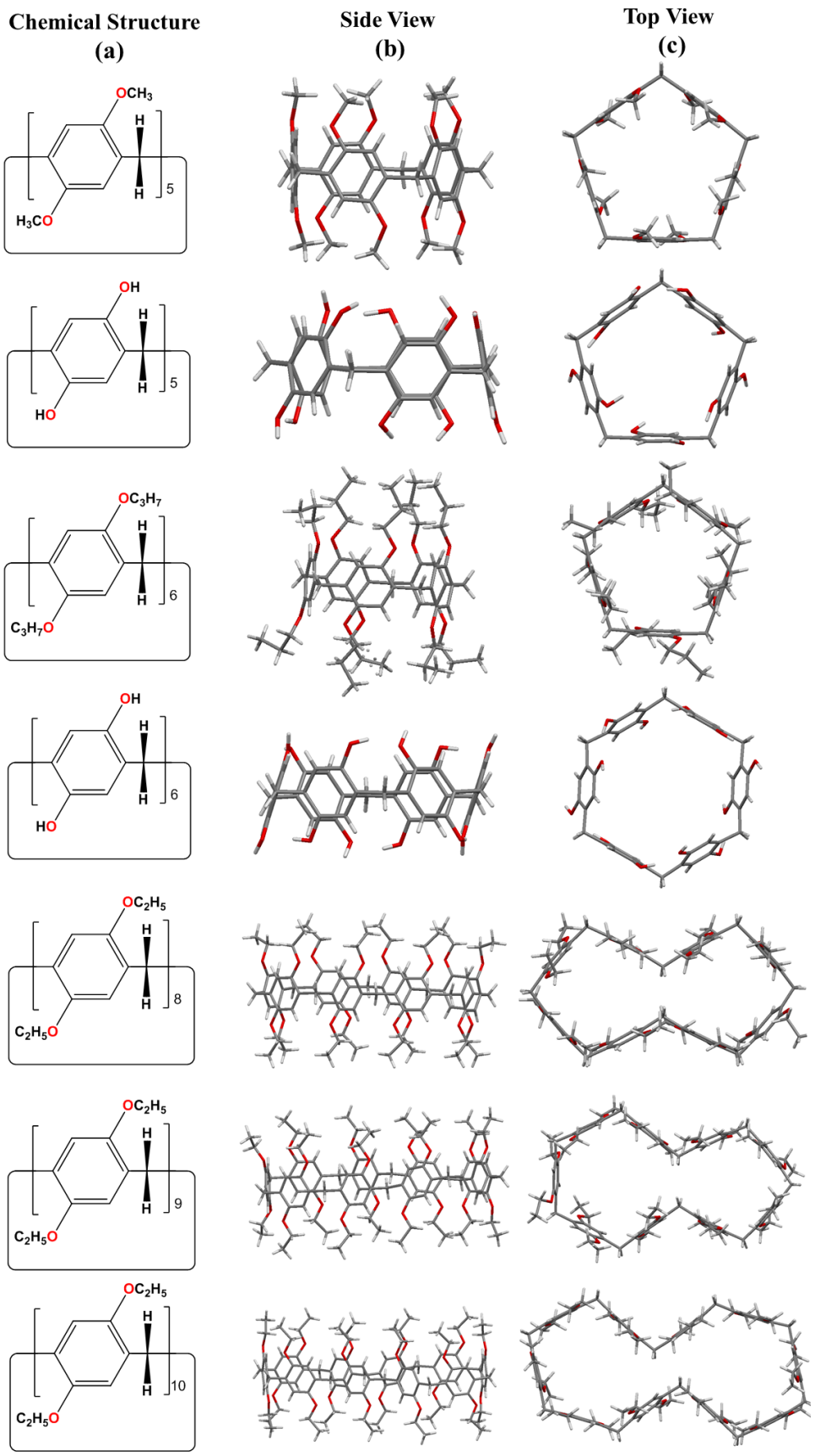

Figure 10. X-Ray structures of different types of pillar[*n*]arene: (from top) n = 5, 6, 8, 9, 10; (a) chemical structures and (b) side and (c) top views crystal structures.[62,86,96]

The X-ray crystal structures of pillar[*n*]arenes, where n = 5 to 10, are shown in Figure 10.[85] P[5]As have a unique, symmetric construction with an internal cavity diameter of around 5Å. P[5]A is geometrically stable because of the 108° average bond angle around the bridging methylene carbon atoms whereas P[6]A is a cyclic hexagonal structure with an internal cavity diameter around 7Å.[85]

1.8 Functionalisation of pillar[*n*]arenes

Functionalisation of pillar[*n*]arenes allows introduction of novel properties which can lead to potential applications. The synthetic approaches and their applications are briefly discussed below.[85]

1.8.1 Mono- fuctionalisation of pillar[5]arenes

Monobromo functionalised P[5]A **16** reacts with sodium azide which generates **17** that will in turn undergo Huisgen reaction to introduce other functional groups. This is the main precursor for a library of mono functionalised P[5]A. For example, P[5]A can be synthesised by incorporating pyrene and azobenzene components (Scheme 9).[79, 95]

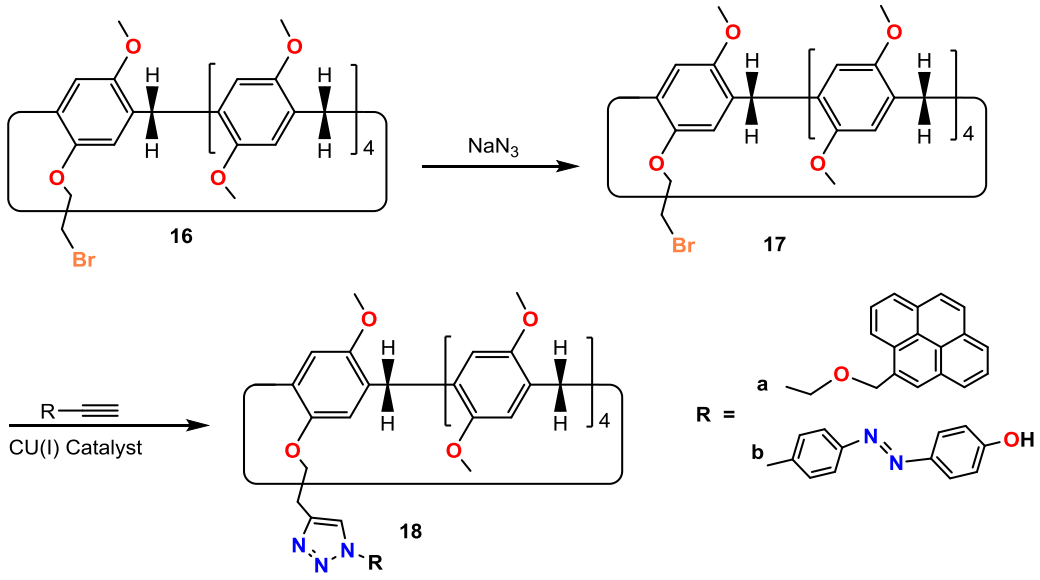

Scheme 9. Schematic representation of mono-functionalised P[5]As.

1.8.2 Pentafuctionalisation of pillar[5]arenes

A naphthalene-containing azide moiety can react with five alkyne groups *via* the Huisgen reaction to give modified P[5]A **20** from peralkyne-functionalised P[5]A **19** shown in Scheme 10.

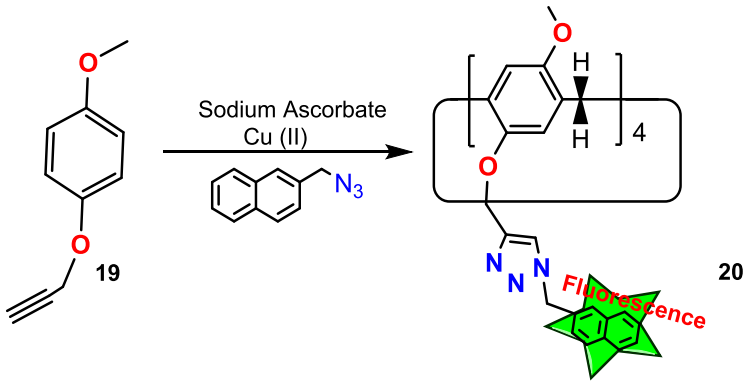

Scheme 10. Schematic representation of synthesis of peralkyne-functionalised P[5]A.

1.8.3 Perfuctionalisation of pillar[5]arenes

Peracid functionalised P[5]A can be synthesised from esterified pillar[5]rene in 90% yield. By analogy with the penta-functionalised P[5]A, the Huisgen reaction between terminal alkynes and azides is high yielding. Peralkyne-functionalised P[5]A reacts with azide or the perazide-functionalised groups to yield substituents with various R groups (Scheme 11).

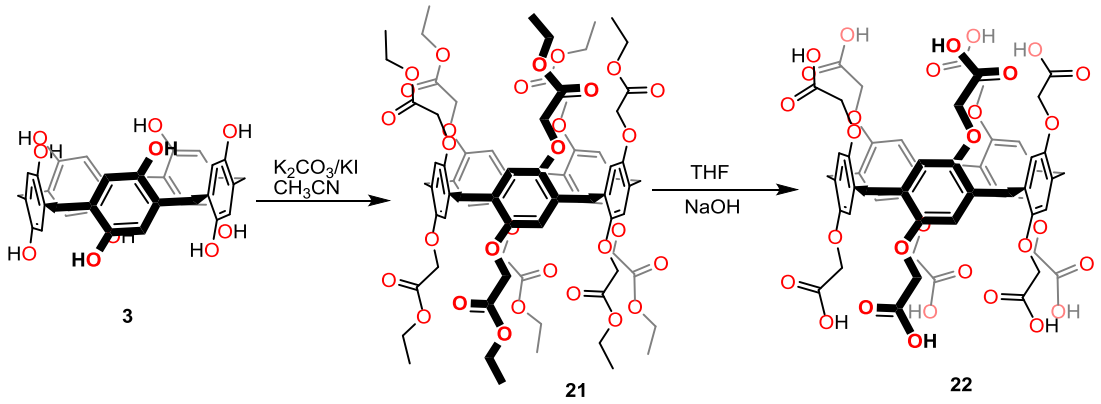

Scheme 11. Schematic representation of synthesis of peracid-functionalised P[5]A.

Nierengarten synthesised a P[5]A azide by a double click reaction between the corresponding decabromide with NaN_3. Subsequent reactions with alkyne

derivatives provides the decasubstituted P[5]As.[79] The azide functionalised pillarenes **23** can also be prepared from **24**.[97]

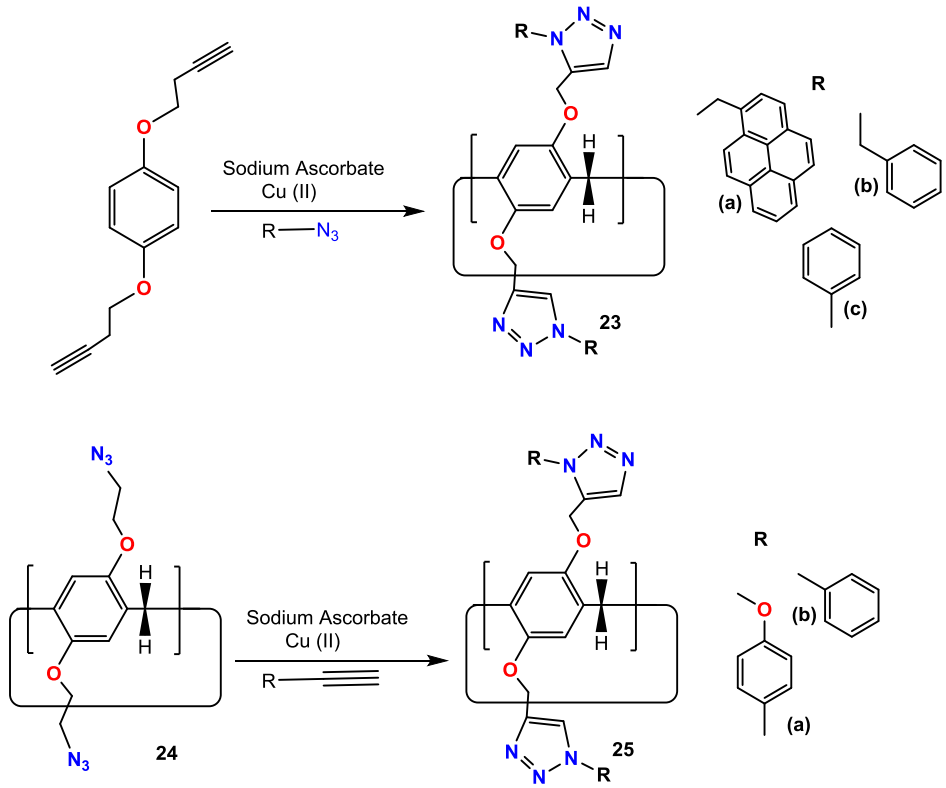

Scheme 12. Schematic representation of synthesis of perfunctionalised P[5]As with various substituents in the 4-position.

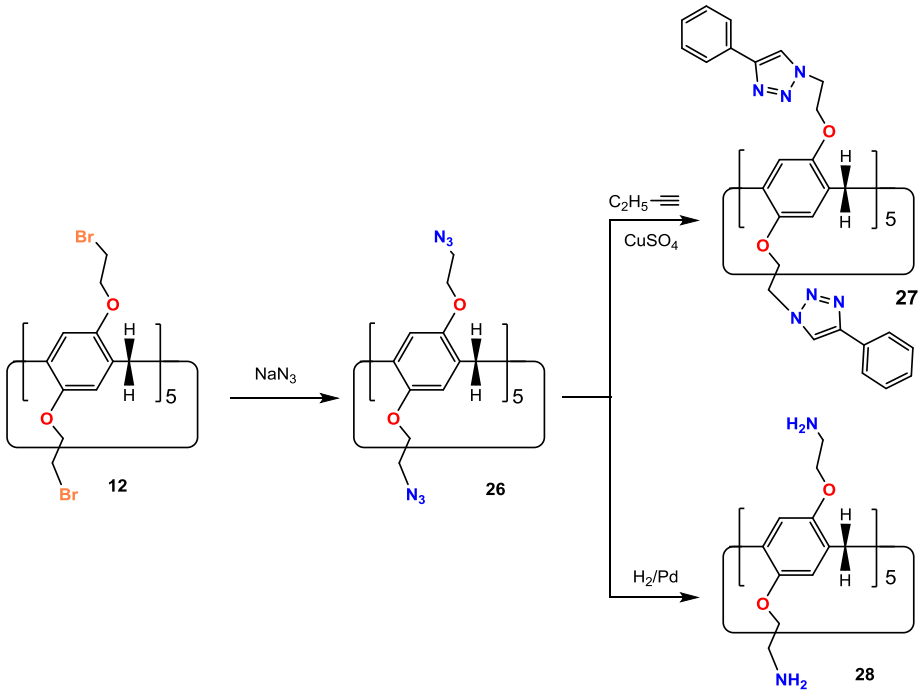

Scheme 13. Schematic representation of synthesis of azide functionalised pillarenes **26**, 1,2,3-triazole **27** and decaamine P[5]A **28**.

The perbromopropylated P[5]A **12** was obtained from the cyclisation of bis(1-bromopropoxy)benzene. Reacting **12** with excess 1-methylimidazole gave the corresponding imidazolium bromide ionic liquid (IL) moieties in good yield (Scheme 14).[98-100]

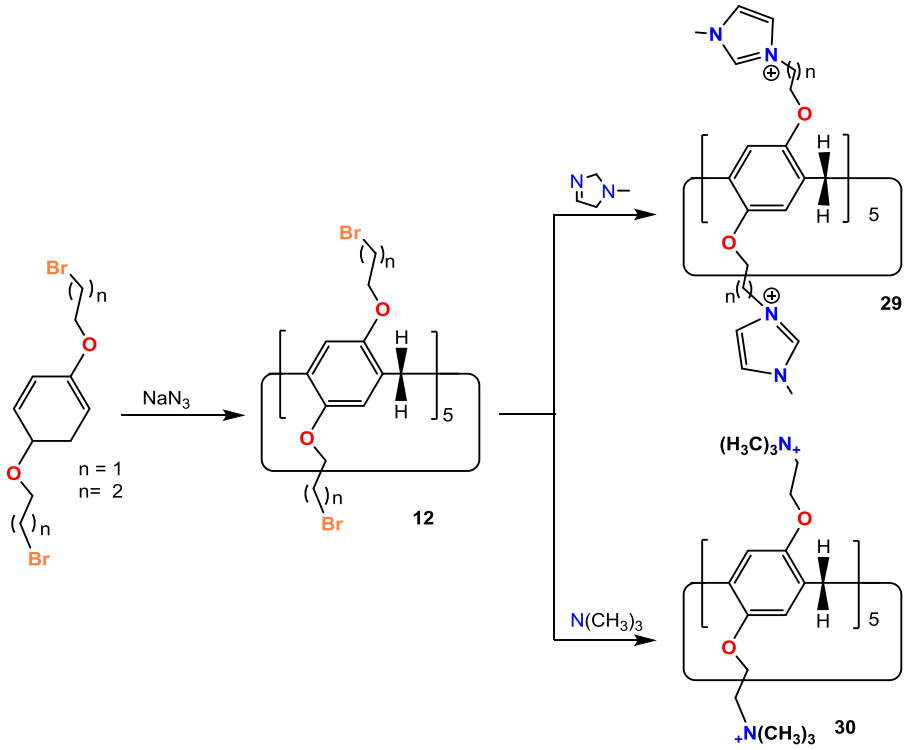

Scheme 14. Schematic representation of synthesis of bromoalkoxy functionalised P[5]As **12**, imidazolium bromide ionic liquids (IL) **29** and a quaternary functional P[5]A **30**.[98-100]

1.8.4 Molecular recognition

For any macrocycle to function as a component in a sensor it must possess a great affinity for the target analyte and a mechanism by which the binding event can be signalled. The molecular recognition aspect is essential if false positives are to be minimised so it is first necessary to survey the current pillar[*n*]arene literature to discover which chemical species are known to bind to the macrocycles.[55] The higher pillar[*n*]arenes have much larger central cavities, as indicated by their crystal structures, and far greater conformational mobility than the pillar[5]- and [6]arenes making the latter more suitable as receptors for small molecules.

From the first crystal structures it was clear that the P[5]A cavity was ideal for small, linear molecules such as acetonitrile,[66] 1,4-dicyanobutane[67] and hexane[68] (Figure 11). Paraquat and its linear derivatives also make good guests for this macrocyclic

host.[62] Later, hydrogen-bonded chains of water molecules were shown to form within the cavities of derivatives such as ester.[101] Most P[5]A crystal structures show the inclusion of solvent or other small molecules either within the macrocycle or associated strongly with the oxygen atoms that surround the two openings.

Ester functionalised P[5]A nanotubes have been synthesised which form rows and stacks in a columnar fashion with the help of hydrogen-boding between column end functional groups.[101]

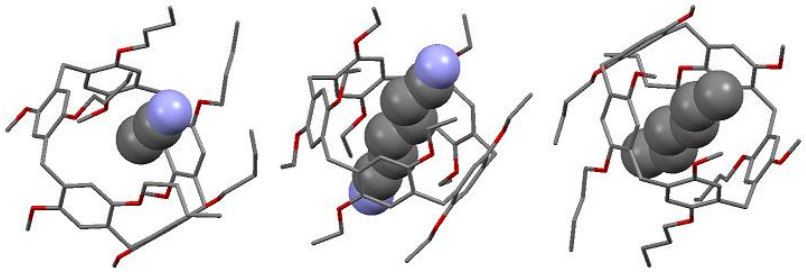

Figure 11. X-Ray structures showing inclusion of (from top) acetonitrile, 1,4-dicyanobutane and hexane (hydrogen atoms removed for clarity).[55]

As proof, P[5]A columns forming long fibres were observed by electron microscopy. The X-ray crystal structure of the compound reveals that these crystals contain hydrogen-bonded water molecules within the fibres as shown in Figure 12.

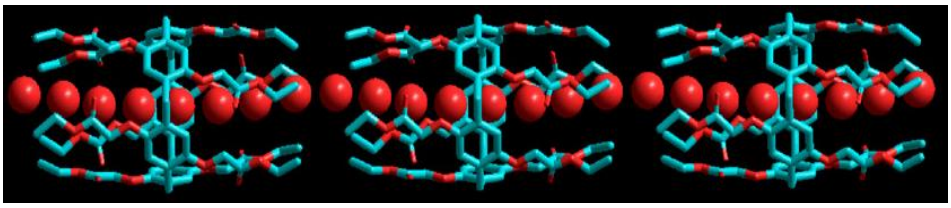

Figure 12. Crystal structure of a P[5]A ester. The crystal packing shows that the encapsulated water molecules (red spheres) crystallise a linear fashion through the columnar statures.[101] (Reproduced with permission from Elsevier)

1.8.5 Pillar[*n*]arenes with sensor applications

Ogoshi's original research, and subsequent work by Li[102,103] demonstrated that cations derived from **1**, 10-bipyridine bound to P[5]A. Ogoshi prepared a water-soluble P[5]A, the ammonium salt of acid **22** formed by cleaving ethyl ester **21**, which led the way to binding analytes in aqueous solution.[69] A stable 1:1 host–guest complex was formed when water-soluble P[5]A reacts with cationic viologen in aqueous media (Figure 13). The water-soluble P[5]A formed an inclusion complex

with viologen in aqueous solution. The conformational freedom of the cavity decreased due to the complexation with viologen.[69] Despite the relatively slow progress in the development of synthetic and complexation protocols, other avenues of research suggest possible targets for inclusion within pillar[*n*]arenes.

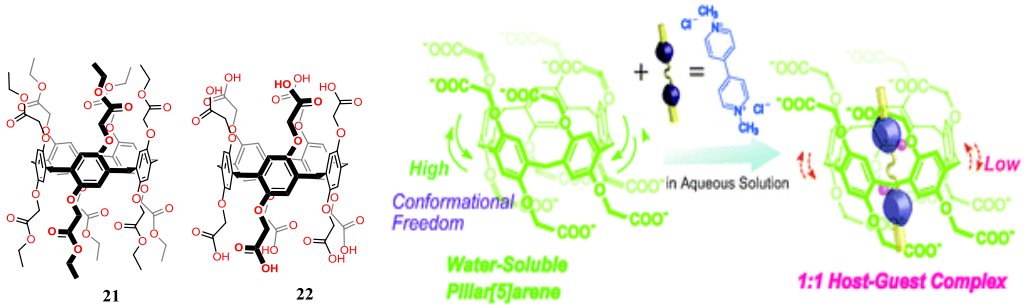

Figure 13. Molecular structure of water-soluble pillarene **22** with ammonium salt of acid. A stable 1:1 host–guest complex forms when water-soluble P[5]A (green) reacts with cationic viologen (blue).[69] (Reproduced with permission from The Royal Society of Chemistry)

Lao and Yu published a DFT computational study of the pillar[n]quinones (n = 3 to 7), first synthesised by Cao and Meier,[81] which indicated that pillar[5]quinone should have a high affinity for Cl^- and Br^-.[104] While such a theoretical approach was interesting, the reactivities of the pillar[n]quinones preclude their use as sensor components. Nevertheless, computer models have had some success in explaining experimental data, if not in actually predicting stable complexes.[86, 105-107]

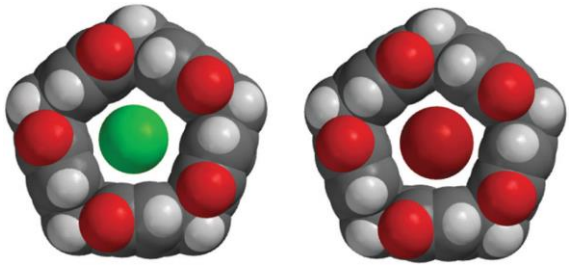

Figure 14. Computer models of pillar[5]quinone inclusion complexes of Cl^- (green) and Br^- (red).[104]

Initial forays into potential pillar[*n*]arene-based sensors can be seen in the work of Huang on a fluoride-complexing derivative **20**, which exhibited substantial fluorescence quenching of the emission peak at 381 nm.[108] The P[5]A was prepared by a Huisgen reaction from the asymmetric propargyl derivative and naphthyl azide which introduced five triazole linkers (Figure 14). Of the four conformers that were formed, fluorescent responses were only determined for the *cone* conformer and,

while the response to F^-, Cl^-, Br^-, I^-, NO_3^-, $F_3CCO_2^-$, $H_3CCO_2^-$ and ClO_4^- were all assessed, only F^- showed any quenching effect. Fluoride was found to have almost no effect on the monomers from which P[5]A was formed, indicating that the pentameric cavity was an essential aspect of the recognition site.

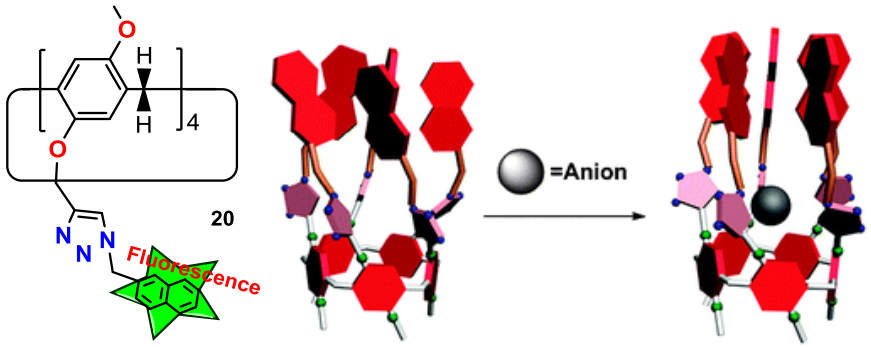

Figure 15. Molecular structure of naphthyl azide pillarene **20**. A cartoon representation shows the unique non-symmetric P[5]A-based anion receptor with high affinity and selectivity for the fluoride anion.[108] (Reproduced with permission from The Royal Society of Chemistry)

Huang also demonstrated that the larger cavity of the P[6]As had the potential to recognise small molecules.[96] 1,4-Dipropoxypillar[6]arene, **31**, was shown to bind a quaternarised azobenzene guest molecule but only as the *trans* isomer which allowed binding to be controlled through the guest's photoresponse to an external stimulus (Figure 16). Although not the focus of the paper, this quality suggests the possibility of a sensor which could detect one isomer over another.

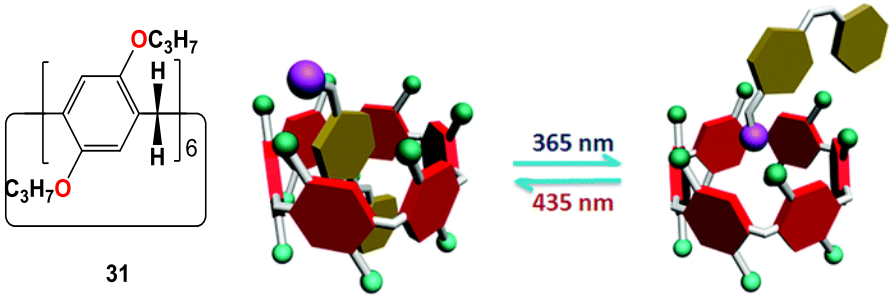

Figure 16. The interconversion between irregular P[6]A aggregates and vesicle-like aggregates is reversibly photocontrolled by irradiation with UV and visible light.[96] (Reproduced with permission from the American Chemical Society)

X-Ray crystallography has been a valuable tool to determine the nature of guest inclusion within pillar[*n*]arenes. It also allows experimentalists to prove that perturbations in signals, such as NMR shifts and intensity changes in UV–vis or fluorescence absorbance peaks, correlate with the guest's position within the

macrocycle. An excellent example of this is the structure of paraquat within a P[5]A with methoxyethylene substituents, (Figure 17).[109] The structure proves that the guest is indeed held entirely within the P[5]A and, moreover, that it is held in place by a multitude of complementary hydrogen-bonds.

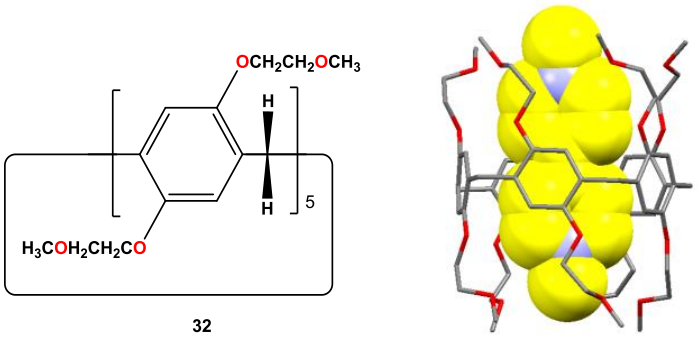

Figure 17. Mono(ethylene oxide) substituted P[5]A host-guest complexation showing the 1:1 complex between P[5]A **32** (in red) and paraquat (in yellow).[109] (Reproduced with permission from the American Chemical Society)

Inclusion of alkyldiamines within a copillar[5]arene in which two methyl groups are replaced by acetates reveals a similarly stabilising hydrogen-bond network (Figure 18).[110] Information of this nature is essential if substrate-specific pillar[*n*]arene derivatives are to be synthesised. In addition to using the novel receptor sites that pillar[*n*]arenes provide, it is sometimes necessary to consider more classical binding motifs for certain guests.[110]

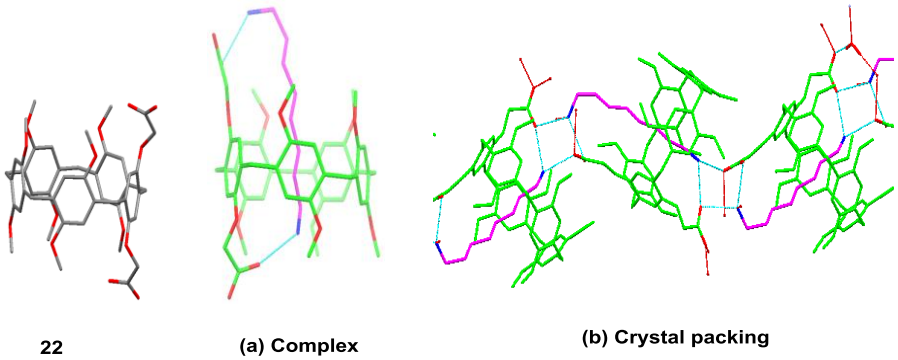

Figure 18. X-ray structure demonstrates host-guest complexation between difunctional P[5]A (host) and alkyldiamine (guest) molecules. (a) H-bond formation between amine and acid functional groups and (b) crystal packing.[110] (Reproduced with permission from the American Chemical Society)

This is particularly important when inorganic species are to be targeted. Fang and Yuan introduced diphenylphosphine oxide termini into a P[5]A, **33**, and demonstrated extraction of thorium(IV) and uranium(VI) over the lanthanide(III) cations while the acyclic, monomeric analogue was ineffectual (Figure 19).

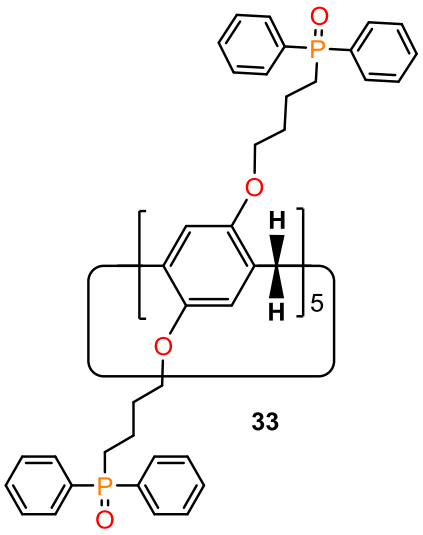

Figure 19. Representation of P[5]A **33** with diphenylphosphine oxide termini.

One of the more exciting aspects of pillar[*n*]arene chemistry is their ability, in water-soluble ionic forms, to act as the capping agents in gold nanoparticle[100,111,112] and quantum dot synthesis. In 2012 Huang showed that cationic P[5]As with *N*-methylimidazolium termini, **29**, were able to facilitate the formation of spherical gold nanoparticles (AuNPs) (Figure 20).[82]

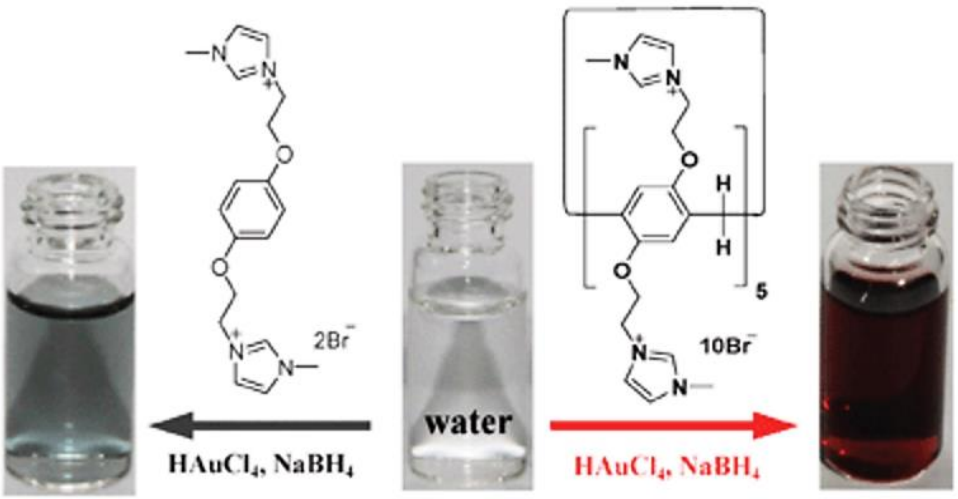

Figure 20. AuNPs formation by P[5]A **29** with N-methylimidazolium termini; the monomeric analogue was ineffective under the same conditions.[82] (Reproduced with permission from The Royal Society of Chemistry)

When added to an aqueous solution of $HAuCl_3$, followed by the addition of $NaBH_4$, the P[5]As formed a wine red solution containing AuNPs that were 1.88 ± 0.58 nm in diameter. As with other applications of P[5]As, the monomeric analogue was ineffective and formed a purple solution under the same conditions. The appearance of a blue/purple colour in AuNP synthesis is generally indicative of particles over 100 nm in diameter being formed. Particles of this size are of little practical use as they usually precipitate from solution spontaneously and so cannot be used to respond to analytes due to the likelihood of false positive results.

The same group later showed that asymmetric amphiphilic P[5]A **34** generated composites with AuNPs that formed microtubes in water. Although the object of the work was to develop green catalysts, the methodology does illustrate another way in which P[5]A-AuNP interactions can be formed (Figure 21).[111]

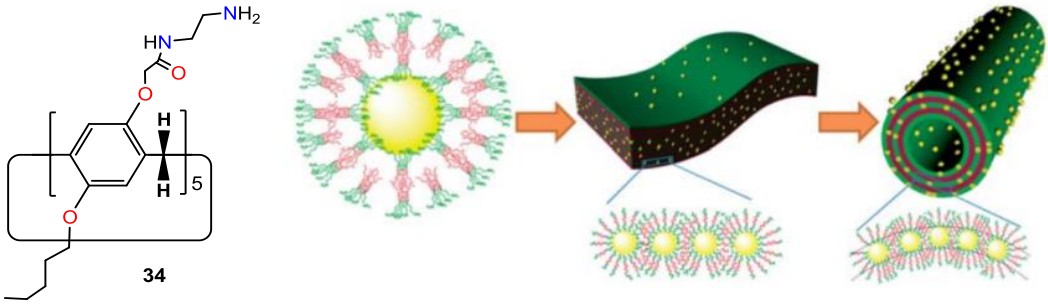

Figure 21. Water soluble AuNPs formed by self-assembled composite microtubes (SCMTs) in water. Molecular structure of symmetric amphiphilic P[5]A.[26, 97] Weiss and Yang employed **22**, by analogy to the more conventional citric acid capping groups, in their synthesis of AuNPs with diameters of 3.1 ± 0.5 nm.[111] (Reproduced with permission from The Royal Society of Chemistry)

Yang used **22** to displace and replace 3-mercaptopropionic acid from CdTe quantum dots.[113] Upon addition of a butyl bridged bis(paraquat) the P[5]A-modified quantum dots precipitated due to analyte-induced aggregation (Figure 22).

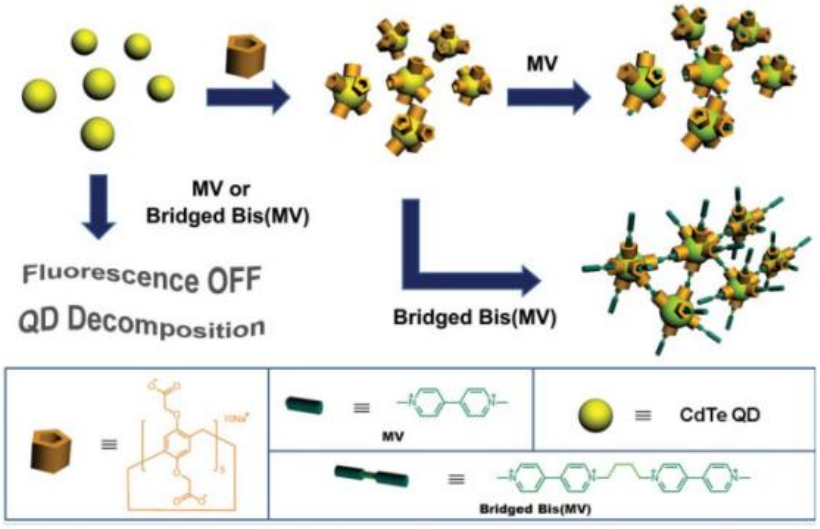

Figure 22. Schematic represents synthesis of P[5]A@QDs. Host–guest interactions of P[5]As and viologens in aqueous solution is shown.[113] (Reproduced with permission from The Royal Society of Chemistry)

Yang and co-workers reported AuNPs stabilized by P[5]A with 10 carboxylate moieties **22** were synthesised by reducing $HAuCl_4$ with $NaBH_4$ in the presence of the **22** shown in Figure 23.[112]

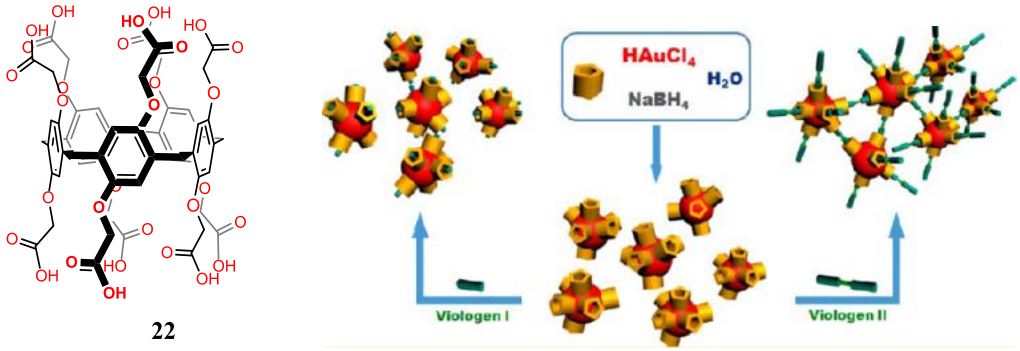

22

Figure 23. The schematic represents synthesis of acid functionalized P[5]A-AuNPs with citric acid capping groups.[112] (Reproduced with permission from American Chemical Society)

Xue demonstrated that **22** could also stabilise silver nanoparticles (AgNPs).[114] In this case the AgNPs were larger than their gold analogues, with diameters of 18.7 ± 2.18 nm, however they aggregated in a similar manner when treated with linear diamines (Figure 24).[114]

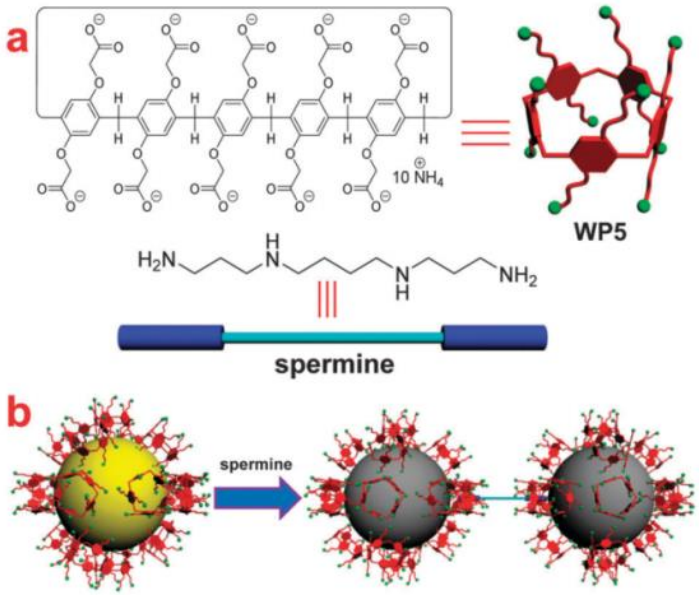

Figure 24. Chemical structures and model representation of water soluble P[5]A **22** and spermine.[114] (Reproduced permission from The Royal Society of Chemistry)

AgNPs can also be stabilised by the P[6]A analogue of Huang's *N*-methylimidazolium P[6]A derivative, **29**.[115] Again, the AgNPs formed are of a larger size than AuNPs formed under similar circumstances, at 13.6 ± 2.18 nm (Figure 25).

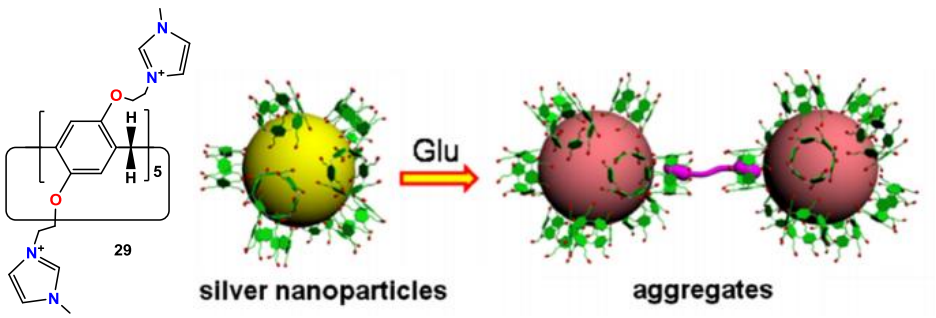

Figure 25. Molecular structure of an *N*-methylimidazolium P[6]A derivative and **29**-AgNPs aggregation with spermine.[115] (Reproduced with permission from Elsevier)

1.8.6 Solution-based binding behaviour of biogenic amines with pillar[5]arene

The unique molecular recognition properties of the pillar[*n*]arenes, and the P[5]As in particular, are indicative of the potential that these macrocycles have to act as substrate-specific receptors. To date sensor applications based on these properties have been limited, as would be expected for a class of compounds that is still in its infancy, but they show significant promise.

In 2010 Stoddart[73] was the first to show that the cavity within P[5]As could be used as a receptor for small molecules and that, furthermore, substrate binding could be signalled through the incorporation of a pyrene substituent.[73] The underlying principle behind this approach was that the recognition site should be altered as little as possible from that of **1** to ensure that the steric and electrostatic properties which made the macrocycle such a good receptor for linear amines was perturbed as little as possible. The starting compound was a copillar[4+1]arene derivative in which one of the methyl groups had been replaced with a bromoethyl group. Using click chemistry, a methoxymethylpyrene substituent was attached to *via* a triazole linker. Substrate binding by **18** (Figure 26) was determined in 1:1 H_3CN:H_2O by observing the intensity of fluorescence emission at 395 nm following excitation at 355 nm. Binding was assumed to involve a 1:1 substrate:sensor stoichiometry, based on Job's plot data, and resulted in quenching of the 395 nm signal through photoinduced electron transfer. The fluorescence quenching studies of alkanediamines containing C_3 to C_8 linkers gave association constants in the range of 10^4 M^{-1}.

From this response, the association constants for a range of alkylamines and alkyldiamines were calculated. No response was observed following the addition of 1,6-hexanediol which highlights the importance of the more extensive hydrogen-bonding networks available to amines.

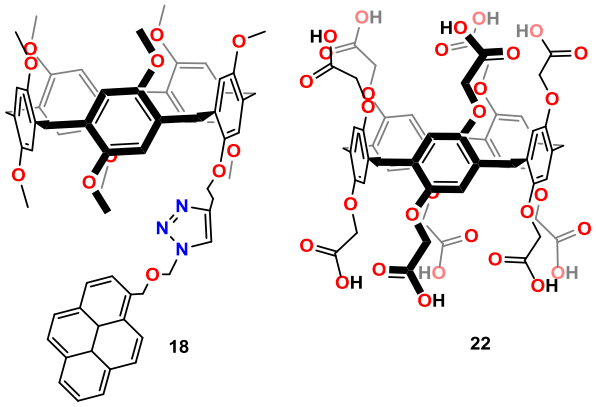

Figure 26. Copillar[5]arene incorporating a pyrene fluorophore **18** and carboxylato-P[5]A **22**.

Table 1. Association constants for P[5]A-amine complexes.[73,110]

Association constant, *Ka* (M^{-1})		
Amines	**(18) (H_3CN/H_2O, 1:1)**	**(22) ($CHCl_3/H_3COH$, 1:1)**
n-Hexylamine	$2.90 \pm 0.30 \times 10^4$	-
n-Octylamine	$1.60 \pm 0.16 \times 10^4$	-
1,3-Diaminopropane	$1.00 \pm 0.20 \times 10^4$	-
1,4-Diaminobutane (PUT)	$1.63 \pm 0.14 \times 10^4$	-
1,5-Diaminopentane	$2.12 \pm 0.10 \times 10^4$	$2.84 \pm 0.23 \times 10^5$
1,6-Diaminohexane	$1.15 \pm 0.14 \times 10^4$	$2.39 \pm 0.24 \times 10^5$
1,7-Diaminoheptane	$1.91 \pm 0.10 \times 10^4$	$3.13 \pm 0.21 \times 10^5$
1,8-Diaminooctane	$3.60 \pm 0.26 \times 10^4$	$2.89 \pm 0.21 \times 10^5$
1,9-Diaminononane	-	$3.45 \pm 0.23 \times 10^5$
1,10-Diaminodecane	-	$3.06 \pm 0.23 \times 10^5$
Spermine (SPR)	$1.02 \pm 0.90 \times 10^4$	-
Spermidine (SPD)	$1.86 \pm 0.80 \times 10^4$	-

As expected alkydiamines were bound more strongly than their monoamine analogues, as shown in Table 1, but relationship between association constants and length of carbon backbone was not straightforward.[35] For example, not only was 1,5-diaminopentane bound better than 1,3-diaminopropane and 1,4-diaminobutane, but also better than 1,6-diaminohexane and 1,7-diaminoheptane. Polyamines spermine and spermidine also bound relatively poorly although there was considerable uncertainty in these determintations. Interestingly, a similar pattern was observed for Yu's system who have synthesised a novel difuntionalised P[5]A with two carboxylic acids in one unit **22** and studied host-guest complexation of **22** with alkanediamnie.[110] The association constant of this complex was in the vicinity of 10^5 M^{-1}, much greater than the **1** and 1,5-pentanediamine complexes determined using fluorescence quenching experiments. The reason for the high constants of these host-guest complexes were due to the co-operative electrostatic interactions between the carboxylate anions of **22** and ammonium cations of the guests, and various CH/π interactions between alkyl chains of alkanediamines.[2] Diamines of the correct length to bind to both openings in the macrocycle will be able to maximise stability through hydrogen-bond formation and, as a corollary to this, diamines

would be expected to bind more strongly than their monoamine analogues. In the case of the polyamines, the act of threading through the P[5]A will initially involve hydrogen-bond formation of primary and secondary amines. As the substrate is drawn further into the cavity it will be necessary to break hydrogen-bonds associated with both amines. It is possible that polyamines cannot overcome this barrier and, consequently, that only one end of each molecule binds. In the case of spermine both termini are derived from 1,3-diaminopropane and a similar association constant to 1,3-diaminopropane is observed. For spermidine, containing both propylamine and butylamine termini, an association constant similar to that of 1,4-butylamine is found. Other factors contributing the ease with which the substrates bind will include the conformations they adopt in the solvent mixture used and any intramolecular hydrogen-bonding that exists in those conformations. Although these influences were not investigated at the time, Stoddart's contribution has been extremely valuable and helped to promote the use of P[5]As as chemical sensors.[55]

1.8.7 Solution binding behaviour of alkali metal ions uisng pillar[5]arene

In 2014 the Stoikov group[116] investigated the binding properties of P[5]As containing acid (**22**), morpholide (**45**) and pyrrolidide (**46**) towards alkali metal cations (Li^+, Na^+, K^+, and Cs^+) (Figure 27).

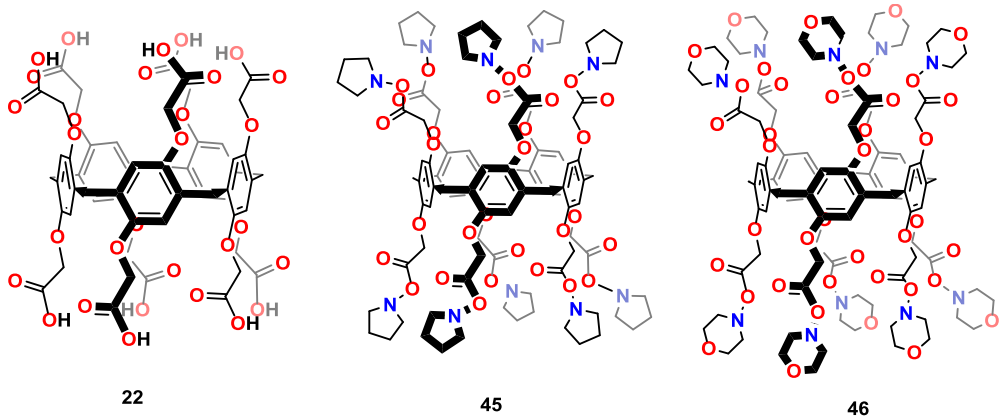

Figure 27. Synthesis of a copillar[5]arene incorporating a pyrene fluorophore **18** and carboxylato-P[5]A **22**.

The association constants of the P[5]As with alkali metal nitrate salts in a 1:1 stoichiometry were determined to be 10^2-10^3 M^{-1} by UV spectroscopy. The interaction between the substrate and guest metal ions were examined by UV-

spectroscopy which have shown significant change in the absorbance spectrum upon formation of the substrate-guest complex. Further, association constants and the stoichiometry of complexes with **45** and **46** have been determine to quantify molecular recognition of the nitrates of these complexes as shown in Table 2. Job's plot have allowed further information of the same complexes' binding stoichiometry at and have proved that Li^+ complexation was the most effective relative to other metal ions as shown in Table 2. Their experiments have also shown that K^+ is bound more strongly than Na^+.

Table 2. Association constants ($logK_{ass}$) for the complexation of P[5]As (**22**, **45** and **46**) with metal ions Li^+, Na^+, K^+, Cs^+) in methanol at 298 K.[116]

Host	**($logK_{ass}$)**			
	Li^+	**Na^+**	**K^+**	**Cs^+**
22	3.33 ± 0.11	2.67 ± 0.18	2.71 ± 0.13	2.52 ± 0.16
45	3.53 ± 0.11	2.19 ± 0.16	2.78 ± 0.12	2.31 ± 0.14
46	3.60 ± 0.7	2.15 ± 0.02	2.46 ± 0.17	2.45 ± 0.12

1.9 Selectivity in host-guest chemistry

Selectivity is one of the important processes in biological receptors and is a key factor in host-guest complexation and synthetic supramolecular chemistry. The extent of selectivity for a specific species requires high sensitivity of the host for a specific guest compound.[117] The ability of a host to form a complex with a specific guest among many competing species is dependent on the selectivity at the point of complexation. The extent of the selectivity can be determined by measuring the ratio of the binding constants (*K*) for the complexes which form. The equilibrium between the host (H) and the guest (G) in a complex (HG) is given in equation 1.

$$\mathbf{[H] + [G] = [HG]} \qquad \mathbf{(1)}$$

When $\Delta G^0 < 0$ a complex is formed spontaneously. ΔG^0 is related to the association (or binding) constant *K* by equation 2.[118]

$$\mathbf{\Delta G^0 = -RT \ln K} \qquad \mathbf{(2)}$$

The term *K* is dependent on the equilibrium activities of the chemical species in the complexation process. The activities are often switched by concentrations for convenience to return more concrete expressions.[118] When a system is in equilibrium, *K* is equal to the concentration of the host–guest complex divided by the product of the concentrations of the distinct host and guest molecules as shown in equation 3.

$$\boldsymbol{K_{\mathrm{a}} = \frac{[\mathrm{HG}]_{\mathrm{eq}}}{[\mathrm{H}]_{\mathrm{eq}}\,[\mathrm{G}]_{\mathrm{eq}}}} \qquad \textbf{(3)}$$

Theoretically, selectivity in supramolecular host–guest complexes can be defined as a difference in binding free energies for structurally related guests, as a function of total binding free energy shows that for certain types of intermolecular interactions a correlation between selectivity and affinity may be observed. However, this correlation is not relevant if the selectivity is due to additional interactions at the secondary binding sites and is seen in complexes with anisotropic guest molecules.[117]

The selectivity can be defined as the ratio of the binding constant for one guest over another in thermodynamic terms as shown in equation 4:

$$\textbf{Selectivity} = \frac{K_{\mathrm{Guest1}}}{K_{\mathrm{Guest2}}} \qquad \textbf{(4)}$$

The selectivity between a host and guests can be influenced by numerous factors such as preorganisation and complementarity.[50]

The solution based complexation of redox active receptors can be explored using electrochemical methods, specifically cyclic voltammetry (CV). In our work, the pillar[5]arene sensors for alkali metals and biogenic amines were redox-active and were performed in solution. Thus the voltammetric analysis can be correlated with electrochemical detection. In the CV method, complexation between the host and guest, where the host is redox-active and the guest is a charged or neutral species, leads to a change in the electrode potential upon complex formation which can be

detected electrochemically. Selectivity of the guest and magnitude of change in the electrode potential (equation 5) in response to the formation of the complex are two important factors in the designing of such supramolecular sensors. Complex formation will lead to changes in binding constants following oxidation or reduction, which in turn results in the redox response.[119]

$$\boldsymbol{K^{+}/K = \exp[-nF\left(E_{[H-G]} - E_{H}\right)/RT]} \quad \textbf{(5)}$$

Here E_H is the host electrode potential, $E_{[H\text{-}G]}$ is the host-guest electrode potential, K^+ is the binding constant of oxidized receptor, K is the binding constant of reduced receptor, F is Faraday's constant, R the universal gas constant, T the temperature in kelvin and n the number of electrons transferred.

The electrode potentials of E_H and $E_{[H\text{-}G]}$ are generally estimated from average of the cathodic and anodic peak potentials from a cyclic voltammogram. Consequently the comparative affinities of the oxidised and reduced host and guest can be determined by CV using a titration method. The half potential ($E_{1/2}$) of a host can be given by equation 6 in which the anionic guest forms a complex with the host in both the oxidised and reduced forms. In this process, the $E_{1/2}$ is obtained by titrating guest with host sample and observing the CV after each addition.[120]

$$\mathbf{E_{1/2}(H) = E_{1/2} + \frac{RT}{2nF} \ln\left[\frac{1+K_{Ox}[G]}{1+K_{Red}[G]}\right]} \quad \textbf{(6)}$$

An alternate method of analysing $E_{1/2}$ which is rather simpler is shown in equation 7. In this method, $E_{1/2}$ is recorded before and after a large proportion of the guest is added to the host solution. In host-guest complexation with strong binding this can be corroborated by NMR where separate peaks for the bound and unbound components can be clearly seen.[120]

$$\mathbf{E_{1/2}\,(H) = E_{1/2}(HG) + \frac{RT}{2nF} \ln\left[\frac{K_{Ox}}{K_{Red}}\right]} \quad \textbf{(7)}$$

Electrochemical methods in general, and CV specifically, are discussed in more detail in section 1.12, below.

As will be seen, our results using electrochemical methods to detect alkali metals and biogenic amine are in line with those of other groups using complementary techniques. Stoddert[73] and Yu's[110] solution based studies by NMR and fluorescent detection. Stoddart and co-workers[73] investigated the host-guest properties of pillar[5]arene with various alkyl amines and confirmed that alkyldiamines were more selective than monoamines, with an apparent dependence on carbon chain length between amine groups, whereas Yu and co-workers study on polyamines have shown that SPR and SPD bound relatively poorly although there was considerable uncertainty in these determinations. Later in 2014, the Stoikov group carried similar studies on alkali metals analysis in solution using UV spectroscopy.[116] Their studies have shown that Na^+ and K^+ were selectively bound to the cavity of functionalised pillar[5]arenes **22**, **45** and **46** and are in agreement with our previously published results.[107] Based on our results and those of others the factors that can influence the selectivity of the pillar[5]arene in electrochemical solution based techniques can be summarised as the size of cavity, its geometry, the charge of the guest as well as probable contributions from mass transfer and steric effects.

1.10 Alkali metal sensors

The first example of an ISE incorporating a macrocycle, a Na^+-responsive calixarene system, was reported by Diamond.[121,122] Since then, macrocycles have been incorporated in polymeric membranes and are widely used as ISE chemical sensors.

Glass pH electrodes have been widely used for almost 60 years.[123,124] Although glass electrodes are widely used there are disadvantages in the areas of food processing and *in vivo* measurements where glass electrodes can easily break. Furthermore, glass electrodes have a relatively large response time because of its high resistivity causing less attraction in the process.[125-127] Polymer-based sensors have several advantages over glass electrodes such as they are disposable, cheap, function over a longer period of time where regular monitoring is required, require less care and do not require sterilisation. Below are some chemical modifiers which have been used to make pH electrodes with PVC membranes (Figure 28).[128-130]

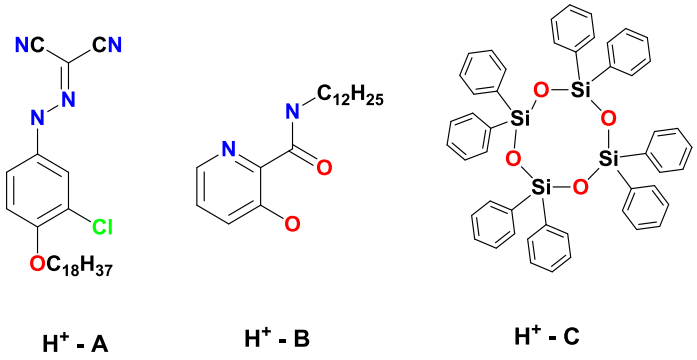

Figure 28. H^+ selective ionophores.

Lipophilic crown ionophores (Li^+-**D** and Li^+-**E**) containing decalino subunits have been reported to be one of the most selectivity to Li^+, with Li^+-**E** the only Li^+ ionophore to show a Li^+/Na^+ selectivity ratio larger than 1000.[131]

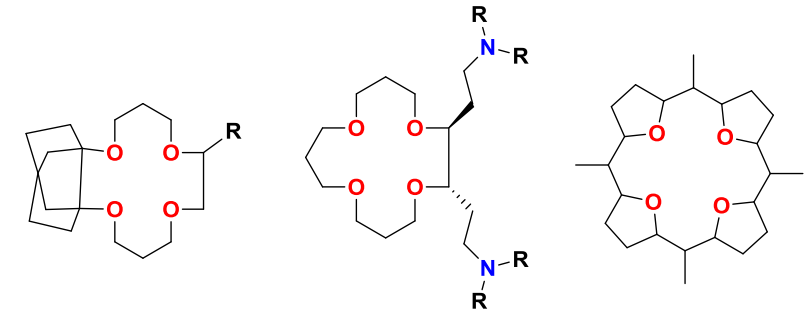

Figure 29. Li^+ selective ionophores.

Dibutyl and diisobutyl diamides (Li^+-**F** and Li^+-**G**), whose bulkiness and ability to provide additional coordination sites seem both to be important, appear to be better Li^+ sensors due to the relatively rigid structure of cyclic polyethers containing furan or tetrahydrofuran units.[132] The sensitivity of the Li^+ can be improved when the ionophore has an ability to contribute supplementary coordination sites as in Li^+-**H** (Figure 29). [133,134]

Although ISE selectivity for numerous metal ions has reported the main focus has always been on Li^+, Na^+ and K^+ for their physiological relevance. The automated method to measure the Na^+ and K^+ potentiometrically was attained in 1972 and has since seen use in clinical measurements.[135,34]

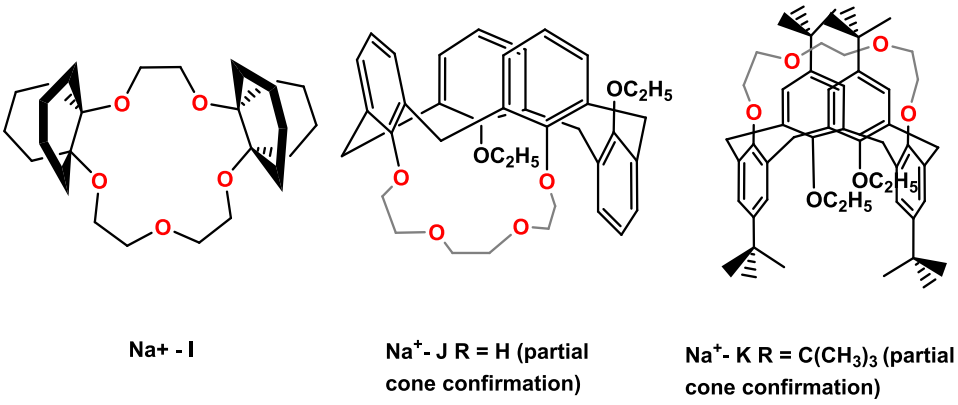

Figure 30. Na^+ selective ionophores.

Two of the highly selective Na^+ ISEs employ bridged calix[4]arenes and 16-crown-5 ether ionophores (Figure 30). These ionophores allow steric hindrance of the molecules thus allows high selectivity.[136,137] Nonetheless, for the most common commercial purpose ISEs containing di-, triamide and bis-crown ether elementary ionophores are most commonly used in clinical applications.

The discovery of high K^+ selectivity of valinomycin (Figure 31) during early ISE research boosted ISE chemistry and, to date, it is the most popular ionophores for this analyte. In clinical applications, the most widely used K^+ sensors incorporate bis(crown ether)s. These ISEs offer high selectivity and are preferred after valinomycin because of the ionophore's lipophilic nature resulting in better lifetimes during clinical use.

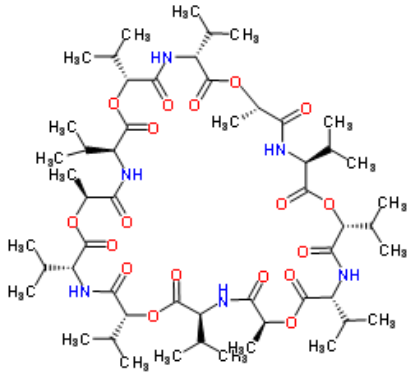

Figure 31. Valinomycin used in K^+ ISE.

More recent improvements include a K^+ ISE with comparatively greater selectivity than the bis-crown ethers based on a calix[4]arene with a crown ether bridge.[36]

Calix[6]arene hexaesters Cs^+-**L** and Cs^+-**M** are the best known Cs^+ ISEs showing high selectivity to Cs^+.[138] Within the bridged calix[4]arenes ionophores Cs^+-**N**, the compounds with ether functional groups have been reported to show good selectivity to Cs^+.

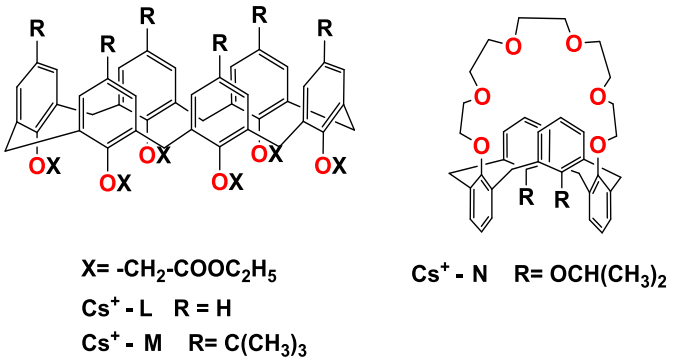

Figure 32. Cs^+ selective ionophores.

Valinomycin is also used in Rb^+ ISEs. Although it is ideal for K^+, it also has good selectivity for Rb^+ over K^+.[139-141] The preference of valinomycin's selectivity to Rb^+ over K^+ can be explained by the fact that the valinomycin-Rb^+ complex is more stable that the K^+-complex.[142] Thiourea groups (Figure 33) containing cryptand ionophores have also been reported to show high selectivity for Rb^+ over Cs^+.[143]

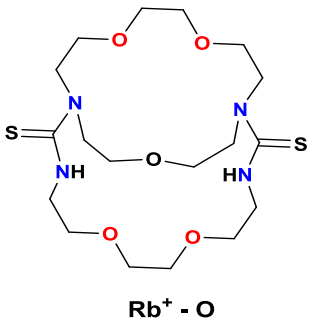

Figure 33. Rb^+ selective ionophores.

Calix[n]arenes have been used widely in the fabrication of ISE's to detect primary organic ammonium ions and alkail metals.[144,145] In general, alkyl ammonium ions form inclusion complexes with calx[6]arene because of its hydrophobic cavity. Hexylammonium ions have shown excellent sensing propertis with calix[6]arene-hexaacetic acid hexaethyl ester,[146] this inophore has been commercially available[147] and under the name 'amine ionophore I'.[148] Ethyl ammonim ions also bind to *p*-tertbutyl calix[6]arene hexaacetic acid hexaethyl ester ISEs.[149]

The larger hydrophobic cavities of calix[8]arene derivatives have been used in the detection of phenylethylamine in the presence of various metals cations. Shvendene reported that the *p-1*-adamantylcalix[8]arene derivative has shown response to phenylalanine methyl ester in addition to 2-phenylethylamine.[150] Thus, cavity of calix[8]arene is larger to encapsulate the bulky organics than the linear molecules. *p-tert*-Butylcalix[8]arene hexaethyl ester shown better selectivity on biologically active norephedrine when compared to calix[8]arene hexaacetic acid hexaethyl ester.[146]

1.11 Biogenic amines (BAs)

The term biogenic amine (BA) encompasses naturally occurring, biologically active small molecules incorporating the amine group.[151] Many are catecholamine derivatives, such as the neurotransmitters dopamine and adrenaline, but two groups are also associated with bacterial enzymatic degradation of proteins by amino acid decarboxylases (Figure 34).[151] The predominant linear BAs (cadaverine, spermine, putresceine and spermidine) are not particularly toxic in themselves (acute oral toxicities: putresceine 2000 $mgkg^{-1}$, spermine and spermidine 600 $mgkg^{-1}$ body weight in wistar rats)[152] but are usually associated with the presence of histamine which has greater health implications. The FDA considers fish containing less than 10 $mgkg^{-1}$ histamine to be of good quality, more than 50 $mgkg^{-1}$ indicates decomposition (the 'caution level'), and over 500 $mgkg^{-1}$ is toxic.[151] In the EU the caution level is between 100 and 200 $mgkg^{-1}$. Histamine toxicity stimulates the release of adrenaline and noradrenaline leading to symptoms including: skin rashes and inflammation, nausea, vomiting, diarrhoea, abdominal cramps, hypotension, headaches and migraine, and respiratory distress.[151] Chronic low level symptoms are also encountered as the well documented condition of histamine intolerance.[153]

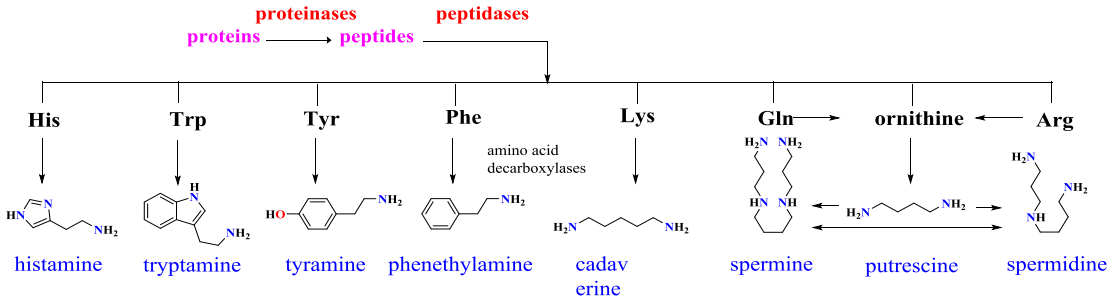

Figure 34. Biosynthesis of biogenic amines.[151]

1.11.1 BA levels in foodstuffs

In a typical study of its type, Park determined the BA content of a range of fish products by UPLC/MS/MS detection of the respective dansyl BA derivatives.[154] The mean values of BAs in different fish varied, as shown in Table 3.[155] Furthermore, numerous species and strains of bacteria produce amino acid decarboxylase enzymes, and generate BAs with specific profiles of BA production as shown in Table 4.[155]

Table 3. Biogenic amines in fish ($mgkg^{-1}$).[155]

Type	putrescine	cadaverine	spermidine	spermine	Histamine
salmon	1.5	7.3	2.2	1.0	2.0
tuna	0.5	0.4	1.7	1.6	0.1
anchovy	20.0	250.5	7.6	2.2	41.1

Table 4. Bacterial biogenic amine profiles ($mgkg^{-1}$).[155]

Type	putrescine	cadaverine	spermidine	Spermine	Histamine
E. coli	32.7	27.0	0.4	0.0	0.1
E.furgusonii	14.0	16.6	0.2	0.0	0.1
M. morganii	16.0	0.2	0.0	0.0	6.8

1.11.2 The need for rapid detection

The detection of bacteria possessing amino acid decarboxylase activity is necessary to estimate the risk of BAs in food and to prevent BA accumulation in food products. The central problem for the food industry is the lack of a fast, reliable test for these compounds. Current methods of determining BAs are almost exclusively chromatographic, requiring trained staff in dedicated facilities, employing protocols such as anion-exchange chromatography with electrochemical detection or HPLC with fluorescence detection.

1.12 Electrochemistry

Electrochemistry can be defined as a study of chemical reactions that can produce electric power or the method where electricity is used to affect chemical processes or systems. In terms of chemistry, electrochemistry can be defined as the branch of chemistry which deals with the study of chemical reactions in presence of aqueous

solution, at the interface between a conducting electrode and the conducting electrolyte solution. In the reaction process, there will a process of electron transfer between the electrode and electrochemical species in the aqueous solution. Electrochemical studies are applicable across a broad range of science including: surface science, biochemistry, analytical techniques, photochemistry, energy storage and nanotechnology.[156]

1.12.1 Cell potentials and electrochemical reactions

In simple terms, a chemical reaction is defined as the process where electron transfer occurs. In the same way, an electrochemical reaction[157,158] is where the transfer of charge is *via* an electron or ion. In a redox reaction, electrons transfers from one chemical species to another and results to change the oxidation state of the chemical compound or species. The redox reaction can take place *via* the utilisation of an external voltage or the usual chemical energy release. There are two processes in a redox reaction, they are oxidation and reduction. Oxidation is the process in which chemical species loses electrons, whereas in reduction it gains electrons. The redox reaction principle explained with Farad's law which states that the quantity of reacted species is directly proportional to the current passing through the cell.[159]

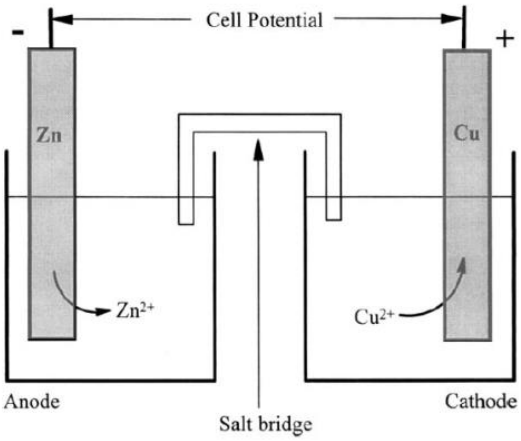

Figure 35. Components of a galvanic cell.[159] (Reproduced with permission from the Wiley publishers).

The following spontaneous reaction (equation 8) is achievable by immersing Zn(0) in a solution containing Cu(II) ions. Zn oxidation can be monitored along with Cu(II) reduction. The same reaction can be done by immersing a Zn strip in a solution of Zn(II) ions and a Cu strip in a solution of Cu(II) ions (Figure 35).

$$\mathbf{Zn_{(s)} + Cu^{2+}{}_{(aq)} \rightarrow Zn^{2+}{}_{(aq)} + Cu_{(s)}} \quad \textbf{(8)}$$

In order to initiate a reaction, pathways must be created for the electrons and ions to move between the sections where the Zn oxidation and Cu(II) reduction processes occur. This can be accomplished by setting up a salt bridge to build electrical association between the two solutions. The salt bridge allows movement of ions and electrons between the two solutions at the same time avoiding mixing. In the redox reaction, electrons move from the Zn electrode (negative) to Cu electrode (positive). The free energy ΔG^O of the overall chemical reaction can be calculates as below (equation 9).[159]

$$\boldsymbol{\Delta G^0 = -nFE^0_{cell}} \quad \textbf{(9)}$$

where, *n* is the total number of electrons transferred in the reaction,

F is the Faraday constant

E^0_{Cell} is the standard cell potential of the cell.

1.12.1.1 The mechanism at the electrode/solution interface

Interactions between solid and liquid electrolyte differ from interactions in a homogeneous liquid cell. The interactions in this case are proportional to the potential applied to the electrodes because of its impact on the charge. The interaction between surface of the electrode and the molecules in a solution will lead to an electrical double layer formation.[160] Charges are impaired on a surface due to the chances of complexion, adsorption or dissociation. The electrostatic shield allows the counterions to become attracted to the surface which results in the neutralising interface. The counterions have capacity to diffuse away and are retained in a dynamic balance through electrostatic interactions. The ionic concentration is directly proportional to its distance from the surface in the diffusion layer which leads to formation of two layers; one with a surface charge and the other with a shielding charge. This alignment of the layers with different charges is the basis of the electrical double layer.[158]

1.9.1.2 Structure of the double layer

The double layer is comprised of two planes; the inner Helmholtz Plane (IHP) and outer Helmholtz plane (OHP). Although ions exchange at the diffuse layer the total charge of the solid is offset by the large counterions at its surface (Figure 36).[158]

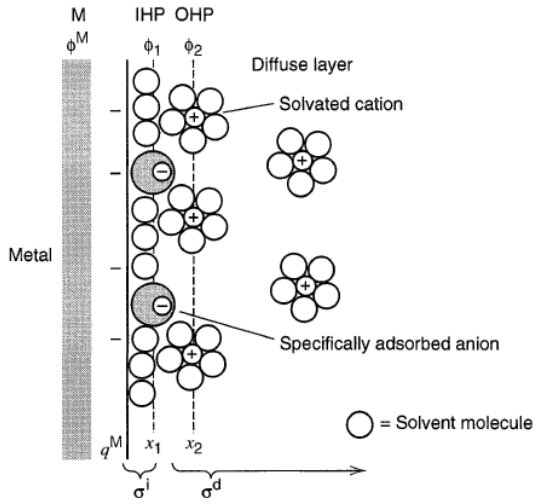

Figure 36. The structure of a double layer.[161]

The rate of the reaction is dependent on the slowest steps of the ions. This may be the mass transport, where the reactant reaches the surface of electrode or the electrode kinetics in which the transfer of electron occurs at the electrical double layer. When the reaction is mass transport-limited, the flux (*J*), where the reaction is held at the rate of reaction *v* and the reagent is imported to the surface from the bulk solution, is expressed as (equation 10):

$$\boldsymbol{J(x,t) = -\frac{i}{zFA}} \qquad \textbf{(10)}$$

where: *J(x,t)* is the flux of species (mol.cm^{-2}s^{-1}),

i is the current (A),

z is the number of electrons involved in the reaction,

F is the Faraday constant (96484.6 C.mol^{-1}) and

A is the electrode area (cm^2)

There are three forms of mass transport which can influence an electrolysis reaction: kinetic, diffusion, convection and migration

Diffusion – Diffusion occurs wherever there is a gradient of concentration in a solution in which, the entropic forces will operate to even the concentration distribution. Diffusion is the main key factor in the process of electrolysis because of which a gradient concentration in the solution interface is possible.

Convection- Natural convection is formed by a gradient of thermal or density factors and acts to incorporate solution in an indiscriminate fashion. Convection can be restrained by introducing simulated convection forces, such as rotating disc or stirrer.

Migration – It is an electrostatic effect. The interface of the electrodes will get charges when a potential is applied. This charged interface and any other similar chemical species near the interface will be get attracted or repelled from it by electrostatic forces. Expressing migration in an equation is very difficult because of ion solvation effects and interaction because of diffusion in the solution.

The rate of mass transport by taking in account of above three processes can be expressed by the Nernst-Planck equation:

$$\boldsymbol{J(x,t)} = -\boldsymbol{D}\frac{\boldsymbol{\partial c(x,t)}}{\boldsymbol{\partial x}} - \frac{\boldsymbol{zFDC\infty}}{\boldsymbol{RT}}\frac{\boldsymbol{\partial \theta(x,t)}}{\boldsymbol{\partial x}} + \boldsymbol{C(x,t)V(c,t)} \qquad \textbf{(11)}$$

where D is the diffusion coefficient ($m^2.s^{-1}$)

R is the ideal gas constant (8.314 $J.K^{-1}$)

C is the concentration of reagent ($mol.L^{-1}$)

V is the velocity of solution

$\frac{\partial \theta(x,t)}{\partial x}$ is the potential gradient in solution

$\frac{\partial C(x,t)}{\partial x}$ is the concentration gradient

Where all three processes are acting the Nernst-Plank equation is valid. To understand the electrochemistry without one of the process, a stable electrolyte is taken in the media and left without stirring so that, there will be no migration process and convection can be treated minimal when compared to the diffusion process. In

this simplest situation, depending on the concentration of reagent, the kinetics of the reaction can be expressed using Fick's law of diffusion[158] (equation 12):

$$\boldsymbol{J\,(x,t) = -D\frac{\partial c(x,t)}{\partial x}} \quad \textbf{(12)}$$

The current from an oxidation can be expressed as a function of the concentration gradient from equation 13:

$$\boldsymbol{i = -zFAD\frac{\partial c(x,t)}{\partial x}} \quad \textbf{(13)}$$

1.12.2 Instrumentation

1.12.2.1 Working electrodes

In an electrochemical system, the working electrode can be defined as the electrode on which the desired reaction takes place. The most commonly used working electrodes are made of a relatively inert metal such as silver, gold, platinum and mercury, or glassy carbon and its surface is inversely proportional to the current density. The geometry of this electrode varies and depends on the application purposes.

Gold electrodes have defined efficiency in the positive potential range because of the surface oxidation. These electrodes are mainly used in the modified electrodes preparation which contains surface structures called self-assembled monolayers (SAMs). The main advantage of gold electrodes is that they have wide cathodic potential range.

Platinum electrodes have excellent electrochemical inter property and can be easily modified into desired forms. The main advantage of platinum is that it is available in the form of wire, flat plate and tubes but has the disadvantage of being very expensive.

Carbon electrodes are excellent anodic potential systems and also enable scanning to more negative potentials when compared to gold and platinum. The most commonly used form is the carbon paste electrode (CPE) which is prepared by packing carbon

paste into an inert electrode body cavity. Glassy carbon electrodes are comparatively high cost, are not suitable in flow cells and are not easy to modify. Their advantages are that they offer a wide potential range and a low background current.

Mercury has classically been used as an electrode compound, usually as a spherical drop formed at the end of a glass capillary. The liquid metal is allowed to flow through a glass capillary. Mercury electrodes offer wide potential range in the cathodic direction, but are restricted in the anodic direction due to oxidation.

1.12.2.2 Reference electrodes

The electrode which has an unalterable electrode potential, and is insensitive to the composition of the analyte solution, is referred to as the reference electrode. When an outward potential is applied to the working electrode, the reference electrode's potential should not change. The most commonly used reference electrodes are the Ag|AgCl calomel electrode and the standard hydrogen electrode (SHE). Our studies are carried out using silver/silver chloride electrode. It consists of a silver wire coated with silver chloride immersed in a saturated potassium chloride solution.

1.12.2.3 Auxiliary electrodes

In the voltammetry studies with a two electrode system containing reference and working electrodes, the current always flows through the reference electrode so that a change in the potential is achieved. In a three electrode system containing reference, working and auxiliary electrodes, the current flows through working and auxiliary electrodes. In the aqueous and non-aqueous medium platinum electrodes are used, whereas in a molten salt medium carbon electrodes are used extensively. The main characteristics of an auxiliary electrode are that it should not dissolve in the medium and the product produced at its end should not react at the working electrode in the electrochemical cell. In the three electrode electrochemical cell set care should be taken of the current is not limited due to the electrodes area therefore, auxiliary electrodes area should be larger than the working electrodes.[158]

1.12.3 Electroanalytical techniques

The electrical properties of the analyte solutions of the electrochemical cell are analysed by a group of quantitative analytical techniques which are commonly

referred as electroanalytical techniques. The electrochemical properties of the analyte are highly sensitive therefore the analytical techniques should be capable of detecting these properties with exceptionally low detection range. These techniques also offer accuracy, precision and high linear dynamic limits. The main advantages of these techniques are they have wealth of characterisation intelligence and capacity to produce anomalous low detection limits characterising the electrochemically addressable systems.[158, 160-162]

These techniques offer a number significant benefits including:

- specificity
- selectivity proceeding from the choice of electrode material
- high sensitivity and low detection ranges
- achievability of furnishing results in real time
- economic cost

The electrochemical techniques are based on measuring the quantitative and qualitative properties of the compounds. Therefore they are two-dimensional concepts where the thermodynamic, kinetic control, mass transit process, rate of the reaction etc. are critical elements to be determined. The basic principles of the electrochemical techniques are to measure selectivity of the compounds. To measure these components it is necessary for the compound to be adsorbed onto the electrode or diffuse to the surface *via* a coupled reaction. One of the important conditions is that the electrical circuit should be proportionately conducting in the medium between the two electrodes. The electroanalytical techniques are typically split into three types: potentiometry, coulometry and voltammetry.

1.12.3.1 Potentiometry

This is based on the principle of measuring the potential of the electrochemical cell without drawing significant current. Analytical potentiometry is the process which comprises a reduction in the analyte compound's concentration and/or movement from the difference in the potential measured between reference and selective electrodes. Silver/silver chloride reference electrodes are the most commonly used.

1.12.3.1.1 Potentiometric response of ion-selective electrodes.

The basic arrangement to measure potentiometry is shown in Figure 37. A high input impedance voltmeter is used to measure the difference in potential between the two electrodes and it swamps the cell resistance (> $10^{12}\,\Omega$).

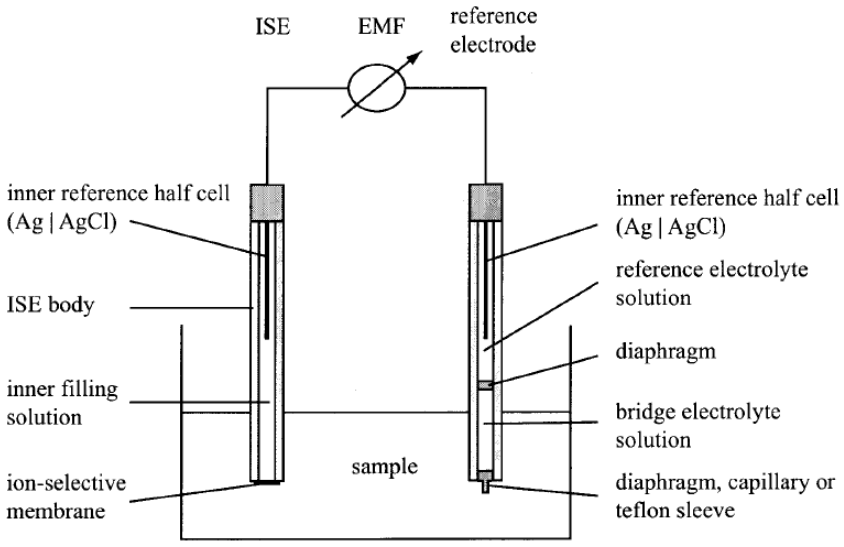

Figure 37. A typical ISE potentiometry cell.

The cell potential can be represented as:

$$E_{cell} = E_{ise} - E_{ref}$$

where E_{cell} is the overall cell potential

E_{ise} is the ion-selective electrode potential

E_{ref} is the reference electrode potential.

Practically, the cell emf consists of a local potential discrepancy proceeding at the solid-solid, solid-liquid or liquid-liquid interfaces. The relation between the electrode potential of a galvanic cell and ion activity can be given by Nernst equation (equation 14)[156,163]

$$\boldsymbol{E_{ise} = E^0 + 2.303\frac{RT}{z_i F} log\ a_i} \qquad \textbf{(14)}$$

where, $\boldsymbol{i}$ is the ion of interest, $\boldsymbol{z_i}$ is its charge and $\boldsymbol{a_i}$ its activity. $\boldsymbol{R}$ is the gas constant, $\boldsymbol{T}$ is the absolute temperature and $\boldsymbol{F}$ is Faraday's constant. The standard electrode potential is $\boldsymbol{E°}$ and will be a constant for the experiment. To the half reactions, standard electrode potentials are determined with reference to the standard hydrogen electrode (E° = 0 V at 298 K and 1 atm pressure). From the Nernst equation, when the constants are multiplied, it will be evident that a change in one unit in the logarithmic term changes the value of the potential by $59.16/z_i$ mV and this type of system behaviour will respond in a Nernstian fashion to changes in analyte activity. One of the important characteristics of ISE is selectivity. It is key property because it determines sensitivity when a sample for analysis contains interfering ions (*J*) and primary ions (*i*). The selectivity coefficient in this case can be determined from the linear part of the response functions of the *J* and *i*. The impact of *J* on the electrode potential is achieved by the semi-empirical extension of the Nernst equation known as the Nikolskii-Eisenmann equation as shown below (equation 15).

$$\boldsymbol{E_M = const + S \ln\left[a_i + \Sigma K_{ij}^{pot} a_j^{z_i/z_j}\right]} \quad \textbf{(15)}$$

where j = interferents,
i = primary ion,
K_{ij}^{pot} = selectivity coefficient,

The expression in the brackets gives a weighting factor to contain *j*'s contribution to the membrane potential. Selectivity coefficient is a measure of selectivity for the membrane for the *i* over *j* and it is revelry proportional to the selective membrane. In an ideal membrane, selectivity coefficient would be equal to 0 for all non-primary ions, and E_M in equation 15 would reduce to Nernst equation. K_{ij}^{pot} is generally expressed in logarithm, log K_{ij}^{pot} due to its wide variation in their values.

1.12.3.1.2 The theory of membrane potential

A potential generating system comprises an interface between two liquid or solid phases. The uneven electrical charge distribution of the charged species between two phases will result in the phase boundary potential. In practical electrode systems, diverse charge carriers are together involved in interfacial processes. Nonetheless,

ISE selectivity will make sure that the transfer reactions are influenced by certain ions. All ion-selective membrane electrodes display reversible behaviour in reality and the electron transfer rate is greater than the mass transport. When describing an ion transport system, both electrical and potential contributions should be taken into account. In the ISE, between the membrane and the external sample solution and between the ion-selective membrane and the internal filling solution in ISE, phase boundary potentials will be created. The boundary potential at any specific membrane interface is given as a function of the activity ratios of transferable ions between the membrane surface and the aqueous solution represented by (equation 16): [156,163]

$$E_B = E_B^0 + \frac{RT}{z_i F} ln \left[\frac{a_{i(aq)}}{a_{i(m)}}\right] \quad \textbf{(16)}$$

The diffusion potential is produced by the diffusion of ions within the membrane. Even though the membrane is considered to be a uniform phase, the free energies of the different membrane components undergo variation with space and time and this results in diffusional flux of ions within the membrane. A membrane diffusion potential then develops to maintain a zero net current state. The diffusion potential may be represented by the Henderson equation (equation 17):

$$E_D = \left[\left(\frac{(\Sigma z_i u_i a_i)' - (\Sigma z_i u_i a_i)''}{(\Sigma z_i^2 u_i a_i)' - (\Sigma z_i u_i a_i)'}\right) \times 2.303 \frac{RT}{F} log \left(\frac{(\Sigma z_i^2 u_i a_i)'}{(\Sigma z_i^2 u_i a_i)''}\right)\right] \quad \textbf{(17)}$$

where u_i is the mobility of membrane component i

Z_i is the charge on membrane component i

a_i is the activity of membrane component i

' and " are the inner and outer membrane boundaries

1.12.3.2 Voltammetry

This electroanalytical technique is based on measuring the current convection at the exterior of an electrode. Depending on the chemical compound at the electrode, the potential will become miscellaneous in precise method to induce oxidation or reduction. Therefore, the current-potential produced is dependent on the nature and concentration of the chemical compound. In this technique three electrodes are used:

working, reference and auxiliary. The auxiliary electrode transmits the current potential; the oxidation or reduction reaction occurs at the working electrode. The controlled potential at the working electrode is the potentiostat, a specially designed circuit which can be altered in the three electrode set up.[158,160]

The voltammetric technique includes the electroactive compound under analysis with three electrode system in a solution. The current always flows through the working electrodes and the potential scanning is established on it. The working electrode material should be selected in such a way that it has small surface area so that it will instantaneously and rigorously estimate the potential established by the electrical circuit. Faraday's Law and Fick's Law are the principle basis of the voltammetric techniques. In simple terms, this technique measures the current complementing to the abundance of the material carried by diffusion and reacting at the surface of the electrode. The magnitude current thus captured or measure is proportional to the concentration of the electrochemical species under study.

Amperometry is a voltammetric technique which measures the current of an electrochemical species at an established operating potential. Current is generated when the electroactive compound in the electrode system undergoes an oxidation or reduction process. The eminence of the current is directly proportional to the concentration of the chemical species similar to the voltammetric technique. A constant current is measured where the electrode set up has a homogenous concentration of the electroactive compound and the flowing stream of constant state transmission is employed.

1.12.3.2.1 Advantages of electroanalytical techniques

- electroanalytical techniques are used to produce or analyse various characterisation knowledge for electroactive chemical species including; qualitative, quantitative, thermodynamic and kinetic data. The equipment used in this technique is inexpensive.
- these techniques are electro sensitive therefore they have capacity to current concentration as low as submicron and subpico-mole of the electroactive species.

- electroanalytical methods are discriminative and so they have ability to regulate the electrode potential thereby making it possible to determine the electrochemical spectrum of the compound of analysis. This method is comparable with the determination of the chemical compounds energy states with the light *via* spectroscopy.

1.12.3.2.1.1 Cyclic voltammetry (CV)

Among various electroanalytical techniques, CV has become one of the most widely used technique in various areas of chemistry.[158,160] The principle of CV is based on the changing the potential applied during current monitoring in both leading and reverse directions at the working electrode. CV technique is used for experiments where a reaction undergoes redox process where, CV makes it possible to understand reaction intermediate and nature of the stability of the reaction products.

The peak potentials (Epc, Epa) and peak currents (Ipc, Ipa) are the two important factors in a CV of cathodic and anodic peaks respectively (Figure 38). Using CV, the electrochemical reaction is said to be reversible if the process of electron transmission is faster than other processes (like diffusion).

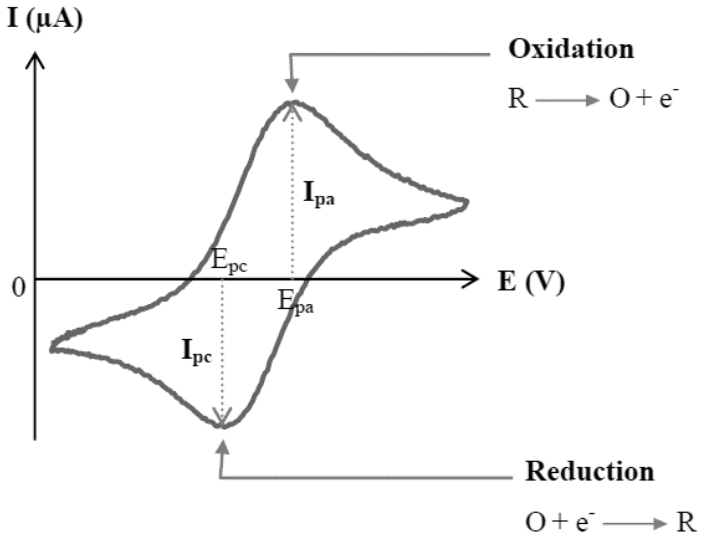

Figure 38. A typical cyclic voltammogram with peak currents.

In such reversible electrochemical reaction, the peak separation is given below equation 18.

$$\Delta E_p = E_{pa} - E_{pc} = 2.303 \frac{RT}{nF} \quad (18)$$

Hence, if a reversible redox reaction with '*n*' electrons and at room temperature, the Δ*Ep* will be 0.0592/*n*V for one electron (≈ 60 mV). Because of the factors such as cell resistance, 60 mV per electron like Δ*Ep* is rarely achievable. The slow electron transfer velocity leading to the irreversibility in the reaction would give Δ*Ep* greater than 0.0592/*n*V. In a reversible redox reaction, the explicit reduction potential is (equation 19):

$$E_0 = \frac{E_{pa} - E_{pc}}{2} \quad (19)$$

The concentration in the reversible redox reaction is dependent on the peak current by the Randles-Sevcik expression equation 20 (at room temperature):

$$I_p = 2.69 \times 10^5 n^{3/2} . A D^{1/2} C_o v^{1/2} \quad (20)$$

where I_p is the peak current

A is the electrode area

D is the diffusion coefficient

C_o is concentration

v is the scan rate

Cyclic voltammetry techniques consist of calculating the current as the adjusted potential is changed linearly with time and at constant rate. At a point in the cyclic process, the sweep direction is inverted following the potential flipping back through the initial potential and these processes occurs at the same rate.[112,114] A typical CV is shown with the potential waveform in Figure 39. The current flow in the CV bears peak shape which is comparable with the linear sweep voltammetry for the two cycles; initial and reverse. The behaviour of the cyclic system is determined by the potential applied at the Vs^{-1} scan rate and is in a triangular wave form. For varied parts of the sweep, the scan rate can be altered otherwise it is usually retained at

constant rate. Figure 39 shows an example CV system demonstrates applied potential and curve responses.

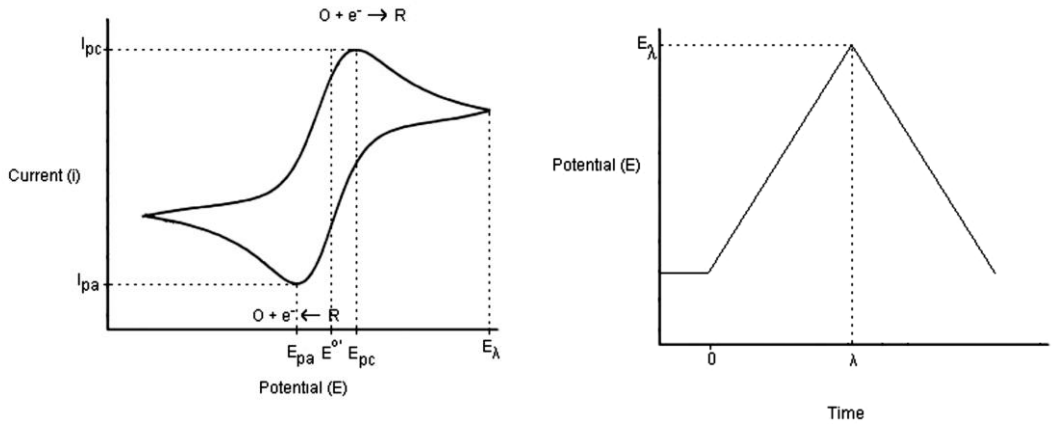

Figure 39. A cyclic voltammogram showing a linear potential applied to the working electrode to change the potential over time.[112]

There are two linear potential sweeps in the CV, where the latter sweep is the reversal of the initial sweep. In cases where there are changes in the processes of initial sweep in the bulk solution, the second sweep's O and R's concentration indicate changes at the surface of the electrodes. The concentration of O and R changes when the volume of O at the surface restricts the mass transfer with the purpose that the reverse sweep follow at a negative $E^{0'}$ potential the second cycle oxidises R back to O.[112]

1.13 Aim

The aim of this project is to synthesise and characterise P[5]A-based receptors for biogenic amines and clinically important metals, and incorporate the receptors in a range of sensors.

1.13.1 Objectives

P[5]A derivatives will be carefully designed to bind alkali metals and biogenic amines with complementary geometric and electrostatic motifs to increase not only the affinities of P[5]As for targets but also their selectivities. This will generate a group of P[5]As with different, but known, binding constants for specific linear biogenic amines (Figure 40). Further functionalisation will facilitate incorporation of P[5]As into carbon paste electrodes or onto gold surfaces so that a variety of

detection platforms, including electrochemical sensor methods, can exploit the novel P[5]As. These techniques are very sensitive to the nature of analyte binding (hydrogen- bonding, electrostatic or hydrophobic interactions) so that differentiation between targets may be possible even with minimal variation to the P[5]A structures.

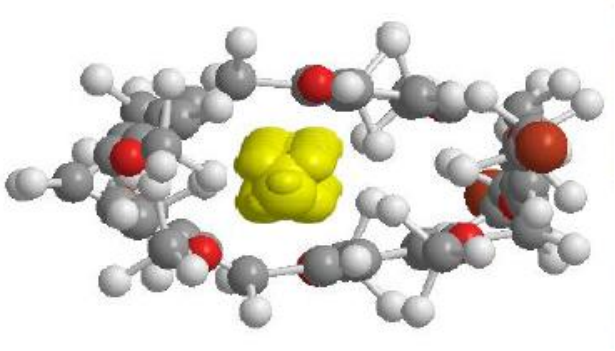

Figure 40. Model of a P[5]A derivative binding to a biogenic amine.

Two classes of sensors are envisaged. The first will use surface modified AuNPs, to give a colorimetric test for the presence of biogenic amines. The second class of sensors, and the main focus of the project, is based on electrochemical methods. The molecular receptors will be incorporated in three different types of electrodes; graphite composites, PVC membrane electrodes and gold surfaces.

The project has been designed to:

- prepare a range of P[5]A receptors designed (with the assistance of computer models) to bind strongly to specific biogenic amines and alkali metals
- determine the binding constants of P[5]A-amine complexes
- functionalise P[5]As so that they can be attached to gold surface.
- prepare and test simple detection systems based on AuNPs
- incorporate P[5]As in composite and ISE electrodes and test responses to biogenic amines and alkali metals.
- attach the thiolated P[5]As to gold electrode surfaces and test the metals and biogenic amines.
- assess electrode stability and performance (sensitivity and selectivity)

CHAPTER - II

Synthesis of pillar[5]arene derivatives

2.1 Experimental

This chapter is concerned with the synthesis of P[5]A and its functionalisation. Their structures, importance in molecular recognition and the mechanism of synthesis have been discussed in detailed in Chapter 1.

2.2 Materials and Methods

All chemicals, solvents and reagents were purchased commercially and used without further purification. All solvents used were of at least reagent plus grade (>98.5%). Compounds **1, 3, 6, 7, 21, 35-38** and **40** were synthesised according to the literature with amendments as described.[62,74,77,99,112,164-167] Compounds **41, 42**, and **44** were synthesised and reported for the first time.[168] Compounds were characterised by NMR, melting point and high resolution mass spectrometry (HRMS) to confirm their identities, through comparison with literature values where possible.[62,74,77,99,112,164-167,169] NMR data were collected by a Bruker Advance DMX-400 spectrometer at 400 MHz for ^{1}H and 100 MHz for ^{13}C with tetramethylsilane (TMS) as the internal reference. Chemical shifts are reported in parts per million (ppm) downfield from TMS (0 ppm) as the internal standard. Multiplicities in the ^{1}H NMR spectra are reported as (s) singlet, (d) doublet, (t) triplet, (q) quartet and (m) multiplet. Electrospray ionisation mass spectra were recorded by a Bruker Daltonics microTOF spectrometer operating in the positive mode. Infra-red absorption spectra were recorded on a Nicolet Avatar 320 FT-IR fitted with a Smart Golden Gate™. Melting points were determined on a BI Barnstead Electrothermal Ltd melting point apparatus and are uncorrected. Gold electrodes (3.0 mm diameter) were mechanically polished and coated with a self-assembled monolayer (SAM) of copillar[4+1]arenes. Electrochemical data were collected with an Ag|AgCl reference electrode using CH instruments software. X-Ray data were collected on a Bruker X8 Apex II CCD diffractometer using a Mo*K*α radiation source (λ = 0.71073 Å). Dye experiments were performed by using an agarose gel membrane incorporating phenolphthalein.

2.3 Synthesis

2.3.1 Synthesis of 1,4-dimethoxypillar[5]arene (1) by method A

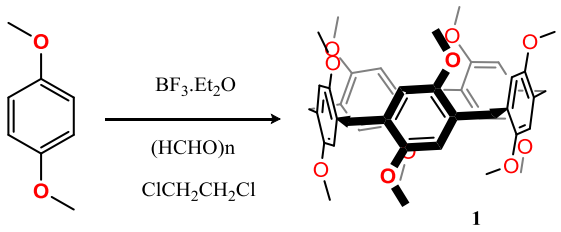

Scheme 15. Synthesis of **1** from 1,4-dimethoxybenezene by method A.

Compound **1** was synthesised by a modification of the reported procedure:[62] 1,4-dimethoxybenzene (1.38 g, 10 mmol) was added to 1,2-dichloroethane (20 ml) followed by addition of paraformaldehyde (0.31 g, 10 mmol) under nitrogen atmosphere. The reaction flask was capped and nitrogen bubbled through the solution for 30 minutes. Then, boron trifluoride diethyl etherate, $BF_3{\cdot}O(C_2H_5)_2$, (1.25 ml, 10 mmol) was added to the solution and the mixture was stirred at room temperature for 3 h. The solution was poured into methanol (30 ml) and the resulting precipitate was collected by filtration. The obtained solid was re-crystallised from CH_3CN which left **1** as a while solid.

1,4-Dimethoxypillar[5]arene (1): yield: 0.33 g (0.44 mmol, 21%); m.p. 248.3-248.8 °C;[62] ^{1}H NMR (400 MHz, $CDCl_3$) δ (ppm): 6.80 (s, 10H, ArH), 3.77 (s, 10H, $ArCH_2Ar$), 3.67 (s, 30H, OCH_3); $^{13}C\{^1H\}$-NMR (100 MHz, $CDCl_3$) δ (ppm): 150.39 (s, C-Ar), 128.24 (s, C-Ar), 113.35 (s, C-Ar), 55.39 (s, C-Ar), 29.26 (s, $ArCH_2Ar$); IR (ν cm^{-1}): 1250 (C-O-C), 1040 (C-OC); HRMS: m/z calcd for $[M+Na]^+$ $C_{45}H_{50}O_{10}Na$, 773.3272, found 773.3296.

2.3.2 Synthesis of 1,4-dimethoxypillar[5]arene (1) by method B

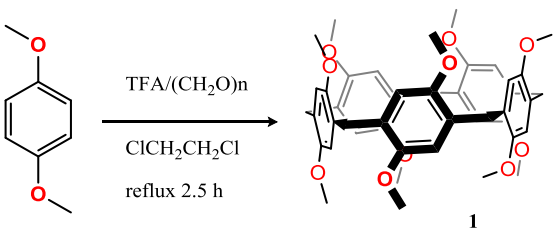

Scheme 16. Synthesis of **1** from 1,4-dimethoxybenezene by method B.

Compound **1** was synthesised by a modification of the reported procedure:[170] 1,4-Dimethoxybenzene (13.82 g, 100 mmol) and freshly ground paraformaldehyde (3.00 g, 100 mmol) were stirred at room temperature in 1,2-dichloroethane (950 ml) for 10 min. TFA (50 ml) was added and the resulting mixture was refluxed for 2.5 h at 90°C. After cooling, the reaction mixture was added into methanol (950 ml). The resulting yellow-green precipitate was collected by filtration and dissolved in $CHCl_3$, initially 150 ml with further solvent added as necessary, before acetone was added (up to 1:1 volume ratio) to give a yellowish white precipitate. The crude product was recrystallised (following treatment with decolourising charcoal) from $CHCl_3$ and washed with acetone which gave **1**.

1,4-Dimethoxypillar[5]arene (1): yield: 10.5 g (14 mmol, 70%); m.p. 248.3-248.8 ^{o}C;[62] ^{1}H NMR (400 MHz, $CDCl_3$) δ (ppm): 6.80 (s, 10H, ArH), 3.77 (s, 10H, $ArCH_2Ar$), 3.67 (s, 30H, OCH_3); $^{13}C\{^{1}H\}$-NMR (100 MHz, $CDCl_3$) δ (ppm): 150.39 (s, C-Ar), 128.24 (s, C-Ar), 113.35 (s, C-Ar), 55.39 (s, C-Ar), 29.26 (s, $ArCH_2Ar$); IR (ν cm^{-1}): 1250 (C-O-C), 1040 (C-OC); HRMS: m/z calcd for $[M+Na]^+$ $C_{45}H_{50}O_{10}Na$, 773.3272, found 773.3296.

2.3.2.1 Preparation of 1,4-dimethoxypillar[5]arene (1) single crystals

Compound **1** (100 mg) was dissolved in the boiling solvent CH_3CN (10 ml) and boiled for 5 min. This solution was filtered into a conical flask. The resulting filtrate was left to evaporate slowly at ambient conditions which left behind **1** in crystalline form. Single crystals of **1** suitable for X-ray diffraction studies were obtained in 3 days.

2.3.3 Synthesis of perhydroxylated-pillar[5]arene (3)

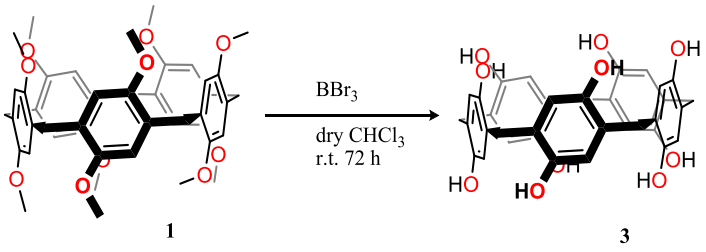

Scheme 17. Synthesis of **3** from **1**.

Compound **3** was synthesised according previously reported procedure:[62,74] **1** (2.0 g, 2.67 mmol) was stirred in anhydrous $CHCl_3$ (150 ml) for 10 min. BBr_3 (5.6 ml, 13.6 g, 54.3 mmol) was then added slowly and the resulting mixture was stirred at room temperature for a further 72 h. Water (100 ml) was then added and the reaction mixture was stirred for 24 h at room temperature. The resulting precipitate was filtered and washed with 0.5 M aqueous HCl which gave **3** as a white powder.

Perhydoxylated-pillar[5]arene (3):[74] yield 1.50 g (2.45 mmol, 82%); ^{1}H NMR (400 MHz, CD_3COCD_3) δ (ppm): 7.99 (s, 10H, OH); 6.68 (s, 10H, ArH); 3.58 (s, 10H, $ArCH_2Ar$); $^{13}C\{^1H\}$-NMR (100 MHz, CD_3COCD_3) δ (ppm): 147.37 (s, C-Ar); 128.02, (s, C-Ar), 118.22 (s, C-Ar), 55.39, (s, OCH_3) 29.26 (s, $ArCH_2Ar$), 30.62, (s, $ArCH_2Ar$); HRMS: m/z calcd for $[M+Na]^+$ $C_{35}H_{30}NaO_{10}$, 633.1904; found, 633.2030.

Note: BBr_3 is highly moisture sensitive and decomposes in air with evolution of HBr. Store under a dry inert atmosphere and transfer by syringe or through a Teflon tube. It reacts violently with protic solvents such as water and alcohols so ether and THF are not appropriate solvents.

2.3.4 Synthesis of pillar[4+1]arene quinone

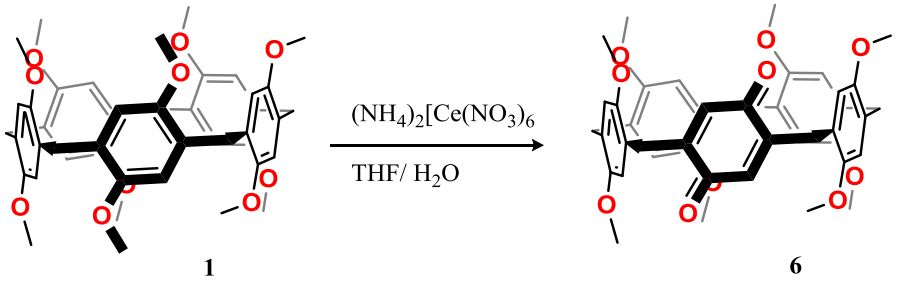

Scheme 18. Synthesis of **6**.

Compound **6** was synthesised by modification of the reported procedure;[164] 1,4-DMP[5]A (3.00 g, 4.00 mmol) and THF (100 ml) was stirred. To this, 25 ml of an aqueous solution (25 ml H_2O) of $(NH_4)_2[Ce(NO_3)_6]$ (2.19 g, 4.00 mmol) was added drop wise and the solution mixture was stirred for 24 h at room temperature. The organic phase was isolated and washed with dichloromethane (DCM) (3 x 50 ml) followed by water (100 ml) and brine (100 ml). The organic phase was dried over

anhydrous Na_2SO_4 and was filtered and the solvent was removed under vacuum. The red solid was purified by flash column chromatography (silica, 230-400 mesh, petroleum ether/DCM, v/v 4:1 to 2:1). The resultant unreacted **1** (1.30 g) and mixture of a red solid was subjected to second column chromatography (petroleum ether/DCM, v/v 1:1), quinone **6** was isolated.

Pillar[4+1]arene quinone (6):[164] yield 285 mg (0.83 mmol, 20%); R_f: 0.6 (petroleum ether:CH_2Cl_2 4:1 to 1:1, silica 40–70 Å); m.p.148.1-148.8 °C;[164] ^{1}H NMR (400 MHz, $CDCl_3$) δ (ppm) 7.15 (s, 2H, Ar-OH), 6.90 (s, 2H, ArH), 6.83 (s, 2H), 6.80 (s, 2H, ArH), 6.60 (s, 2H, ArH), 6.58 (s, 2H, ArH), 3.83 (s, 6H, -OCH_3), 3.76 (br, 12H, -OCH_3), 3.73 (s, 6H, -OCH_3), 3.68 (s, 6H, Ar-CH_2-Ar), 3.67 (s, 4H, Ar-CH_2-Ar); $^{13}C\{^1H\}$-NMR (100 MHz, $CDCl_3$) δ (ppm): 188.66 (s, Ar-C=O), 151.07 (s, Ar-C-O), 150.82 (s, Ar-C-O), 150.72 (s, Ar-C-O), 146.49 (s, Ar-C-O), 133.37 (s, Ar), 129.32 (s, Ar-CH_2), 128.34 (s, Ar-CH_2), 127.86 (s, Ar-CH_2), 127.86 (s, Ar-CH_2), 123.48 (s, Ar-CH_2), 114.25 (s, Ar), 114.21 (s, Ar), 113.81 (s, Ar), 113.70 (s, Ar), 55.95 (s, OCH_3), 55.85 (s, OCH_3), 55.71 (s, OCH_3), 55.41 (s, OCH_3), 29.39 (s, Ar-CH_2-Ar), 28.02 (s, Ar-CH_2-Ar); HRMS: m/z calcd for $[M+Na]^+$ $C_{43}H_{44}O_{10}$ Na, 743.24, found 743.2250.

2.3.5 Synthesis of pillar[4+1]arene quinone

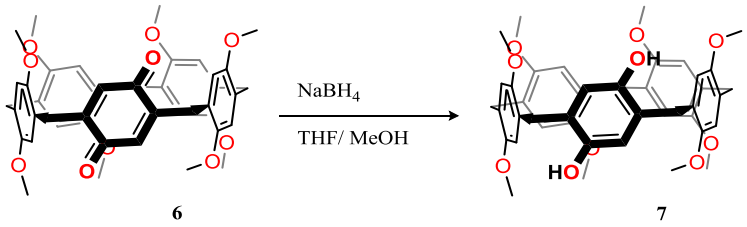

6 7

Scheme 19. Synthesis of **7**.

Compound **6** was synthesised according to previously reported procedure;[83] Quinone **6** (285 mg, 1 mmol) and THF (20 ml) were stirred for 5 min. To this solution $NaBH_4$ (120 mg 3 mmol) in methanol (4 ml) was added slowly. The reaction mixture was stirred for 30 min at room temperature before being quenched by addition of 1M HCl. DCM (100 ml) was added and the mixture washed with deionised water (3 x 50 ml). The organic layer was dried over anhydrous Na_2SO_4 and filtered. A white solid, **7**, was obtained after removing solvent by rotary evaporation.

Pillar[4+1]arene-hydroquinone (7):[164] yield 280 mg (0.38 mmol, 98%); m.p. 173.1-174.6°C;[164] ^{1}H NMR (400 MHz, $CDCl_3$) δ (ppm) 7.15 (s, 2H, Ar-OH), 6.90 (s, 2H, ArH), 6.83 (s, 2H), 6.80 (s, 2H, ArH), 6.60 (s, 2H, ArH), 6.58 (s, 2H, ArH), 3.83 (s, 6H, -OCH_3), 3.76 (br, 12H, -OCH_3), 3.73 (s, 6H, -OCH_3), 3.68 (s, 6H, Ar-CH_2-Ar), 3.67 (s, 4H, Ar-CH_2-Ar); ^{13}C{^{1}H}-NMR (100 MHz, $CDCl_3$) *δ* (ppm): 152.65 (s, Ar-C-O), 150.25 (s, Ar-C-O), 150.74 (s, Ar-C-O), 149.74 (s, Ar-C-O), 147.15, (s, Ar-C-O), 129.11 (s, Ar-CH_2), 128.57 (s, Ar-CH_2), 128.24 (s, Ar-CH_2), 127.75 (s, Ar-CH_2), 127.10 (s, Ar-CH_2), 126.25 (s, Ar-CH_2), 115.83 (s, Ar), 114.39 (s, Ar), 114.03 (s, Ar), 113.93 (Ar), 56.05 (s, OCH_3), 55.82 (s, OCH_3), 55.79 (s, OCH_3), 55.76 (s, OCH_3), 30.65 (s, Ar-CH_2-Ar), 29.88 (s, Ar-CH_2-Ar), 29.80 (s, Ar-CH_2-Ar); HRMS: *m/z* calcd for $[M+Na]^+$ $C_{43}H_{46}O_{10}Na$, 745.3091; found, 745.3156.

2.3.6 Sythesis of pillar[5]arene ethyl ester (21)

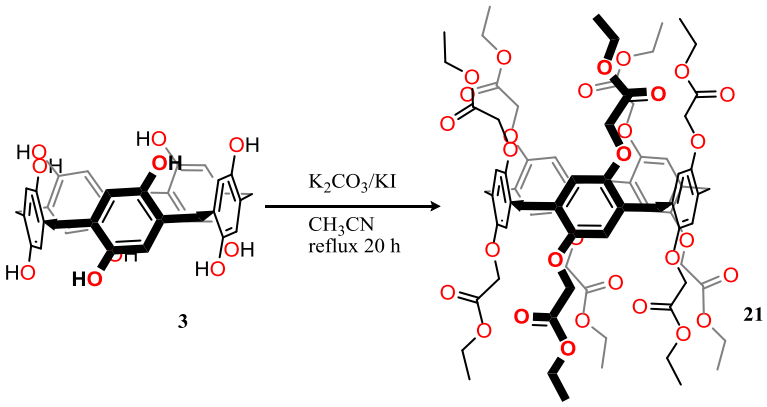

Scheme 20. Synthesis of **21** from **3**.

Hydroxylated pillar[5]arene **3** (1.5 g, 2.4 mmol) was disolved in CH_3CN (70 ml). To this, K_2CO_3 (3.6 g, 26 mmol) was added and the mixture was stirred for 45 min. at room temperature. KI (35 mg) and excess ethyl bromoacetate (4.97 ml, 45 mmol) were added to the reaction mixture which was refluxed for 20 h under nitrogen. After cooling the reaction mixture it was flitered and washed with chloroform (20 ml). Solvent was removed from the pale yellow coloured organic layer under reduced pressure. The resulting pale yellow oily solid was subjected to the column chromotography (silica gel 40–70 Å mesh; CH_2Cl_2:acetone, 100:0 to 90:10). The second fraction to elute (R_f: 0.75) was collected and recrystallised from acetone which left **21** as a white crystalline product.

Esterified pillar[5]arene (21):[112] yield 2.89 g (1.96 mmol, 82%); R_f: 0.75 (CH_2Cl_2:acetone, 100:0 to 90:10 silica 40–70 Å); m.p. 196.2-196.9 °C;[112] ^{1}H NMR (400 MHz, $CDCl_3$) δ (ppm): 7.04 (s, 10H, ArH), 4.56 (q, *J* = 8.4 Hz, 20H, Ar-OCH_2), 4.09 (m, Hz, 20H, OCH_2), 3.86 (s, 10H, $ArCH_2Ar$), 0.99 (t, *J* = 7.0 Hz, 30H, CH_3); ^{13}C{^{1}H}-NMR ($CDCl_3$, 100 MHz) δ (ppm): 169.3 (s, C=O), 148.96 (s, Ar), 128.69 (s, Ar), 114.45 (s, C-Ar), 65.70 (s, *O*-CH_2), 60.85 (s, *O*-CH_2CH_3), 29.21 (s, $ArCH_2Ar$), 13.81 (s, CH_3); HRMS: m/z calcd for $[M+Na]^+$ $C_{75}H_{90}NaO_{30}$, 1493.5414; found, 1493.6281.

2.3.7 Synthesis of 1,4-bis(bromoethyoxy)benzene (35)

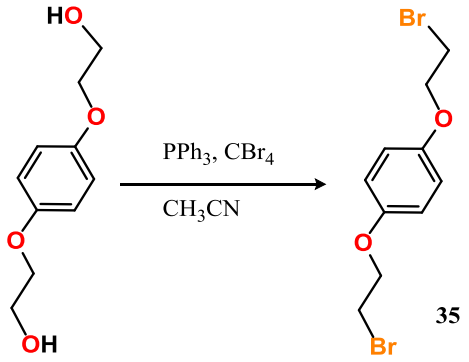

Scheme 21. Synthesis of **35**.

Compound **35** was synthesised according previously reported procedure:[99] 1,4-Bis(hydroxyethoxy)benzene (5.00 g, 25.2 mmol) was mixed with triphenylphosphine (15 g, 60 mmol) in CH_3CN. The white mixture was stirred and cooled to 0°C. Carbon tetrabromide (20.00 g, 60 mmol) was slowly added in small portions to a solution with stirring, at 0°C. The reaction mixture was left to warm to room temperature and the resulting clear solution was stirred for another 4 h under N_2 gas. Then cold water (100 ml) was added to precipitate a white solid which was collected by vacuum filtration. The solid was then recrystallised from hot methanol (200 ml) producing white needle-crystals. **35** formed as white flake-like crystals following vacuum filtration.[168]

1,4-Bis(bromoethyoxy)benzene (35): yield 6.54 g (20 mmol, 80%); m.p. 112.1-113.0 °C;[168] ^{1}H NMR (400 MHz, $CDCl_3$) δ (ppm): 6.85 (s, 4H, ArH), 4.23 (t, *J* = 6.35 Hz, 4H, -CH_2O), 3.59 (t, 4H, *J* = 6.4 Hz, -CH_2Br); ^{13}C-NMR (100 MHz, $CDCl_3$) δ (ppm): 152.89 (Ar-C-0), 116.49(Ar), 116.17 (Ar), 115.8 (Ar), 68.81

(OCH_2), 29.38 CH_2Br); HRMS (m/z): calcd for $[M + Na]^+$, $C_{10}H_{12}Br_2O_2 \cdot Na\ C_2HO_2$, 391.9063; found, 391.9195. Note: the molecular ion could not be detected for this compound and was always observed as the sodium orthoformate complex.

2.3.8 Synthesis of 1,4-bis(thioethoxy)benzene (36)

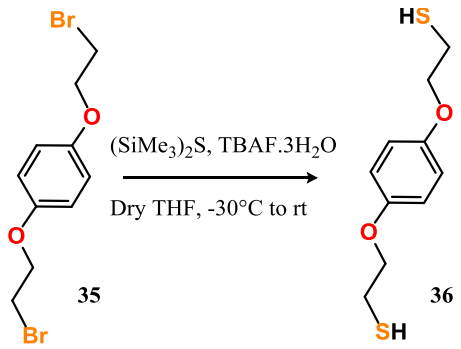

Scheme 22. Synthesis of **36**.

Compound **36** was synthesised according previously reported procedure:[165] 1,4-Bis(bromoethyoxy)benzene (0.897 g, 3.25 mmol) was dissolved in dry THF (30 ml) at -30°C under a nitrogen atmosphere. To this, $(SiMe_3)_2S$ (1.64 ml, 7.78 mmol) was added followed by addition of tetrabutylammonium fluoride trihydrate, $TBAF \cdot 3H_2O$, (2.26 g, 7.16 mmol). The resulting light green reaction mixture was stirred overnight and allowed to warm to room temperature. The solvent was evaporated and deionised water (50 ml), and DCM (50 ml) were added to the resulting residue. The organic layer was separated and washed three times with water before the organic layer was dried with anhydrous Na_2SO_4 and filtered. Solvent was removed by rotary evaporation to give 1,4-bis(bromoethyoxy)benzene, **36**, as a colourless oil mixture following an ethanol wash.

1,4-Bis(thioethyoxy)benzene (36): yield 0.56 g (2.43 mmol, 78%); m.p. 64–66 °C;[169] ^{1}H NMR (400 MHz, $CDCl_3$) δ (ppm): 6.84 (s, 4H, ArH), 4.06 (t, J = 8, 4 Hz , H, -CH_2O), 2.89 (dt, J_1 = 8, J_2 = 8.5 Hz, 4 H, CH2-S-), 1.67 (t, J = 8 Hz, 2 H, SH); ^{13}C-NMR (100 MHz, $CDCl_3$) δ (ppm): 153.11 (Ar-C-O), 116.49 (Ar), 116.51 (Ar), 70.11 (OCH_2), 24.31 (CH_2S)

2.3.9 Synthesis of ethyl-2-(4-methoxyphenoxy)acetate (37)Method A

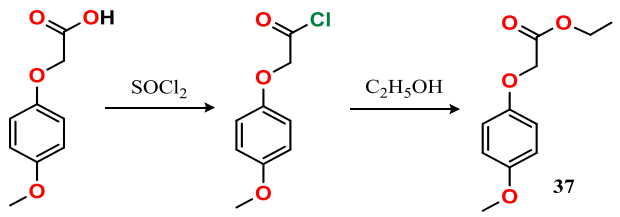

Scheme 23. Synthesis of **37**.

2-(4-Methoxyphenoxy)acetic acid (9.1 g, 50 mmol) was added to thionyl chloride (5 ml, 65 mmol), and was dissolved at 84-86°C. A brown mixture was obtained which was stirred and refluxed for 30 min with a $CaCl_2$ guard tube fitted to the reaction flask. The brown solid was dissolved in absolute ethanol (3 ml, 50 mmol). This solution mixture was heated and refluxed for 15 min. The brown liquid was left to cool at the room temperature. Later unreacted $SOCl_2$ was removed by treating with deionised water (10 ml). The aqueous layer was separated by adding diethyl ether (50 ml). The basicity of the solution was increased by adding aqueous $NaHCO_3$ (100 ml). The solution obtained was later dried with anhydrous $MgSO_4$ and later filtered. A brown oily liquid was obtained under reduced pressure.

Ethyl-2-(4-methoxyphenoxy)acetate (37): 6.2 g (29.5 mmol, 57%); m.p. 96.5–97.5 °C; ^{1}H NMR (400 MHz, $CDCl_3$) δ (ppm): 6.84-680 (m, 4H, ArH), 4.55 (s, 2H, OCH_2C=O), 4.3 (q, *J* = 7.3 Hz, 2H, -OCH_2CH_3), 3.74 (s, 3H, OCH_3), 1.3 (t, *J* = 7.3 Hz, 3H, OCH_2CH_3); ^{13}C-NMR (100 MHz, $CDCl_3$) *δ* (ppm): 169.17 C=O), 154.55 (Ar-C-O), 152.07 (Ar-C-O), 115.89 (Ar), 114.66 (Ar), 66.39 (*O*-CH_2CH_3), 61.22 (*O*-CH_2), 55.61 (OCH_3), 14.14 (CH_3); HRMS (*m*/*z*): calcd for $[M + Na]^+$, $C_{11}H_{14}NaO_4$ found, 233.1028.

2.3.10 Synthesis of ethyl-2-(4-methoxyphenoxy)acetate (37), Method B

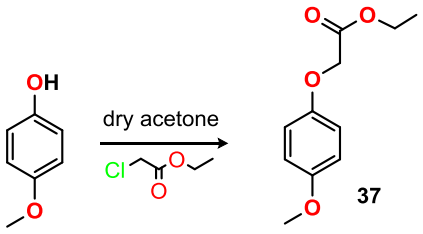

Scheme 24. Synthesis of **37**.

Compound **37** was synthesised according to previously reported procedure:[167] 4-methoxyphenol (5 g, 40.27 mmol) was disolved in dry actone (50 ml). K_2CO_3 (6.2 g, 134.5 mmol) and ethyl chloroacetate (4.8 g, 40 mmol) was added to the reaction mixture, which was then refluxed for 8h. After cooling the reaction mixture, the solvent was removed under reduced pressure. The residual mass was triturated with ice water to remove K_2CO_3 and extracted with ether (3 × 50 ml). The ether layer was washed with 10% NaOH solution (3 × 30 ml) followed by water (3 × 30 ml) which was dried over anhydrous Na_2SO_4 and evaporated to dryness to get crude solid. The crude product was recrytsalised with ethanol to give **37** as a white crystalline product.

Ethyl-2-(4-methoxyphenoxy)acetate (37):[167] yield 6.72 g (32 mmol, 80%); m.p. 96.5–97.5 °C; ^{1}H NMR (400 MHz, $CDCl_3$) δ (ppm): 6.84-6.80 (m, 4H, ArH), 4.55 (s, 2H, OCH_2C=O), 4.3 (q, *J* = 7.3 Hz, 2H, -OCH_2CH_3), 3.74 (s, 3H, OCH_3), 1.3 (t, *J* = 7.3 Hz, 3H, OCH_2CH_3); ^{1}H-NMR (100 MHz, $CDCl_3$) *δ* (ppm): 169.17 (C=O), 154.55 (Ar-C-O), 152.07 (Ar-C-O), 115.89 (Ar), 114.66 (Ar), 66.39 (*O*-CH_2CH_3), 61.22 (*O*-CH_2), 55.61 (OCH_3), 14.14 (CH_3); HRMS (*m*/*z*): calcd for $[M + Na]^+$, $C_{11}H_{14}NaO_4$ found, 233.1028.

2.3.11 Synthesis of diethyl 2,2'-(1,4-phenylenebis(oxy))diacetate (38), method A

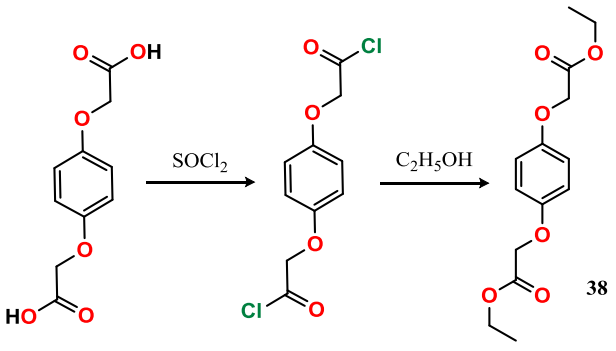

Scheme 25. Synthesis of **38**.

2,2'-(1,4-Phenylenebis(oxy))diacetic acid (5.2 g, 50 mmol) was added to thionyl chloride (5 ml, 65 mmol), and dissolved at 84-86°C. A brown mixture was obtained

which was stirred and refluxed for 30 min with a $CaCl_2$ guard tube fitted. The brown solid was dissolved in absolute ethanol (3 ml) and was heated to reflux for 15 min. The resultant brown liquid was left to cool to room temperature. Unreacted $SOCl_2$ was removed by treating with deionised water (10 ml) and the aqueous layer was separated by adding diethyl ether (50 ml). The basicity of the solution was increased by adding aqueous $NaHCO_3$ (100 ml). The solution obtained was later dried with anhydrous $MgSO_4$ and later filtered. A brown oily liquid **38** was obtained under reduced pressure.

Diethyl 2,2'-(1,4-phenylenebis(oxy))diacetate (38): yield 6 g (21.27 mmol, 64%); ^{1}H NMR (400 MHz, $CDCl_3$) δ (ppm): 6.85 (s, 4H, ArH), 4.55 (s, 4H, $OCH_2C{=}O$), 4.26 (q, 4H, *J* = 7.2 Hz, $-OCH_2CH_3$), 1.28 (t, *J* = 7.13 Hz, 6H, OCH_2CH_3); ^{13}C-NMR (100 MHz, $CDCl_3$) *δ* (ppm): 169.08 (C=O), 154.59 (Ar), 152.83 (Ar), 115.89 (Ar), 66.26 (*O*-CH_2CH_3), 61.32 (*O*-CH_2), 14.16 (CH_3); HRMS (*m*/*z*): calcd for $[M + Na]^+$, $C_{14}H_{18}NaO_6$ 305.1010 found, 305.1281.

2.3.12 Synthesis of diethyl 2,2'-(1,4-phenylenebis(oxy))diacetate (38), method B

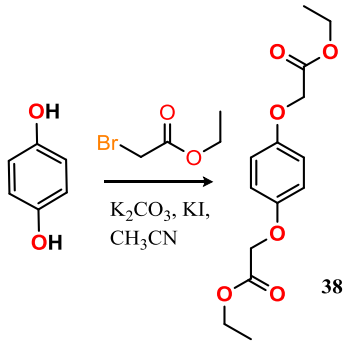

Scheme 26. Alternative synthesis of **38**.

Hydroquinone (5 g, 45.4 mmol) was disolved in CH_3CN (80 ml). K_2CO_3 (6.2 g, 134.5 mmol) was added and the mixture stirred for 45 min. at room temperature. KI (35 mg) and excess ethyl bromoacetate (14.92 ml, 134.9 mmol) were added to the reaction mixture which was then refluxed for 24 h under nitrogen. After cooling the reaction mixture it was flitered and washed with chloroform (20 ml). Solvent was removed from the pale yellow coloured organic layer under reduced pressure. The crude product was recrytsalised with methanol to give **38** as a white crystalline product.

Diethyl 2,2'-(1,4-phenylenebis(oxy))diacetate (38): yield 7.5 g (26.58 mmol, 80%); ^{1}H NMR (400 MHz, $CDCl_3$) δ (ppm): 6.85 (s, 4H, ArH), 4.55 (s, 4H,

$OCH_2C{=}O$), 4.26 (q, 4H, *J* = 7.2 Hz, -OCH_2CH_3), 1.28 (t, *J* = 7.13 Hz, 6H, OCH_2CH_3); ^{13}C-NMR (100 MHz, $CDCl_3$) *δ* (ppm): 169.08 (C=O), 154.59 (Ar), 152.83 (Ar), 115.89 (Ar), 66.26 (*O*-CH_2CH_3), 61.32 (*O*-CH_2), 14.16 (CH_3); HRMS (*m*/*z*): calcd for $[M + Na]^+$, $C_{14}H_{18}NaO_6$ 305.1010 found, 305.1281.

2.3.13 Synthesis of 1,4-bis(bromoethyoxy)copillar[4+1]arene (40), method A

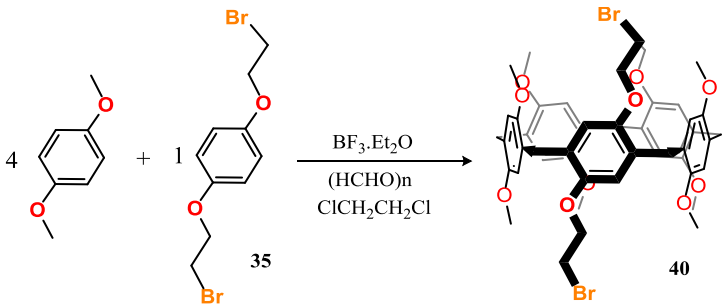

Scheme 27. Synthesis of **40**.

1,4-Bis(bromoethyoxy)benzene (1.62 g, 5 mmol) and 1,4-dimethoxybenzene (2.76 g, 20 mmol) and freshly ground paraformaldehyde (0.775 g, 25 mmol) were dissolved in CH_2Cl_2 (140 ml) under nitrogen atmosphere in a round bottom flask followed by $BF_3{\cdot}O(C_2H5)_2$ (3.1 ml, 25 mmol) which was added by syringe. The green/blue mixture was stirred for 2 h. To this mixture, deionised water (100 ml) was added which gives milky solution that was stirred overnight. The solvent was removed under reduced pressure. To the crude product, distilled water was added and extracted with DCM (3 x 70 ml). The combined organic extracts were dried with anhydrous Na_2SO_4 and filtered. The organic layer was collected and the solvent removed under vacuum. The pale yellow solid was purified by flash column chromatography (silica, 230-400 mesh, 3.5 x 25.5 cm column, 100% DCM). The fractions with an R_f of 0.8 were combined and the solvent removed to leave white crystals of **40**.[168]

1,4-Bis(bromoethyoxy)copillar[4+1]arene (40): yield 0.777 g (0.83 mmol, 18%); Rf: 0.8 (CH_2Cl_2 silica 40–70 Å); m.p. 127.1-127.9 ºC; ^{1}H NMR (400 MHz, $CDCl_3$) δ (ppm) 6.77 (s, 2H, -Ar*H*), 6.76 (s, 4H, -Ar*H*), 6.74 (s, 2H, -ArH), 6.71 (s, 2H, -ArH), 4.05 (t, *J* = 6.3 Hz, 4H, CH_2O), 3.78 (s, 10H, $ArCH_2Ar$), 3.66 (s, 18H, OCH_3), 3.61 (s, 6H, OCH_3), 3.55 (t, *J* = 6.3 Hz, 4H, -CH_2Br); ^{13}C{^{1}H}-NMR (100 MHz, $CDCl_3$)

δ (ppm): 150.85 (s, Ar-C-O), 150.78 (s, Ar-C-O), 150.74 (s, Ar-C-O), 149.74 (s, Ar-C-O), 129.11 (s, Ar-CH_2), 128.57 (s, Ar-CH_2), 128.24 (s, Ar-CH_2), 128.15 (s, Ar-CH_2), 127.82 (s, Ar-CH_2), 115.83 (s, Ar), 114.39 (s, Ar), 114.03 (s, Ar), 113.93 (s, Ar), 68.74 (s, OCH_2), 56.05 (s, OCH_3), 55.82 (s, OCH_3), 55.79 (s, OCH_3), 55.76 (s, OCH_3), 34.00 (s, Ar-CH_2-Ar), 29.88 (s, CH_2Br), 29.80 (s, CH_2Br); HRMS: m/z calcd for $[M+Na]^+$ $C_{47}H_{52}Br_2NaO_{10}$, 959.1804; found 959.2047.

2.3.13.1 Preparation of bis(bromoethyoxy)copillar[4+1]arene (40) single crystals

Compound **40** (50 mg) was dissolved in DMF and methanol (1:1, 6 ml) in a conical flask. The solution was filtered into a conical flask at room temperature. The filtrate was then allowed to slowly evaporate at room temperature which gave crystalline **40** as colourless needles. Single crystals of **40** suitable for X-ray diffraction studies were obtained in 4 days.

2.3.14 Synthesis of 1,4-bis(bromoethyoxy)copillar[4+1]arene (40), method B

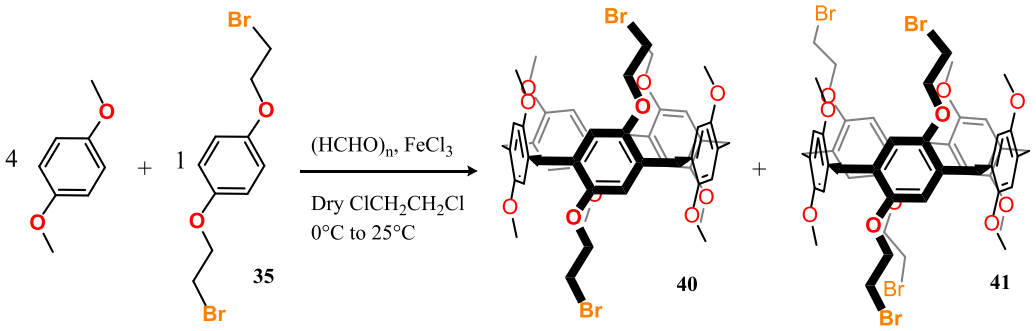

Scheme 28. Synthesis of **40** and **41**.

1,4-Dimethoxybenzene (11.96 g, 86.56 mmol), 1,4-bis(bromoethyoxy)benzene (1.75 g, 5.41 mmol) and paraformaldehyde (7.80 g, 259.68 mmol) were dissolved in CH_2Cl_2 (350 ml). After cooling to 0°C, $FeCl_3$ (2.19 g, 13.53 mmol) was added under nitrogen atmosphere, then the mixture was stirred at 0°C for 30 min, as the solution turns light green, and then it was raised to room temperature for 3h whereupon the solution turns dark green. After completion of the reaction, the organic layer was washed with water (100 ml), saturated brine (100 ml) and dried over Na_2SO_4. Following removal of the drying agent, solvent was removed under vacuum and

diethyl ether (100 ml) was added to the dried impure solid. This was filtered on a Büchner funnel and washed with further diethyl ether (20 ml). The organic layer was collected and the solvent removed under vacuum. The residue was purified by silica-gel flash column chromatography (silica, 230-400 mesh, 3.0 x 25.5 cm column) using petroleum ether/CH_2Cl_2 (2:1 to 1:1) as the eluent. Compounds **40** and **41**were obtained as white solids.

1,4-Bis(bromoethyoxy)copillar[4+1]arene (40): yield 1.56 g (16.6 mmol, 33%); R_f: 0.66 (petroleum ether:CH_2Cl_2 1:1 silica 40–70 Å); m.p. 127.1-127.9 °C;[168] ^{1}H NMR (400 MHz, $CDCl_3$) δ (ppm) 6.77 (s, 2H, -Ar*H*), 6.76 (s, 4H, -Ar*H*), 6.74 (s, 2H, -ArH), 6.71 (s, 2H, -ArH), 4.05 (t, *J* = 6.3 Hz, 4H, CH_2O), 3.78 (s, 10H, $ArCH_2Ar$), 3.66 (s, 18H, OCH_3), 3.61 (s, 6H, OCH_3), 3.55 (t, *J* = 6.3 Hz, 4H, -CH_2Br); $^{13}C\{^1H\}$-NMR (100 MHz, $CDCl_3$) *δ* (ppm): 150.85 (s, Ar-C-O), 150.78 (s, Ar-C-O), 150.74 (s, Ar-C-O), 149.74 (s, Ar-C-O), 129.11 (s, Ar-CH_2), 128.57 (s, Ar-CH_2), 128.24 (s, Ar-CH_2), 128.15 (s, Ar-CH_2), 127.82 (s, Ar-CH_2), 115.83 (s, Ar), 114.39 (s, Ar), 114.03 (s, Ar), 113.93 (s, Ar), 68.74 (s, OCH_2), 56.05 (s, OCH_3), 55.82 (s, OCH_3), 55.79 (s, OCH_3), 55.76 (s, OCH_3), 34.00 (s, Ar-CH_2-Ar), 29.88 (s, CH_2Br), 29.80 (s, CH_2Br); HRMS: m/z calcd for $[M+Na]^+$ $C_{47}H_{52}Br_2NaO_{10}$, 959.1804; found 959.2047.

1,4-Bis(bromoethyoxy)copillar[3+2]arene (41): yield 0.607 g (0.54 mmol, 10%); R_f: 0.8 (petroleum ether:CH_2Cl_2 1:1, silica 40–70 Å); m.p. 140.1-140.8 °C;[168] ^{1}H NMR (400 MHz, $CDCl_3$) δ (ppm) 6.81 (s, 2H, -ArH), 6.80 (s, 4H, -ArH), 6.77 (s, 2H, -ArH), 6.76 (s, 2H, -ArH), 4.11 (q, *J* = 6.3 Hz, 8H, -OCH_2), 3.80-3.78 (s, 10H, $ArCH_2Ar$), 3.72 (s, 6H, OCH_3), 3.69 (s, 6H, OCH_3), 3.52 (t, *J* = 6.2 Hz, 8H, -CH_2Br); $^{13}C\{^1H\}$-NMR (100 MHz, $CDCl_3$) *δ* (ppm): 150.82 (s, Ar-C-O), 150.80 (s, Ar-C-O), 150.73 (s, Ar-C-O), 149.73 (s, Ar-C-O), 129.26 (s, Ar-CH_2), 129.12 (s, Ar-CH_2), 128.24 (s, Ar-CH_2), 128.55 (s, Ar-CH_2) (s, Ar), 128.23 (s, Ar-CH_2), 127.95 (s, Ar-CH_2), 115.78 (s, Ar), 114.34 (s, Ar), 114.28 (s, Ar), 113.92 (s, Ar), 68.83 (s, OCH_2), 68.74 (s, OCH_2), 56.05 (s, OCH_3), 55.82 (s, OCH_3), 55.79, 31.84 (s, Ar-CH_2-Ar), 31.53 (s, Ar-CH_2-Ar), 29.95 (s, CH_2Br), 29.92 (s, CH_2Br), 29.67 (s, CH_2Br), 29.64 (s, CH_2Br); HRMS: m/z calcd for $[M+Na]^+$ $C_{49}H_{54}Br_4NaO_{10}$, 1145.0308; found, 1144.9071.

2.3.14.1 Preparation of bis(bromoethyoxy)copillar[3+2]arene (41) single crystals

The chromatographic fraction (50 mg) believed to be the copillar[3+2]arene, synthesised using method B and the end product was dissolved in DMF and methanol (1:1, 6 ml). The solution was filtered into a conical flask and the filtrate was then allowed to slowly evaporate at room temperature which gave crystalline **41** as colourless needles. Single crystals of **41** suitable for X-ray diffraction studies were obtained in 3 days.

2.3.15 Synthesis of 1,4-bis(thioethyoxy)copillar[4+1]arene (42)

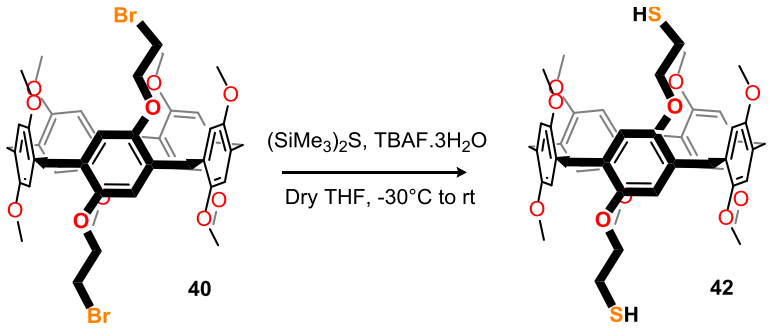

Scheme 29. Synthesis of **42**.

1,4-Bis(bromoethoxy)copillar[5]arene, **40**, (0.200 g, 0.213 mmol) was dissolved in dry THF (10 ml) under nitrogen at -30°C. $(SiMe_3)_2S$ (0.09 ml, 0.426 mmol) and tetrabutylammonium fluoride trihydrate (TBAF:$3H_2O$) (0.296 g, 0.941 mmol) were added to the reaction mixture. The resulting light green solution was allowed to warm to room temperature while being stirred overnight. The resultant colourless mixture was evaporated to remove THF before deionised water (20 ml) and DCM (20 ml) were added. The organic layer was separated and washed three times with deionised water. The organic layer was dried with anhydrous Na_2SO_4, filtered and the solvent removed by rotary evaporation to give the crude product as a pale yellow solid. Further recrystalisation was carried with methanol to give **42** as a yellowish white solid.[168]

1,4-Bis(thioethyoxy)copillar[4+1]arene (42):[168] yield 155 mg (0.18 mmol, 85%); m.p. 188.9-190.1 ºC;[168] ^{1}H NMR (400 MHz, $CDCl_3$) δ (ppm): 6.77-6.73 (m, 10H, -

ArH), 4.12 (t, *J* = 6.3 Hz, 4H, -CH_2O), 3.77 (s, 10H, $ArCH_2Ar$), 3.74-3.65 (s, 24H, -OCH_3), 3.02 (m, 4H, -CH_2SH), 1.42 (m, 2H, -SH); $^{13}C\{^1H\}$-NMR (100 MHz, $CDCl_3$, 20 °C) δ (ppm) 150.93 (s, Ar-C-O), 150.87 (s, Ar-C-O), 128.66 (s, Ar-CH_2), 128.44 (s, Ar-CH_2), 128.20, (s, Ar-CH_2), 114.39 (s, Ar), 114.23 (s, Ar), 65.79 (OCH_2), 56.06 (s, OCH_3), 55.91 (s, OCH_3), 55.84 (s, OCH_3), 50.80 (s, OCH_3), 29.73, (s, CH_2SH); HRMS (*m*/*z*): calcd for $[M+Na]^+$ $C_{47}H_{54}NaO_{10}S_2$, 865.3056; found, 865.3141.

2.3.16 Attempted synthesis of monoester functionalised copillar[4+1]arene (43)

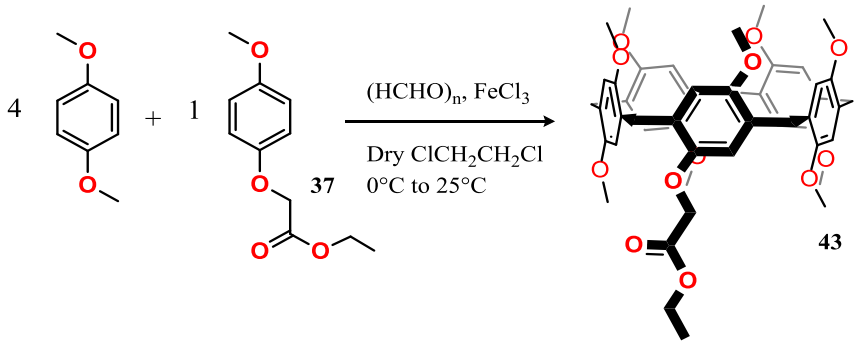

Scheme 30. Synthesis of **43**.

Ethyl 2-(4-methoxyphenoxy)acetate (1.05 g, 5.0 mmol) and 1,4-dimethxybenzene (2.76 g, 20 mmol) mixtures were added to dry 1,2-dichloethane (140 ml) in a 250 ml round-bottom flask. Freshly grounded paraformaldehyde (0.775 g, 25 mmol) was added under a nitrogen atmosphere followed by $BF_3{\cdot}O(C_2H5)_2$ (3.1 ml, 25 mmol) which was added by syringe. The green mixture was stirred at room temperature for 4 h. before the solvent was removed by rotary evaporation. To the crude mixture, DCM (100 ml) was added and then washed with deionised water (3 x 50 ml). The organic layer was dried over anhydrous Na_2SO_4 and filtered. The green solid was obtained after removing solvent by rotary evaporation. Separation was not good enough to get a clean NMR spectrum.

2.3.17 Synthesis of ester copillar[4+1]arene (44), method A

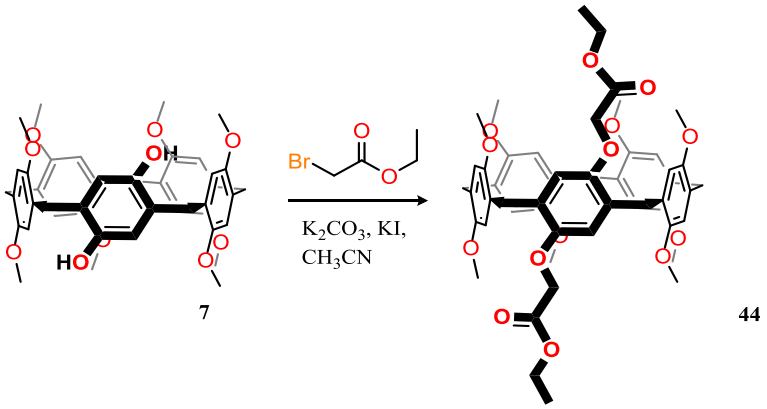

Scheme 30. Synthesis of **44**.

Copillar[**4+1**]arene **7** (1.1 g, 3.00 mmol) was dissolved in CH_3CN (50 m) in a 250 ml round bottom flask. Ethyl bromoacetate (2.59 g, 24.0 mmol) and K_2CO_3 (6.62 g, 48.0 mmol) were added the mixture refluxed for 14 h under a nitrogen atmosphere. The reaction mixture was cooled, filtered and washed with chloroform. The filtrate was evaporated under vacuum and the residue dissolved in a mixture of methanol and chloroform to precipitate crystals. The crystals were then filtered and washed with methanol and finally dried under vacuum to yield **44**.

Ester copillar[4+1]arene (44): yield 2.36 g (2.63 mmol, 91%); m.p. 165.5−167.9°C; ^{1}H NMR (400 MHz, $CDCl_3$) δ (ppm) 7.07 (s, 4H, ArH), 7.06 (s, 2H), 7.00 (s, 2H, ArH), 6.93 (s, 2H, ArH), 4.77 (s, 4H, ArH), 3.99-3.98 (s, 10H, Ar-CH_2-Ar), 3.97(s, 6H, -OCH_3), 3.92 (s, 6H, -OCH_3), 3.91 (s, 6H, -OCH_3), 3.90 (s, 6H, -OCH_3), 3.37 (q, *J* = 7.1 Hz, 4H, Ar-CH_2C(O)-), 0.017 (t, *J* = 7.0 Hz, *O*-CH_2-CH_3); ^{13}C{^{1}H}-NMR (100 MHz, $CDCl_3$) *δ* (ppm): 169.3 (s, C=O), 150.66 (s, Ar-C-O), 150.64 (s, Ar-C-O), 150.41 (s, Ar-C-O), 150.34 (s, Ar-C-O), 149.41 (s, Ar-C-O), 128.72 (s, Ar-CH_2), 128.60 (s, Ar-CH_2), 128.50 (s, Ar-CH_2), 128.00 (s, Ar-CH_2), 114.51 (Ar), 114.42 (s, Ar), 113.74 (s, Ar), 113.62 (s, Ar), 113.37 (s, Ar), 65.98 (*O*-CH_2), 60.74 (s, *O*-CH_2CH_3), 55.80 (s, OCH_3), 55.71 (s, OCH_3), 55.66 (s, OCH_3), 55.58 (s, OCH_3), 29.57(s, Ar-CH_2-Ar), 29.49 (s, Ar-CH_2-Ar), 28.97 (s, Ar-CH_2-Ar), 12.28 (s, CH_3); HRMS: *m/z* calcd for $[M+Na]^+$ $C_{51}H_{58}O_{14}Na$, 917.38, found 917.41.

2.3.18 Synthesis of ester copillar[4+1]arene (44), method B

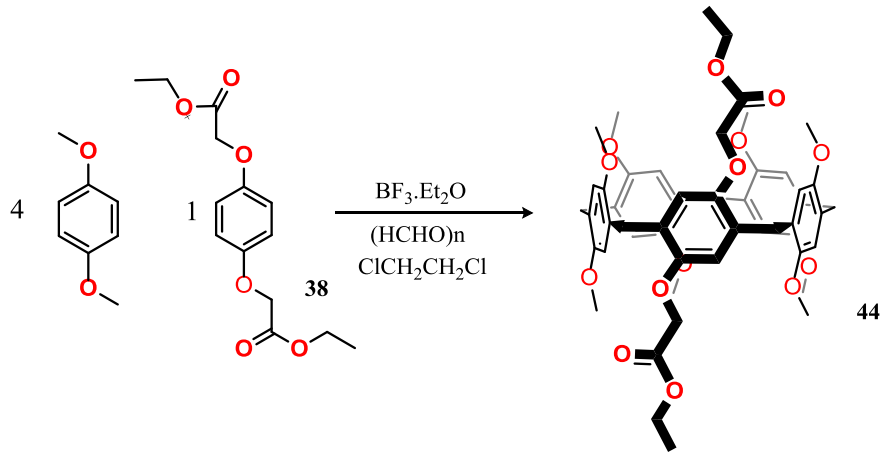

Scheme 31. Synthesis of **44**.

Diethyl 2,2'-(1,4-phenylenebis(oxy))diacetate (1.41 g, 5.0 mmol) and 1,4-dimethxybenzene (2.76 g, 20 mmol) mixtures were added to dry 1,2-dichloethane (140 ml). To this solution, freshly grounded paraformaldehyde (0.775 g, 25 mmol) was added under a nitrogen atmosphere followed by $BF_3{\cdot}O(C_2H_5)_2$ (3.1 ml, 25 mmol) using a syringe. The green mixture was stirred at room temperature for 4 h. To this mixture, deionised water (100 ml) was added which gives milky solution and was stirred overnight. The solvent was removed under reduced pressure. To the crude product, distilled water was added and extracted with DCM (3 x 70 ml). The combined organic extracts were dried with anhydrous sodium sulfate and filtered. The organic layer was collected and the solvent removed under vacuum. The yellow oily solid was purified by flash column chromatography (silica, 230-400 mesh, 3.5 x 25.5 cm column, petroleum ether:CH_2Cl_2 1:1). The fractions with an R_f of 0.7 were combined and the solvent removed to leave white crystals of **44**.

Ester copillar[4+1]arene (44): yield 0.75 g (0.84 mmol, 19%); m.p. 165.5-167.9 °C; ^{1}H NMR (400 MHz, $CDCl_3$) δ (ppm) 7.07 (s, 4H, ArH), 7.06 (s, 2H), 7.00 (s, 2H, ArH), 6.93 (s, 2H, ArH), 4.77 (s, 4H, ArH), 3.99-3.98 (s, 10H, Ar-CH_2-Ar), 3.97(s, 6H, -OCH_3), 3.92 (s, 6H, -OCH_3), 3.91 (s, 6H, -OCH_3), 3.90 (s, 6H, -OCH_3), 3.37 (q, *J* = 7.1 Hz, 4H, Ar-CH_2C(O)-), 0.017 (t, *J* = 7.0 Hz, *O*-CH_2-CH_3); ^{13}C{^{1}H}-NMR (100 MHz, $CDCl_3$) *δ* (ppm): 169.3 (s, C=O), 150.66 (s, Ar-C-O), 150.64 (s, Ar-C-O), 150.41 (s, Ar-C-O), 150.34 (s, Ar-C-O), 149.41 (s, Ar-C-O), 128.72 (s, Ar-CH_2), 128.60 (s, Ar-CH_2), 128.50 (s, Ar-CH_2), 128.00 (s, Ar-CH_2), 114.51 (Ar),

114.42 (s, Ar), 113.74 (s, Ar), 113.62 (s, Ar), 113.37 (s, Ar), 65.98 (*O*-CH_2), 60.74 (s, *O*-CH_2CH_3), 55.80 (s, OCH_3), 55.71 (s, OCH_3), 55.66 (s, OCH_3), 55.58 (s, OCH_3), 29.57(s, Ar-CH_2-Ar), 29.49 (s, Ar-CH_2-Ar), 28.97 (s, Ar-CH_2-Ar), 12.28 (s, CH_3); HRMS: *m*/*z* calcd for $[M+Na]^+$ $C_{51}H_{58}O_{14}Na$, 917.38, found 917.41.

2.4 Results and Discussion

Three compounds, P[5]A **1**, esterified P[5]A **21** and thiolated copillar[4+1]arene **42**, were identified as targets capable of binding alkali metal cations and biogenic amines based on reports in the literature and apparent complementarity between these hosts and the size of the guests. In particular the unique fivefold symmetric tubular structures of the P[5]As were expected to demonstrate novel binding motifs not available to planar macrocycles such as porphyrins and phthaocyanins, funnel-shaped calixarenes and resorcinarenes, or hard to functionalise cucurbiturils. These three P[5]A derivatives were used as modifiers for sensors with **1** incorporated into ISE sensors to bind alkali metal cations, **21** as a potential conduit for protons and **42** as a derivative capable of attachment to gold electrodes and nanoparticles.

2.4.1 Synthesis of 1,4-dimethoxypillar[5]arene (1)

Following the first report of **1** in 2008,[62] and subsequent improvements in its synthesis that made the novel macrocycle available in multigram quantities, compound **1** appeared to be a good candidate as an electrode modifier to enhance ion selectivity. Hence, **1** was synthesised and used in the fabrication of composite and ISE sensors to investigate alkali metal selectivities as detailed in Chapter 3 and 4.

Compound **1** was synthesised through condensation of 1,4-dimethoxybezene with paraformaldehyde using a Lewis acid catalyst.[62] It is a symmetrical host macrocyclic compound and is therefore comparable to calix[5]arene, however, the aromatic moieties of **1** are linked by methylene bridges at the 2- and 5-positions. Its synthesis was attempted by two literature methods to determine which had the better yield and simplest purification method. The key difference between the two methods was the choice of catalyst used: $BF_3{\cdot}O(C_2H_5)_2$ was used in method A[62,74] and TFA was used in method B (Scheme 33).[170]

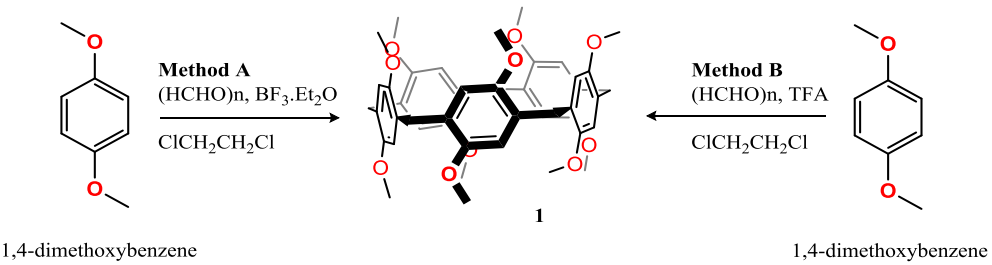

Scheme 32. Compound **1** synthesised by two methods.

2.4.1.1 Synthesis of 1 by method A

Following the original synthesis procedure reported by Ogoshi[62] **1** was synthesised by a 1:1 molar ratio condensation of 1,4-dimethoxybenzene and paraformaldehyde catalysed by Lewis acid; $BF_3{\cdot}O(C_2H_5)_2$. Immediately following addition of the catalyst, the colour of the reaction mixture went from light green to dark green and, after a further 15 min, a black product was obtained. The disadvantage of this method was the consistency of the material obtained which was not optimal for the recrystallisation of the pentamer which, when successful, only gave a yield of around 10%. Optimisation of the conditions, as reported by Ogoshi where three equivalents of paraformaldehyde per equivalent of 1,4-dimethoxybenzene were used, resulted in an observable colour change of the reaction mixture from light green to dark green very quickly after introduction of the catalyst.[74] Compound **1** was isolated from crude product by adding methanol, collecting the precipitate, and recrystallisation from CH_3CN. Alternatively, the precipitate could be extracted into chloroform and the product isolated by recrystallisation from chloroform/acetone (1:1 v/v) to yield white crystalline **1**.

The advantages of the 1:3 paraformaldehyde:1,4-dimethoxybenzene ratio over the 1:1 ratio are fewer polymeric impurities and a yield of 70%. This method also takes less time but the reaction is moisture sensitive. The reaction was scaled up but the yields were poor and separation was always challenging.

2.4.2 Synthesis of 1 by method B

In this method, **1** was synthesised by adapting reported procedure using TFA.[170] The reaction involved a direct 1:1 condensation between 1,4-dimethoxybenzene and paraformaldehyde in 1,2-dichloroethane catalysed by TFA to give **1**. During the

reaction, the reaction mixture changed colour from light yellow to light green upon addition of TFA. Following reflux for 20 min, the colour then changed to dark green. This reaction mixture was further refluxed for 2.5 h at 90°C. The crude product was isolated from the reaction mixture and recrystallised by the same method as in method A, however, pale yellow crystals were obtained instead of the expected white crystals.[170]

To enhance purity of the **1**, the pale yellow product was dissolved in chloroform and mixed with decolourising charcoal which has aromatic and delocalisation properties enabling it to trap coloured impurities. Compound **1** obtained after purification was a white crystalline solid in 65% yield. It was also possible to synthesise **1** on a larger scale (13 g) by this method. The advantages of this method are that the solvents are available cheaply, require no additional drying, can be used for large scale synthesis and, most importantly, the procedure is moisture-insensitive. The purity of the crystalline **1** was confirmed by the melting point experiments which is in the range of 248.3-248.8 ºC and in agreement with literature reports.[62,74,170]
Compound **1** was characterised using NMR and single crystal X-ray crystallography techniques. The ^{1}H NMR spectrum revealed that cyclisation had been successful through the characteristic methylene bridge protons at 3.76 ppm. ^{1}H and ^{13}C NMR spectra were consistent with those reported previously.[62,74,170]

2.4.2.1 X-ray crystal structure of 1·CH_3CN

Crystal data for **1**·CH_3CN: colourless block; $C_{47}H_{53}O_{10}N$; *Fw* = 795.10; tetragonal, space group $I4_1/a$; unit cell dimensions: a = 14.9866(11), b = 14.9866(11), c = 39.368(4)Å, α = 90°, β = 90°, γ = 90°; V = 8842.0(16) Å^3; Z = 8; D_c = 1.195 g cm^{-3}; T = 274 (2) K; μ = 0.084 mm^{-1}; θ-range for data collection 2.82-28.00°; 5349 measured reflections, 886 independent reflections, 281 parameters, 0 restraints; F(000) = 3389; final R-indices [$I > 2\sigma(I)$]: R_1 = 0.1113, $wR2$ = 0.1862, R-indices (all data): R_1 = 0.3210, $wR2$ = 0.4464; max. residual density 1.523 eÅ^3, and goodness-of-fit (F^2) = 0.926.

The structure of **1,** determined by X-ray crystallography, is shown in Figure 41. The crystals were obtained by slow evaporation of CH_3CN. The X-ray crystallography

studies of **1** confirmed that the structure was the cyclic pentamer with aromatic units connected by methylene bridges at the 2- and 5-positions.

Structure of **1** reveals a regular pentagonal architecture and, from the side, shows a symmetrical pillar structure. The angle of the bridging carbons (Ar-CH_2-Ar) is 110.68° which is very close to the 109.28° angle of sp^3 hybridised carbon atoms. The X-ray structure of **1** also shows inclusion of CH_3CN in its cavity. The structure was solved in the tetragonal space group $I4_1/a$ with a high R-factor due to the poor crystal quality. However, from the gross connectivities, we can infer that the pillarene backbone adopts a symmetrical pillar-like structure.

The orientation of CH_3CN in **1** was found to be different from that reported in the literature in which C and N were connected the other way round.[62] The correct connectivity of CH_3CN the cavity is evident although the solvent molecule is badly disordered due to the poor quality of the crystal which limited the amount of diffraction data that could be collected. It was not possible to model the CH_3CN guest effectively but thermal ellipsoid plots aid the interpretation of the crystallographic results as shown in Figure 42. The ellipsoids for the methoxy carbon atoms are very elongated or flattened and it can also be noted that the CH_3CN nitrogen ellipsoid is larger than should be expected.

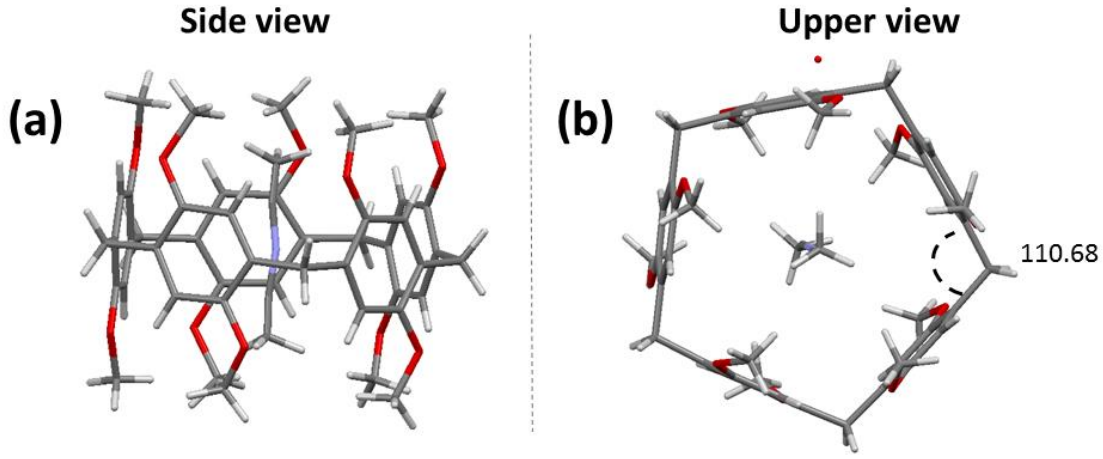

Figure 41. Single crystal X-ray structure of **1** with included CH_3CN. (a) side view of crystal structure (b) upper view of crystal structure with included CH_3CN and methylene bridge bond angle 110.68.

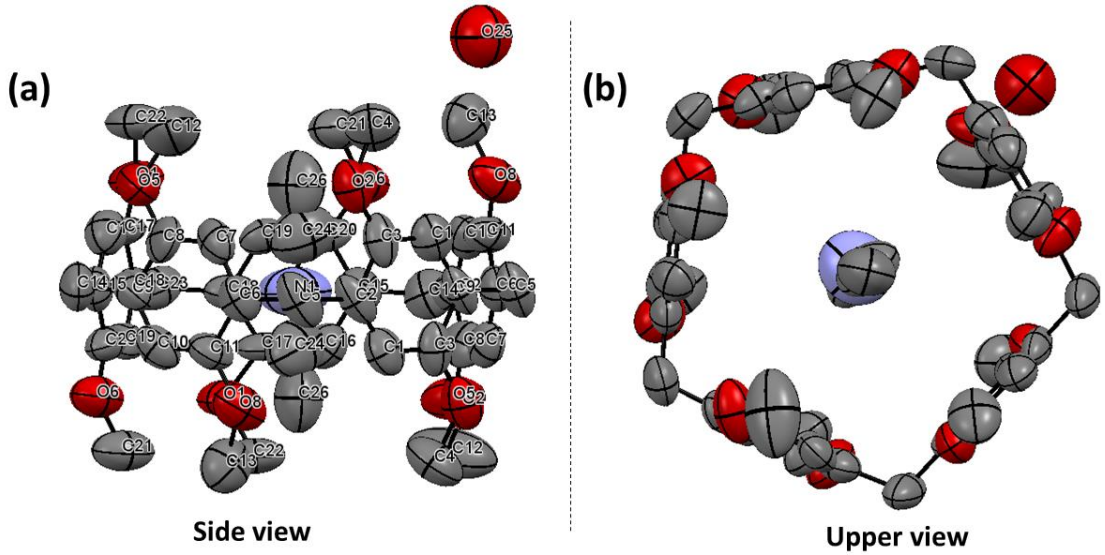

Figure 42. Thermal ellipsoid structures of **1** (Hydrogen atoms are omitted for clarity).

2.4.3 Synthesis of esterified pillar[5]arene 21

In order to achieve the aim of using functionalised P[5]As in sensors, fully esterified pillar[5]arene **21** was synthesised. It was chosen because of its extended ester functional groups that could have molecular recognition properties. Wen demonstrated that in the solid state molecules of **21** align to form tubes which absorb guest water molecules[101] and related ester functionalised pillarenes had shown activity as transmembrane channels for water and amino acids[171] thus it was expected that this compound could be used as a sensor modifier.

Compound **21** was synthesised by adapting the reported procedure[112] and was attempted several times, aiming to improve yield of the product (Scheme 34). The reaction was carried in two steps from **1**.

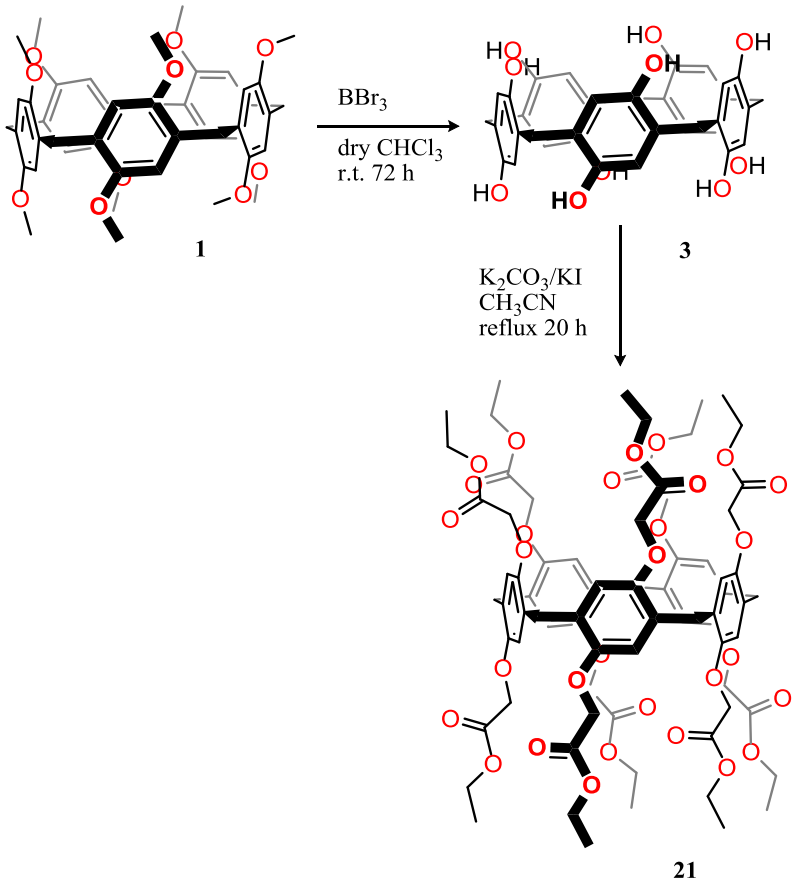

Scheme 33. Preparation of **21** from **1**.

In the first step, **1** was treated with BBr_3 in dry chloroform, resulting in a clear solution, and was stirred for 72 h. The reaction proceeds through a complex formed between the BBr_3 and **1** in which deprotection of methoxy substituents takes place. Mechanisms used to explain the demethylation by BBr_3 suggests that it coordinates to ethereal oxygens and promotes C-O bond cleavage to a methyl bromide and a methoxy borane that was hydrolysed to an alcohol during reaction. Upon addition of water to the reaction mixture a white suspension was observed; stirring for 24 h resulted in the formation of a white precipitate. During this process, the boronate ester hydrolyses to leave $B(OH)_3$ and HBr which are both water soluble.

The white precipitate was filtered and washed with HCl which afforded compound **3** in 90% yield as a white powder. Upon standing the colour changes to brown due to oxidation (Figure 43 (**A**)), so any subsequent reaction steps usually need to be carried immediately. However, this issue was addressed by the simple expedient of storing the compound under deionised water (Figure 43 (**B**)) immediately after

isolation renders the compound stable for several days.[171] Compound **3** was characterised by NMR and mass spectrometry. The ^{1}H NMR spectrum indicated the appearance of hydroxyl signal of proton, a singlet at 7.85 ppm, and the disappearance of the methoxy protons of **1**. The spectra were consistent with those reported previously.[69, 112]

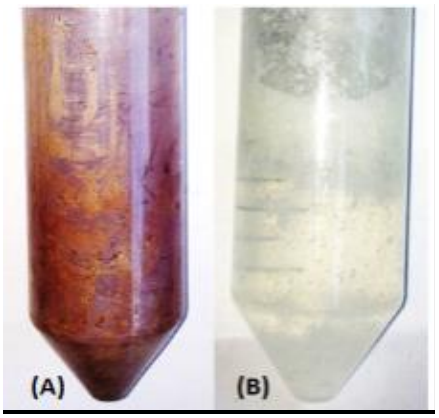

Figure 43. Compound **3** stored in absence (A) and presence of water (B).[171]

In the second step, **3** was dissolved in CH_3CN followed by addition of K_2CO_3. To the reaction mixture, excess ethyl bromoacetate was added slowly and the solution refluxed under nitrogen. In this reaction, ethyl bromoacetate and K_2CO_3 served as the alkylating agent and base respectively. As is clear from the X-ray structure of **3**, reported by Ogoshi,[69] the P[5]A phenolic units are able to freely rotate around the methylene bridges. Subsequent introduction of substituents at both rims inhibits the rotation of the phenolic units and immobilises the conformation. Once the first *O*-alkylation occurs the pseudo-D_5 conformation is restored. After cooling the reaction mixture, the product was filtered and CH_3CN removed by rotary evaporation. The resulting pale yellow oily solid was subjected to column chromatography; the second fraction to elute was recrystallised from acetone to give **21** as a white crystalline product.

Column chromatography could be avoided by careful recrystallisation from methanol and DCM. The crude product was dissolved in warm methanol and DCM was added to just dissolve the product before heating until the solution was just boiling. The hot solution was then allowed to cool to room temperature which gave

white solid which was filtered under vacuum and washed with methanol. The product was dried to give white crystalline ethyl ester, **21**, in 82% yield.[171] Thus, an alternative to column chromatography had been devised to purify **21**. The process was repeated several times ensure reproducibility. The purity of crystalline **21** was confirmed by melting point and NMR experiments. The sharp melting point was in the range of 196.2-196.9 ºC and is in agreement with literature reports.[69,112] Compound **21** was characterised using NMR which proved that peralkylation **3** had taken place to give **21.** Characteristic is the disappearance of hydroxyl signal of proton at 8.01 ppm and the appearance of substituent Ar-O-$CH_2C(O)OCH_2CH_3$ protons at 4.56, 4.09 and 0.99 ppm. ^1H and ^{13}C NMR spectra were consistent with those reported previously.[69,112]

2.4.4 Synthesis of 1,4-bis(thioethyoxy)copillar[4+1]arene 42

In order to achieve the aim of attaching thiol functionalised P[5]A to gold surfaces to study sensing properties, the dithiol functionalised copillar[4+1]arene **42** was synthesised.[168] It was selected because of the well-known affinity of sulfur for gold and the assumption that macrocycles that are covalently bound to gold electrodes will respond to electrical conductance changes upon guest binding.

Compound **42** seemed appropriate as only one of the aromatic rings would be involved in gold surface attachment while the remaining rings remain free to change conformation to optimise guest binding. Short linkers between the P[5]A and the terminal thiols were also required to bind the macrocycle close to the gold surface so that, in the case of electrochemical applications, the effect of guest inclusion could be transmitted directly to the electrode.

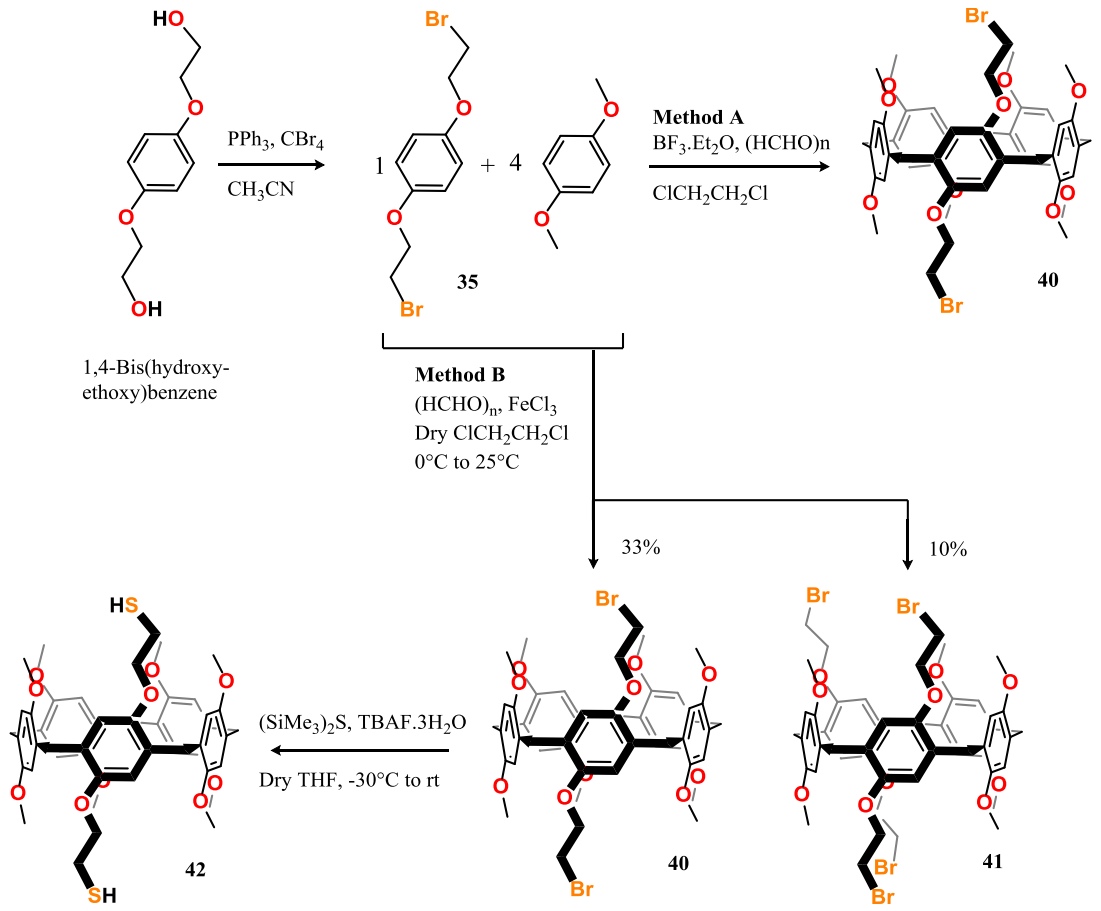

Scheme 34. Preparation of thiolated copillar[4+1]arene **42**.

By contrast, Zhou's[172] monothiol has a single four carbon spacer which allows the macrocycle to lie further from the metal surface. While this is ideal for the promotion of particle aggregation it is less amenable to guest detection by electrochemical methods. Dithiol **42** is a novel compound.[168] The first three reaction steps have been reported in literature but the novelty of **42** is the introduction of a dithol P[5]A derivative which could lie parallel to a gold surface (Scheme 35).

2.4.4.1 Synthesis of 1,4-bis(bromoethoxy)benzene 35

The first step of the reaction proceeds as reported by Huang.[100] 1,4-Bis(hydroxyethoxy)benzene was dissolved in CH_3CN then triphenylphosphine followed by carbon tetrabromide were slowly added in small portions. The reaction mixture was then left to warm to room temperature and the resulting clear solution was stirred for another 4 h followed by recrystallisation which afforded **35** in 80% yield. It was noticeable that both the yield and purity of the product were reduced if

powdered, rather than crystalline, 1,4-bis(hydroxyethoxy)benzene was used. The purity of crystalline **35** was confirmed by the melting point experiments which gave a range of 112.1-113.0 ºC and in agreement with literature reports.[100] Compound **35** was characterised using NMR. The ^{1}H NMR spectrum provided evidence that bromine had substituted for the hydroxyl groups due to the disappearance of the hydroxyl protons at *ca.* 4.90 ppm. NMR spectra and other data were consistent with those reported previously.[100]

2.4.4.2 Synthesis of 1,4-bis(bromoethyoxy)copillar[4+1]arene 40

1,4-Bis(bromoethyoxy)copillar[5]arene **40** was synthesised from **35** by methods A and B. In method A compound **40** was synthesised by the general method reported by Zhang and Yang in 19% yield[77] but with $BF_3{\cdot}O(C_2H_5)_2$ used using trifluoromethanesulfonic acid (TFMSA). The $BF_3{\cdot}O(C_2H_5)_2$ catalysed condensation reaction between 1,4-dimethoxybenzene and **35**, with 1 equivalent of compound **35** per 4 of 1,4-dimethoxybenzene, and freshly ground paraformaldehyde proceeded smoothly. $BF_3{\cdot}O(C_2H_5)_2$ was added by syringe to the other reagents and the heterogeneous mixture was stirred for 2 h. During this process, an observable colour changes from light to dark green. Upon completion, deionised water was added which resulted in milky white mixture. Solvents were removed under vacuum and the crude product extracted into DCM. The combined organic extracts were dried with anhydrous sodium sulfate and filtered. The filtrate was dried under vacuum which gave a pale yellow solid which was purified by flash column chromatography, from fractions that had an R_f of 0.8, to give a white crystalline product in 18% yield. This compares favourably with the 19% reported by Zhang and Yang for the **40** prepared with catalytic TFMSA.[77] The purity of crystalline **40** was confirmed by a melting point determination which gave a narrow range of 127.1-127.9 ºC. The ^{1}H NMR spectrum was more complex than that of parent **1**, with four aromatic proton singlets between 6.77 and 6.71 ppm and triplets at 4.05 and 3.43 ppm corresponding to –OCH_2 and –CH_2Br, respectively, was consistent with the literature report.[77]

Method B was that published by Meier.[173] The reaction of 1,4-dimethoxybenzene, **35** and freshly ground paraformaldehyde was catalysed by $FeCl_3$ but with 16 equivalents of **35** per equivalent of 1,4-dimethoxybenzene rather than the 4:1 ratio

used in method A. This reaction mixture was dissolved in CH_2Cl_2, cooled to 0°C and $FeCl_3$ added under nitrogen. As the mixture was stirred at 0°C an observable colour change to light green was noticed but the reaction mixture turned to dark green upon standing at room temperature. The reaction mixture was washed with water and saturated brine, dried over Na_2SO_4 and the resulting filtrate was dried under vacuum. The residue was purified by silica-gel flash column chromatography to give **40** and **41** as white solids in 33% and 10% yield, respectively. The formation of **41** in a reasonable yield was unexpected; using other literature reaction conditions mass spectrometric evidence for [4+1] and [3+2] regioisomers are observed but not for these conditions. Analytical data for **40** were consistent with those reported previously and from the sample prepared by method A.[77] The purity of crystalline **41** was confirmed by a sharp melting point between 140.1-140.8 °C. Compound **41** was synthesised for the first time and has been published.[168]

2.4.4.3 X-Ray crystallography of 40 and 41

Crystal data for **40**·DMF·0.5 H_2O: white block; $C_{50}H_{60}Br_2NO_{11.50}$; *Fw* = 1017.80; monoclinic, space group $P2_1/n$; unit cell dimensions: a = 11.956(2), b = 24.061(5), c = 16.901(3) Å, α = 90°, β = 93.72(3)°, γ = 90°; V = 4851.8(17) Å^3; Z = 4; D_c = 1.393 g cm^{-3}; T = 123 (2) K; μ = 1.732 mm^{-1}; θ-range for data collection 2.81-29.40°; 11517 measured reflections, 5887 independent reflections, 606 parameters, 0 restraints; $F(000)$ = 2112; final R-indices [$I > 2\sigma(I)$]: R_1 = 0.0750, $wR2$ = 0.1550, R-indices (all data): R_1 = 0.1663, $wR2$ = 0.2133; max. residual density 1.023 eÅ^3, and goodness-of-fit (F^2) = 1.023. CCDC: 1404413.

Single crystals of **40** and what was believed to be **41** were grown from solutions in DMF/methanol. The crystal structures were solved by direct methods and refined based on full-matrix least-squares methods on F^2 with SHELX-97.[174] All non-hydrogen atoms were refined with anisotropic displacement parameters, all hydrogen atoms with free positional parameters and isotropic displacement parameters. For **40**·DMF·0.5 H_2O the occupancies of the terminal bromine were refined to 0.921(2) for Br1 and 0.079(2) for Br1'.

The single crystal X-ray structure of **40** showed that it crystallises as the DMF solvate with a single solvent guest in the macrocyclic cavity. It is presumed that the water came from atmospheric moisture. The structure was solved in the $P2_1/n$ space group with one bromine atom disordered over two sites, with occupancies of 92% and 8%, and a water molecule modelled at 50% occupancy. Simple P[5]As crystallise out in racemic planar chiral forms and consequently the unit cell of **40** contains two molecules with *pS* and two with *pR* chirality. For simplicity, only the *pR* form is illustrated in Figure 44. Thermal ellipsoid plots were also used to interpret crystallographic results of **40** as shown in Figure 45 and show large ellipsoids for bromine and the oxygen in DMF.[168]

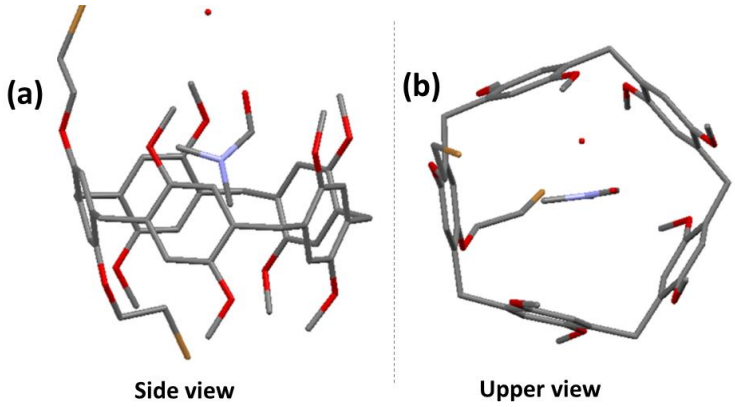

Figure 44. X-Ray structure of **40** DMF·0.5 H_2O (hydrogen atoms removed for clarity).[168]

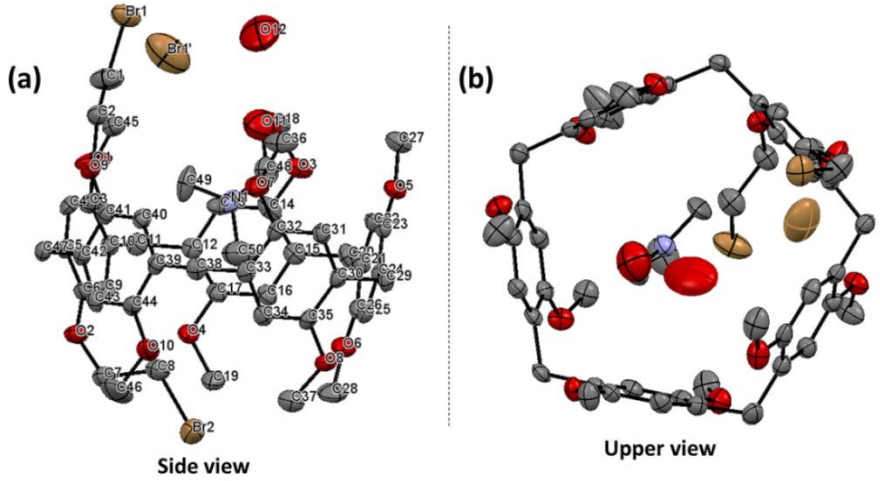

Figure 45. Thermal ellipsoid structures of compound 40; (a) and (b) side and upper view respectively (hydrogen atoms removed for clarity).

2.4.4.4 Co-crystallised copillar[5]arenes 40 and 41.

It was possible to demonstrate that **41**, synthesised using method B as detailed in Chapter 2, had ethoxybromide substituents on the alternate rings, rather than

adjacent rings, in agreement with NMR data. The structure of copillar[4+1]arene **41** was problematic to solve and could only be resolved as a 4:1 co-crystallised mixture of DMF and DMF·CH_2Cl_2. Appearance of CH_2Cl_2 solvent could be possibly due to mobile phase which was used in column chromatograaphy. Co-crystallisation is consistent with the appearance of both **40** and **41** (molecular structures shown in Figure 46) in the mass spectra for chromatographic fractions despite the fraction giving an apparent single spot by TLC with a single R_f value of 0.6. The X-ray data confirmed formation of co-crystals which explains the apparent contradiction of two derivatives with identical R_f values. The two compounds co-crystallise in a 4:1 ratio suggesting that they co-elute under the chromatographic conditions used. The quality of the single crystal X-ray diffraction data collected for co-crystal was limited due to poor crystal quality thus it was difficult to resolve the structure satisfactorily.

Crystal data for co-crystallised **40**·DMF·CH_2Cl_2 and **41**·DMF: white block; $C_{49}H_{54}Br_4O_{10}$ (0.75), $C_{47}H_{52}Br_2O_{10}$ (0.25), C_3H_7NO, CH_2Cl_2 (0.25); Fw = 1170.43; monoclinic, space group $P2_1/c$; unit cell dimensions: a = 18.987(4), b = 12.955(3), c = 21.903(4) Å, α = 90°, β = 103.27(3)°, γ = 90°; V = 5244.0(18) $Å^3$; Z = 4; D_c = 1.482 g cm^{-3}; T = 100 (2) K; μ = 2.773 mm^{-1}; θ-range for data collection 1.84-25.92°; 9965 measured reflections, 8409 independent reflections, 668 parameters, 48 restraints; F(000) = 2390; final R-indices [$I > 2\sigma(I)$]: R_1 = 0.0987, $wR2$ = 0.1187, R-indices (all data): R_1 = 0.2715, $wR2$ =0.3151; max. residual density 0.849 e$Å^3$, and goodness-of-fit (F^2) = 1.060.[168]

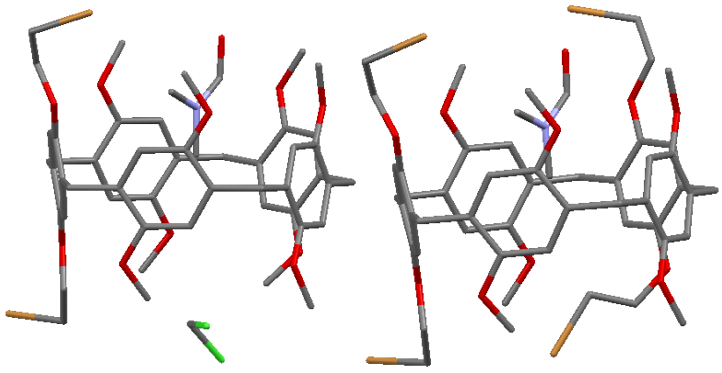

Figure 46. Molecular structures of copillar[5]arenes **40** (left) and **41** (right).[168]

2.4.5 Synthesis of 1,4-bis(thioethyoxy)copillar[4+1]arene 42

1,4-Bis(thioethyoxy)copillar[5]arene, **42**, was synthesised using the low temperature approach of Hu and Fox.[165] The reaction involves an activated thiol derivative and

subsequent deprotection step. In this reaction, **40** was dissolved in dry THF under nitrogen at -30°C using dry ice. To this, $(SiMe_3)_2S$ and tetrabutylammonium fluoride trihydrate were added which rapidly react to give tetrabutylammonium trimethylsilylthiolate, which in turn reacts with the alkyl bromides of **40**. During this step, the reaction mixture changed colour from pale yellow to light green before being stirred overnight and allowed to warm to room temperature. Solvent was evaporated and resultant organic layer dried with anhydrous Na_2SO_4 before being filtered. The solvent was removed by rotary evaporation to give the crude product as a pale yellow solid. Further recrystallisation was carried from methanol to give **42** as a yellowish white solid in 85% yield. Sample purity of crystalline **42** was indicated by its sharp melting point of 188.9-190.1 ºC. Compound **42** was initially characterised using ^{1}H NMR which showed a singlet at 3.77 ppm, corresponding to $ArCH_2Ar$ protons, two singlets at 3.65 and 3.63 ppm, corresponding to OCH_3 groups, triplets at 4.11 ppm, corresponding to $–CH_2O$ and multiplets at 1.44 ppm corresponding to CH_2SH. Compound **42** was synthesised for the first time and has been reported.[168]

2.4.6 Attempted synthesis of monoester copillar[4+1]arene 43

Derivative **43** was designed to have a single point of attachment to a surface. Unlike **42**, the cavity of this P[5]A would be expected to lie perpendicular, rather than parallel, to a surface. This would allow these two binding modes to be compared. Furthermore, it was decided to introduce a carboxylic acid, protected as the ethyl ester, to facilitate surface binding. Carboxylated P[5]As have been reported as capping agents for AuNPs,[112] but could also react with suitably protected cysteine to introduce both a sulfur for surface attachment and a carboxylic acid for guest recognition. As such, a Cys-P5A derivative would be able to bind biogenic amines whilst attached to a gold electrode. Precursor **37** was synthesised from 4-methoxyphenol by modification of the procedure reported by the Rangappa group.[167] After the work up, a solid was obtained which was further purified by recrystallisation with ethanol to give white crystals in 80% yield. Sample purity of crystalline **37** was indicated by its sharp melting point of 96.5–97.5 ºC. The compound was characterised using NMR and found to be consistent with data from the literature.[167]

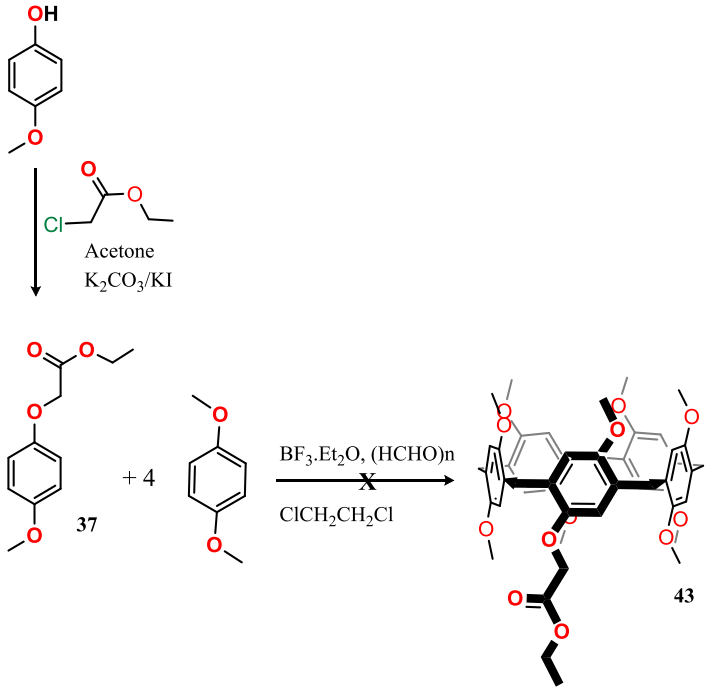

Scheme 35. Attempted preparation of copillar[4+1]arene **43**.

The synthesis of **43** was attempted through the $BF_3{\cdot}O(C_2H_5)_2$-catalysed condensation of **37**, 1,4-dimethoxybenzene (in a 1:4 molar ratio) with paraformaldehyde under nitrogen. During this process, an observable changes from light to dark green was noted as had been seen in previously successful co-condensation reactions but the crude product was difficult to separate using column chromatography and analysis by NMR was inconclusive (Scheme 36).

2.4.7 Synthesis of esterified copillar[4+1]arene 44

Despite the lack of success in preparing **43**, a cysteine-substituted copillar[4+1]arene was still of interest as a compound capable of being attached on to a gold electrode which would allow biogenic amine affinities and selectivities to be optimised through interactions with terminal carboxylic acids. Consequently a more symmetric copillar[5]arene was designed with esterified copillar[4+1]arene **44** as the key intermediate. The final cysteine-containing derivative was no longer required as **42** was found to discriminate between biogenic amines, however, the synthesis of **44** is reported here. Three further steps, ester cleavage followed by reaction with a suitably protected cysteine derivative and eventual de-protection, would yield the $(Cys)_2$-P5A derivative originally devised.

2.4.7.1 Synthesis of 6 from 1

In a method adapted from that reported by Chengyou[110] and Huang,[164] **1** and THF were mixed. To this solution, aqueous $(NH_4)_2[Ce(NO_3)_6]$ was added drop wise for 45 min. During this step, an observable change in colour from white to pale orange was noticed. The reaction mixture was left stirring for 24 h at room temperature before being washed with DCM, water and brine, and dried over anhydrous Na_2SO_4. The crude product was purified by column chromatography to give quinone **6** in 25%. It was challenging to purify **6** using column chromatography because of the poor separation with the R_f values of **1** and **6** found to be 0.7 and 0.6 respectively. To overcome this issue, two columns were used. In the first, unreacted **1** and product **6** were eluted as a mixture with petroleum ether/DCM. The second column gave desired pure red crystalline **6**. The purity of **6** was indicated by a narrow melting point range of 148.1-148.8 ºC, in agreement with the literature.[164] The ^{1}H NMR spectrum showed that partial oxidisation of **1** had given the desired product, **6**, as indicated by benzoquinone aromatic protons appearing at 6.84 ppm with those on the benzene rings next to the benzoquinone unit split into two singlets at 6.80 and 6.79 ppm. Bridging methylene protons were also split into two singlets at 3.78 and 3.59 ppm. The spectrum was consistent with that reported previously.[164]

2.4.7.2 Synthesis of 7 from 6

Compound **7** was prepared from **6** and using the literature method.[83] Methanolic $NaBH_4$ was added to a solution of quinone **6** in THF. The reaction mixture was stirred for 30 min at room temperature before being quenched by HCl. DCM was added and the two phase mixture washed with deionised water. The organic layer was dried over anhydrous Na_2SO_4 and filtered to give hydroquinone **7** as a white solid.

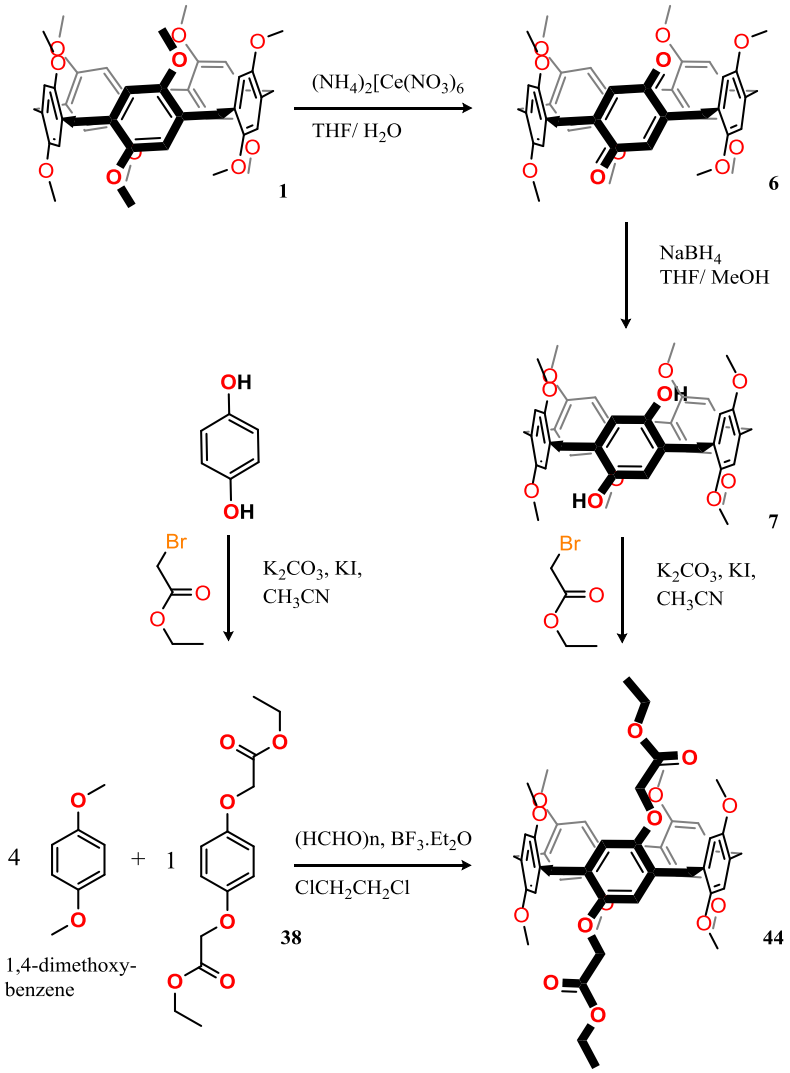

Scheme 36. Preparation of ester copillar[4+1]arene **44**.

Compound **7** undergoes oxidation quickly and it should be used without delay, however, storing under nitrogen appears to slow down the rate of oxidation. The purity of the crystalline **7** was indicated by the compound's sharp melting point of 173.1-174.6 ºC, in agreement with literature.[164] The ^{1}H NMR spectrum of **7** showed the reduction of **6** that gave the desired product, **7** as indicated by similar peaks to **6** except one new peak at 7.15 ppm corresponding to protons on the hydroxyl groups of the hydroquinone moiety. The spectrum was consistent with that reported in the literature.

2.4.7.3 Synthesis of 44 from 7

In an adaptation of the method reported by the Chengyou group,[110] ethyl bromoacetate was used as the alkylating agent instead of methyl chloroacetate. In

this method, **7** was dissolved in CH_3CN and ethyl bromoacetate and K_2CO_3 added. The reaction mixture was refluxed under nitrogen before being cooled, filtered and washed with chloroform. The filtrate was evaporated under vacuum and the residue dissolved in a mixture of methanol and chloroform to precipitate crystals. The crystals were then filtered and washed with methanol to give ester copillar[4+1]arene **44** in 91% yield. The ^{1}H NMR spectrum showed the characteristic disappearance of the hydroxyl signal of proton at 8.01 ppm and the appearance of peaks associated with two ethyl ester groups.

2.4.7.4 Synthesis of 44 from 38 (alternative method)

An alternative synthesis of compound **44** was attempted through direct cyclisation of 1,4-dimethxybenzene and **38**. The reaction conditions were optimised from the copillar[4+1]arene **40** method.[168] Precursor **38** was synthesised from hydroquinone by a modification of the procedure reported by Kyte where hydroquinone was dissolved in CH_3CN before K_2CO_3, KI and excess ethyl bromoacetate were added.[166] The reaction mixture was refluxed under nitrogen. The crude product was recrystallised from methanol to give **38** as a white crystalline product in 80% yield.

Compound **44** was synthesised through the $BF_3{\cdot}O(C_2H_5)_2$-catalysed condensation of **38**, 1,4-dimethoxybenzene (in a 1:4 molar ratio) with paraformaldehyde under nitrogen. As expected an observable colour change was observed. The challenge of this synthesis was formation of an apparently polymeric material which was difficult to extract. This issue was overcome by filtering the product on silica gel to give a light green crude solid which was purified by flash column chromatography. Fractions containing a single product at R_f of 0.7 were combined and solvent removed to afford **44** as a white crystalline product in 19% yield. Crystalline **44** had a slightly broad melting point range of 165.5-167.9 ºC, however, NMR did not indicate any impurities. The ^{1}H NMR spectrum of **44** gave four singlets between 7.48 and 6.93 ppm corresponding to the aromatic protons, a singlet at 4.77 ppm corresponding to Ar-OCH_2, a quartet at 3.36 ppm corresponding to the OCH_2 protons and the bridging methylene protons at 3.97 ppm, which confirmed successful cyclisation. The reaction was successful and this route has several advantages over

the first: it required just one step, consumes fewer reagents, is more economic and takes less time. However, the yield was low.

2.4.8 Conclusions

Most of the compounds required for the sensors were prepared successfully and, although they would have made an interesting comparison, the proposed cysteine-containing copillar[4+1]arene derivatives were eventually found to be unnecessary. Most of the cyclisation reactions took many attempts to optimise conditions, particularly with regard to chromatography solvents, but were ultimately successful in producing several novel copillar[4+1]arenes in good yields.

CHAPTER - III

Pillar[5]arene-based ion selective electrodes

3.1 Introduction

This chapter focuses on the synthesis and fabrication of sensors incorporating **1** and **21**. The P[5]As were incorporated into PVC membranes and used to detect both inorganics (alkali metals) and organics (biogenic amines) to assess the potential to detect host-guest interactions using electrochemical techniques.

Analytical potentiometry determines analyte concentration from the potential difference between reference and selective electrodes. ISEs are widely used in industrial and clinical applications due to their unique abilities to sense and react to changes in the activity of ions.[175,176] They are effective where an analytical technique is required which is selective, definitive, rapid and cheap. ISEs are used in the food industry to determine chloride and fluoride in milk,[121-177] sodium in smoked bacon[178] and sulfides in beer.[179] The main advantage of ISE over other methods is that they are not concerned by colour or turbidity of the compound to be analysed. In medical applications, ISEs are used for the everyday pH monitoring and determination of essential blood elements like Na^+, K^+ and Cl^-. Most biological fluids are intricate composites of ions in which their distribution may differ noticeably with respect to time. ISEs respond promptly to changes in ion activities and can alert clinicians to toxic levels of undesirable chemical species.

3.1.1 Ion selective electrodes (ISEs)

ISEs can be defined as electrochemical sensors that allow the potentiometric analysis of the activity of a chemical ionic species in the presence of other ions in solution. In the potentiometric determination of an analyte, the ISE reacts to ionic activity for which the logarithmic value is directly proportional to the electrical potential of its membrane measured corresponding to a reference electrode. ISEs have been used extensively for the past 30 years in various applications like metals and organic chemical sensing purposes in aqueous solutions. Chemical sensors for almost 60 different analytes have been reported by various polymeric based ISEs.[3,180]

3.1.1.1 ISE sensing components

ISEs are broadly divided into three types based on the membrane: glass, crystalline (or solid) and polymeric (or liquid). The most commonly known glass ISE is the glass pH electrode in which, the electrode is made of both glass and reference electrode fitted into one body. Solid or crystalline membrane ISEs are generally used in environmental control systems for metal ions like Cu^{2+}, Cd^{2+} and Ag^{+}. Although glass and crystalline membranes have great selectivity, a disadvantage is that they are used for specific ions only. A liquid or polymeric membrane is generally used to isolate solution mixtures containing a solution of interest from other test solution. Ion-selective membranes are made up of four components. The chemical sensor's characteristics are dependent on the nature and the amount of these components. Normally, the sensing membrane is made of 33% (w/w) polyvinyl chloride (PVC) as polymeric matrix, 66% plasticizer and 1% ionophore.[144] The plasticizer is used to homogenise the matrix. The four membrane components are:

- polymeric matrix
- plasticizer (membrane solvent)
- ionophore (membrane–active recognition)
- lipophilic additive salt (ionic additives)

PVC is most commonly used compound as the polymer matrix with Shatkay reporting the first use as a homogenous membrane in 1967.[181] The purpose of the PVC matrix is to give mechanical strength and structural integrity to the ISE membrane as the polymer matrix is not designed to be a chemically active compound.[181]

The plasticizer is one of the key components of ISE membrane and its purpose is to provide plasticity, turning the solid brittle plastic into a delicate flexible elastomer by decreasing the PVC glass transition temperature (Tg) below room temperature. Plasticizer components should be inactive and not form complexes with ions. The plasticizer together with polymer matrix provides a homogenous and miscible system in the ISE by dissolving the ionophore and lipophilic ionic supplements. The most well-known and commonly used plasticizers are adipates, phthalates, sebacates and phenyl ethers.[144]

The ionophore component is an active chemical species rich of electrons that can readily bind to particular ion. Ionophores can be charged or neutral macrocyclic compound which has cavities to circle the objective ions. The ionophore is responsible for the selectivity and sensitivity of the ISE which is dependent on the extent of binding between the ionophore and the ion of interest. Hence, the ionophore is one of the key ISE membrane components. The ions will be transported *via* an organic membrane by carrier translocation. Ionophore and target complexes are proportional to the affinity of the bonding. Therefore, in presence of counterions or interfering-ions, the ionophore and target ions complexation is not strong and are reversible.

Ionic additives are ion exchangers and the addition of lipophilic components to an ISE membrane will enhance the electrode response time, stability, reproducibility and selectivity. However, they will not be effective if the membrane does not have ionic sites because they will not react to the changes in concentration of the target ions. Most common examples of lipophilic additive salts are tetraphenyl borate and tetraalkyl ammonium salts for cation- and anion-selective electrodes respectively.

3.1.2 Function and construction of ISEs

An ISE is made up of a galvanic half-cell which contains an ion-selective membrane, an internal contacting solution or a solid contact and an internal reference electrode shown in Figure 47. The other half cell contains extraneous reference electrode. In the reference electrode setup, there is a salt bridge that will connect two half of the galvanic cells *via* form of an electrolyte. The detailed theory of ISE potentiometric technique has been described in Chapter 1.

In the ISE, the membrane containing the ionophore is in contact with the electrolyte solutions and can exchange ions selectively at the liquid or solution-membrane boundary. As a result, this will result in increase in the potential which is the fundamental step of how ISE functions.

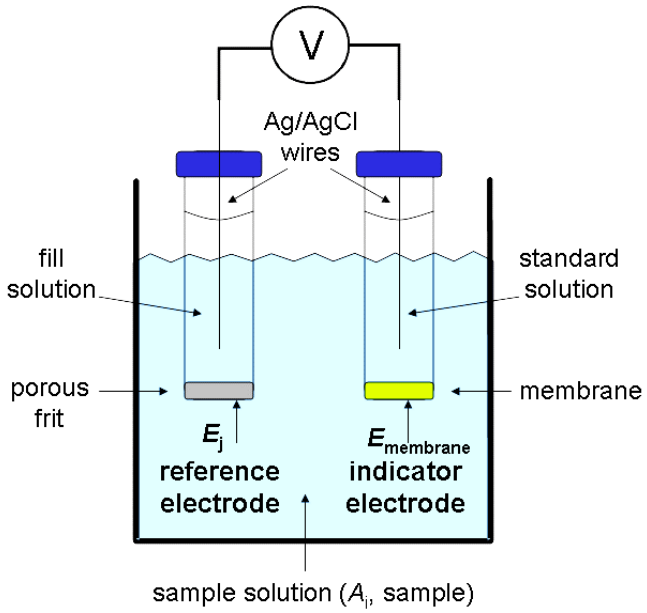

Figure 47. Typical ISE assembly for potentiometric measurements.

The changes in potential and the activity of ions in the solution in an ideal membrane scenario can be expressed by Nernst equation[129] and, for an ideal membrane, *S* is 59.16 mV dec^{-1}.

$$\mathbf{E_M} = \mathbf{Const} + \boldsymbol{S}\mathbf{ln}\,\boldsymbol{a_i} \qquad \textbf{(21)}$$

where, E_M is the membrane potential

a_i is the activity of the ion in solution, and

S is the response slope in mV dec^{-1}

3.2 Goal of the ISE research

ISEs have been used extensively in metal cation and organic chemical sensing in aqueous solutions. The polyamine content of food represents a useful indicator of spoilage, especially of meat and fish. Certain polyamines are hazardous to health because of their ability to react with nitrite to from carcinogenic nitrosamines.[182] Stoddart described inclusion properties of linear alkyl amines with P[5]A[73] which suggested the possibility that a P[5]A-based ISE could be used to detect biogenic amines.

3.3 Experimental Methods

3.3.1 Chemicals and Materials

All chemicals, solvents and reagents were purchased commercially and used without further purification. Compounds were synthesised according to the literature with amendments as described in Chapter 2. All compounds were characterised by NMR and mass spectrometry, as detailed in section 2.2, to confirm their identities through comparison with literature values. Dye experiments were performed by using an agarose gel membrane incorporating phenolphthalein. ISEs were manufactured according to the published procedure.[183] Electrolytes were prepared in the range of pH 0.5 to 7. Electrochemical data were collected with an Ag|AgCl reference electrode using CH instruments software. 0.05M Tris. HCl buffer solution prepared. Alkali and alkaline metal chlorides prepared with HPLC grade water. Electrochemical data were collected using CH Instruments' software and analysed using Igor (4.03 version) software.

3.3.2 Assessment of H^+ ions transportation of 21 using agar membrane

The H^+ ions transportation assessment was carried by an agar membrane experiment as shown in Figure 48.

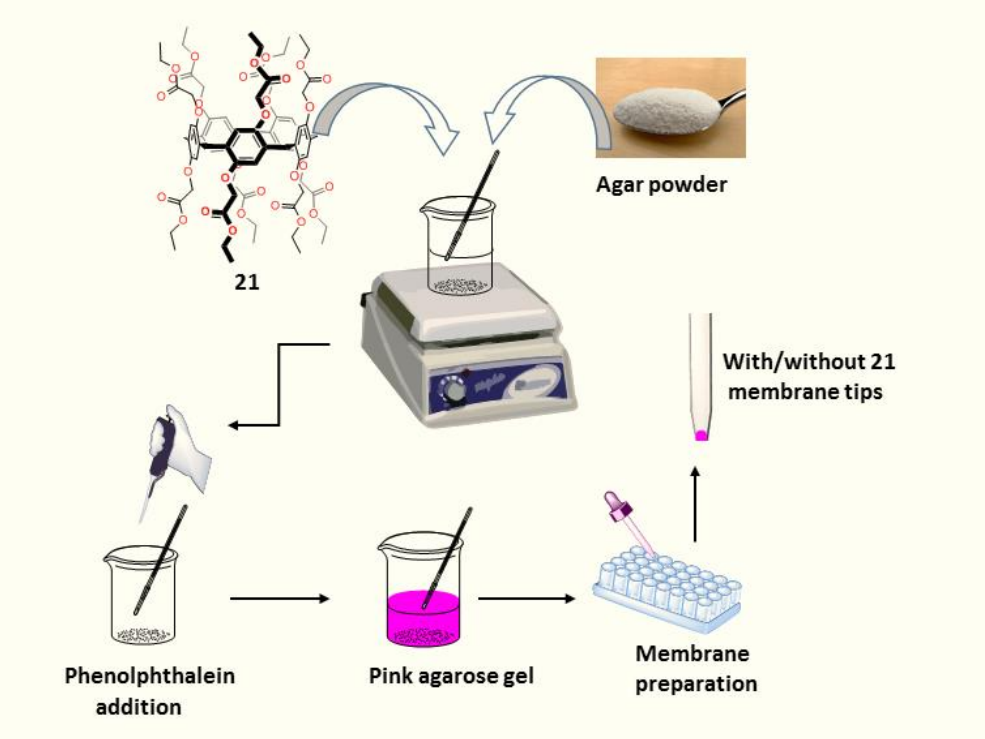

Figure 48. Fabrication of an agar indicator membrane incorporating **21.**

The agar membrane was prepared by adding 1% agar and 0.5% of **21** in water and boiling for 10 min. When solution was slightly warm, 1.25% phenolphthalein[184] by weight in 0.1 M sodium hydroxide was added and the resulting pink solution was thoroughly mixed. Clean pipettes tips (10 × 1 ml) were dipped in the pink solution and the outside surface of these tips were cleaned by wiping with tissue to remove any residual membrane solution (Figure 48). The tips were left vertical with the membrane side facing down. These set of tips were dried at room temperature for 2 h. Control membranes were prepared in similar way but omitting **21**. In a preliminary experiment, 0.1 M HCl was added to the upper surface of gels within the tips. These tips were then inserted in the 1M HCl (10 ml). The proton diffusion was compared with and without **21** membrane tips at 100 s time intervals.

3.3.3 Assessment of H^+ ions transportation of 21 using ISE

Assessment of H^+ ion transportation by **21** was divided into three phases as discussed below.

3.3.3.1 ISE fabrication (PVC-based ISE preparation)

ISEs were manufactured according to the published procedure.[183] Compound **21** or **1** (5 mg) was dissolved in THF (2.5 ml) to give a 2.0 mg ml^{-1} solution (A). Potassium tetrakis(4-chlorophenyl)borate (2.0 mg) was dissolved in THF (20 ml) to give a 0.1 mg/ml solution (B). Using a 200 µl micropipette, bis(2-ethylhexyl)sebacate (164 µl, 150 mg) and PVC (66 mg) were mixed to give (C). All vessels were sealed with SubaSeals (or placed in glass beakers with plastic lids that could be pierced with a needle) to avoid evaporation. THF (1 ml) was added to C followed by B (1 ml) and finally A (1 ml). This mixture was covered with Parafilm and stirred for 2 h before being left to evaporate in a fume hood until it had set as a transparent plastic membrane (12-24 h).

Table 5. Reagents for ISE preparation.

Solutions	**Container**
(A) 5.0 mg of (**x**) + 2.5 mL THF = [2.0 $mgml^{-1}$] (**x**) = **21** or **1**	Round bottomed flask
(B) 2.0 mg KTCIPB (borate) + 20 mL THF = [0.1 $mgml^{-1}$]	Round bottomed flask
(C) 66 mg PVC + 164 µL DOS (use a 200µL micropipette; equivalent to 150 mg of sebacate)	Glass beaker

THF (1ml) was added using a glass syringe to re-dissolve the dried membrane and the mixture stirred with a glass pipette until the polymer membrane completely dissolved (*ca*. 3-5 minutes). Using a new glass pipette, a drop of the membrane solution was transferred onto a clean glass slide to give a thin layer of the solution. One end of the micropipette tip electrode was dipped on to the drop quickly to form a thin membrane. The exterior of the electrode body was wiped with a tissue to remove any residual membrane solution. The electrode body was kept upright with the membrane side facing down. Cast membranes were left to dry overnight at room temperature**.**

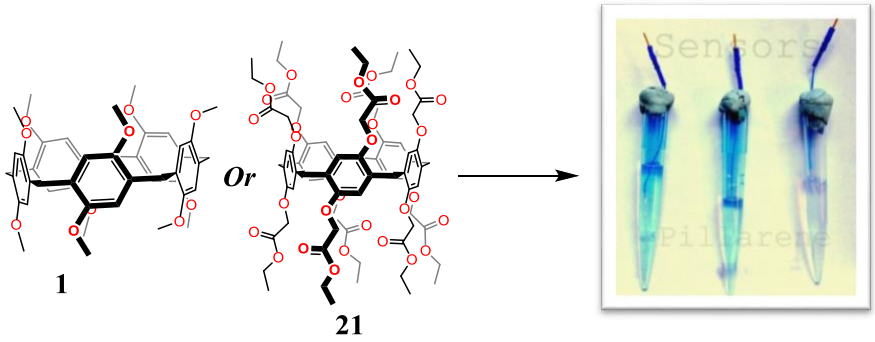

Figure 49. ISEs incorporating **1** and **21** separately (Ag|AgCl wire and suitable internal solution).[162]

3.3.3.2 Assembling the ISE

Silver wire was cleaned with ethanol and rinsed before being placed in a beaker with 3M KCl solution. A current of about 0.3 mA was applied for 15-20 seconds and a platinum counter electrode was used to complete the circuit. Chloridised (Ag|AgCl) wires were rinsed with deionised water and then with 0.1M KCl. The wire was inserted inside the electrode body and placed 5 mm from the membrane. The electrode body was threaded with connection wire inside Portex tubing (ensuring enough overlap between the silver and connection wire). To avoid inducing air bubbles, a small amount of glue was applied at the tubing interface and the wire was positioned as close to the membrane as possible. Excess glue was wiped off and the assembly left to dry with the membrane side down. ISEs were stored in same as internal solution such as 0.1M KCl, 0.1M ACSF at 4°C when not in use (Figure 50).

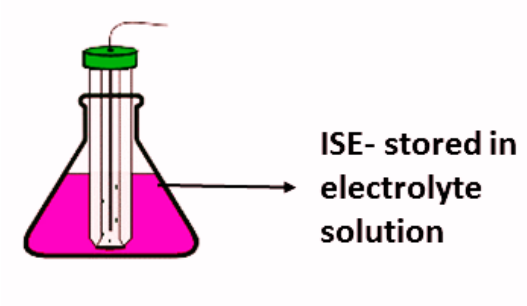

Figure 50. ISE storage.

3.3.3.3 Testing 21 ISEs for H^+ ion transport

The electrodes were rinsed in deionised water before each recording. Compound **21** ISEs were tested for their satiability and reproducibility for the potentiometric experiments over the range of pH. Five ISEs were selected and were used in the experiments. ISEs containing **21** were tested against range of 0.1M KCl solutions from pH 0.5 to 4.0 in steps of 0.5 pH units. Open circuit potential was monitored with Ag|AgCl as the reference electrode. The mean voltage observed during each pH range was recorded. All the potentiometric measurements were carried out under defined voltage/time parameters at room temperature.

3.3.4 Assessment of alkali metals using 1

Potentiometry measurements were carried out in 10 mM solutions of alkali and alkaline metal cations (Li^+, Na^+, K^+, Rb^+, Cs^+, Mg^{2+}, Ca^{2+}) and NH_4^+ prepared from their chloride salts. The electrochemical properties of the ISEs were investigated in the routine configuration. The measuring electrochemical cell containing **1** in the ion membrane selective electrode was filled with 0.1M ACSF for all ISE electrodes. This was used as the internal filling solution and Ag|AgCl as the reference electrode. About 10 ml of sample solution was placed in the cell with a syringe. The dynamic response curves were produced by adding standard solutions of analyte (0.1 M ACSF, pH 7.2). Measurable changes in concentration were obtained from concertation graph. All the potentiometric measurements were carried under defined voltage/time parameters at room temperature. Samples were prepared freshly using HPLC grade water.

3.3.5 Assessment of biogenic amines using 1

Potentiometry measurements were carried out in 1 mM solutions of biogenic amines (PA, PUT, SPD and SPR) which were prepared in fresh Tris HCl buffer (0.05 M, pH 7.2). The measuring electrochemical cell containing **1** incorporated in the ion membrane was filled with fresh Tris HCl buffer (0.05 M, pH 7.2). These were used as the internal filling solution. About 10 ml of the sample solution were placed in the cell with a syringe. Calibration plots were prepared and the alkyl amines were analysed in triplicate. The electrodes were rinsed with distilled water in each experiment. Four biogenic amines were analysed against the Ag|AgCl reference electrode. Tris HCl was used as background solution and the alkyl amine response was compared against it. The alkyl amine response was collected after a 100 s time lapse. A maximum recovery time of 200 s was allowed in each experiment. The dynamic response curves were produced by adding standard 0.05 M solutions of analyte at pH 7.2. Measurable changes in concentration were obtained from a concentration graph. All the potentiometric measurements were carried under defined voltage/time parameters at room temperature. Samples were prepared freshly using HPLC grade water.

3.4 Results and discussion

3.4.1 Inorganic and organic ion detection by pillar[5]arene ion selective electrodes

Potentiometric detection by a PVC-based electrode incorporating P[5]A derivatives was used to determine concentrations of protons, alkali metal cations and biogenic amines.

3.4.1.1 H^+ ion transportation of 21 in an agar membrane

Compound **21** was investigated for its ability to facilitate the transport of protons through an indicator agar gel matrix containing phenolphthalein. Proton diffusion was monitored over time (0 to 300 s) to determine the effect of the **21** at 100 s time intervals. The results were analysed with naked eye and photographs were collected (Figure 51). It can be noted that pink coloured **21** containing membrane at 0 s gradually turned to colourless at 300 s suggesting whereas, pink colour of the

control membrane faded relatively less. This suggested that the **21** had the ability to facilitate H^+ ion transfer.

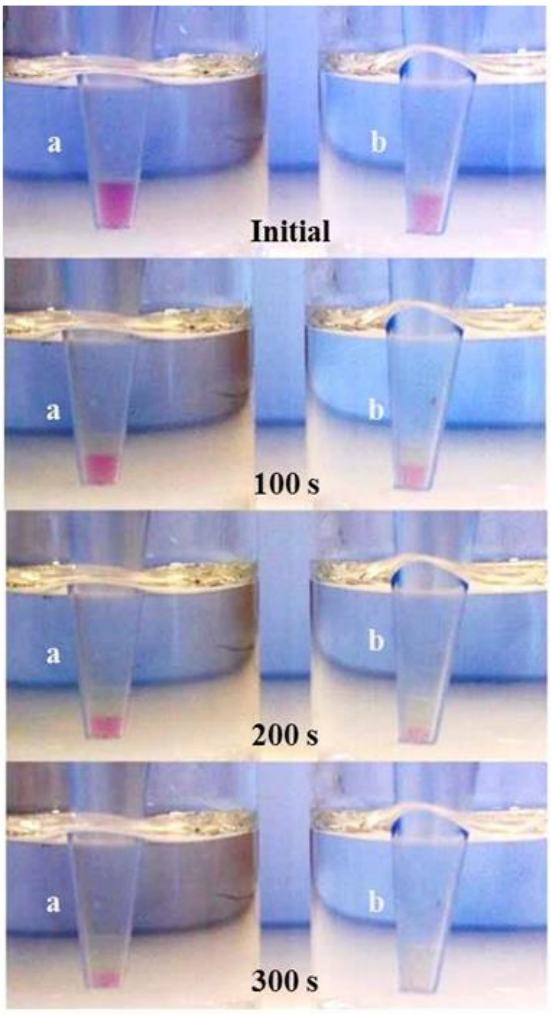

Figure 51. Response of the indicator agar to 0.1 M HCl from 0 to 300 s in the absence **(a)** and presence **(b)** of **21**.

The overall population data from multiple trials gave the time taken for the indicator to completely turn clear in the absence of **21** as 413 ± 69 s (n=16). Protonation of phenolphthalein was significantly faster when **21** was present ($p < 0.001$, t-test) as the time taken for the indicator to turn clear decreased to 289 ± 70 s (n=14) shown in Figure 52.

This behaviour indicates that **21** has the potential to facilitate the transport of protons when incorporated within an agar matrix.[171] Investigations were also carried out at 0.05 M and 0.01 M HCl, where similar results were observed in the presence of **21**.

Under both conditions the time taken for the indicator to decolourise was significantly greater than in those membranes where **21** was not present population data (mean ± S.D, n=6).

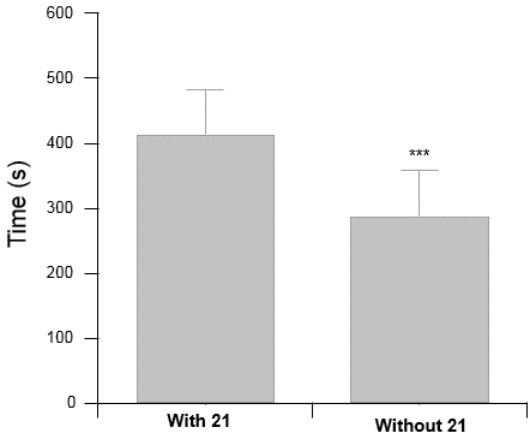

Figure 52. Time taken for the phenolphthalein indicator to turn clear in the absence and presence of **21**. Data shown as mean ± S.D, n=14-16, ***p<0.001.

3.4.1.2 Assessment of H^+ ion transport by 21 in an ISE

To further understand the role of **21** in transport of protons, an ISE incorporating **21** was fabricated in an analogous fashion to valinomicin-containing ISEs for K^+.[183] Measurements were made in solutions ranging from pH 1 to 4.

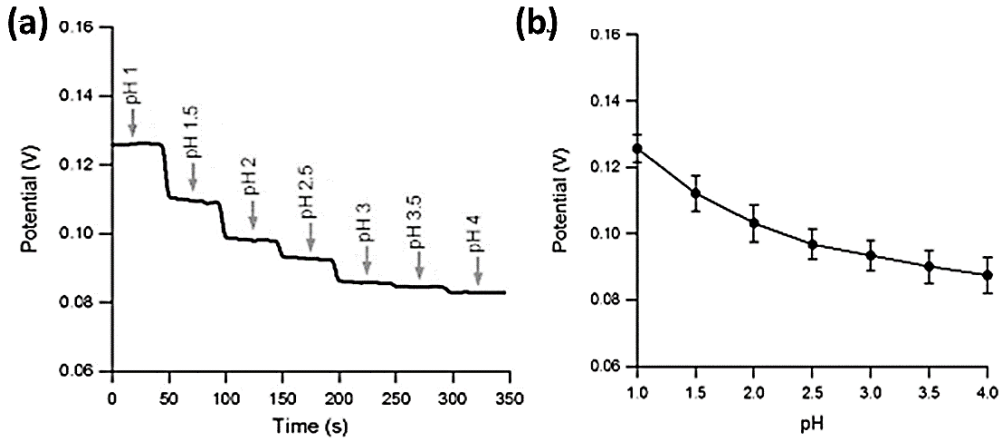

Figure 53. Non-linear response to pH observed for ISEs prepared with 15: **(a)** raw data and **(b)** population data (mean ± S.D, n = 5).[171]

In Figure 53 an experimental trace is shown for the ISE which exhibits a decrease in the open-circuit potential with decreasing pH. The electrode also shows minimal drift at each pH step, indicating good stability during measurements. The population

data from various ISEs are shown in Figure 53 which reveals a non-linear pH dependence. From these measurements it can also be shown that the variance in the response is limited indicating good reproducibility in electrode response.

In conventional electrochemical pH sensors the response to changes in analyte concentration is Nernstian, with a linear -59 mV per pH unit dependency, yet the data in Figure 53 are clearly non-Nernstian. While the reason for this is not clear, it may be due to a flux-dependent catalytic process.[185] Another feature of interest is that the time taken to respond to consecutive 0.5 pH unit increases appears almost the same from pH 1 to 3 implying that the response is concentration independent.

3.4.1.2.1 Electrochemical analysis

Five ISEs containing **21** were tested against range of 0.1 M KCl solutions from pH 0.5 to 4.0 in steps of 0.5 pH units with Ag|AgCl as the reference electrode. The mean voltage observed during each pH range was recorded. The values of sensor response over the pH range 1-4 are given in Table 6.

Table 6. Data for individual ISEs.

pH	Sensor response (mV)						
	ISE 1	**ISE 2**	**ISE 3**	**ISE 4**	**ISE 5**	**Mean**	**St. Dev.**
1	128.9	126.1	118	126	130	125.80	4.70
1.5	116	109.7	105	110	120	112.14	5.88
2	107.4	101.1	96.7	98	111	102.84	6.15
2.5	99.4	94.1	91.8	92.3	103	96.12	4.88
3	94	90.7	87.7	91	101	92.88	5.06
3.5	87	88.1	87.5	86	99	89.52	5.36
4	84	85	84.8	83	97	86.76	5.78

Note that if data from the best three ISEs are used the mean error drops from 5.40 to 2.05. Importantly, the errors at pH 3.5 and 4.0, where the potential difference is small, drop from ± 5.36 and ± 5.78 to ± 0.86 and ± 0.82, respectively; the differences in the data points then become statistically significant (Figure 54).

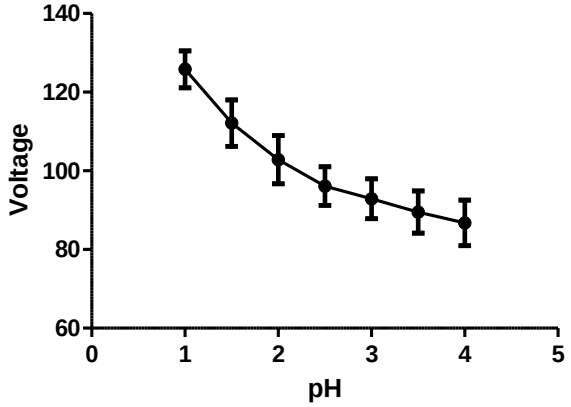

Figure 54. pH dependence fitted to a third order function ($y = -0.0014\ x^3 + 0.0151\ x^2 - 0.0584\ x + 0.1706$; $R^2 = 0.9997$).

3.4.1.3 Detection of potassium ions

There has been much recent interest in sensing materials for K^+-selective electrodes[136,186-188] It has been demonstrated that **1**, when incorporated within a graphite matrix performs well as a Na^+-selective modifier across the physiological concentration range.[107] Consequently, we wished to determine if given its ability to show sensing properties of **1** at the molecular level could be translated into a metal sensing device. The ionophoric properties of **1** towards alkali metal cations were assessed using potentiometry.

The electrochemical properties of the ion-selective electrodes were investigated in the routine configuration. The hydrophobic cavity of **1** contains ten oxygen atoms of which five are in upper rim and reaming five are in lower rim. In our previous studies, **1** was incorporated in graphite paste and was shown to have selectivity for clinically important Na^+.

ISEs containing **1** were prepared and 10 mM solutions of alkali metal (Li^+, Na^+, K^+, Rb^+ and Cs^+), alkaline earth metals (Mg^{2+} and Ca^{2+}) and NH_4^+ ions were analysed potentiometrically. All the potentiometric experiments were carried between -3 V and +3 V at room temperature. ISEs containing a non-cyclic P[5]A precursor, 1,4-dimethoxybenzene were used as controls.

K^+ was shown to have a significant response when compared to the other metal cations, and ammonium ions also gave a considerable response. Previous reports

gave similar results for valinomycin, crown[189] and calixarene derivatives.[190, 191] In the case of the valinomycin ISE, the selectivity order was; $H^+ > Rb^+ > K^+ > Cs^+ > Na^+$.[192] Incorporation of **1** into PVC membrane for the first time succeeded in showing lower pH detection range.[171]

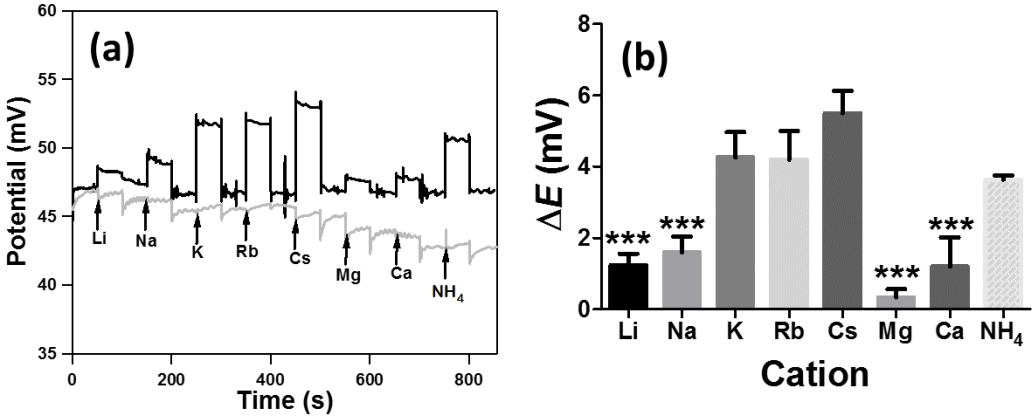

Figure 55. The potentiometric response **(a)** of ISEs containing **1** against monomer ISEs and (**b)** changes observed in the voltage response with **1** (data shown as mean ± st. dev., where ***p <0.05 vs K^+, Rb^+ and Cs^+. There is no significant difference between K^+, Rb^+ and Cs^+ when compared to Li^+. NH_4^+ has **p<0.05 vs Li^+ and a significant difference**.**

The results shown that the complexation and extraction of ion transport selectivity of ISEs containing **1** are in the decreasing order of: $Cs^+ \sim Rb^+ \sim K^+ > NH_4^+ > Na^+ > Li^+ > Mg^{2+} > Ca^{2+}$. The control experiments with the monomer gave no ion selectivity or transportation as shown in Figure 55 (a). Figure 55 (b) shows the significant difference in selectivity of metal ions with K^+, Rb^+ and Cs^+ ions giving similar responses. As the human body does not naturally contain Rb^+ and Cs^+ ion these are of no physiological importance so, under these conditions, ISEs containing **1** are K^+-selective. Conversely, graphite composite electrodes incorporating **1** and gold electrodes with **42** attached to the surface demonstrated selectivity towards Na^+ and Li^+ respectively as discussed in Chapters 4 and 5. The difference in the selectivity by the same macrocycle appears to be due to its arrangement in the three different types of sensors. In ISEs, the macrocycle integrates with PVC to make upper and lower rims readily available for complex formation and may have a little conformational freedom. In composite sensors, the macrocycle is held in a very rigid D_{5h} geometry so that the target analyte must be an ideal fit. In gold electrodes, one of the aromatic rings will be involved in surface attachment *via* its substituents leaving the remaining rings free to change conformation and accommodate ions such as Li^+

which may only bind two methoxy groups rather than five, as is likely for larger cations. Therefore, the nature of ion selectivity with the same macrocycle can be different depending on the type of electrode employed.

3.4.1.3.1 Dynamic range

The dynamic range defines the concentration limit of the ion for which the ISE will produce an analytically useful signal. All instrumental methods have a degree of noise associated with signal measurement that limits the amount of analyte that can be detected. This measurable change in response may be described as the lowest concentration level that can be determined to be statistically different from an analyte blank. The general limit of detection of an ISE in direct potentiometry is approximately 10^{-4} M of the analyte.

3.4.1.3.1.1 Potassium ion concertation response

Figure 56 (a) shows that the potential response of K^+ ions increases with the concentration of solution, however it can be seen that from 10^{-2} M data that the error in the signal is quite high. The potential data were obtained by increasing the K^+ concentration in steps from 10^{-6} M to 10^{-1} M at a constant time interval against a blank solution. The detection limit of K^+ ions was 10^{-3} M as shown in Figure 56 (b) as this concentration was statistically significant to the blank solution.

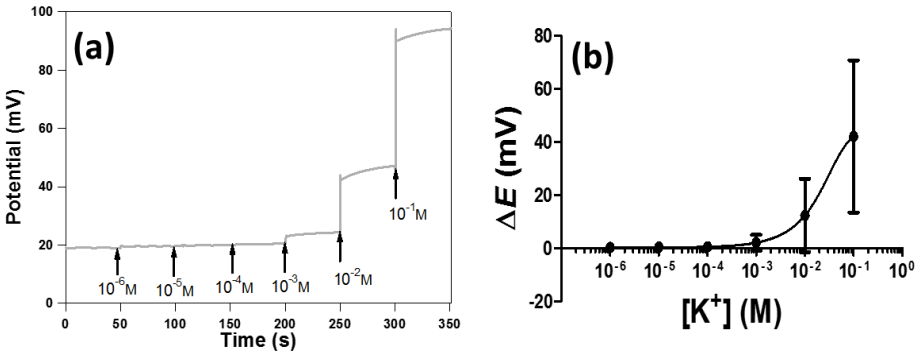

Figure 56. The concentration response **(a)** for K^+ based on ISEs containing **1** at pH 7.2 **(b)** The change in concertation limit determination for K^+.

3.4.1.4 Biogenic amine selectivity using 1

An ISE containing **1** was constructed in a similar manner to the P[5]A pH sensor[171] and was used for biogenic amine detection. Biogenic amine solutions (1 mM) were prepared freshly in Tris HCl buffer (0.05 M at pH 7.2). Pentylamine (PA)

demonstrated a greater response to the ISE when compared to di- and polyalkyl amines. Putrescine (PUT), spermidine (SPD) and spermine (SPR) has no response indicating that the polyamines may not be suitable for the transportation through the P[5]A cavity (Figure 57). This could be because of the competition among amine groups involved in the molecular interaction with oxygen atoms around the macrocycle.

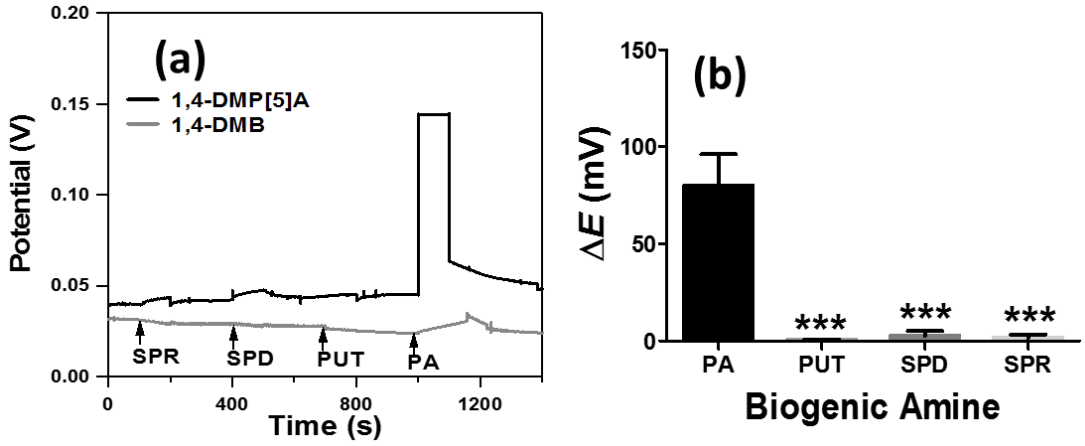

Figure 57. The potentiometric response **(a)** of ISEs containing **1** to the biogenic amines compared to control ISEs. Changes observed in the voltage response with **1** (data shown as mean ± st.dev., where ***$p < 0.05$ PAVs PUT, SPD and SPR. **(b)** There is no significant difference between PUT, SPD and SPR when compared to PA.

3.4.1.4.1 The pentylamine (PA) concentration response

Figure 58 (a) shows that the potential response of PA increases with the concentration of solution. The potential data were obtained by increasing PA concentration in steps from 10^{-6} M to 10^{-2} M at constant time interval against a blank solution. The detection limit of PA was 10^{-4} M as shown in Figure 58 (b) where the signal was determined to be statistically distinct against blank solution.

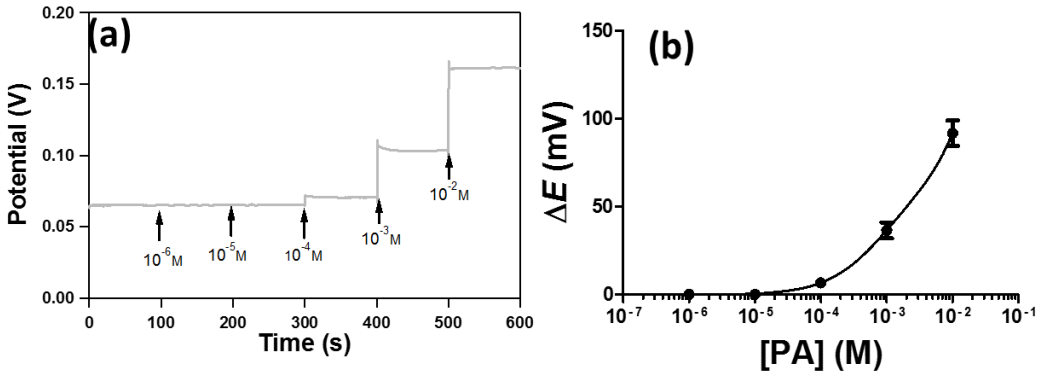

Figure 58. The concertation response **(a)** for pentylamine (PA) by ISEs containing **1** at pH 7.2 in 0.05 M Tris HCl solutions **(b)** The detection limit of 10^{-3} M for PA.

3.5 Conclusion

Compounds **1** and **21** have been successfully incorporated in PVC membranes to construct ISEs for proton, alkali metal cation and the biogenic amine detection. The hydrophobic cavities generated by the aromatic walls of benzene moieties are essential for analyte detection. ISEs containing **21** have been shown to promote molecular scale transport of protons through the macrocycle cavity in a nonlinear dependence between pH 1 to 4. Compound **1** has been shown to be an excellent host for primary alkylamines, specifically pentylamine, as well as for K^+.

CHAPTER - IV

Modification of graphite-epoxy electrodes with 1,4-dimethoxypillar[5]arene and its recognition of alkali metal cations

4.1 Introduction

This chapter is focused on carbon composite electrode fabrication with **1**. These graphite epoxy P[5]A composite electrodes were tested for the detection of both inorganics (alkali metals) and organics (biogenic amines) to assess host-guest molecular interactions using electrochemical techniques.

Carbon has been used in electrode manufacture due to its advantageous properties over other compounds such as electrical conductivity, chemical inertness and wide potential range.[193,194] Carbon forms such as graphite and carbon fibres are used extensively as the conductive phase in the composite electrodes applicable for electrochemical sensors.[195-197] In the development of sensor devices, the use of composite materials functioning through a conductive phase discharged within an insulating polymer has played a key role.[198-205] The fabrication of electrochemical sensors can be achieved by constructing electrodes using a combination of desired carbon phase and insulating matrix materials. The main advantage of using fabricated electrodes is that their surface can be easily renewed by polishing.[206]

New commercial carbon graphite materials research has led to considerable use of these carbon materials.[35,207-222] Most common composite electrodes are made of carbon, glassy carbon, graphite and binders like paraffin, epoxy resins, methacrylate, silicon, polyester and silica gel. In 1958 Adams first developed composite electrode conducting materials using carbon paste.[221] Since then, various procedures have been reported in developing a variety of carbon paste electrodes. In the work presented in this chapter, carbon paste electrodes were employed with graphite used in the composite electrodes.

4.1.1 Composite sensors and their characteristics

A composite material is made by combining two or more compounds together. Carbon paste electrodes (CPE) have been used in this work in which the carbon paste was made with graphite powder and epoxy resin as a binder. CPEs are the preferred type of composite electrode due to the material's adaptability to various chemical and biological applications. The insulating liquids in the composite electrodes must be insoluble in the solutions, possess low vapour pressure, be mechanically stable, have a long lifetime and be electrochemically inert when potential is applied in the studies of interest during voltammetric and amperometric applications. The most commonly used insulating liquids in CPEs are silicon oil, paraffin oil and tricresylphosphate. CPEs are favoured among composite electrodes because carbon paste is cheap and easily available. In organic and inorganic electrochemistry, the electrodes made in this way can form exceptionally selective sensors.[206, 223]

4.1.2 Chemically modified graphite – epoxy composite electrodes

Graphite is used as one of components in the composites because it exhibits good electrical conductivity, chemical inertness and has a wide potential range.[194] Graphite has multiple planar layers in which each layer is organised in a hexagonal lattice. The carbon atoms are arranged in the form of honeycomb where each lattice is offset by 0.142 nm with a 0.335 nm distance between the planes. The graphite-epoxy composite (GEC) composite electrodes have several advantages when compared to carbon paste composites as GECs are resistant to organic solvents. In amperometric studies, which may require regeneration of the electrodes surface by polishing, they give greater reproducibility.[206] Among various rigid composite combinations, graphite and epoxy resins are widely used in aqueous and nonaqueous media. GECs can be fabricated in ranges of shapes and sizes, allowing easy modifications to be made to the electrodes depending on their anticipated use, including flow-through, screen-printing and conventional moulding. GEC surfaces can be easily polished to make smooth surface thus making it possible to display the active chemical compound or material to be used in a new assessments or analysis. There are several advantages of the composite electrodes including flexibility in fabrication, geometry, use over a large pH range and range of solvents, good electric

conduction, stability, broad potential range and being economical compared to metallic or expensive diamond materials.[206]

4.1.3 Composite sensors in supramolecular chemistry

Chemically modified carbon paste electrodes have earned widening attention in supramolecular chemistry because of their potential use in variety of analyses. Early chemically modified electrode (CME) studies focused on metal analysis. CPEs, when modified with macrocycles such as cyclodextrins, calixarenes, crown ethers and cucurbit[8]urils produce functionalized electrodes with the analytically valuable functional groups attached to achieve selectivity and sensitivity. CPEs functionalised with calixarenes and their derivatives have had applications as electrochemical sensors for metal ions including Hg(II)[224] Cd(II)[225] and Cu(II) from tap water.[226]

Recently, CPE-functionalised sensor interest has moved to the analysis of organic compounds. These are of great importance in industrial and biological applications. The CPEs with macrocyclic compounds are used in the investigating electrochemical behaviour of organic compounds using voltammetric and impedance measurements.[223] CPEs modified by cucurbit[8]uril have been used in recognising phenols by capturing electrochemical response.[227] CMEs were used to determine vitamin riboflavin,[228] *p*-aminobenzoic acid[229] and ascorbic acid,[230] nicotinamide,[231] depending on the macrocyclic compounds.

4.2 Goal of the research

To an extension to the studies on P[5]A ISEs for biogenic amines, as discussed in Chapter 3, composite electrodes will be employed. Alkali metal cation detection has been chosen as one target and biogenic amines (PA, PUT, SPD and SPR) as another.

4.3 Experimental Methods

4.3.1 Chemical and Materials

All the reagents were of analytical grade and used without further purification, unless when specified. Compound **1** was prepared as described in Chapter 2, reprecipitated from $CHCl_3$:acetone (1:1 v/v) as a pale yellow powder then further purified by treatment with decolourising charcoal (50 mg per 1 g of **1**) in $CHCl_3$ (60

ml/g). Aqueous solutions of alkali metal cations (Li^+, Na^+, K^+, Rb^+, Cs^+) were prepared in deionised water from their respective PF_6^- salts (Sigma-Aldrich Co Ltd).

4.3.1.1 Apparatus

All voltammetric measurements were carried out using a CHI 1030 potentiostat (CH Instruments, Austin, TX) controlled with CH Instruments software. All electrochemical measurements were carried out using a three electrode system, consisting of an Ag|AgCl (3 M KCl) reference electrode, a platinum wire auxiliary electrode and a 3 mm graphite composite electrode with or without **1** as the working electrode. Scanning electron microscopy was performed in a Zeiss-DSM 940-A apparatus, operated at 5 kV, with different magnitudes. Buehler Isomet low speed sectioning saw.

4.4 Graphite composite electrodes incorporating 1

4.4.1 Fabrication of the graphite epoxy composite electrodes

Composite electrodes containing **1** were composed of 10% **1**, 30% graphite powder (Ultra F, Union Carbide) and 60% epoxy resin and monomer composite electrodes were composed of 10% 1,4-dimethoxybenzene, 30% of graphite and 60% epoxy resin (Robnor Resins Ltd) by mass. Graphite composite electrodes were composed of 30% graphite powder and 70% epoxy resin by mass. The components were mixed and cast in 3 mm (internal diameter) plastic tubes and left to set for 48 hours at 20-21°C. The resulting composites containing **1** and control graphite composites were cut into 2 mm thick slices using a diamond wafering blade attached to a Buehler Isomet low speed sectioning saw. Electrical contact was achieved using a wire connected to one side of the composite discs using silver-loaded epoxy resin (Circuit Works, RS Components, Corby, UK). The final electrodes were produced by encasing these entire constructs in epoxy resin and leaving them to set for 48 hours at 20 - 21°C shown in Figure 59. The electrodes were cut once again with the diamond wafer blade to expose a graphite composite disc electrode. The dimensions of the final electrodes disc were 1 mm in thickness and 3 mm in diameter. Prior to electrochemical studies, electrodes were polished with 1200 grit sandpaper.

Following this, electrodes were polished sequentially, 0.3µm and 0.05µm alumina slurry to reduce surface roughness.

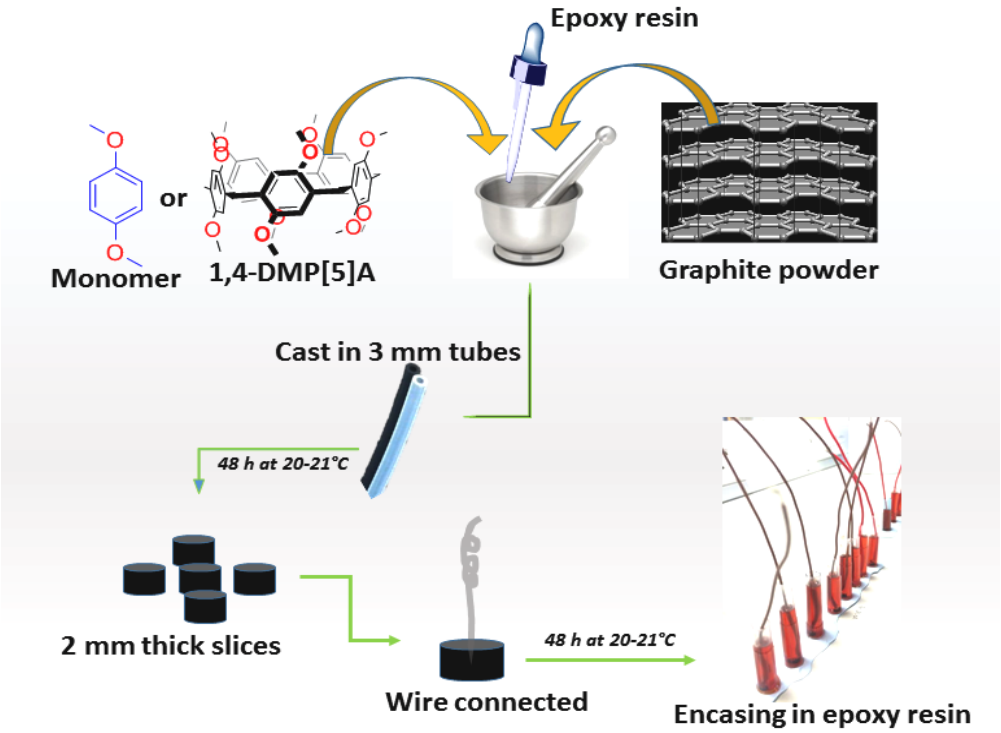

Figure 59. Schematic representation of fabrication of graphite composite electrodes with **1**.

4.4.2 Preparation of composite electrodes for SEM analysis

The composite electrode paste was filled in plastic tube (3mm diameter) and left for 48h at room temperature to solidify. After two days, the composite containing plastic tubes were sliced into 3mm sized pieces. Before SEM analysis, the electrodes were polished on (1200 grit) sandpaper, followed by 0.3 and 0.05µm alumina, cleaned thoroughly with methanol and HPLC grade water, and left to dry at room temperature. Later, composite electrodes were taken on to the platinum coated stab for the SEM analysis.

4.4.3 Computational methods

Computer simulations were carried out using Spartan.10,[232] installed on a desktop computer equipped with an Intel Core i7-2600 processor running at 3.40 GHz. Molecular mechanics energy minimisation methods (Merck Molecular Force Field) were used to optimise the geometries of the solvated cations (M^+ = Li^+, Na^+, K^+,

Rb^+, Cs^+), ligand **1** and solvated **1**·M^+ complexes. Thermodynamic data were calculated for these species following further geometry optimisation at the PM3 (tm)[232] semiempirical level in the gas phase. Structures were visualised using Mercury 3.0.[233]

4.4.4 Composite electrode application

Composite electrodes containing **1** were tested on both alkali metals (Li^+, Na^+, K^+, Rb^+ and Cs^+) and biogenic amines (PA, PUT, SPD and SPR) to see the behaviour of the macrocyclic composite electrodes with respect of its monomer as a control electrode.

4.4.4.1 Detecting alkali metal cations with composite electrodes

4.4.4.1.1 Assessment of selectivity and sensitivity of alkali metals

Prior to measurements in aqueous solutions containing the hexafluorophosphate salts of the target cations, the electrode conductive areas of the composite electrodes were assessed using the standard hexaammineruthenium(III) chloride (RuHex) redox couple in deionised water. Experiments were carried out between -0.5 to +0.1 V using a scan rate of 0.1 Vs^{-1}. For selectivity measurements, voltammetric scans were carried out in 10 mM solutions of alkali metal cations (Li^+, Na^+, K^+, Rb^+, Cs^+) prepared from their PF_6^- salts. Recordings were carried out between -0.3 and +0.3 V at a 0.1 Vs^{-1} scan rate. The electrodes were rinsed in deionised water between each recording. The change in the capacitive signal, measured as the difference in the current observed at 0 V over the scan rate, was monitored in order to measure the effect of the salts on the voltammetric response. For sensitivity recordings, calibration responses were recorded at concentrations of Na^+ and K^+ based on their range of clinical interest. Recordings were made at 0 V vs Ag|AgCl for 50 s on both control and graphite composite electrodes containing **1** at each concentration.

4.4.4.1.2 Reproducibility, stability and response time

Electrode reproducibility was assessed by comparing voltammetric data from six fabricated sensors containing 10% **1**, 30% graphite powder and 60% epoxy resin. Measurements were made in 10 mM Li^+, Na^+ and K^+ salt solutions and were carried out between -0.3 and +0.3 V at a 0.1 Vs^{-1} scan rate. The capacitance was measured

as the difference in the current observed at 0 V over the scan rate. The stability of the sensors containing **1** was assessed in the same manner using 10 mM Na^+ and K^+ salt solutions over a duration of seven days. To measure the response time, recordings were carried out at 0 V using amperometry. The sensors containing **1** were held in deionised water for 50 s and then placed in 10 mM solutions of either Na^+ or K^+ salts for 50 s. The sensor was then placed back in deionised water and the time required for the current to return to its baseline prior to cation measurements was recorded.

4.4.4.2 Detecting alkyl amines with composite electrodes

Biogenic amines were purchased from Sigma, UK. Four alkyl amines were selected to screen on composite electrodes containing **1** and control composite electrodes. Pentylamine**,** putrescine, spermidine and spermine (1 mM) were freshly prepared each time in aqueous solution.

4.4.4.2.1 Method for selectivity biogenic amines

Prior to measurements in aqueous solutions containing the hexafluorophosphate salts of the target cations, the electrode conductive areas of the composite electrodes were assessed using the standard hexaammineruthenium(III) chloride (RuHex) redox couple in deionised water. Experiments were carried out between -0.5 to +0.1 V using a scan rate of 0.1 Vs^{-1}. For selectivity measurements, voltammetric scans were carried out in 1 mM solutions of biogenic amines such as pentylamine, putrescine, spermidine and spermine freshly prepared in HPLC grade water. Recordings were carried out between -0.3 and +0.3 V at 0.1 Vs^{-1} scan rate. Composite electrodes incorporating **1** were used to assess the biogenic amines. 1,4-Dimethoxybenzene-containing and graphite composite electrodes were used for the control experiments. Electrodes were rinsed in deionised water between each recording. The change in the capacitive signal, measured as the difference in the current observed at 0 V over the scan rate, was monitored in order to measure the effect of the biogenic amines on the voltammetric response.

4.5 Results and Discussion

4.5.1 Graphite composite electrodes incorporating 1

4.5.1.1 Surface characterisation of the composite electrodes

SEM images of fractured surfaces of the composites were observed for the bulk distribution and the structure of the conductive carbon filler. SEM images can provide information about the structure and distribution of graphite particles in epoxy resin and for examining the morphology of the electrode surface.

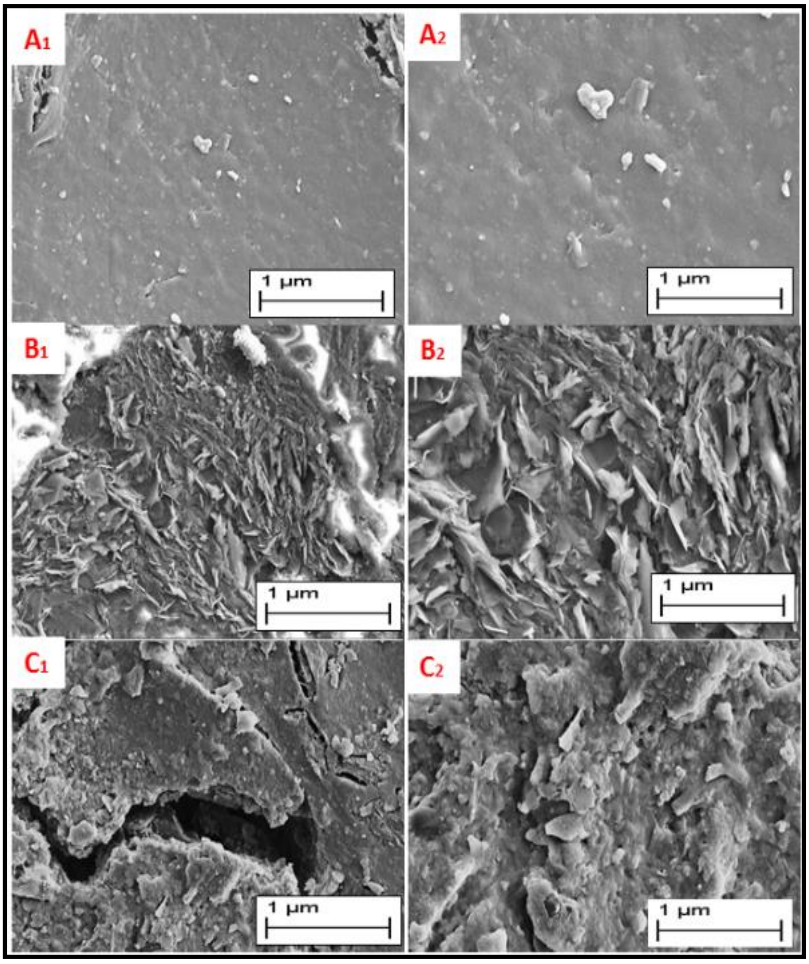

Figure 60. Scanning micrographs of graphite composite electrodes at different magnifications. (A1) graphite (30% + 70% epoxy resin) at (10k mag.), (B1) 1,4-dimethoxybenzene (monomer) (30%graphite + 10% monomer + 60% epoxy resin) at (10k mag.) and (C1) **1** (30% graphite + 10% **1** + 60% epoxy resin) at (10k mag.) (A2), (B2) and (C2) at 20k magnification.

Figure 60 shows scanning electron micrographs of a graphite composite electrode with **1** and a monomer composite electrode. The electrochemical performance of the composite electrodes is strongly affected by the presence of the modifier and its

chemical composition. From the SEM images, it can be seen that the graphite flakes are well distributed in both composite electrodes. However, some differences were noticed in case of the surfaces of composite electrodes incorporating **1** which exhibits roughness, some porosity and fractured surfaces**.**

4.5.1.2 Computational chemistry insights

Computational chemistry has advanced in recent years such that now relatively sophisticated simulations can be performed on desktop computers. This is of particular importance for host-guest systems where solvation, desolvation and an array of non-covalent interactions contribute to complexation.[234] Nevertheless it would appear that, despite advances in computer power, gaining accurate insights into supramolecular phenomena may be impossible. Fortunately it is possible to design computer models which provide useful information without having to optimise every interaction. For example, molecular mechanics methods are now so thoroughly parameterised, where ideal bond lengths and angles have been determined from vast test sets, that accurate structures can be created in seconds. Furthermore Sheehan has shown[235] that the effects of solvation and desolvation can be omitted with little effect on the accuracy of the resulting supramolecular complexes if they are modelled using the semiempirical PM3 (Parameterized Model number 3) model.[236] Consequently, 'gas phase' calculations, which do not consider the effects of solvent, can be carried out rapidly. While the electron density and thermodynamic data are generally less accurate than those calculated by *ab initio* methods, the simulations give a good indication of general trends.

Initially, molecular mechanics were used to determine, firstly, which alkali metal cations could fit within the P[5]A cavity. The widely used Merck Molecular Force Field generated structures of the 1:1 host:guest complexes with Li^+ through to Cs^+. From inspection (Figure 61) it was clear that Rb^+ and Cs^+ were too large to fit inside the macrocyclic cavity. It was noticeable that Li^+, preferring a tetrahedral coordination geometry, had perturbed the rings of the P[5]A. As the macrocycle had been immobilised in the carbon electrode without cations being present it would not be possible for the cation to induce this geometry. To investigate these complexes further they were modelled using PM3(tm), a variation of the semi-empirical PM3

method parameterised for transition metals and heavier *s*-block elements,[232] and their thermodynamic parameters calculated. For these calculations it was assumed that the following process occurred (equation 22).

$$\mathbf{1 + M^{+}(H_2O)_6 \rightarrow [1 \cdot M^{+}(H_2O)_2]\ 4\ H_2O} \qquad \mathbf{(22)}$$

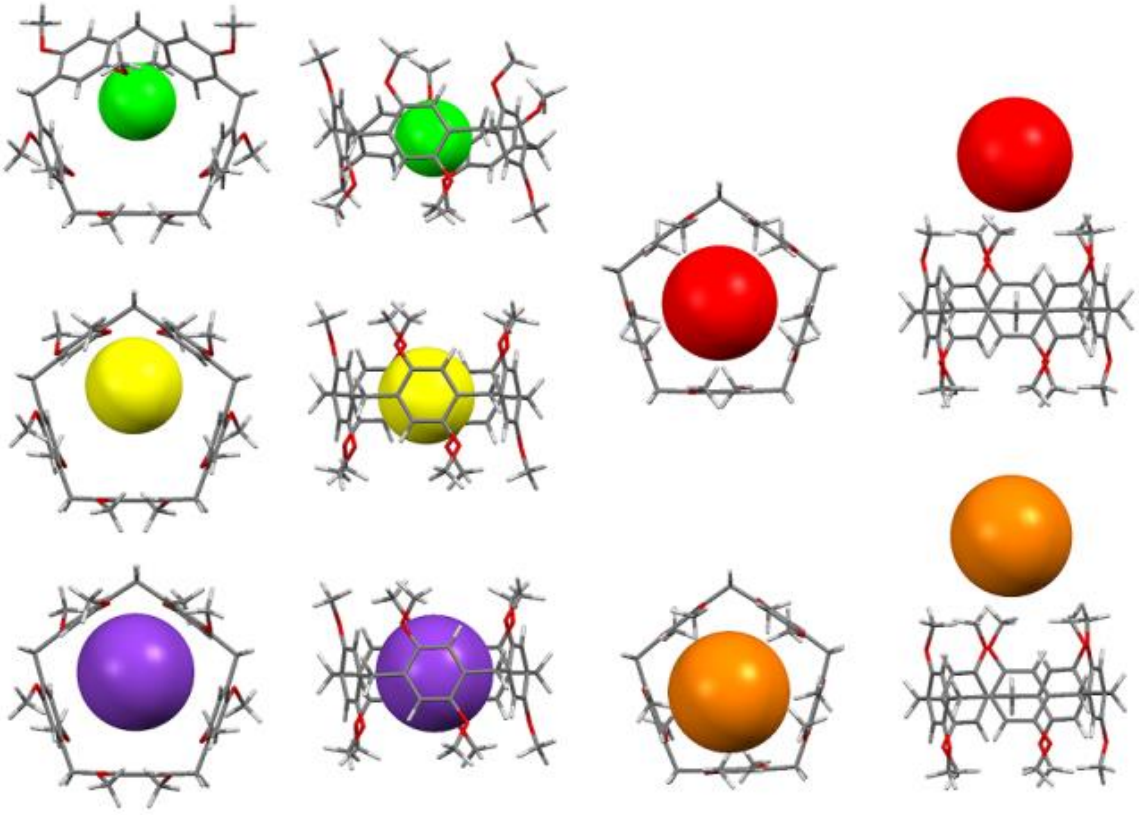

Figure 61. Top and side views of MMFF geometry optimised **1**·M^{+} complexes: (left, from top) Li^{+}, Na^{+}, K^{+}, (right, from top) Rb^{+}, Cs^{+}.

For the Li^{+} and Na^{+} systems it was assumed that only four of the six water molecules were ligated to the cation but the overall effect was the same. It was also assumed that two water molecules would coordinate axially to the cation as this has been observed by the Cragg group for an extended calix[4]arene complex with Na^{+}.[237] The overall Gibbs free energies for complex formation were calculated from equation 23:

$$\mathbf{G_{(complex)} - [G_{(host)} + G_{(guest)}]} \qquad \mathbf{(23)}$$

4.5.1.3 Computationally determined thermodynamics of binding

Molecular mechanics simulations described the simple size exclusion of Rb^+ and Cs^+ they did not adequately explain the differences in binding between Li^+, Na^+ and K^+ so simulations using the PM3(tm) model were undertaken.

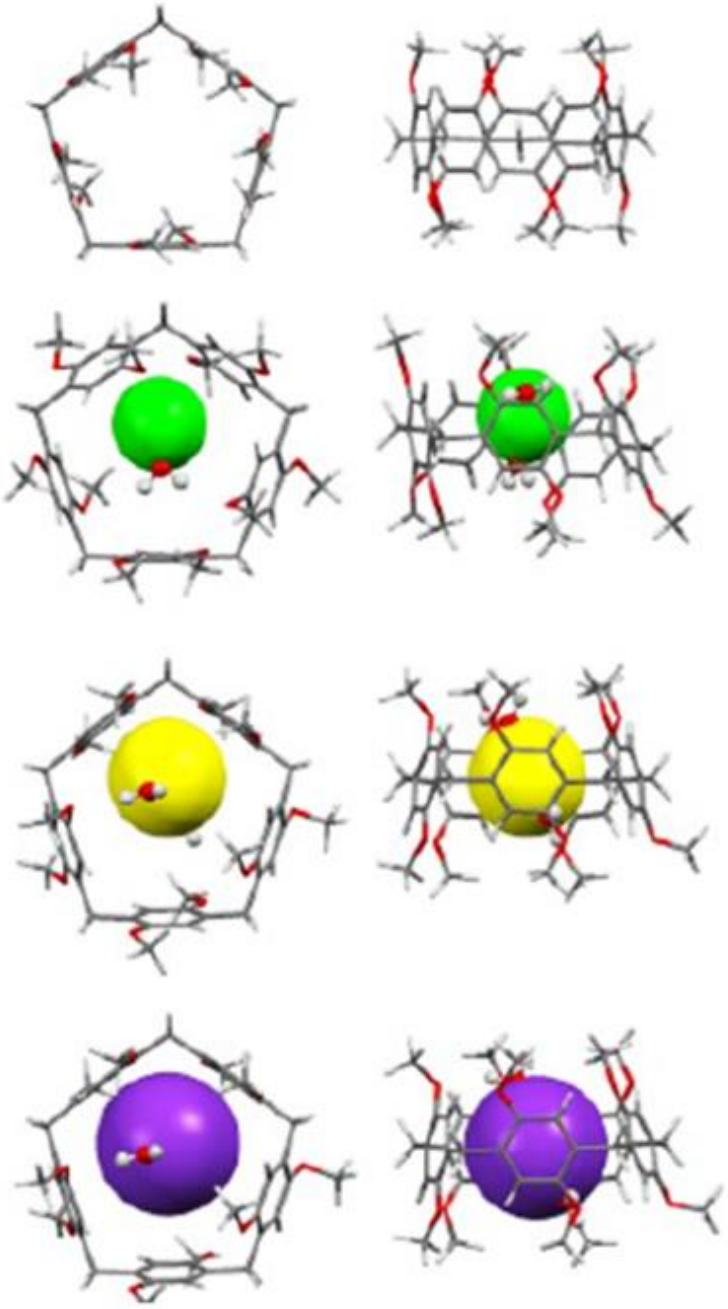

Figure 62. PM3 (tm) geometry optimised structures: (from top) **1**, [**1**·Li^+·2 H_2O], [**1**·Na^+·2 H_2O], [**1**·K^+·2 H_2O] (non-coordinated solvent removed for clarity).

To reflect the aqueous solutions used, the model included six water molecules which were allowed to coordinate to the cation. For Li^+ and Na^+ this resulted in four water molecules binding to the cation whereas in all other cases (K^+, Rb^+ and Cs^+)

octahedral coordination, incorporating all six water molecules, was observed. Binding affinities were determined by analysing thermodynamic data calculated for the hydrated cations, the free macrocycle and the hydrated macrocyclic-cation complex. Resulting structures for the Li^+, Na^+ and K^+ complexes are shown in Figure 62. Inspection of the geometry optimised structures shows that in each case two water molecules remain coordinated to the cation and all three complexes required changes from the geometry found for cation-free **1**. Analysis of the simulated thermodynamic data suggests (Table 7) that the Gibbs free energies of binding for the Li^+, Rb^+ and Cs^+ complexes would be unfavourable relative to the species existing as free macrocycles and their respective hydrated cations.

Table 7. PM3 (tm) determined thermodynamic data

	H° ($kJmol^{-1}$)	ΔH° ($kJmol^{-1}$)	G° ($kJmol^{-1}$)	ΔG° ($kJmol^{-1}$)
$Li(H_2O)_4 \cdot 2\ H_2O$	-120.664	-	-267.995	-
$Na(H_2O)_4 \cdot 2\ H_2O$	-28.126	-	-179.092	-
$K(H_2O)_6$	61.878	-	-102.162	-
$Rb(H_2O)_6$	208.691	-	57.224	-
$Cs(H_2O)_6$	208.986	-	55.809	-
1	3096.176	-	2817.418	-
[**1**·$Li(H_2O)_2$]·4 H_2O	2947.662	-27.85	2579.758	30.34
[**1**·$Na(H_2O)_2$]·4 H_2O	2960.509	-107.54	2598.334	-39.99
[**1**·$K(H_2O)_2$]·4 H_2O	3013.524	-144.53	2650.141	-65.12
1·Rb·6 H_2O	3276.824	-28.04	2911.768	37.13
1·Cs·6 H_2O	3258.195	-46.97	2894.873	21.65

A surprising feature was that K^+, which should only just fit in the macrocyclic cavity, was predicted to bind more strongly than Na^+ by 25 $kJmol^{-1}$, however, the route by which the cation enters the macrocyclic cavity has not been considered in this simulation. The route by which the cation enters the macrocyclic cavity has not been considered in the simulation. Binding of the larger cation may be impeded by the macrocycle's methyl substituents rotating to partially block entrance to the central cavity, the energetics of cation dehydration, displacement of encapsulated solvent or other phenomena, leading to the observed selectivity of Na^+ over K^+. The predicted binding affinity for K^+ over Na^+ does, however, reflect the observed difficulty with which the former is removed from the sensor containing **1**, as

discussed in 4.5.1.7 below. A similar observation was made by Gokel for hydraphiles involving 18-crown-6.[238] His explanation was that the size complementarity between K^+ and the macrocycle was so good that association was strong and dissociation slow whereas the poorer fit between Na^+ and 18-crown-6 meant that it could be bound only slightly less well than K^+ but released with much greater ease. The binding affinity of K^+ in ISEs using **1** was observed to be more selective than other alkali metals (discussed in 3.5.1.3) which is also in agreement with the results of these simulations.

4.5.1.4 Electrochemical behaviour of electrodes containing 1

The electrochemical behaviour of the composite electrodes was investigated. A ratio of 30:70 graphite to nonconductive elements was used as the mass ratio as this composition has been shown to have a good electrical conductance and low resistance.[205] The electrochemical behaviour of the control electrodes and those composed of 10% by mass of **1** was assessed using the standard redox couple of RuHex. There was a 3% variation in the faradaic current between the control composite electrode and those containing **1**. This response was utilised to normalise the response obtained from the cations to ensure the effects observed were not due to differences in the conductive area of the composite electrodes.

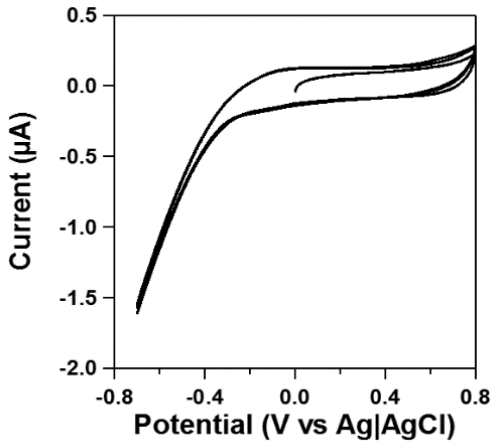

Figure 63. Voltammetric response of a graphite composite electrode containing **1** in deionised water.

The first concern with **1** was the possibility that the macrocycle could be electrochemically oxidised to the quinone or hydroquinone as *O*-alkylated pillar[*n*]arenes are known to undergo facile oxidation to the mono- or polyquinone species under mild chemical conditions. As shown in Figure 63, there was no

observed oxidation or reduction on the voltammatogram over the wide potential range investigated. A significant change in the current was observed at negative potential, however, this was due to the reduction of oxygen.

4.5.1.5 Effects of alkali metal cations on capacitive current

To investigate the effects of cations on capacitive current, a voltammetric response was obtained in an electrolyte-free solution to negate any influences from cation or anion interactions with **1** during voltammetric scans. Figure 64 (a) shows voltammetric scans in the presence of various cations, where the only differences in the capacitive signal were observed for Na^+ and K^+. However, some voltammetric features were observed in scans of Li^+, Na^+ and K^+, where an increase in the current was observed on the anodic sweep of the voltammogram. This decrease in potential was associated with the reduction of oxygen; interestingly this effect was not observed in Rb^+ and Cs^+. The overall alterations in the capacitive signal were measured at 0 V and the results are shown in Figure 64 (b).

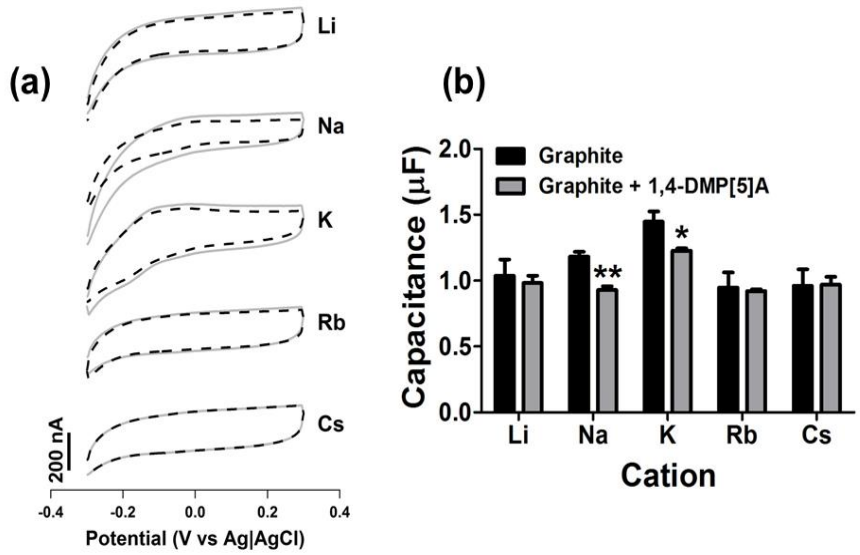

Figure 64. Capacitive responses of alkaline metal PF_6^- salts on 3 mm composite sensors: (a) voltammograms (0.1 Vs^{-1}) for electrodes with 10 mM Li^+, Na^+, K^+, Rb^+ and Cs^+ with (solid line) and without (dashed line) 1,4-DMP[5]A, (b) data comparison (mean ± s.d., n=3).

No significant differences were observed in the capacitive signal for Li^+, Rb^+ or Cs^+ on the control and the electrode containing **1**. The capacitive current for Na^+ decreased significantly from 1.18 ± 0.03 µF on the control electrode to 0.92 ± 0.03 µF on the electrode containing **1** ($p < 0.01$, $n = 3$). The capacitive current for K^+ also decreased significantly from 1.44 ± 0.08 µF on the control electrode to 1.22 ± 0.02

μF on the electrode containing **1** ($p < 0.01$, $n = 3$). This suggested that the capacitive current was reduced and potentially facilitated by **1** on the electrode. This could occur if the cations were bound by **1** and thus, during the establishment of the double layer, would not need to migrate towards the electrode surface. If Na^+ and K^+ were held on the electrode, the capacitive current would also allow the double layer to form more rapidly. The decrease in the capacitive current could also be explained by the effect of PF_6^- on the electrode surface but, as the same anion was utilised for all the cations studied, this can be ruled out as a reduction in the capacitance is only observed for the Na^+ and K^+ salts. Overall the electrochemical responses suggest that **1** has the potential to bind Na^+ and K^+ on the electrode and can provide a means to analytically detect these key clinical cations.

4.5.1.6 Sensitivity of electrodes containing 1

The sensitivity of sensors containing **1** to varying concentrations of Na^+ and K^+ salt solutions was assessed with a particular interest in detection across the physiological range of Na^+, 100 to 180 mM, and K^+, 1 to 10 mM. Experimental responses towards Na^+ are shown in Figure 65 (a), where clear stepwise reductions in the current were observed with each addition. Calibration responses of the sensors containing **1** and control graphite composite electrodes are shown in Figure 65 (b) and (c). A significant difference can be seen in the response of the sensor containing **1** towards Na^+ in the range 40 and 200 mM ($p < 0.001$, $n = 3$, Figure 65 (b)). There is a linear relationship between current and Na^+ cation concentration, with a sensitivity of 4.2 pA mM^{-1}, and a limit of detection (LOD, 3 x s.d. of the y intercept) of 40.81 mM. This is suitable to determine Na^+ at clinically relevant concentrations as the LOD is far below the lowest expected value. For the calibration of K^+, a linear relationship was also observed, where the sensitivity was slightly greater at 13.9 pA mM^{-1}. The limit of detection was 2.28 mM. Although this is adequate, it is above the lowest physiological concentration of K^+. Another concern is the response of the control sensor in the K^+ calibration (Figure 65 (c)). A significant difference in the current response between the control and sensor containing **1** was only observed at 10 ($p<0.05$, $n=3$) and 12 mM ($p<0.01$, $n=3$). Therefore, no detectable differences between the modified and control sensors were observed below 10 mM despite the limit of detection being lower. Overall the sensor containing **1** was capable of

monitoring Na^+ within the cations expected clinical range, but was not ideal for the detection of K^+ due to the small difference between the control and sensors containing **1** at concentrations of K^+ below 8 mM.

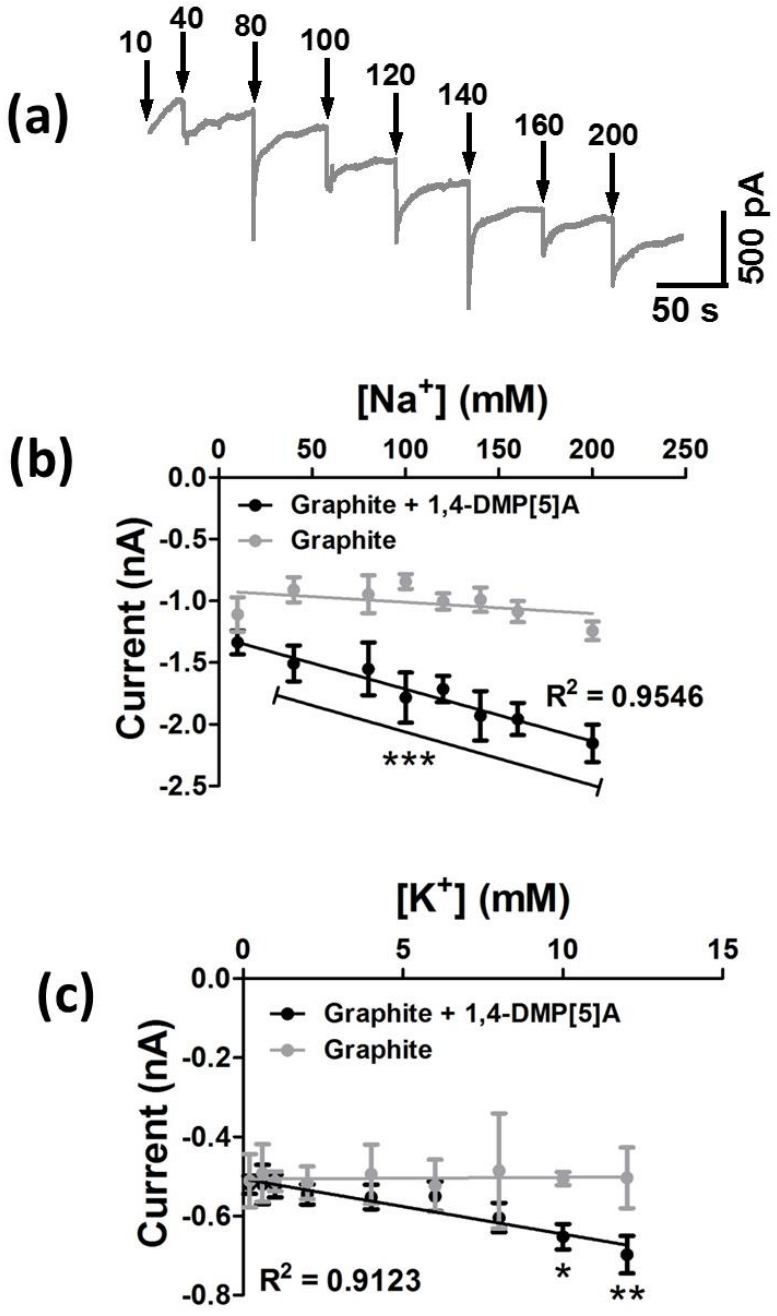

Figure 65. Calibration responses: (a) Clear stepwise reductions in the current with each addition (b) responses of the control and sensors containing 1 in varying concentrations of Na^+, (c) responses of the control and sensors containing **1** in varying concentrations of K^+ (mean ± s.d., n=3,*p<0.05, **p<0.01.

4.5.1.7 Reproducibility, stability and response time of sensors containing 1

After determining the selectivity for the electrodes towards Na^+ and K^+ salts, the analytical performance of the sensor was investigated further. First the reproducibility of the sensors was determined. Carbon composite sensors can suffer some variability in response, compared to solid state electrodes, as the inherent surface areas of the electrodes can vary during sensor production. Figure 66 (a) shows the mean response from six electrodes in their detection of Li^+, Na^+ and K^+ salts.

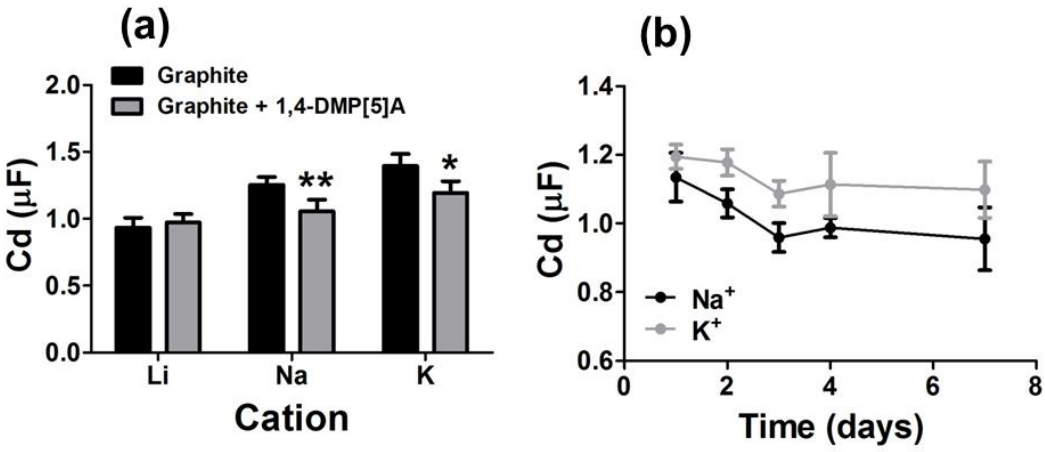

Figure 66. Reproducibility and stability of sensors containing **1**: (a) capacitive responses from various fabricated electrodes in 10 mM Li^+, Na^+ and K^+. (b) stability of the 1,4-DMP[5]A-containing electrode over seven days (mean ± s.d., n=6, *p<0.05 and **p<0.01).

Similar responses were observed, suggesting that the use of electrodes prepared in different batches does not account for the different voltammograms observed. More importantly, there was no difference in the variance between the control and sensors containing **1**. This indicates that the addition of **1** does not have a major impact in the sensor structure and available active surface area. The stability of the electrodes was assessed over a seven-day period. The electrodes were kept under normal laboratory conditions and evaluated in 10 mM Na^+ and K^+ salt solutions. Figure 66 (b) shows that the there was no significant difference in the stability of the sensors containing **1** (n = 6), however, there is an increase in the variation of the response with increasing time. This suggests that sensor performance, or their potential to regenerate over time, is limited. The response time of the sensor was investigated to understand if cation binding to the electrodes containing **1** could be reversed to restore the sensor to its initial state.

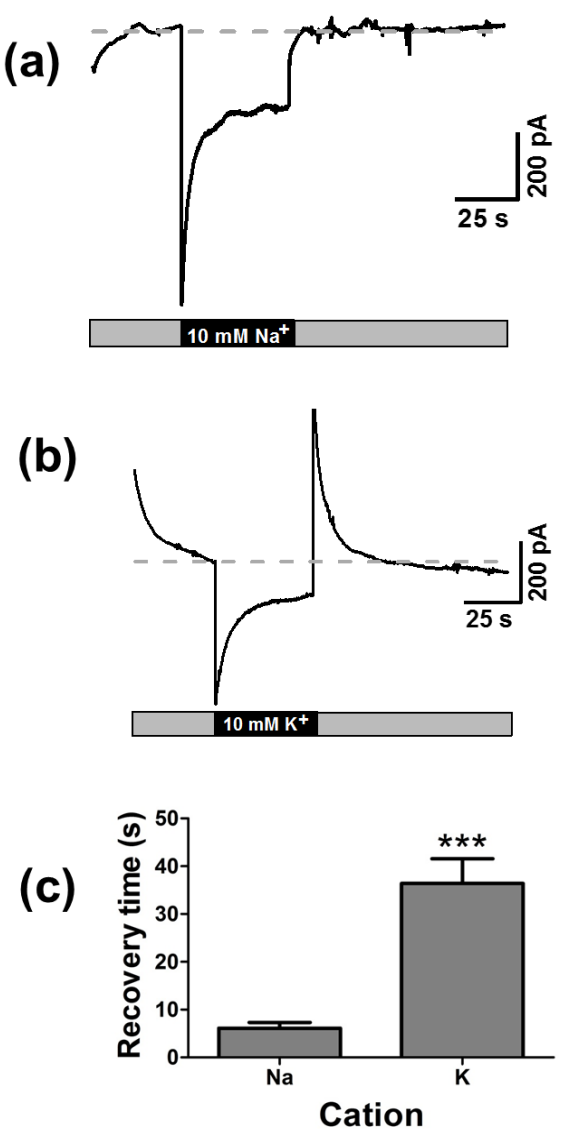

Figure 67. Recovery time of the 1,4-DMP[5]A-containing graphite composite sensors: (a) experimental trace of sensors containing 1 exposed to 10 mM Na^+, (b) experimental trace of sensors containing **1** exposed to 10 mM K^+, **(c)** data comparison (mean ± s.d., n=3, ***p<0.001).

Figure 67 shows the response of electrode stability. The representative traces in Figure 67 (a) and (b) show a decrease in the current when sensors were exposed to either 10 mM Na^+ or K^+ salt solutions but clear differences in their ability to recover to baseline were evident. Figure 67 (c) shows that the recovery time was significantly greater when the sensor was exposed to K^+, *ca*. 36 s, compared to Na^+, *ca*. 6 s, ($p < 0.001$, $n = 5$). The increase in recovery time for K^+ is likely to be related to a stronger binding affinity of **1** for K^+ than for Na^+. Consequently it takes much longer for K^+ to leach back into deionised water than for Na^+.

4.5.2 Effects of biogenic amines on capacitive current

The overall alterations in the capacitive signal were measured at 0 V. Figure 68 (b) shows voltammetric scans in the presence of biogenic amines where the only differences in the capacitive signal were observed between monomer composite electrodes and composite electrodes with **1**. Low capacitance was observed in composites with **1** when compared to graphite and monomer composites as shown in Figure 68 (c). The capacitance signal is less for all biogenic amines when compared to graphite, this provides evidence for the host–guest interactions but no selectivity was observed. Furthermore, the significant difference in capacitance was not observed among biogenic amines. Although there was no significant differences in capacitive signal among four biogenic amines against the graphite control, SPD (*P<0.01, n = 3) and SPR signals were slightly less when compares to PA and PUT.

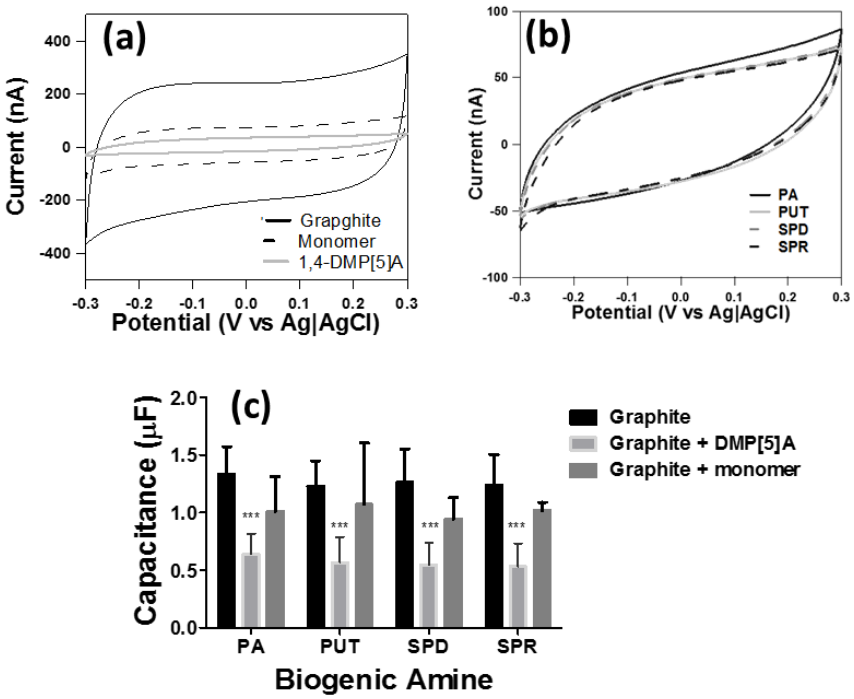

Figure 68. Capacitive responses of biogenic amines on 3 mm composite sensors: (a) voltammograms (0.1 Vs^{-1}) for graphite, **1** and monomer composite electrodes with SPD (b) voltammograms (0.1 Vs^{-1}) for composite electrodes containing **1** with (PA, PUT, SPD and SPR (c) The capacitance data comparison (graphite + **1** mean ± s.d., n = 3, ****p < 0.0001).

4.6 Conclusion

The first electrochemical study on alkali metal cations binding to **1** has been undertaken and showed the macrocycle to be electrochemically stable with respect to oxidation and also to respond to Na^+ and K^+, both of which are important electrolytes

to monitor in clinical and environmental settings. No significant differences were observed in the capacitive signal for Li^+, Rb^+ or Cs^+ on either the control or electrodes containing **1** but the capacitive current of the latter decreased significantly in the presence of Na^+, from 1.18 ± 0.03 μF (control) to 0.92 ± 0.03 μF (with **1**), and K^+, from 1.44 ± 0.08 μF to 1.22 ± 0.02 μF. The anion, PF_6^-, was common to all experiments and was therefore not responsible for the electrochemical activity. Reproducibility of the data acquired from sensors was high and no loss of stability of the sensors incorporating **1** was observed over a seven-day period. The recovery time of the sensors incorporating **1** following exposure to Na^+ was significantly greater than that of K^+, indicating the differences in binding affinities. Finally, the sensor incorporating **1** was able to detect Na^+ concentrations in the physiological range, whereas this was not possible for K^+. Computational models gave insights into the binding preferences observed and indicated that complexation of Li^+, Rb^+ and Cs^+ is disfavoured on thermodynamic grounds. A higher binding affinity for K^+ over Na^+, consistent with a longer sensor recovery time, was predicted by the theoretical model. Further optimisation of electrode composition is ongoing with the intent to develop a Na^+ selective electrode, based on the easily prepared macrocycle **1**, for use in electrochemical sensors. No significant difference in capacitance was observed among biogenic amines hence the selectivity of biogenic amines was not observed.

CHAPTER – V

Synthesis and self-assembled monolayers of copillar[4+1]arene dithiols

5.1 Introduction

The focus of this chapter is the synthesis of a thiolated P[5]A and the fabrication of gold sensors and to assess its affinity towards alkali metals and selected biogenic amines.

Using supramolecular chemistry as a tool for the recognition was first considered in the late 1960s.[45] Tremendous progress has since been made in cation recognition in supramolecular chemistry using a vast range of cyclic compounds and other receptors. The sensing capability of molecular and ionic receptors using supramolecular principles has resulted in applications from biological processes and food chemistry to environmental monitoring and medical diagnostics. In electrochemical research, for the past 15 years' extensive research has been carried out on electrodes covered with organised monolayers of supramolecular assemblies. These assemblies have given researchers in supramolecular chemistry remarkable insights into molecular processes at the electrode-solution interface. Organised monolayer assemblies on electrode surfaces can be prepared by various methods, of which the most well-known Langmuir-Blodgett technique depends on forced mechanical organisation of the compounds at the air-water interface.[239] Due to the high number of weak or moderate interactions, self-assembly will spontaneously produce organised interfacial structures.

Self-assembled monolayers (SAMs) were first reported in 1991 and, in the present era, they have become one of the important aspects of material science. Some of the most well-known SAMs are silanes on silicon surfaces,[240] sulfur-containing molecules on gold[12,241,242] and carboxylic acids on metal oxides.[243] Organosulfur SAMs on gold surfaces can be achieved by adsorption of thiol, thioether, disulfide, or thioctic ester derivatives and are especially useful due to their greater level of structural organisation, ease of preparation and specific terminal functionalities

which can be located at the surface of a monolayer. SAMs made of host molecules for molecular recognition on the monolayer have been prepared in highly efficient ways.[244] Well-organised and densely arranged SAMs afford a prearranged molecular sensing system. In aqueous environments, Immobilisation of receptors onto the surface of the electrode will promote sensing anions. SAMs together with molecular recognition factors produce an excellent tool to monitor the sensing mechanism at the monolayer interface.[245]

5.2 Self-assembled monolayers

SAMs can be described as a layer of molecules that spontaneously organise themselves into a distinct and reproducible monolayer at the interface between two phases. The whole process of SAM formation is directed by minimisation of the interaction energy between the molecules. SAMs are significant as a method to functionalise the surface of an electrode and are thus able to achieve specific chemical or physical properties thereby broadening the field of application. Langmuir and Blodgett first carried out studies on molecular monolayer films, subsequently named Langmuir-Blodgett films, in the 1930's.[246,247] These films contain amphiphilic molecules which were transferred from liquid to solid surfaces. For this work Langmuir was awarded the Nobel Prize in 1932.[248] In 1946, Zisman first reported a SAM which consisted of surfactant molecules on metal surfaces.[249]

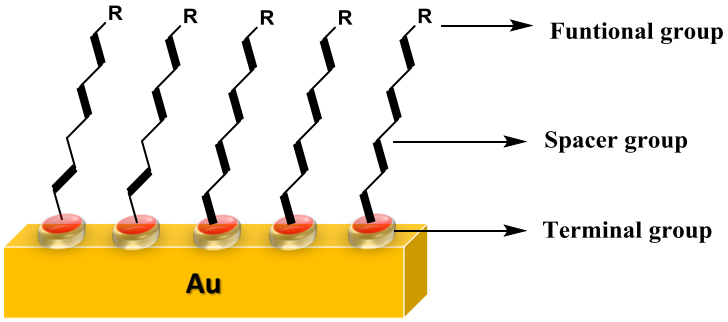

Figure 69. Schematic of SAM at solid-liquid interface.

A schematic of a SAM at a solid-liquid interface is shown in Figure 69. The molecules comprising the monolayer have three important features; terminal, spacer and functional groups. The terminal, or anchoring group is covalently bonded to the surface of the substrate following spontaneous exothermic chemisorption. The spacer group defines the nature and arrangement of the final layer of the SAM. This is due

to the organisation of the SAM through the forces and interactions between the molecules such as van der Waals forces or dipole interactions. The functional group defines the properties of the surface as this entity interacts precisely with the chemicals in the liquid phase.

SAMs can be formed on discrete substrates like glass,[12] silicon, liquid mercury, gold, silver, copper or iron. In 1983 Nuzzo and Allara reported the first thiol SAMs on gold and, since then, thiol SAMs on gold surface have been studied largely and are now the most common SAM used.[250-255,]

5.2.1 Preparation of thiol-SAMs

Thiol SAM preparation consists of immersing a clean gold substrate in a dilute solution of an alkanethiol. The gold used in the immersion must be extremely clean to avoid interference of unwanted chemical entities. It normally takes about 1 to 24 hours to form a monolayer on the gold's surface. In monolayer formation, the S-H bonds break followed by simultaneous formation (equation 24) of Au-S strong bond energy of ~190 $kJmol^{-1}$,[256] The Au-S formed in monolayer is very strong thus the monolayer is stable in both organic and aqueous solvents. Furthermore, the monolayer is well adaptable to electrochemistry applications because of the nature of the resistance of the bond to a large potential range.

$$\mathbf{RS\text{-}H + Au \rightarrow RS\text{-}Au + \tfrac{1}{2}\, H_2} \qquad \textbf{(24)}$$

The process of the electron transfer between the surface of electrode and the species in solution over modified SAM in the electroanalysis can follow in three ways: the electron can be transferred through the monolayer *via* a tunnelling method; the functional or electroactive species can pass through the monolayer and interact with the surface of electrode; or the electroactive species can disperse to an uncovered spot such as a pinhole, on the electrode.[257]

The extent to which the process happens is dependent on the nature of the chemical species and the structure of the SAM. SAMs with short alkyl chains can be prepared but defects and pinhole formations often occur. Kinetic parameters, surface coverage

and structures of SAM can be analysed electrochemically using CV and EIS techniques. According to Marcus theory, in cases of SAMs without a pinhole, the electron transfers across monolayer *via* tunnelling method which attributes to the current and the current produced is altered as the thickness increases.[258] In a SAM made up of long hydrocarbon chains (n > 9), which leads to a compact structure, electrochemical processes can be suppressed[257] SAMs with unsaturated or aromatic moieties which results in the difference of the tunnelling effect can be determined *via* impedance spectroscopy.[259]

SAMs deposited on gold, those based on alkane thiols are gaining considerable interest in the field of electro-analysis and biosensor development.[255, 260] SAM-modified gold electrodes may be applied to the analysis of surfactants by ion pair formation with a redox marker.[261] Other approaches are based on selective adsorption, complexation or permeation[5] through a SAM on gold for discrimination between analyte and interferents or for identifying pinholes and studying the monolayer. SAMs are consequently an important aspect of smart-functional interfaces.[5,262] SAMs can be formed with supramolecular structures such as crown ether,[262] cyclodextrin,[263] and calixarene derivatives[264] by immobilising them onto a suitable substrate surface. These SAMs can determine molecular recognition *via* host-guest interactions, for example, SAMs incorporating crown ethers selectively binding K^+ in aqueous solution as reported by Echegoyen.[263] β-Cyclodextrin SAMs have been used to demonstrate the inclusion of electrochemically active compounds like ferrocene and quinone derivatives by Kaifer and Park.[264] Calix[4, 6, 8]arene derivatives were proven to show polyamine selectivity.[265] Calixarene compounds have excellent complexation activity with neutral molecules along with amino acids and pesticides.[265]

5.3 Goal of the research

The focus of this chapter is the synthesis of thiolated P[5]A and the fabrication of surface modified gold sensors. Gold electrodes with copillar[4+1]arene attached were characterised using CV and EDX and investigated for their affinity for alkali metals and the biogenic amines (PA, PUT, SPD and SPR).

5.4 Experimental Methods

5.4.1 Apparatus

All the measurements were made using a conventional three-electrode system: the reference electrode, the counter electrode and the working electrode. Platinum wire acted as the auxiliary electrode. All the potentials are referred to an Ag|AgCl/KCl saturated reference electrode. The gold electrode (2.0 mm diameter) was used as working electrode. All the electrochemical experiments were carried out at room temperature (25°C) without. The potential scan was carried out between –0·3 and +0·3 V at 100 mVs^{-1}.

5.4.2 Preparation of gold electrodes

The gold electrode (2.0 mm diameter) was mechanically polished with two micropolish alumina suspensions of 0.3μm followed by 0.05μm for 3 min each and washed with distilled water. Subsequent ultrasonic cleaning with absolute ethanol removed the residual alumina powder.

Figure 70. Gold macro electrode (2 mm).

After mechanical cleaning, the gold electrode was immersed in piranha solution (H_2SO_4/H_2O_2, 3:1 v/v) for 10 min at room temperature and finally washed with distilled water. Prior to sensor fabrication, a gold working electrode was electrochemically cleaned by cycling between -0.3 and 1.5 V at a scan rate 0.1 V/s versus Ag|AgCl in 0.5 M sulfuric acid until gold oxide formation was detected in the voltammogram. The electrodes were washed thoroughly with distilled water and dried in a nitrogen stream to obtain a clean gold surface.

5.4.3 Attachment of copillar[4+1]arene (42) to gold electrode

Electrode modification was carried out by placing the gold electrode in a solution of thiolated **42** (20 mg in 2 ml THF) for varying durations (20 mins to 6 hours) at ambient temperature before being washed several times with pure ethanol and then with double distilled water. The modified gold electrodes were kept in double distilled water prior to electrochemical characterisation (Scheme 37).

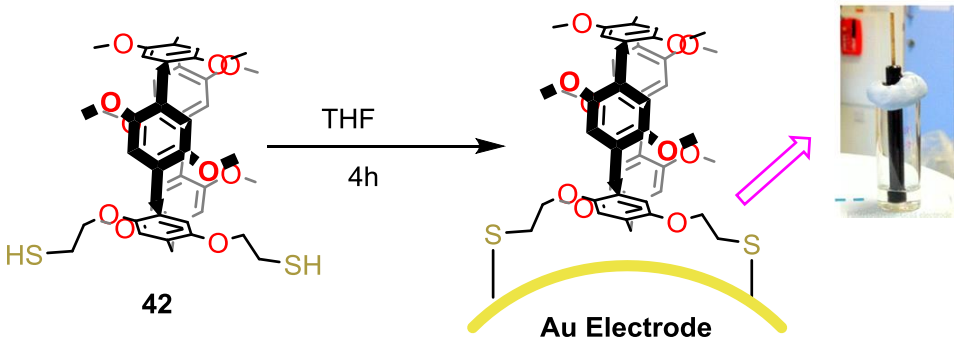

Scheme 37. Schematic representation of **42** adsorption onto a gold electrode surface.

5.4.4 Characterisation of modified gold electrode surface

5.4.4.1 Attachment confirming by CV

The modified electrodes were characterised by cyclic voltammetry. All cyclic voltammetric measurements were taken using Ag|AgCl as a reference electrode and platinum wire as a counter electrode. A solution of 10 mM K4[Fe(CN)6 in 0.1 M KCl (pH 7.0) was used as a redox probe and scanned at 0.1 Vs^{-1} from -0.1 to +0.6V.

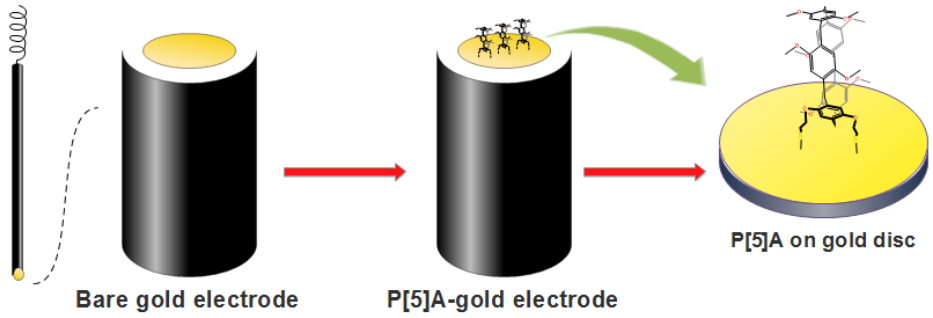

Figure 71. Representation of **42** attached to the bare gold electrode.

5.4.4.2 Surface analysis by SEM and EDX

Attachment of **42** to gold electrodes was assumed to be complete after 4 h. as no further changes in peak current were observed. To confirm this, unmodified and

modified electrodes were imaged by SEM and surface composition determined by energy dispersive X-ray spectroscopy (EDX).

5.4.5 Electrochemical assessment of alkali metals and biogenic amines using copillar[4+1]arene-functionalised gold electrodes

P[5]A functionalised gold electrodes were used to detect alkali metal and biogenic amines by CV. Specific aspects of this study are given below.

5.4.5.1 Assessment of alkali metals using copillar[4+1]arene-functionalised gold electrode

Voltammetric scans were carried out in 10 mM solutions of alkali metal cations (Li^+, Na^+, K^+, Rb^+, Cs^+) were prepared from their PF_6^- salts. Recordings were carried out between -0.3 and +0.3 V at 0.1 Vs^{-1} scan rate. The control experiments were also carried with a bare electrode and an electrode coated with monomer **36**. All cyclic voltammetric measurements were taken using Ag|AgCl as a reference electrode and platinum wire as a counter electrode. The control experiments were also carried with bare electrode and monomer attached gold electrode. Electrodes were rinsed in deionised water between each recording. The change in the capacitive signal, measured as the difference in the current observed at 0 V over the scan rate, was monitored in order to measure the effect of the salts on the voltammetric response. All experiments were conducted in triplicate.

5.4.5.2 Assessment of Li^+ in ACSF using 42 attached to a gold electrode

ACSF (126 mM NaCl, 3.5 mM KCl, 1.3 mM $MgCl_2$ and 2 mM $CaCl_2$) and 10mM Li^+ in ACSF were prepared from their salts and used for the ion inference analysis experiments. Between all recordings the electrodes were rinsed in distilled water. In order to measure the effect of cation salts on the voltammetric response, the change in the capacitive signal was monitored on both a gold electrode attached with **42** and a bare gold electrode. The capacitance was measured as the difference in the current observed at 0 V over the scan rate. All experiments were conducted in triplicate. Cyclic voltammetric measurements were taken using Ag|AgCl as a reference electrode and platinum wire as a counter electrode.

5.4.5.3 Assessment of biogenic amines using a copillar[4+1]arene-modified gold electrode

Voltammetric scans were carried out in 1 mM solutions of pentylamine, putrescine, spermidine and spermine freshly prepared in HPLC grade water. Recordings were carried out between -0.3 and +0.3 V at a 0.1 Vs^{-1} scan rate. All cyclic voltammetric measurements were taken using Ag|AgCl as a reference electrode and platinum wire as a counter electrode. The control experiments were also carried with a bare electrode and one coated with **36**. Electrodes were rinsed in deionised water between each recording. The change in the capacitive signal, measured as the difference in the current observed at 0 V over the scan rate, was monitored in order to measure the effect of the salts on the voltammetric response. All experiments were conducted in triplicate.

5.4.5.4 Assessment of SPR using copillar[4+1]arene-modified gold electrodes at various concentrations

Voltammetric scans were carried out in 0.1, 0.2, 0.4, 0.6, 0.8 and 1 mM solutions of freshly prepared SPR in HPLC grade water. Recordings were carried out between -0.3 and +0.3V at a 0.1 Vs^{-1} scan. All cyclic voltammetric measurements were taken using Ag|AgCl as a reference electrode and platinum wire as a counter electrode. Electrodes were rinsed with deionised water between each recording. Anodic current (I_PA) and cathodic current (I_PC) were recorded and plotted a graph against concentration of SPR.

5.5 Results and Discussions

5.5.1 Bare gold electrode surface analysis

Gold electrode was mechanically polished and electrochemically cleaned using piranha solution. Gold working electrode were electrochemically cleaned by cycling between -0.3 and 1.5 at a scan rate 0.1 Vs^{-1} versus Ag|AgCl in 0.5 M sulfuric acid until the gold oxide formation region between 1.15-1.5V of the voltammograms as shown in Figure 72. The cathodic peak was observed at 0.9 V, which indicates that the gold electrode surface was successfully cleaned and characterised.

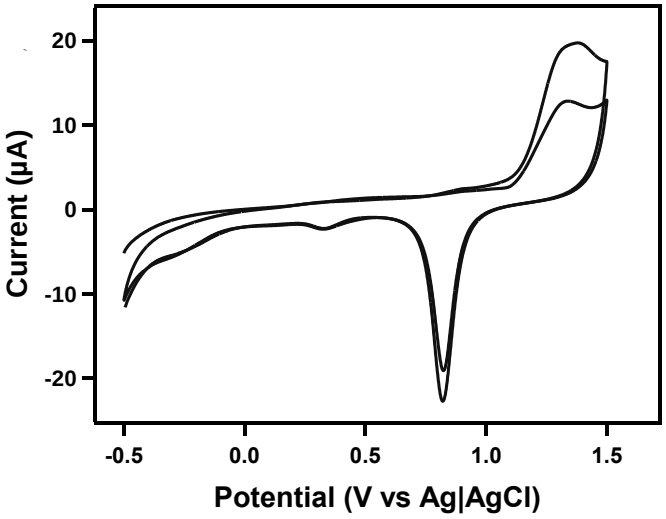

Figure 72. Voltammetric scans for a clean, bare gold electrode in a 0.5 M H_2SO_4 solution

5.5.2 Modified gold electrode surface analysis by CV

Cyclic voltammetry was used to determine if **42** could be successfully attached to gold electrodes and function as an electrode modifier. The standard dipping method was adopted to attach **42** to the surface of a gold electrode and cyclic voltammograms of the redox couples of $K_4[Fe(CN)_6]$ before and during the process were compared shown in Figure 73. Both the capacitive and faradic current were attenuated with increasing time (Figure 73 (a)), consistent with a coating of the macrocycle on the conductive gold surface. After 4 hours, no significant oxidation or reduction peak current for $K_4[Fe(CN)_6]$ was observed on the gold electrode, suggestive of maximum coverage by **42** within this time (Figure 73).

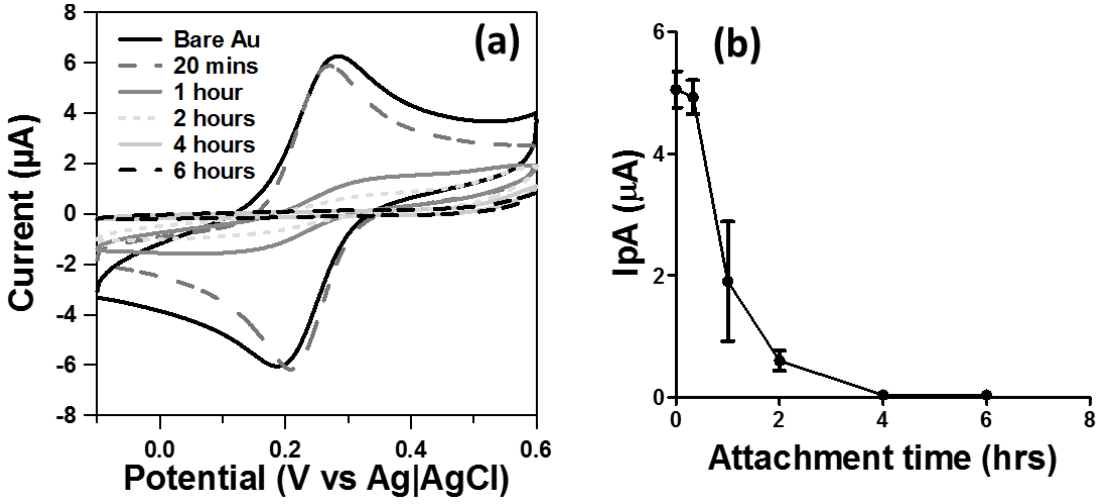

Figure 73. Cyclic voltammetry during attachment of **42**: (a) the effect of attachment time with **42** on a gold electrode and (b) the oxidation peak current decrease with time (0.01 M $K_4[Fe(CN)_6]$ in 0.1 M KCl supporting electrolyte.

5.5.3 Modified gold electrode surface analysis by SEM EDX

The gold electrode disc surface was observed under SEM. Figure 74 shows a bare gold electrode surface (a) and a surface modified by **42** (b) with the roughness of the surface clearly visible in (b). EDX analysis was carried to confirm the composition for the both bare (c) and modified gold electrodes (d) shown in Figure 74. SEM images show a broadly smooth gold surface, with a little pitting, which becomes uniformly uneven following addition of **42**. No sulfur is evident on the surface prior to attachment of **42** but EDX shows it to be present after addition. The theoretical ratio of carbon to sulfur in **42** is 1: 0.114; the ratio from EDX is 1.00 (±0.024) : 0.095 (±0.03) which falls within the expected range and proves that **42** has bound to the electrode surface. Elemental analysis of the sample (d) Wt% (C = 16.87, O = 3.65 Al = 0.44 S = 1.59 Au = 77.45).[168]

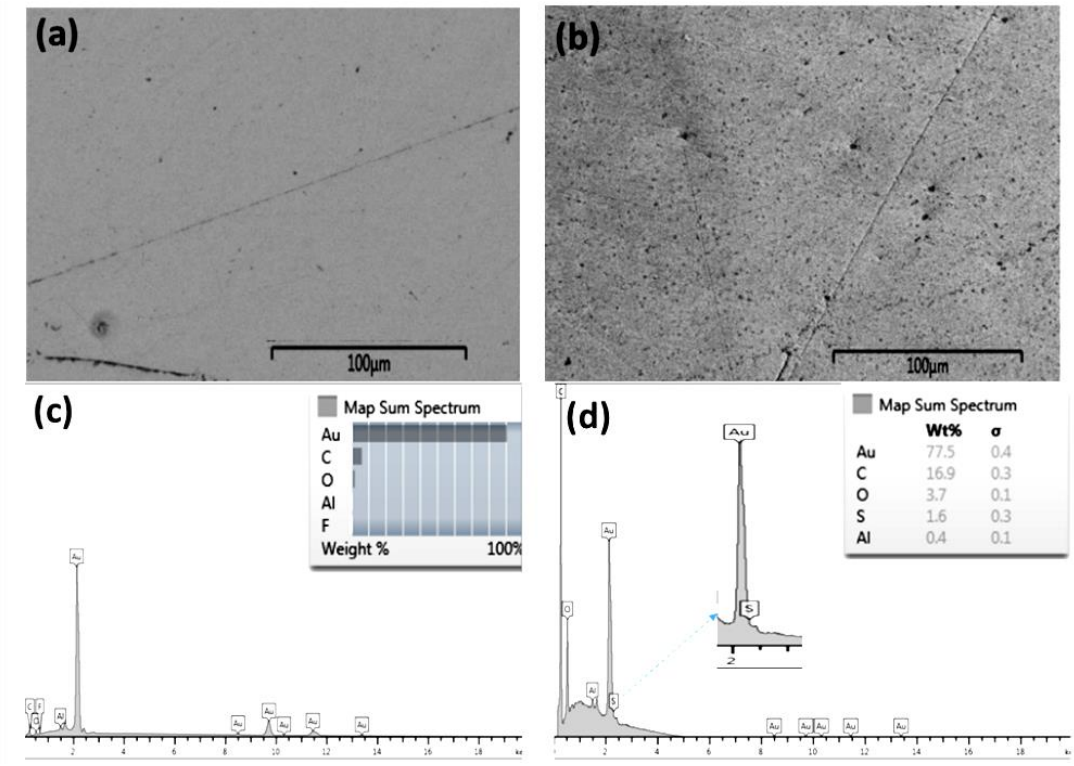

Figure 74. Scanning electron microscopy images of bare electrode disc (a) and modified gold disc surface by 42 (b). EDS analysis shows the electrode composition for bare (c) and modified gold electrode disc (d).

5.5.4 Detection of alkali metals with gold electrodes functionalised with 42

Cyclic voltammetry was utilised to characterise the capacitive signal, which is the measure of difference in capacitance of the current observed at 0 V over the scan

rate, for 10 mM solutions of alkali metal cations (Li^+, Na^+, K^+, Rb^+ and Cs^+) using gold electrodes with **42** attached. Bare and monomer (1,4-dithioethoxybenzene, **36**) attached electrodes were used as controls. Cyclic voltammograms of Figure 75 (a) and (b) shows the capacitive responses of Li^+ and Cs^+ respectively.

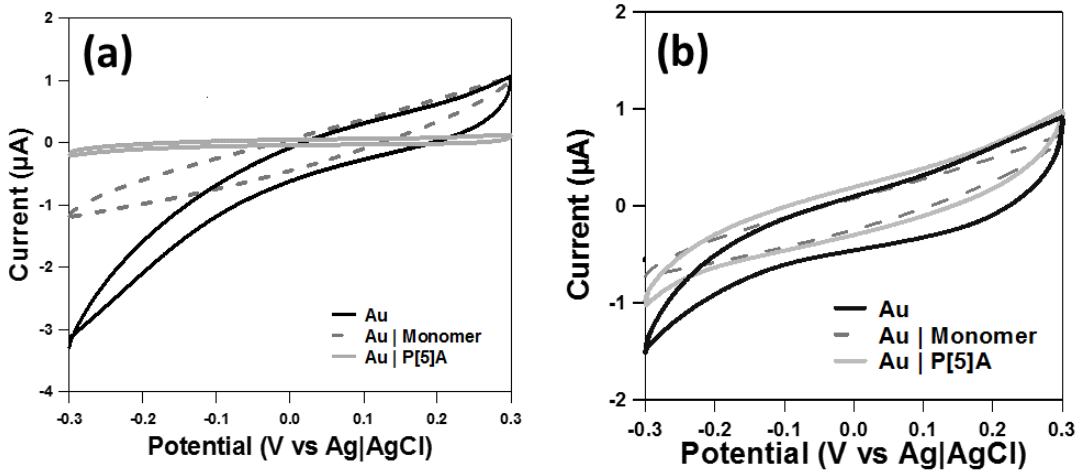

Figure 75. CVs of bare, monomer and **42** attached gold electrode. (a) Li^+ (10mM) response and (b) Cs^+ (10mM) response.

The grey solid line represents the decreased capacitance of Li^+ when compared to bare (solid black) and monomer (dashed line) coated electrode. For Cs^+, no significant change in the capacitance was noticed. Figure 76 shows the statistical significant difference in capacitance between alkali metals.

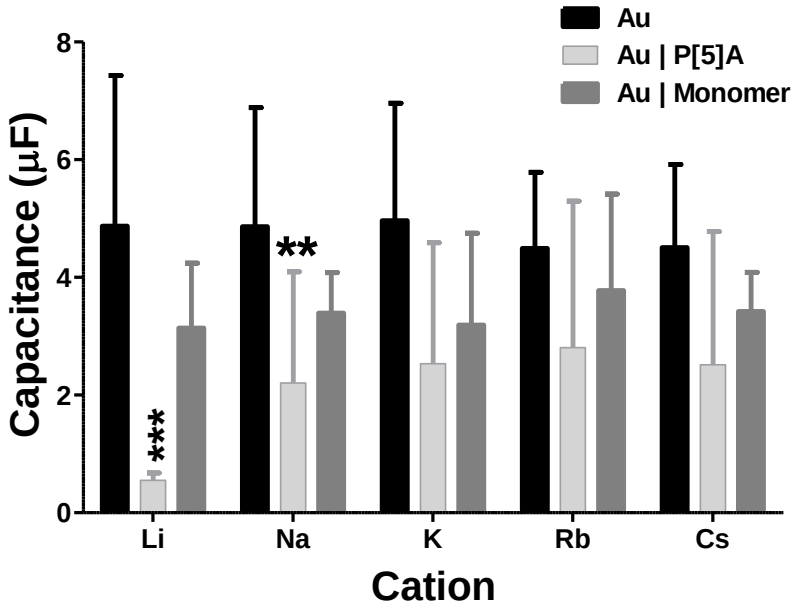

Figure 76. Changes observed in the capacitance signal on bare gold electrodes and gold electrodes coated with monomer **36** or **42** (data shown as mean ± st. dev., where, **p < 0.05 and ***p < 0.001 vs the bare gold electrode).

In the presence of these cations, significant differences in the capacitive signal were observed for Li^+, Na^+ and K^+ salts with the greatest reduction was observed for Li^+ with, as mean ± st. dev $^{**}p < 0.05$ and $^{***}p < 0.001$ vs the bare gold electrode. Although not statistically significant, some reduction in the capacitive signal was also observed with Rb^+ and Cs^+. The decrease of the capacitance is due to changes in the double layer in the vicinity of the electrode which alter the capacitive current at the electrode surface. If Li^+ is held within the P[5]A the electrode surface is less accessible to the free ions in solution, which are repelled, thus the double layer profile is influenced and the net capacitance is reduced. The electrochemical response follows the unusual Eisenman sequence XI in which transport follows the order of ionic radii ($Li^+ > Na^+ > K^+ > Rb^+ > Cs^+$) rather than the order of dehydration.[266] The selectivity on gold surfaces is ascribed to a combination of cation size and complementarity to the cavity of the P[5]A when locked into a rigid pentagonal geometry. When the macrocycle is attached to a surface through substituents on one aromatic ring, as is the case for **42**, the remaining rings are free to change conformation. They can therefore adopt the coordination geometry preferred by each cation. As a consequence, Li^+ could be bound effectively without the need to be completely dehydrated which is energetically unfavourable. This is consistent with the observations of Shurpik who reported the binding constants for the Li^+, Na^+, K^+ and Cs^+ with acid, pyrrolidine and morpholine functionalised **42** in methanol. In all cases log K_{ass} was highest for Li^+ over the other cations[116] Selectivity for the lightest alkali metal is of note as Li^+ detection remains a challenge in analytical chemistry.

Further experiments were carried out to determine if the Li^+ response with **42** would suffer from ion interference. ACSF was used as the background solution and a gold electrode coated with **42** was analysed with ACSF and 10mM Li^+. Cyclic voltammetric scans shown in the presence of ACSF solution and Li^+ where, the change in capacitance was almost negligible. However, in the presence of Li^+, the capacitance slightly increased. This indicates that the ions (Na^+ and K^+) from the ACSF solution interferes with Li^+ against binding site of the **42**. The overall alterations in the capacitive signal were measured at 0 V and the results are shown in Figure 77 (a).

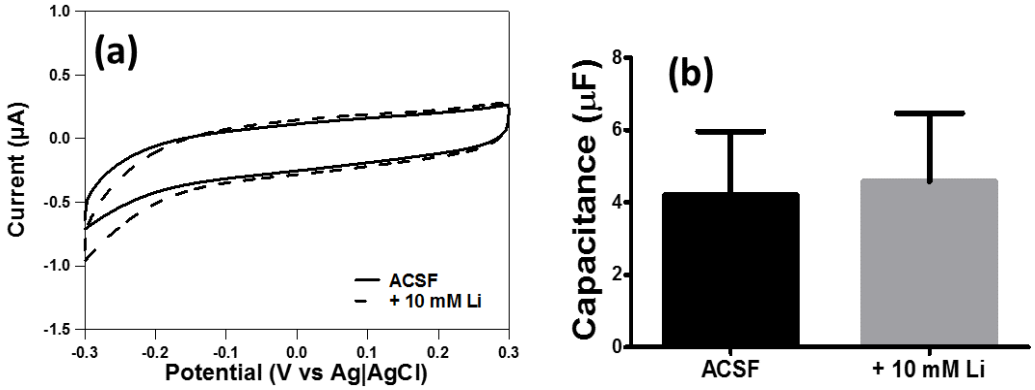

Figure 77. (a) ACSF lithium and Li^+ in ACSF. (b) no significant difference in capacitance observed.

In Figure 77 (b) no statistically significant differences were observed in the capacitive current for Li^+ against background ACSF. This suggested that the capacitive current was not changed potentially facilitated by the copillar[4+1]arene sensor in the presence of mixture of metals.

5.5.5 Biogenic amine detection using copillar[4+1]arene gold electrode

P[5]A SAMs were also used to investigate host-guest interactions with biogenic amines. Similar work has been reported with calixarenes which demonstrated excellent complexation with neutral molecules.[265] Furthermore, SAMs of calix[4, 6, 8]arene derivatives showed selective binding of polyamines.[264] It was therefore possible that copillar[4+1]arene **42** could exhibit similar interactions with biogenic amines. Figure 78 (a) shows the cyclic voltammograms of four biogenic amines, pentylamine**,** putrescine, spermidine and spermine, that were analysed using **43** attached to a gold electrode. CVs of PA (solid black line), PUT (dark grey line), SPD (light grey line) and SPR (broken line) are overlaid. Biogenic amines produced oxidative and reductive peaks with the **42**-modified gold electrode with PA having the smallest oxidation peak and no noticeable reduction peak. PUT, SPD and SPR have noticeable shifts in oxidation and reduction peak potentials.

Systematically changing the number of amine groups in linear alkyl chains in the biogenic amines resulted in a significant response with **42**. The anodic and cathodic peak currents were observed in di- and polyamines due to the electron transfer through the SAM-modified electrode when the biogenic amine guest molecule is presumably captured by the host molecule *via* co-ordination to oxygen atoms of the

P[5]A. Control experiments were carried out with bare and monomer electrodes where no peak current was observed as shown in Figure 78 (b).

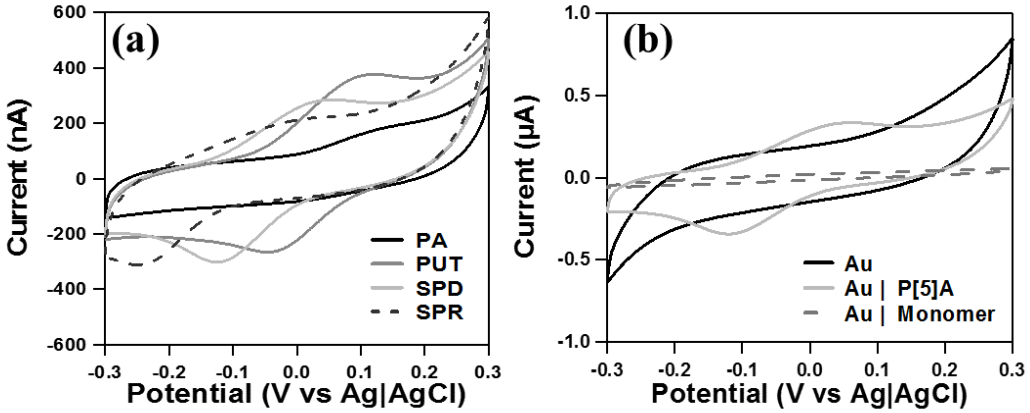

Figure 78. (a) shows the cyclic voltammograms biogenic amines (b) CVs of SPD with bare, monomer and a gold electrode coated with **42**.

The current peaks seen for biogenic amines with a P[5]A-modified electrode could be due to the biogenic amines become electrochemically active through electrostatically induced complexation upon binding to the P[5]A, and the redox active macrocycle facilitates electron transfer from the bulk solution to the gold electrode through the SAM.

The PA, PUT and SPD capacitance difference was also measured and the difference in the current was observed at +0.24 V over the scan rate. The control experimental capacitance was measured under the copillar[4+1]arene gold electrode conditions. There is a significant increase in the capacitive current of the copillar[4+1]arene electrode when compared to bare and monomer electrodes ($p < 0.05$, $n = 3$). Figure 78 (b) shows the comparison of interactions between SPD and bare gold electrodes and those with monomer or **42** attached. There was no peak observed for SPD with bare and monomer-attached electrodes but, in case of the electrode with **42** attached both oxidation and reduction peaks were observed. Biogenic di- (PUT) and polyamines (SPD and SPR) have shown a greater response to the copillar[4+1]arene cavity. The hydrophobic cavity of **42** presumably facilitated tunnelling of electrons through the monolayer hence the peaks in negative potential direction during complexation. This suggests that the macrocycle has catalytic and host-guest properties.

Figure 79 (a) shows no significant response in capacitive signals for any biogenic amine with **42**. The peak current values Epa and Epc were analysed statistically as shown in Figure 79 (b) and (c). Figure 79 (b) shows the Epc linearity of the curve was 0.95 and Epa was 0.91. In Figure 72 (c) PA only has an oxidation current peak which significantly differs when SPR is present. Figure 79 (d) shows a difference in Epa and Epc, where SPR ($p < 0.05$, $n = 3$) is significantly different from PUT. Therefore, it is evident from the results of the cathodic current that biogenic amines are in the order SPR > SPD > PUT > PA. This further suggests that SPR has a greater response to a gold electrode modified with **42**, possibly due to a redox response from the combination of BA and **42**. It appears therefore that **42** is a suitable host for the alkyl polyamine guests.

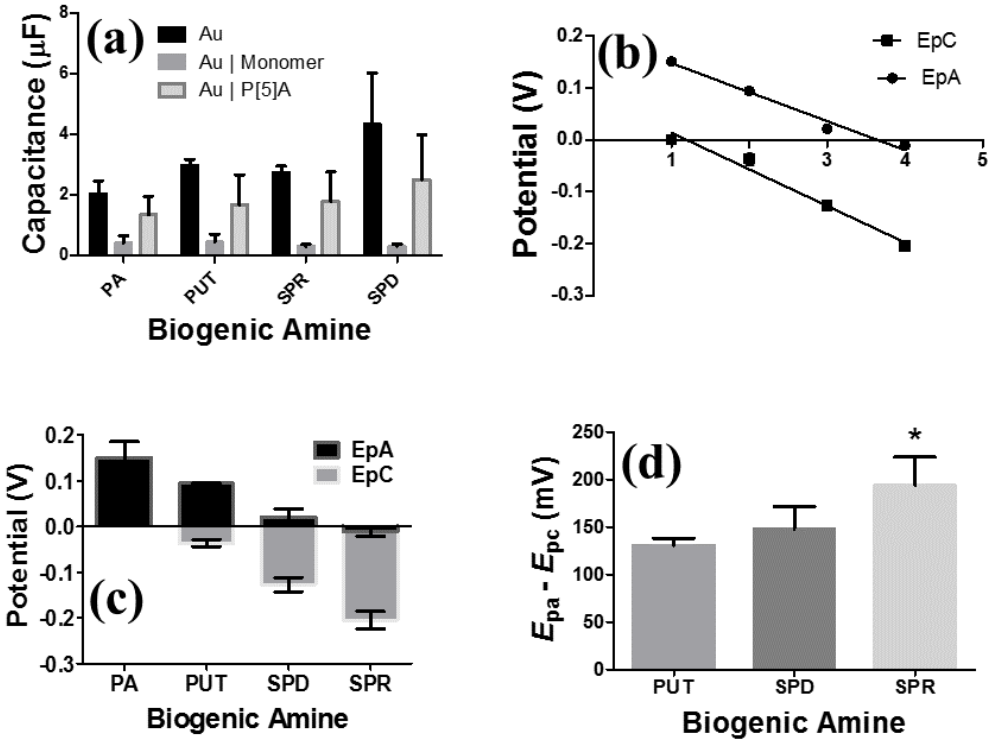

Figure 79. (a) biogenic amines capacitance P <0.0001. (b) and (c) shows peak current values, Epa and Epc were analysed statistically, Epc R= 0.9576 and Epa R = 0.9153. (d) SPR ($p<0.05$, $n =3$) is significantly varied with PUT.

5.5.5.1 Concentration response of SPR

Cyclic voltammetry experiments were carried with SPR at various concentrations to determine its response to, and the detection limit of, a gold electrode with **42** attached. Figure 80 (a) shows as series of voltammograms recorded in at various concentrations of SPR in HPLC grad water (0.1 0.2, 0.4, 0.6 0.8 and 1mM).

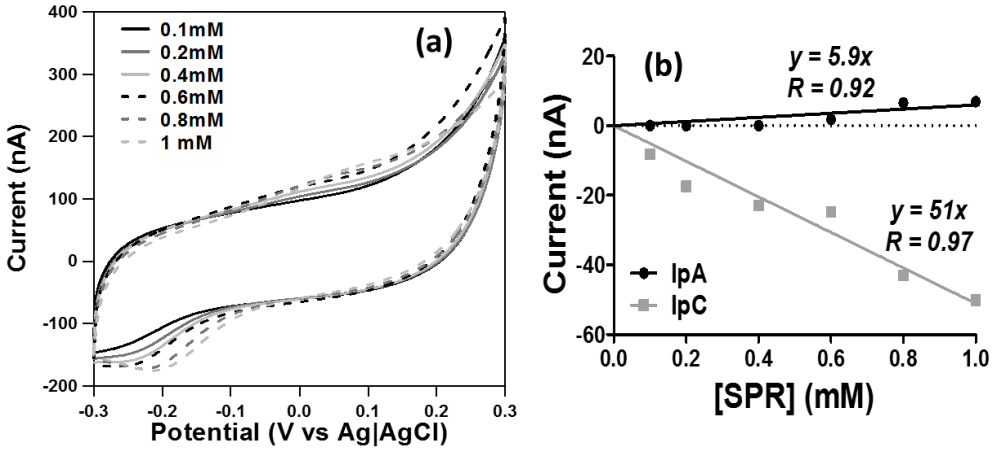

Figure 80. (a) shows the cyclic voltammograms of SPR with various concertation response on **42** attached gold electrode. (b) Intensity between IpA and IpC linearity of the curve.

The cathodic current indicates that reduction took place with increasing SPR concentration. In Figure 80 (b), it is clear that the CV reduction current increased when the concertation of SPR was increased in the solution. Anodic currents (I_PA) and cathodic currents (I_PC) were recorded and plotted against SPR concentration. An I_PC linear response (R = 0.97) was clearly observed as the concentration increased in the solution. This demonstrated that a P[5]A-modified sensor could be fabricated by the SAM method and used to detect alkyl polyamines such as SPR.

5.6 Conclusion

A novel copillar[4+1]arene derivative was synthesised and characterised. SAM of thiolated copillar[4+1]arene and monomer **36** (2,2'-(1,4-phenylenebis(oxy))bis-ethane-1-thiol) were attached to bare gold electrodes by a dipping technique and characterised by SEM, EDX and CV experiments. Attachment to a gold surface by two thiol groups allows copillar[4+1]arene **42** to lie parallel to the surface so that guest species can pass through. The electrochemical response to alkali metal salts by **42** indicates selectivity for Li^+ over the other cations. Biogenic amines were analysed using **42** attached to gold electrodes and a selective electrochemical response to SPR was detected by a monolayer of **42** on a gold surface.

CHAPTER - VI

Direct synthesis of copillar[4+1]arene-capped gold nanoparticles

6.1 Introduction

This chapter focuses on the synthesis and characterisation of copillar[4+1]arene-capped gold nanoparticles (AuNPs) followed by an assessment to investigate their selectivity to biogenic amines (PA, PUT, SPD and SPR).

AuNPs have been used extensively in fields of chemistry, biology, materials science, medicinal and electrochemistry for many years. Even though the area of gold nanoparticle synthesis has been comprehensively explored, there is still scope for novelty in the synthesis of nanoparticles with novel properties. AuNPs were used historically by artists for colouring stained glass, and ceramics. The gold used in those artistic works is "colloidal gold" because the AuNPs are in the form of a suspension, commonly water. Later, colloidal gold forms were also used in medicinal purposes.[267]

Faraday, at the end of 19th century, carried out studies on properties of colloidal gold.[3] He reported that the optical properties of the AuNPs are dependent on several experimental conditions including concentration of the colloidal gold suspension, thickness, in case of gold films, or the applied mechanical compression. Currently, there are various methods of AuNP synthesis,[268-270] but there is also a focus on improving the synthetic methods that produce particles with desired physico-chemistry such as specific size and shape dependent optical, electronic and magnetic properties.[271-274]

6.1.1 Synthesis of AuNPs

Nanomaterial studies requires careful selection of an appropriate synthetic method which produces particles with distinct dimensions and monodispersity.[275] The earliest approaches are known as "liquid chemical methods". In 1951, Turkevich

introduced the method for the first time and this is the basis of current classic method of nanoparticles synthesis.[268] In this method, AuNPs were prepared that are spherical 10-20 nm in size by reduction of $HAuCl_4$ in water by sodium citrate. Later, a method of AuNP synthesis with a broad range of diameters, from 10 to 147 nm was reported by Frens using this process. [269, 270]

Later, Brust and Schiffrin synthesised gold clusters in a liquid-liquid (water-toluene) system based on Faraday's original work.[271] In the Brust and Schiffrin synthesis, shown in Figure 81, the gold precursor and tetraoctylammonium bromide (TOAB) were dissolved in an aqueous phase. Tetrachloroaurate was transferred into the organic phase by stirring vigorously. Dodecanethiol was added to the organic phase, followed by sodium borohydride, where they act as binding and reducing agents respectively. This method of synthesising gold particles which can be easily suspended in the organic phase had a vast impact on the advancement of novel procedures.

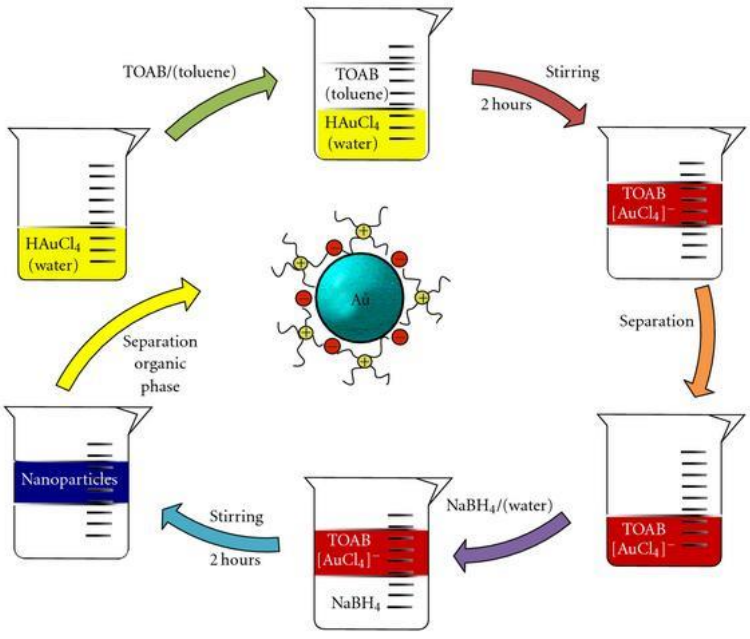

Figure 81. Schematic representation of the Brust and Schiffrin synthesis of AuNPs.[275]

6.1.2 Surface Plasmon Resonance (SPR)

A valuable spectroscopic characteristic of noble metal nanoparticles (NPs) is their surface plasmon resonance (SPR) which gives a sharp and intense absorption band in the visible range. The research work presented here includes the synthesis of surface modified AuNPs. AuNPs are excellent optical probes for sensing applications due to

their capacity to scatter light intensely in the SPR wavelength region which makes them detectable by the naked eyes.[276] By changing the size and shape of the AuNPs their SPR wavelength can be varies from the visible to the near IR region. Their size-reliant optical properties are because of the surface plasmon band (SPB which is observed in transmission of NPs size larger than 2 nm in suspension.

Absorption is a physical process where collective resonant oscillation of the free electrons of the conduction band of the metal takes place.[277] The free conductive valence electrons on the AuNP surface oscillate because of the accumulating attraction effect of the atomic nuclei's positive charge. This oscillation leads to electron density, or surface plasmon, waves. SPR is an optical phenomenon caused by the interaction of the surface plasmon with the incident electromagnetic radiation at a particular resonant frequency. The nature of the metals such as its size, shape, the refractive index of the medium, the dielectric constants and other factors will determine the extent of the plasmon effect. For certain metals, the plasmon energy can corresponds to the energy of a UV photon. The optical properties of AuNPs are dependent on the surface chemistry and the inter-particle interactions. They occur due to exclusive localised surface plasmon resonance (LSPR) shown in Figure 82. LSPR is the cumulative oscillation of the nanostructure's conduction band electrons in resonance with the incident electromagnetic field.[278] In metal NPs, the local field effect around them causes changes in their dielectric function resulting in surface polarisation. The localised surface plasmon oscillations bring about to the profound colours of these NPs and/or very strong scattering. Noble metal NPs possess active UV–vis absorption bands, not usually seen in the bulk metals NPs, an absorption phenomenon known as Mie resonance. Mie theory explains the correlation between SPR band intensity and wavelength with factors affecting the electron charge density on the NP surface like its type, particle size, shape, structure, composition and the dielectric constant of the surrounding medium.[279] Like AuNPs, silver and copper NPs show SPR bands in the visible electromagnetic spectrum while other metals show vast and weak SPR band in the UV region.[6]

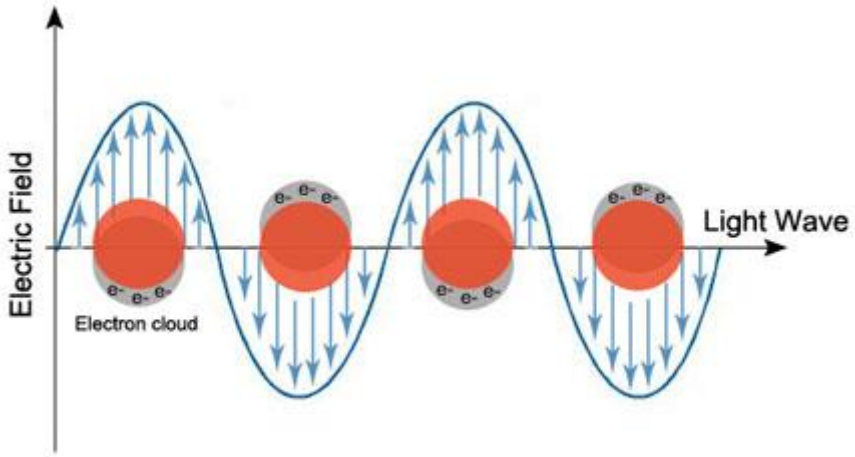

Figure 82. Scheme of LSPR due to collective oscillation of AuNPs surface with a particular wavelength of light.[280]

AuNPs show SPR band near 520 nm in the visible region. AuNPs smaller than 10 nm have phase changes, unlike larger particles, because of the increased rate of the electron-surface collisions which will affect the SPR band of the NPs. The size of the NPs is proportional to the SPR intensity and wavelength as larger NPs give red shifts.[279, 280]

6.1.3 Macrocycle capped AuNPs in sensors

Nanoparticles are an excellent option to achieve colorimetric signalling in experimental studies. AuNPs are especially attractive due to their high extinction coefficients when compared to other organic dyes and exhibit distance-dependent optical properties.[281] Dispersed and aggregated AuNPs are red and purple or blue in colour, respectively. Due to these properties, AuNPs make an excellent medium for sensitive colorimetric detection with minimal material use.[282] AuNPs are well organised due to the assembly of the NPs from solution.[52] Methods using hydrogen-bonding,[283, 284] host-guest,[285] van der Waals,[286] electrostatic interactions have been reported as ways to construct AuNPs. Self-assembly process and host–guest interactions have been promoted by various surface-bound macrocyclic compounds such as cyclodextrins [287] crown ethers[288] cucurbiturils[289] and calixarenes [290, 291] because of their excellent recognition properties. Pochini used 1,3-dialkoxycalix[4]arene-modified and *p*-sulfonatocalix[6]arene-modified AuNPs as colorimetric probes to detect quaternary ammonium cations[292] and diaminobenzene,[293] respectively. Calix[4]arene crown ethers recognise amino group

with high specificity *via* the host–guest interactions.[294] It has also been reported that calix[4]arene-crown ether capped AuNPs enable the visual detection of diamines.[295] AuNPs functionalised with 15-crown-5 recognise K^+ in water,[296] and Li^+ [297] and heavy metal ions[298] were recognised using AuNPs-based sensors.

6.1.4 Pillar[5]arene-capped gold and silver nanoparticles

Recently functionalised AuNPs and AgNPs have been synthesised by capping P[5]As. Huang reported P[5]A-capped AuNPs using an imidazolium P[5]A derivative, and AuNPs formed from $HAuCl_4$ in aqueous solution reduced by $NaBH_4$. The AuNP sizes were controlled by the concentration of P[5]A added.[299] Yang and Weiss used a carboxylate P[5]A derivative to prepare AuNPs in which they proposed that strong carboxyl-gold binding interactions stabilised the AuNPs and that, additionally, growth of the AuNPs during the reduction step was suppressed.[112] Later Xue reported carboxylate derivative that could be used to control the AuNP's size.[300] Similar surface functionalisation by capping AuNPs can be found in the work of Li[301] Diao[302] and Jia.[303] In all these methods, a basic principle is that the P[5]A attaches to the metal surface *via* one of its functionalised rims so that the resultant AuNPs become covered in macrocyclic receptors. For example, Zhou prepared sodium citrate stabilised monothiolate AuNPs and determined successful attachment through FTIR and UV–vis spectroscopy,[172] Zhou reported that the AuNPs reversibly assembled as an effect of the photocycloaddition of anthracene guest species. Pillar[5]- and [6]arene-capped nanoparticles have been used to detect alkylpolyamines[304] hybrid AuNPs which form active P[5]A-incorporated polymers,[305] carboxylated P[5]A-coated AuNPs with peroxidase activity,[306] P[6]A-altered AuNPs and nanorods are used in pH and NIR-triggered restrained discharge.[307] Cationic P[5]A-incorporated AuNPs are used to detect observe pyrene by surface-enhanced Raman scattering spectroscopy.[308]

6.2 Experimental methods

6.2.1 Materials and methods

For nanoparticle synthesis, hydrogen tetrachloroaurate(III) trihydrate ($HAuCl_4 \cdot 3H_2O$, 99.9%), tetraoctylammonium bromide (TOAB, $[CH_3(CH_2)_7]_4N^+Br^-$, >98%) and sodium borohydride ($NaBH_4$, >98%) were purchased from Sigma-

Aldrich. All solvents used were of at first reagent plus grade (>98.5%). Compounds were synthesised according to the literature with amendments as described. SEM experiments wereZeiss EVO LS-15)

6.2.2 Synthesis copillar[4+1]arene gold nanoparticles

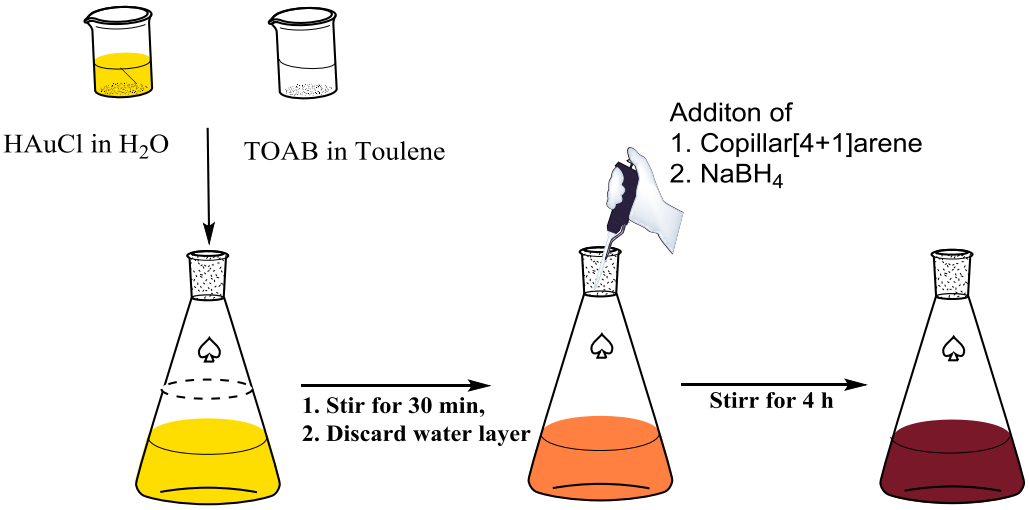

Figure 83. Schematic representation of direct synthesis of **42** capped AuNPs.

A direct synthesis of AuNPs was achieved in toluene upon addition of **42**. Hydrogen tetrachloroaurate (III) trihydrate (7.75 mg, 19.7 μmol) was dissolved in distilled water (0.7 ml) and added at once to 40 mM TOAB in toluene (10 ml, 0.215 g, 20 equiv.) solution. The biphasic mixture was stirred for 30 minutes at room temperature and the aqueous phase subsequently discarded to afford gold(III) TOAB in toluene solution. Copillar[4+1]arene **42** (6.4 mg, 2 mM in SH groups) was added to the mixture under vigorous stirring for 30 minutes. Addition of freshly prepared aqueous 0.4 M sodium borohydride (0.5 ml, 7.44 mg, 10 equiv.) solution was added drop wise at a rate of approximately 20 μl per 15 seconds, whilst continuing to vigorously stir (Figure 83). The initial colour of the gold (III) solution turned brown with 90 seconds at which point the remainder of the sodium borohydride solution was added. The mixture was stirred for approximately 4 h and the aqueous phase was subsequently discarded. The final toluene solution (10ml) contained ≈ 0.2 mM of gold and 40 mM of TOAB and was stored in a glass container in the dark for characterisation using UV–vis spectroscopy and transmission electron microscopy. A control experiment was carried out using the same procedure in the absence of **42**.

6.2.3 Characterisation of copillar[4+1]arene gold nanoparticles

6.2.3.1 Fourier transform infrared spectroscopy (FTIR)

P[5]A-capped AuNPs and TOAB stabilized AuNPs surface was studied by Fourier Transform Infrared (FTIR). The samples were dried under air. FTIR spectroscopy was recorded at a resolution of 4 cm^{-1} and analysed in the region of 4000–400 cm^{-1} over 600 scan in a FTIR spectroscopy (Perkin Elmer Spectrum GX FTIR, USA).

6.2.3.2 Ultraviolet–visible spectroscopy (UV–vis)

The UV–vis spectra of P[5]A-capped AuNPs and TOAB stabilized AuNPs recorded by Lambda 25-Perkinelmer spectrophotometer. Solution spectra were obtained by measuring the absorption of dilute solutions in a quartz cell with a path length of 1 cm; the solvent used was 80% toluene: 10% THF.

6.2.3.3 Scanning electron microscopy (SEM)

SEM is a widely used and powerful imaging technique and is used to record images of surface features in the micro- and nanometre range.[309] The sample is subjected to a focused electron beam which is transmitted from 'electron gun' which accelerates the electrons.[310] The electron beam is focused by condenser lenses followed by passing through deflection coils before it scans the sample. A detector collects the information and produces high quality images in high resolution, however, in some analysis, it may be necessary to use a detector that can collect backscattered electrons.[309] Thus, samples containing various components images can be obtained with high compositional contrast. In this work thin films of platinum were used to coat AuNPs.

6.2.4 Transmission electron microscopy (TEM)

In TEM, electrons produce images by screening the samples studied. The electron beam is partly transmitted over the sample and then recorded on a fluorescent screen.[311,312] The beam is accelerated by an anode in the range 40 – 400 keV (compared to 0.2 - 40 keV in SEM). The specimen used in TEM is very thin as thick may result in scattering of the electron beam. There are few disadvantages with the technique such as the sample preparation, which can be very complicated, but the maximum resolution achievable will be in the sub-Ångström range.[313] For these reasons, samples in the form of thin foils, nanostructures and powders are ideal for

TEM analysis. In the present work, a Hitachi-7100 with Gatan Ultrascan was used to image TOAB and copillar[4+1]arene stabilised AuNPs. The samples were prepared on a copper grid by adding a drop of the nanoparticles dispersed in toluene and left to dry for about 30 min.

6.2.5 Assessment of biogenic amines using copillar[4+1]arene capped AuNPs

Four biogenic amines on interest (pentylamine, putrescine, spermidine and spermine each of 1mM) and **42**-capped AuNPs (1mM) were prepared in THF/toluene (80:10). These two solutions were mixed in 1:1 ratio and were further analysed using UV–vis (Perkin Elmer Lambda 25). TOAB capped AuNPs were used as control in these analysis.

6.3 Results and Discussions

6.3.1 Copillar[4+1]arene stabilised AuNPs

Compound **42** was used as a capping agent in the synthesis of AuNPs and was achieved successfully by the Brust-Schiffrin method[314] as modified by Katz for use with mercaptocalixarenes[315] and further confirmed by using UV–vis spectroscopy and transmission electron microscopy. The final P[5]A-capped AuNPs appeared dark brown in colour as shown in Figure 84.

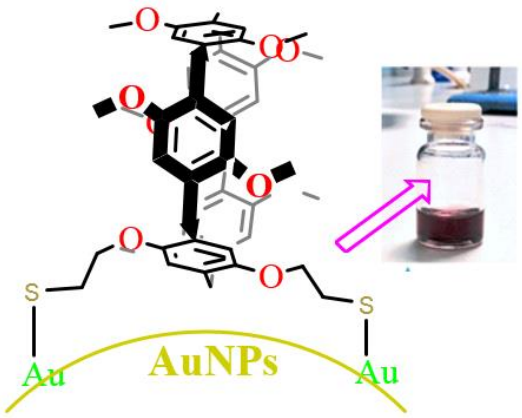

Figure 84. A representation of direct synthesis of AuNPs capped with **42**.

6.3.2 FTIR spectra analysis

Directly synthesised P[5]A-capped AuNPs were characterised by FTIR**.** The P[5]A-capped AuNP spectra **(a)** compared with TOAB AuNPs **(b) as** shown in Figure 85.

A characteristic absorption peak was observed at 3200 and 1600 cm^{-1} was indicative of aromatic compounds.[248]

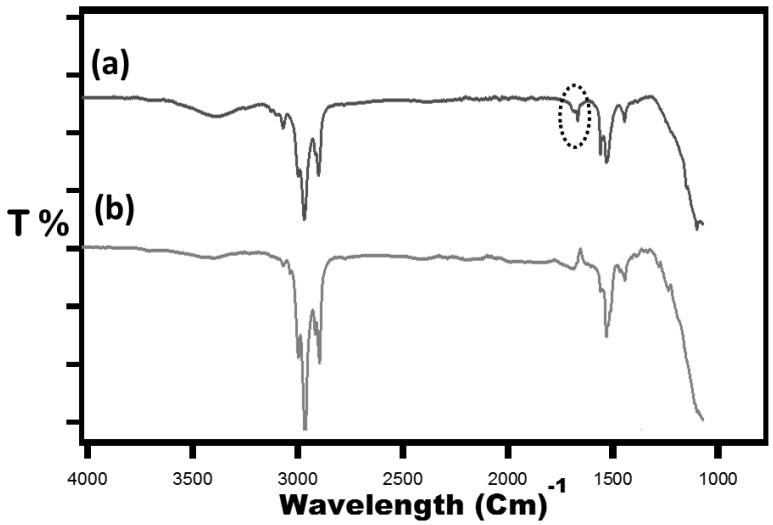

Figure 85. Fourier transform IR spectra of (a) P[5]A-stabilised AuNPs and (b) TOAB-AuNPs.

6.3.3 Ultraviolet–visible spectroscopy (UV–vis) analysis

AuNPs capped by **42** and TOAB-AuNPs were dispersed in 80% toluene: 10% THF and analysed by UV–vis. The plasmon bands of the gold nanoparticles are observed in the range of 450-700 nm. The broad Surface plasmon resonance of capped AuNPs was observed at ~520 nm shown in Figure 86.

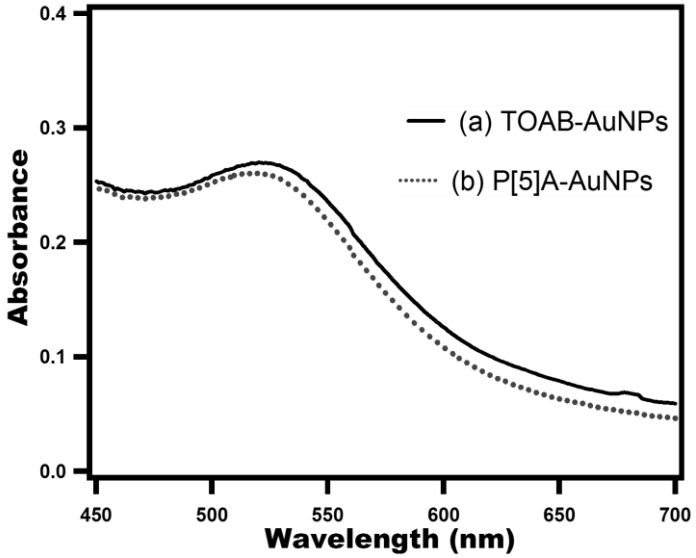

Figure 86. Ultraviolet–visible spectroscopy of (a) TOAB-AuNPs and (b) AuNPs stabilised with **42**.

UV–vis scans of the AuNPs show subtle changes around 520 nm which indicate that replacement of TOAB by **42** though the peaks are too broad to be used to extrapolate changes in AuNP sizes as a consequence of TOAB replacement.

6.3.4 Analysis of transmission electron microscopy (TEM)

TEM images revealed that the AuNPs capped by **42** were 2.9 ± 0.9 nm in diameter, similar in size to those prepared by Yang and Weiss (3.1 ± 0.5 nm).[112] AuNPs prepared without **42** exhibited a broad distribution from 1 to 5 nm indicating that the pillar[4+1]arene is able to control particle size (Figure 87).

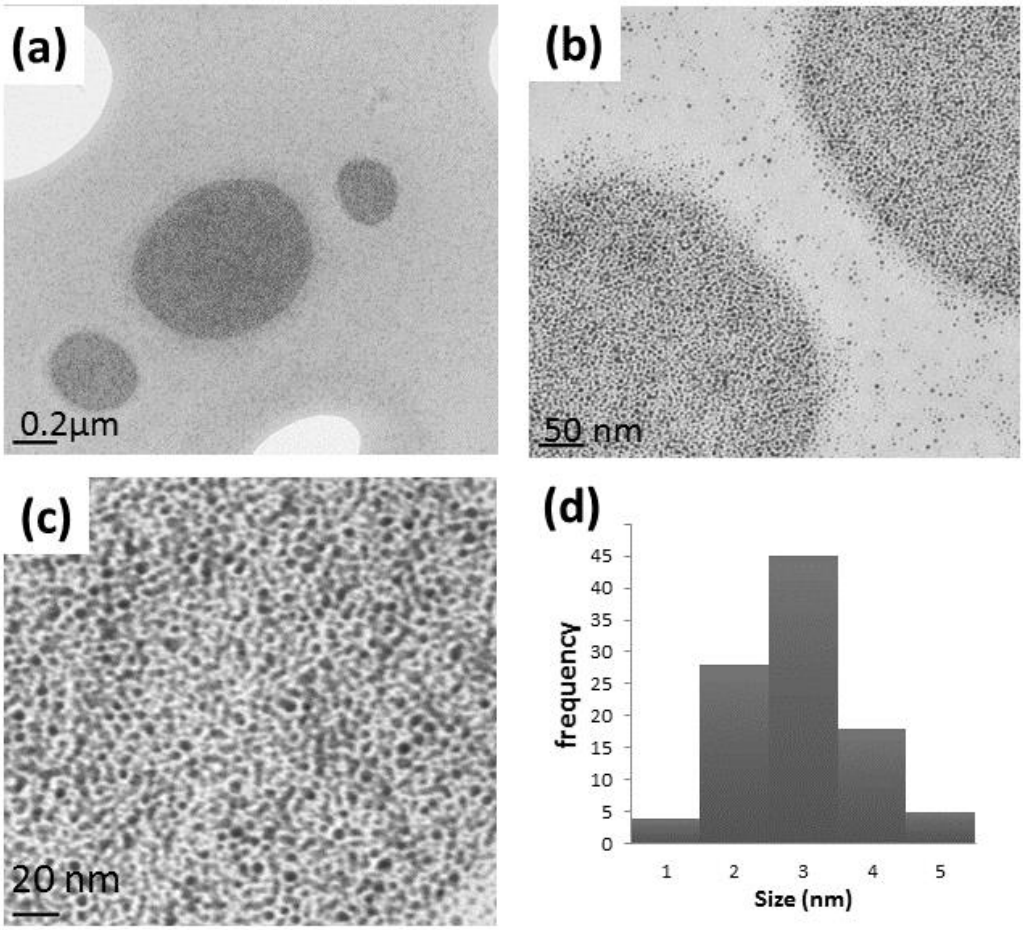

Figure 87. TEM images of AuNPs capped by **42** magnified (from top) by x 10,000, x 30,000 and x 100,000 Analysis of (Hitachi-7100 with Gatan Ultrascan) transmission electron microscopy (TEM) images revealed that the AuNPs were 2.9 ± 0.9 nm in diameter.

6.3.5 Scanning electron microscopy (SEM) of 42-capped AuNPs

Compound **42** stabilised AuNPs were centrifuged and dried under vacuum. The solid particles were imaged under SEM. **42** capped AuNPs were aggregated as shown in

Figure 88 with low to higher magnification. The image of **42**-coated AuNPs shows that the AuNPs assemble in clusters. The AuNPs in this case had rough surfaces and a much larger size of 250 nm. The EDS profile shows the element peaks C, O, S and Au.

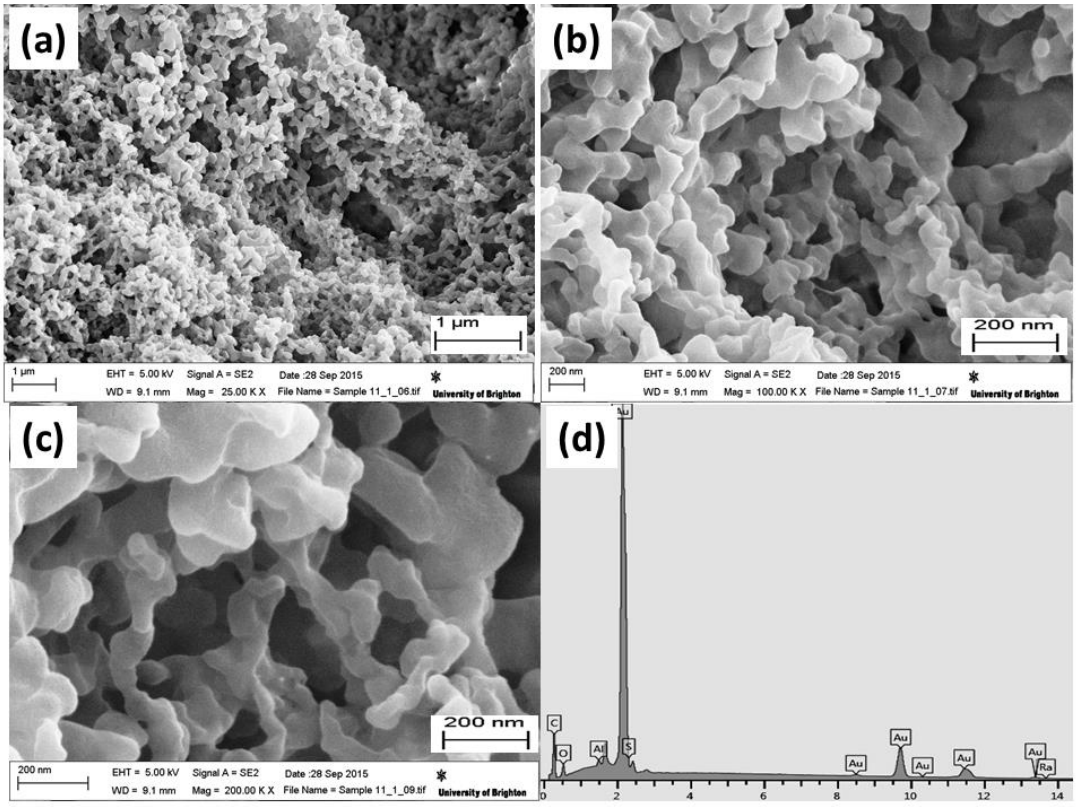

Figure 88. Scanning electron microscopy images of **42** stabilised AuNPs (a),(b) & (c) at low to high magnification. (d) EDS analysis for the element composition of **42**-AuNps

6.4 Detection of biogenic amines

UV–vis spectroscopy is used to determine complexation of **42** and biogenic amines. Biogenic amines (1 mM) used in this method were prepared in THF/toluene (80:10). The guest molecules of interest are pentylamine, putrescine, spermidine and spermine were dispersed separately with **42**-capped AuNPs and characterised. Figure 89 shows the characteristic spectral peaks of host **42** (a) as control and host-guests of pentylamine, putrescine, spermidine and spermine as b, c, d and e, respectively. It is clearly evident from the spectra that the spermine was had the lowest intensity compared to the rest of the **42**-capped AuNPs-biogenic amine combinations. The decreasing order of intensity for the four biogenic amines is pentylamine > putrescine > spermidine > spermine. This suggests that macrocyclic complexation occurred strongly with spermidine and spermine compared to pentylamine and

putrescine. Furthermore, the strong interaction between spermine and **42** can be explained by its rapid complex formation unlike other three biogenic complexes in which the particles aggregated and precipitated due to the smaller alkyl chain that connects it to the surface of the AuNPs. Thus this arrangement provides possible H-bonds with oxygen atoms of **42.**

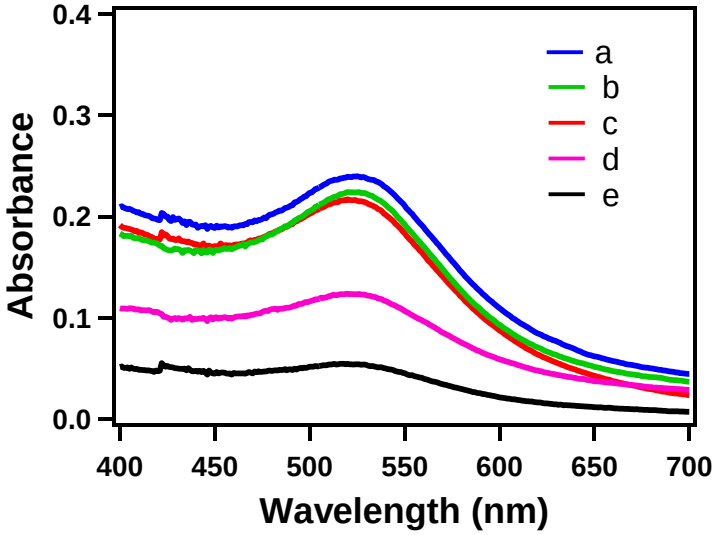

Figure 89. UV of **42**-stabilised AuNPs with four biogenic amines (a) absence of biogenic amine (b) 42-stabilised AuNPs with PA (c) **42**-stabilised AuNPs with PUT (d) **42**-stabilised AuNPs with SPD (e) **42**-stabilised AuNPs with SPR.

6.5 Conclusions

The novel dithiol copillar[4+1]arene (**42**) was synthesised in three steps for the first time and attached to AuNPs which were successfully characterised using FTIR, TEM, UV, SEM and EDX techniques. The host-guest interactions among selected four biogenic amines were studied and analysed with UV–vis spectroscopy. Successful complex formation of SPR was observed. Our findings can potentially be implemented in future in chemical and biological sensor applications.

CHAPTER - VII

7.1 Summary and Conclusions

Supramolecular chemistry can be defined as *'chemistry beyond the molecule'*. It can be broadened to include concepts such as 'inclusion phenomena', 'host–guest chemistry' or 'molecular recognition'. The concept of supramolecular chemistry can be applied to aspects of the life sciences such as the functions of enzymes and antibodies, and the integrity of phospholipid membranes. Macrocyclic compounds play a key role in supramolecular chemistry due to their defined shape, nanoscale size, and molecular selectivity. This selectivity can be applied in the design of sensor molecules for specific analytes. For example, crown ethers, calixarenes, porphyrins, cucurbiturils and cyclodextrins have all been used to detect inorganic metal ions and organic species.

Pillar[*n*]arene chemistry has become a chemical focus following the first report of P[5]A by Ogoshi in 2008. In particular the unique fivefold symmetric tubular structures of the P[5]As were expected to demonstrate novel binding motifs not available to planar macrocycles such as porphyrins and phthaocyanins, funnel-shaped calixarenes and resorcinarenes, or hard to functionalise cucurbiturils. To date sensor applications based on these properties have been limited, as would be expected for a class of compounds that is still in its infancy and with only a handful of papers concerned with molecular recognition by the higher pillar[*n*]arenes, but they show significant promise. From the first crystal structures it was clear that the P[5]A cavity was ideally for small, linear molecules such as CH_3CN, 1,4-dicyanobutane, hexane, alkyldiamines and paraquat. In 2010, Stoddart[73] was the first to show that the cavity within P[5]As could be used as a receptor for linear alkylamines. We believed that these recognition properties could be exploited to generate P[5]A-based sensors and chose to target their potential electrochemical response to guest binding.

Electrochemical sensors have a crucial job in the field of chemical analysis because they allow many specific ions to be measured and monitored.[231,316] Electrodes modified to incorporate macrocycles have earned widening attention in

supramolecular chemistry because of their molecular and electrochemical sensing properties to detect a range of metal ions and chemical species.[2,159]

7.1.1 Novel contributions and findings

The aim of this project was to synthesise, test and optimise P[5]A-based receptors and to incorporate these receptors in a range of sensors. The molecular receptors were incorporated in three different types of electrodes; PVC membrane, graphite composites and gold electrodes. They were additionally used to surface modify AuNPs, to give a colorimetric test for the presence of biogenic amines.

Chapter 2 presented details about the synthesis, characterisation and optimisation of P[5]A based receptors. The parent compound, **1**, an esterified derivative, **21**, and a thiolated copillar[4+1]arene, **42**, were synthesised and characterised. These three derivatives were used as modifiers for sensors.

The key challenges encountered included the synthesis of the ester via hydroxylated P[5]A, which undergoes oxidation upon standing, and the multistep synthesis of the entirely novel dithiol derivative which required numerous purification proceses.

Compound **1** was synthesised using $BF_3O(C_2H_5)_2$ or TFA as the catalyst by two different methods; that of Ogoshi, with $BF_3O(C_2H_5)_2$ as the catalyst, and a second method with TFA as the catalyst, as reported by Boinski and Szumna, which was adopted as it resulted in a much cleaner reaction. The end product was pale yellow but could be further purified by recrystallising the compound in the presence of charcoal to give the macrocycle as a fine white crystalline powder in an overall 60% yield.

A dithiolated copillar[5]arene was synthesised and characterised for the first time. The reaction was carried in three steps. In the first step 1,4-bis(bromoethoxy)benzene was synthesised by Huang's method in an 80 % yield. It was noticeable that both the yield and purity of the product were reduced if powdered, rather than crystalline dimethoxybenzene was used. In the second step the alkyl bromide copillar[4+1]- and [3+2]arenes were prepared using Meier's iron-

catalysed method which were isolated in 33% and 10% yield, respectively, following column chromatography. The challenge in this step was the extraction and filtration after the synthesis due to the presence of insoluble polymer-like impurities. The problem was overcome by using flash chromatography in a short silica column and eluting with DCM. In the third step the dibromo derivative was treated with hexamethyldisilathiane to give the dithiol at low temperature using the method of Hu and Fox method to give a yield of 85%.

Chapter 3 focused on fabrication of a pillar[5]arene-based ISE and to test it against H^+, alkali metal cations and biogenic amines to investigate sensing properties. Esterified P[5]As were successfully incorporated in PVC membrane to construct an ISE for proton transportation. The published X-ray crystal structure of this compound revealed that the crystals contain hydrogen-bonded water molecules threaded through the P[5]As which suggested that a pH-sensitive device could be constructed to take advantage of that effect. Our studies have proved that the ester P[5]A ISE exhibited excellent molecular scale transport of protons through the macrocycle cavity with a nonlinear dependence on pH between pH 1 to 4. A similar analysis with a ISE modified with **1** assessed sensing properties for alkali metals and biogenic amines. Four important linear biogenic amines; pentylamine (PA), putrescine (PUT), spermidine (SPD) and spermine (SPR) were chosen as analytical targets. Ion transport selectivity of these electrodes in the order: $Cs^+ \sim Rb^+ \sim K^+ > NH_4^+ > Na^+ > Li^+ > Mg^{+2} > Ca^{+2}$. The human body does not contain rubidium and caesium ions, as they are not of physiological importance making this ISE a K^+-selective sensor.

For biogenic amines, this ISE demonstrated a greater response to pentylamine. Putrescine, spermidine and spermine has no response in transportation through the macrocycle indicating that the polyamines may not be suitable for the transportation through the P[5]A cavity. This could be because of the competition among amine groups involved in the molecular interaction with oxygen atoms around the macrocycle. Therefore, it appears that the ISE was suitable for the transportation and selectivity of K^+ and PA against alkali metal ions and other biogenic amines respectively.

Chapter 4 focused on the fabrication of composite sensors incorporating **1** and to assess them as detectors of alkali metals and biogenic amines. The studies revealed that the macrocycle is electrochemically stable with respect to oxidation and responds to Na^+ and K^+, both of which are important electrolytes to monitor in clinical and environmental settings. No significant differences were observed in the capacitive signal for Li^+, Rb^+ or Cs^+. The composite sensor was able to detect Na^+ concentrations in the physiological range, whereas K^+ concentrations were well above those encountered *in vivo*. Computational models gave insights into the binding preferences observed and indicated that complexation of Li^+, Rb^+ and Cs^+ is disfavoured on thermodynamic grounds. The composite electrodes did not show significant differences in capacitance for biogenic amines. Therefore, a composite sensor incorporating **1** was suitable to detect Na^+ and K^+ over alkali metal ions and unaffected by the presence of biogenic amines.

Chapter 5 focused on the synthesis of a novel thiolated copillar[4+1]arene, **42**, and its attachment to the gold electrode surface followed by characterisation by CV, SEM and EDX. These surface modified gold electrodes were tested against alkali metals and biogenic amines to investigate their sensing properties. The studies demonstrated that gold electrodes modified with **42** were most selective to Li^+ over other alkali metal cations. Attachment to a gold surface by two thiol groups allows **42** to lie parallel to the surface so that guest species can pass through.

Chapter 6 focused on the synthesis of AuNPs capped with **42** followed by characterisation by UV, TEM, IR and SEM. The **42**-capped AuNPs were successfully synthesised, characterised and assessed for biogenic amine selectivity. From the UV–vis measurements, spermine had the lowest intensity compared to the rest of the AuNP-biogenic amine combinations. The order of intensity of four biogenic amines in the decreasing order of intensity is pentylamine > putrescine > spermidine > spermine. Thus complexation occurred strongly with spermidine and spermine compared to pentylamine and putrescine.

Overall, the common purpose of the research presented in this thesis was to assess P[5]A macrocycle for its selectivity of alkali metals and biogenic amines. The

difference in the nature of ion selectivity by the same macrocyclic binding motif appears to be due to its arrangement in three different types of electrodes. In the ISE, the crystalline macrocycle integrates with PVC which make the upper and lower-rim functional groups available for complex formation. In composite sensors, the alignment of the macrocycles is very rigid making complex formation reliant on the guest fitting into the rigid macrocyclic cavity. In gold electrodes, one of the aromatic rings was involved in surface attachment which makes the remaining rings to freely change their conformations. Therefore, the nature of ion selectivity with the same five-membered macrocycle could be different with various electrodes and is possibly because of the nature of the macrocycle such as rigidity, flexibility and availability of the functional groups

7.1.2 Suggestions for future work.

The research presented in this thesis is focused on the P[5]A synthesis, functionalisation and assessment of the macrocycles as sensors. Extensive studies of the P[5]A sensors were undertaken to optimise selectivity, however, an alternative approach to the synthesis of P[5]As with functional groups such as alkyl chains terminating in carboxylic acids or amides, and single amino acids could be used to enhance biogenic amine affinities and selectivities. Copillar[4+1]arene dithiols were attached to gold surfaces to enhance selectivity, however this may be achieved by altering the alkyl chain length of copillar[4+1]arene dithiols and also by using monofunctionalised thiols. This approach could be extended to thiol-capped AuNPs sensors which could also be assessed for selectivity of alkali metals and biogenic amines. The selectivity studies could also be carried out using g old microelectrode arrays for simultaneous detection of different bacterial produced biogenic amines. The copillar[4+1]arene dithiol modified gold sensors have shown Li^+ selectivity which was validated by CV. For a more detailed electrochemical response, these sensors' sensitivity for Li^+ could also be studies using EIS. Finally, P[5]A-based detection of important cations and biogenic amines could have a significant impact if the macrocycles could be incorporated in disposable devices for use in clinical or industrial settings.

REFERENCES

1. A. Hulanicki, S. Glab and F. Ingman, *Pure Appl. Chem.*, 1991, **63**, 1247-1250.
2. E. García-España, M. T. Albelda and J. C. Frías, in *Applications of supramolecular chemistry*, ed. H.-J. Schneider, CRC Press, New York, 2012, pp. 11-48.
3. P. Bühlmann, E. Pretsch and E. Bakker, *Chem. Rev.*, 1998, **98**, 1593-1688.
4. G. D. Christian, *Sensors*, 2002, **2**, 432-435.
5. I. Rubinstein, S. Steinberg, Y. Tor, A. Shanzer and J. Sagiv, *Nature*, 1988, **332**, 426-429.
6. C. Henke, C. Steinem, A. Janshoff, G. Steffan, H. Luftmann, M. Sieber and H. J. Galla, *Anal. Chem*, 1996, **68**, 3158-3165.
7. H. Adams, F. Davis and C. J. M. Stirling, *J. Chem. Soc., Chem. Commun.*, 1994, 2527-2529.
8. A. Friggeri, F. C. J. M. van Veggel, D. N. Reinhoudt and R. P. H. Kooyman, *Langmuir*, 1998, **14**, 5457-5463.
9. M. T. Rojas, R. Koeniger, J. F. Stoddart and A. E. Kaifer, *J. Am. Chem. Soc.*, 1995, **117**, 336-343.
10. A. J. Moore, L. M. Goldenberg, M. R. Bryce, M. C. Petty, A. P. Monkman, C. Marenco, J. Yarwood, M. J. Joyce and S. N. Port, *Adv. Mater.*, 1998, **10**, 395-398.
11. S. Flink, B. A. Boukamp, A. van den Berg, F. C. J. M. van Veggel and D. N. Reinhoudt, *J. Am. Chem. Soc.*, 1998, **120**, 4652-4657.
12. R. G. Nuzzo and D. L. Allara, *J. Am. Chem. Soc.*, 1983, **105**, 4481-4483.
13. S. Flink, F. C. J. M. van Veggel and D. N. Reinhoudt, *J. Phys. Chem. B*, 1999, **103**, 6515-6520.
14. G. Zhang, J. Zhan and H. Li, *Org. Lett.*, 2011, **13**, 3392-3395.
15. H. Liu, S. Liu and L. Echegoyen, *Chem. Commun.*, 1999, 1493-1494.
16. S. G. Liu, H. Liu, K. Bandyopadhyay, Z. Gao and L. Echegoyen, *J. Org. Chem.*, 2000, **65**, 3292-3298.
17. R. A. Sachleben, A. Urvoas, J. C. Bryan, T. J. Haverlock, B. A. Moyer and B. P. Hay, *Chem. Commun.*, 1999, 1751-1752.
18. S. Zhang and L. Echegoyen, *Tetrahedron Lett.*, 2003, **44**, 9079-9082.
19. D. M. Roundhill, *Extraction of metals from soils and waters, 1. ed*, Kluwer Academic/Plenum Publ., New York, , 2001.
20. P. J. Dijkstra, J. A. J. Brunink, K. E. Bugge, D. N. Reinhoudt, S. Harkema, R. Ungaro, F. Ugozzoli and E. Ghidini, *J. Am. Chem. Soc.*, 1989, **111**, 7567-7575.

21. P. D. Beer, P. A. Gale, Z. Chen, M. G. B. Drew, J. A. Heath, M. I. Ogden and H. R. Powell, *Inorg. Chem.*, 1997, **36**, 5880-5893.
22. D. A. Doyle, J. M. Cabral, R. A. Pfuetzner, A. Kuo, J. M. Gulbis, S. L. Cohen, B. T. Chait and R. MacKinnon, *Science*, 1998, **280**, 69-77.
23. G. W. Gokel, *Chem. Commun.*, 2000, 1-9.
24. J. de Mendoza, F. Cuevas, P. Prados, E. S. Meadows and G. W. Gokel, *Angew. Chem. Int. Ed.*, 1998, **110**, 1650-1653.
25. G. D. Christian, *Anal. Chem.*, 1969, **41**, 24A-40A.
26. J. Koch-Weser, *N. Engl. J. Med.*, 1972, **287**, 227-231.
27. Y. Kim, T. Nguyen and D. G. Churchill, in *The Alkali Metal Ions: Their Role for Life*, Springer,New York, 2016, pp. 1-10.
28. C. J. Pedersen, *Angew. Chem. Int. Ed. Engl.*, 1988, **27**, 1021-1027.
29. J.-M. Lehn, *Angew. Chem. Int. Ed. Engl.*, 1988, **27**, 89-112.
30. J. Pick, K. Tóth, E. Pungor, M. Vasák and W. Simson, *Anal. Chim. Acta*, 1973, **64**, 477-480.
31. P. Schulthess, Y. Shijo, H. V. Pham, E. Pretsch, D. Ammann and W. Simon, *Anal. Chim. Acta*, 1981, **131**, 111-116.
32. J. Tarcali, G. Nagy, K. Tóth, E. Pungor, G. Juhász and T. Kukorelli, *Anal. Chim. Acta*, 1985, **178**, 231-237.
33. K. Kimura, H. Tamura and T. Shono, *J. Chem. Soc., Chem. Commun.*, 1983, 492-493.
34. H. Yamamoto and S. Shinkai, *Chem. Lett.*, 1994, 1115-1118.
35. A. Kamenev and K. Lushov, *J. Anal. Chem.*, 2001, **56**, 380-383.
36. A. Casnati, A. Pochini, R. Ungaro, C. Bocchi, F. Ugozzoli, R. J. Egberink, H. Struijk, R. Lugtenberg, F. Jong and D. N. Reinhoudt, *Chem. Eur. J.* , 1996, **2**, 436-445.
37. K. Kimura, H. Oishi, T. Miura and T. Shono, *Anal. Chem.*, 1987, **59**, 2331-2334.
38. K. Kimura, H. Yano, S. Kitazawa and T. Shono, *J. Chem. Soc., Perkin Trans. 2*, 1986, 1945-1951.
39. J. A. Thoma and D. Koshland Jr, *J. Am. Chem. Soc.*, 1960, **82**, 3329-3333.
40. J.-M. Lehn, *Pharm. Acta Helv.*, 1995, **69**, 205-211.
41. P. Ehrlich, *The relations existing between chemical constitution, distribution and pharmacological action.*, John Wiley & Sons Ltd, New York, 1906.
42. M. Sherburn, *Aust. J. Chem.*, 2002, **55**, 357-358.
43. P. J. Cragg, *Supramolecular Chemistry: from Biological Inspiration to Biomedical Applications* Springer, Dordecht, London, 2010.

44. J.-M. Lehn, *Pure Appl. Chem.* , 1978, **50**, 871-892.
45. C. J. Pedersen, *J. Am. Chem. Soc.*, 1967, **89**, 7017-7036.
46. J. W. Steed, D. R. Turner and K. Wallace, *Core concepts in supramolecular chemistry and nanochemistry*, John Wiley & Sons, West Sussex, U.K, 2007.
47. F. J. Hoeben, P. Jonkheijm, E. Meijer and A. P. Schenning, *Chem. Rev.* , 2005, **105**, 1491-1546.
48. J.-M. Lehn, M. Mascal, A. Decian and J. Fischer, *J. Chem. Soc., Chem. Commun.*, 1990, 479-481.
49. J. Sponer, J. Leszczynski and P. Hobza, *J. Biomol. Struct. Dynam.*, 1996, **14**, 117-135.
50. J. W. Steed and J. L. Atwood, in *Supramolecular Chemistry*, John Wiley & Sons, Ltd, New York, 2009, pp. 1-47.
51. K. Müller-Dethlefs and P. Hobza, *Chem. Rev.*, 1999, **100**, 143-168.
52. J.-M. Lehn and J. Sanders, *Angew. Chem. Int. Ed.* , 1995, **34**, 2563-2563.
53. L. Trembleau and J. Rebek, *Science*, 2003, **301**, 1219-1220.
54. N. L. Strutt, H. Zhang, S. T. Schneebeli and J. F. Stoddart, *Acc. Chem. Res.*, 2014, **47**, 2632-2642.
55. R. R. Kothur, B. A. Patel and P. J. Cragg, *Sci. Lett. J.*, 2015, **4** 1-8.
56. Y. Ma, Z. Zhang, X. Ji, C. Han, J. He, Z. Abliz, W. Chen and F. Huang, *Eur. J. Org. Chem.*, 2011, **2011**, 5331-5335.
57. P. J. Cragg and K. Sharma, *Chem. Soc. Rev.*, 2012, **41**, 597-607.
58. A. Dandridge and H. Drescher, *GB patent*, **322169**.
59. J. Lagona, P. Mukhopadhyay, S. Chakrabarti and L. Isaacs, *Angew. Chem. Int. Ed.* , 2005, **44**, 4844-4870.
60. K. Uekama, F. Hirayama and T. Irie, *Chem. Rev.*, 1998, **98**, 2045-2076.
61. T. Ogoshi and T. Yamagishi, in *Pillararenes*, The Royal Society of Chemistry, Chembridge, U.K, 2016, pp. 90-133.
62. T. Ogoshi, S. Kanai, S. Fujinami, T. Yamagishi and Y. Nakamoto, *J. Am. Chem. Soc.*, 2008, **130**, 5022-5023.
63. T. Ogoshi and T. Yamagishi, in *Pillararenes*, The Royal Society of Chemistry, Chembridge, U.K, 2016, pp. 23-43.
64. T. Ogoshi, D. Yamafuji, T. Aoki and T. Yamagishi, *J. Org. Chem.*, 2011, **76**, 9497-9503.
65. T. Ogoshi, K. Kitajima, T. Aoki, S. Fujinami, T. Yamagishi and Y. Nakamoto, *J. Org. Chem.*, 2010, **75**, 3268-3273.

66. Y. Kou, H. Tao, D. Cao, Z. Fu, D. Schollmeyer and H. Meier, *Eur. J. Org. Chem.*, 2010, **2010**, 6464-6470.
67. X. Shu, S. Chen, J. Li, Z. Chen, L. Weng, X. Jia and C. Li, *Chem. Commun.*, 2012, **48**, 2967-2969.
68. C. Han, F. Ma, Z. Zhang, B. Xia, Y. Yu and F. Huang, *Org. Lett.*, 2010, **12**, 4360-4363.
69. T. Ogoshi, M. Hashizume, T. Yamagishi and Y. Nakamoto, *Chem. Commun.*, 2010, **46**, 3708-3710.
70. T. Ogoshi, K. Kitajima, T. Aoki, T. Yamagishi and Y. Nakamoto, *J. Phys. Chem. Lett.*, 2010, **1**, 817-821.
71. H. Deng, X. Shu, X. Hu, J. Li, X. Jia and C. Li, *Tetrahedron Lett.*, 2012, **53**, 4609-4612.
72. X. Shu, J. Fan, J. Li, X. Wang, W. Chen, X. Jia and C. Li, *Org. Biomol. Chem.*, 2012, **10**, 3393-3397.
73. N. L. Strutt, R. S. Forgan, J. M. Spruell, Y. Y. Botros and J. F. Stoddart, *J. Am. Chem. Soc.*, 2011, **133**, 5668-5671.
74. T. Ogoshi, T. Aoki, K. Kitajima, S. Fujinami, T. Yamagishi and Y. Nakamoto, *J. Org. Chem.*, 2011, **76**, 328-331.
75. C. Li, X. Shu, J. Li, J. Fan, Z. Chen, L. Weng and X. Jia, *Org. Lett.*, 2012, **14**, 4126-4129.
76. M. Holler, N. Allenbach, J. Sonet and J. F. Nierengarten, *Chem. Commun.*, 2012, **48**, 2576-2578.
77. K. Wang, L. Tan, D. X. Chen, N. Song, G. Xi, S. X. Zhang, C. Li and Y. W. Yang, *Org. Biomol. Chem.*, 2012, **10**, 9405-9409.
78. S. Santra, I. S. Kovalev, D. S. Kopchuk, G. V. Zyryanov, A. Majee, V. N. Charushin and O. N. Chupakhin, *RSC Adv.*, 2015, **5**, 104284-104288.
79. I. Nierengarten, S. Guerra, M. Holler, J. F. Nierengarten and R. Deschenaux, *Chem. Commun.*, 2012, **48**, 8072-8074.
80. Y. Chen, H. Q. Tao, Y. H. Kou, H. Meier, J. L. Fu and D. R. Cao, *Chin. Chem. Lett.*, 2012, **23**, 509-511.
81. D. Cao, Y. Kou, J. Liang, Z. Chen, L. Wang and H. Meier, *Angew. Chem., Int. Ed.*, 2009, **48**, 9721-9723.
82. M. Pan and M. Xue, *Eur. J. Org. Chem.*, 2013, **2013**, 4787-4793.
83. T. Ogoshi, D. Yamafuji, D. Kotera, T. Aoki, S. Fujinami and T. Yamagishi, *J. Org. Chem.*, 2012, **77**, 11146-11152.
84. K. I. Shivakumar and G. J. Sanjayan, *Synthesis*, 2013, **45**, 896-898.

85. T. Ogoshi and T. Yamagishi, *Eur. J. Org. Chem.*, 2013, **2013**, 2961-2975.
86. X. B. Hu, Z. Chen, L. Chen, L. Zhang, J. L. Hou and Z. T. Li, *Chem. Commun.*, 2012, **48**, 10999-11001.
87. T. Ogoshi, D. Yamafuji, T. Aoki and T. Yamagishi, *Chem. Commun.*, 2012, **48**, 6842-6844.
88. T. Ogoshi, H. Kayama, D. Yamafuji, T. Aoki and T. Yamagishi, *Chem. Sci.*, 2012, **3**, 3221-3226.
89. T. Ogoshi, K. Demachi, K. Kitajima and T. Yamagishi, *Chem. Commun.*, 2011, **47**, 7164-7166.
90. Z. Zhang, B. Xia, C. Han, Y. Yu and F. Huang, *Org. Lett.*, 2010, **12**, 3285-3287.
91. Z. Zhang, G. Yu, C. Han, J. Liu, X. Ding, Y. Yu and F. Huang, *Org. Lett.*, 2011, **13**, 4818-4821.
92. T. Ogoshi, K. Kitajima, S. Fujinami and T. Yamagishi, *Chem. Commun.*, 2011, **47**, 10106-10108.
93. G. Yu, Z. Zhang, J. He, Z. Abliz and F. Huang, *Eur. J. Org. Chem.*, 2012, **2012**, 5902-5907.
94. Z. Zhang, G. Yu, C. Han, J. Liu, X. Ding, Y. Yu and F. Huang, *Org Lett*, 2011, **13**, 4818-4821.
95. D. Cao and H. Meier, *Asian J. Org. Chem.* , 2014, **3**, 244-262.
96. G. Yu, C. Han, Z. Zhang, J. Chen, X. Yan, B. Zheng, S. Liu and F. Huang, *J. Am. Chem. Soc.*, 2012, **134**, 8711-8717.
97. X. B. Hu, L. Chen, W. Si, Y. Yu and J. L. Hou, *Chem. Commun.*, 2011, **47**, 4694-4696.
98. T. Ogoshi, N. Ueshima, T. Yamagishi, Y. Toyota and N. Matsumi, *Chem. Commun.*, 2012, **48**, 3536-3538.
99. Y. Ma, X. Ji, F. Xiang, X. Chi, C. Han, J. He, Z. Abliz, W. Chen and F. Huang, *Chem. Commun.*, 2011, **47**, 12340-12342.
100. Y. Yao, M. Xue, X. Chi, Y. Ma, J. He, Z. Abliz and F. Huang, *Chem. Commun.*, 2012, **48**, 6505-6507.
101. W. Si, X. B. Hu, X. H. Liu, R. Fan, Z. Chen, L. Weng and J. L. Hou, *Tetrahedron Lett.*, 2011, **52**, 2484-2487.
102. C. Li, Q. Xu, J. Li, F. Yao and X. Jia, *Org. Biomol. Chem.*, 2010, **8**, 1568-1576.
103. C. Li, S. Chen, J. Li, K. Han, M. Xu, B. Hu, Y. Yu and X. Jia, *Chem. Commun.*, 2011, **47**, 11294-11296.
104. K. U. Lao and C. H. Yu, *J. Comput. Chem.*, 2011, **32**, 2716-2726.
105. S. R. Peerannawar and S. P. Gejji, *Comput. Theor. Chem.*, 2012, **999**, 169-178.

106. S. R. Peerannawar and S. P. Gejji, *Spectrochim. Acta Mol. Biomol. Spectrosc.*, 2013, **104**, 368-376.
107. L. E. Dube, B. A. Patel, A. Fagan-Murphy, R. R. Kothur and P. J. Cragg, *Chem. Sens.*, 2013, **3**, 1-6.
108. G. Yu, Z. Zhang, C. Han, M. Xue, Q. Zhou and F. Huang, *Chem. Commun.*, 2012, **48**, 2958-2960.
109. X. Chi, M. Xue, Y. Yao and F. Huang, *Org. Lett.*, 2013, **15**, 4722-4725.
110. G. Yu, B. Hua and C. Han, *Org. Lett.*, 2014, **16**, 2486-2489.
111. Y. Yao, M. Xue, Z. Zhang, M. Zhang, Y. Wang and F. Huang, *Chem. Sci.*, 2013, **4**, 3667-3672.
112. H. Li, D. X. Chen, Y. L. Sun, Y. B. Zheng, L. L. Tan, P. S. Weiss and Y. W. Yang, *J. Am. Chem. Soc.*, 2013, **135**, 1570-1576.
113. D. X. Chen, Y. L. Sun, Y. Zhang, J. Y. Cui, F. Z. Shen and Y. W. Yang, *RSC Adv.*, 2013, **3**, 5765-5768.
114. Y. Yao, K. Jie, Y. Zhou and M. Xue, *Chem. Commun.*, 2014, **50**, 5072-5074.
115. Y. Yao, K. Jie, Y. Zhou and M. Xue, *Tetrahedron Lett.*, 2014, **55**, 3195-3199.
116. D. N. Shurpik, L. S. Yakimova, L. I. Makhmutova, A. R. Makhmutova, I. K. Rizvanov, V. V. Plemenkov and I. I. Stoikov, *Macroheterocycles*, 2014, **7**, 351-357.
117. H.-J. Schneider and A. K. Yatsimirsky, *Chem. Soc. Rev.*, 2008, **37**, 263-277.
118. K. Hirose, in *Analytical Methods in Supramolecular Chemistry*, Wiley-VCH Verlag GmbH & Co. KGaA, New York, 2007, pp. 17-54.
119. J. Tucker, in *Encyclopedia of Supramolecular Chemistry*,, eds. J. W. Steed and J. L. Atwood, Dekker, New York, 2004, vol. 1, pp. 505-519.
120. J. W. Steed and J. L. Atwood, in *Supramolecular Chemistry*, John Wiley & Sons, Ltd, West Sussex, U.K., 2009, pp. 223-284.
121. D. Diamond, G. Svehla, E. M. Seward and M. A. McKervey, *Anal. Chim. Acta*, 1988, **204**, 223-231.
122. D. Diamond and M. A. McKervey, *Chem. Soc. Rev.*, 1996, **25**, 15-24.
123. T. Grady, A. Cadogan, T. McKittrick, S. J. Harris, D. Diamond and M. A. McKervey, *Anal. Chim. Acta*, 1996, **336**, 1-12.
124. J. Koryta, *Anal. Chim. Acta*, 1990, **233**, 1-30.
125. A. O. Siggaard, P. D. Wimberley, A. Fogh, N and I. H. Gøthgen, *Scand. J. Clin. Lab. Invest.*, 1988, **48**, 7-15.
126. D. Ammann and I.-S. Microelectrodes, Springer-Verlag, Berlin, 1986.
127. U. Chaudhry and R. Bhat, *Am. J. Dis. Child.* , 1985, **139**, 1049-1053.

128. K. Hiratani, T. Okada and H. Sugihara, *Bull. Chem. Soc. Jpn.* , 1986, **59**, 2015-2016.
129. K. Suzuki, H. Yamada, K. Sato, K. Watanabe, H. Hisamoto, Y. Tobe and K. Kobiro, *Anal. Chem.*, 1993, **65**, 3404-3410.
130. S. Faulkner, R. Kataky, D. Parker and A. Teasdale, *J. Chem. Soc., Perkin Trans. 2*, 1995, 1761-1769.
131. S. J. Kim, S. O. Jung, S. S. Lee and S. J. Kim, *Bull. Korean Chem. Soc.*, 1993, **14**, 123-123.
132. J. S. Cha, O. Kown and S. Y. Kwon, *Bull. Korean Chem. Soc.*, 1995, **16**, 1009-1011.
133. Y. Umezawa, P. Bühlmann, K. Umezawa, K. Tohda and S. Amemiya, *Pure Appl. Chem.*, 2000, **72**, 1851-2082.
134. S. Sawada, H. Torii, T. Osakai and T. Kimoto, *Anal. Chem.*, 1998, **70**, 4286-4290.
135. K. Suzuki, K. Sato, H. Hisamoto, D. Siswanta, K. Hayashi, N. Kasahara, K. Watanabe, N. Yamamoto and H. Sasakura, *Anal. Chem.*, 1996, **68**, 208-215.
136. K. Kimura, T. Tsuchida, T. Maeda and T. Shono, *Talanta*, 1980, **27**, 801-805.
137. K. Toth, J. Fucsko, E. Lindner, Z. Fehér and E. Pungor, *Anal. Chim. Acta*, 1986, **179**, 359-370.
138. A. Cadogan, D. Diamond, M. R. Smyth, G. Svehla, M. A. McKervey, E. M. Seward and S. J. Harris, *Analyst*, 1990, **115**, 1207–1210.
139. K. A. Brooks, J. R. Allen, P. W. Feldhoff and L. G. Bachas, *Anal. Chem.*, 1996, **68**, 1439-1443.
140. L. Y. Heng and E. A. Hall, *Anal. Chim. Acta*, 1996, **324**, 47-56.
141. L. S. Park, Y. J. Hur and B. K. Sohn, *Sens. Actuators A*, 1996, **57**, 239-243.
142. E. Eyal and G. Rechnitz, *Anal. Chem.*, 1971, **43**, 1090-1093.
143. N. Lukyanenko, N. Y. Titova, N. Nesterenko, T. Kirichenko and S. Scherbakov, *Anal. Chim. Acta*, 1992, **263**, 169-173.
144. E. Bakker, P. Bühlmann and E. Pretsch, *Chem. Rev.*, 1997, **97**, 3083-3132.
145. R. Ludwig, *Fresenius J. Anal. Chem.*, 2000, **367**, 103-128.
146. T. Katsu, N. Okaki, K. Watanabe, K. Takaishi and H. Yokosu, *Anal. Sci.*, 2003, **19**, 771-774.
147. Fluka Chemika Selectophore, Fluka, Buchs, Switzerland, 1996.
148. T. Katsu, D. Xu, K. Tsuji and T. Nagamatsu, *Anal. Chim. Acta*, 1997, **354**, 301-305.
149. T. Katsu, M. Akagi, T. Hiramatsu and T. Tsuchiya, *Analyst*, 1998, **123**, 1369-1372.
150. M. Jańczyk, A. Kutyła-Olesiuk, X. Ceto, M. del Valle, P. Ciosek and W. Wroblewski, *Sens. Actuators B*, 2013, **189**, 179-186.
151. A. R. Shalaby, *Food Res. Int*, 1996, **29**, 675-690.

152. H. Til, H. Falke, M. Prinsen and M. Willems, *Food Chem. Toxicol.*, 1997, **35**, 337-348.
153. L. Maintz and N. Novak, *Am. J. Clin. Nutr.*, 2007, **85**, 1185–1196.
154. J. S. Park, C. H. Lee, E. Y. Kwon, H. J. Lee, J. Y. Kim and S. H. Kim, *Food Control*, 2010, **21**, 1219-1226.
155. F. Durlu-Özkaya, K. Ayhan and N. Vural, *Meat Science*, 2001, **58**, 163-166.
156. A. Kaifer and M. Gómez-Kaifer, in *Supramolecular Electrochemistry*, Wiley-VCH Verlag GmbH, New York, 2008, pp. 11-21.
157. R. S. Nicholson, *Anal. Chem.*, 1965, **37**, 1351-1355.
158. A. J. Bard and L. R. Faulkner, in *Electrochemical methods: Fundamentals and applications*, John Wiley & Sons, Ltd, New York, 2001, pp. 632-658.
159. A. Kaifer and M. Gómez-Kaifer, in *Supramolecular Electrochemistry*, Wiley-VCH Verlag GmbH, New York, 2007, pp. 1-10.
160. J. Wang, in *Electroanalytical techniques in clinical chemistry and laboratory medicine*, VCH Publishers, Inc., New York, 1988, pp. 1-42.
161. A. J. Bard and L. R. Faulkner, in *Electrochemical methods: Fundamentals and applications*, John Wiley & Sons, Ltd., New York, 2001, pp. 1-43.
162. P. Kissinger, C. R. Preddy, R. E. Shoup and W. R. Heineman, in *Laboratory Techniques in Electroanalytical Chemistry, revised and expanded*, eds. P. Kissinger and W. R. Heineman, MARCEL DEKKER, INC., New York, 1996, pp. 11-49.
163. S. Walsh, PhD thesis, Dublin City University, 1997.
164. C. Han, Z. Zhang, G. Yu and F. Huang, *Chem. Commun.*, 2012, **48**, 9876-9878.
165. J. Hu and M. A. Fox, *J. Org. Chem.*, 1999, **64**, 4959-4961.
166. A. B. Kyte, K. A. Owens, I. O. Sutherland and R. F. Newton, *J. Chem. Soc., Perkin Trans. 1*, 1987, 1921-1927.
167. K. R. Sathisha, S. A. Khanum, J. N. N. S. Chandra, F. Ayisha, S. Balaji, G. K. Marathe, S. Gopal and K. S. Rangappa, *Bioorg. Med. Chem.*, 2011, **19**, 211-220.
168. R. R. Kothur, F. Fucassi, G. Dichello, L. Doudet, W. Abdalaziz, B. A. Patel, G. W. Cave, I. A. Gass, D. K. Sarker, S. V. Mikhalovsky and P. J. Cragg, *Supramol. Chem.*, 2016, **28**, 436-443.
169. R. Kamiński, J. Kowalski, I. Mames, B. Korybut-Daszkiewicz, S. Domagała and K. Woźniak, *Eur. J. Inorg. Chem.*, 2011, **2011**, 479-488.
170. T. Boinski and A. Szumna, *Tetrahedron*, 2012, **68**, 9419-9422.
171. R. R. Kothur, J. Hall, B. A. Patel, C. L. Leong, M. G. Boutelle and P. J. Cragg, *Chem. Commun.*, 2014, **50**, 852-854.

172. Q. Zhou, B. Zhang, D. Han, R. Chen, F. Qiu, J. Wu and H. Jiang, *Chem. Commun.*, 2015, **51**, 3124-3126.
173. L. Liu, D. Cao, Y. Jin, H. Tao, Y. Kou and H. Meier, *Org. Biomol. Chem.*, 2011, **9**, 7007-7010.
174. L. J. Barbour, *J. Supramol. Chem.*, 2001, **1**, 189-191.
175. J. Koryta, *Anal. Chim. Acta*, 1977, **91**, 1-85.
176. A. W. M. Sweetsur, *Analyst*, 1974, **99**, 690-692.
177. J. Stuart, *Analyst*, 1970, **95**, 1032-1038.
178. J. Halliday and F. Wood, *Analyst*, 1966, **91**, 802-805.
179. G. Moody and J. Thomas, in *Ion-Selective Electrodes in Analytical Chemistry*, ed. H. Freiser, Plenum Press, New York, 1978, vol. 1, pp. 339-433.
180. M. S. Frant, *Analyst*, 1994, **119**, 2293–2301.
181. A. Shatkay, *Anal. Chem.*, 1968, **40**, 458-458.
182. C. P. Oliveira, M. B. A. Gloria, J. F. Barbour and R. A. Scanlan, *J. Agric. Food Chem.*, 1995, **43**, 967-969.
183. M. Dror, E. Bergs and R. Rhodes, *Sens. Actuators*, 1987, **11**, 23-36.
184. A. L. Odom and P. V. Kelly, *Sci. Educ.*, 2001, **85**, 615-635.
185. W. Nernst, *Z. Phys. Chem.*, 1889, **4**, 129–181.
186. Z. Brzozka, B. Lammerink, D. N. Reinhoudt, E. Ghidini and R. Ungaro, *J. Chem. Soc., Perkin Trans. 2*, 1993, 1037-1040.
187. K. M. O'Connor, M. Cherry, G. Svehla, S. J. Harris and M. A. McKervey, *Talanta*, 1994, **41**, 1207-1217.
188. B. S. Creaven, D. F. Donlon and J. McGinley, *Coordin. Chem. Rev.*, 2009, **253**, 893-962.
189. Y. H. Cho, S. G. Rha, S. K. Chang, T. D. Chung, K. Cho and H. Kim, *J. Inclusion Phenom. Macrocyclic Chem.*, 1998, **31**, 119-129.
190. B. Mokhtari, K. Pourabdollah and N. Dalali, *J. Inclusion Phenom. Macrocyclic Chem.*, 2011, **69**, 1-55.
191. T. Katsu, Y. Yokoyama, K. Ueda, K. Kohno and T. Yamato, *Anal. Sci.*, 2005, **21**, 175-178.
192. T. E. Andreoli, M. Tieffenberg and D. C. Tosteson, *J. Gen. Physiol.*, 1967, **50**, 2527-2545.
193. Y. Tu, Y. Lin, W. Yantasee and Z. Ren, *Electroanalysis*, 2005, **17**, 79-84.
194. I. Corb, F. Manea, C. Radovan, A. Pop, G. Burtica, P. Malchev, S. Picken and J. Schoonman, *Sensors*, 2007, **7**, 2626-2635.

195. L. Rassaei, M. Sillanpää, M. J. Bonné and F. Marken, *Electroanalysis*, 2007, **19**, 1461-1466.
196. L. Zhu, C. Tian, J. Zhai and R. Yang, *Sens. Actuators B*, 2007, **125**, 254-261.
197. M. Pumera, A. Merkoçi and S. Alegret, *Sens. Actuators B*, 2006, **113**, 617-622.
198. F. Céspedes, E. Martinez-Fàbregas and S. Alegret, *TrAC, Trends Anal. Chem.*, 1996, **15**, 296-304.
199. S. Ramírez-García, S. Alegret, F. Céspedes and R. J. Forster, *Analyst*, 2002, **127**, 1512-1519.
200. T. Gabay, B. M. David, I. Kalifa, R. Sorkin, R. A. Zeev, B. E. Jacob and Y. Hanein, *Nanotechnology*, 2007, **18**, 035201-035211.
201. J. Manso, M. Mena, Y. P. Sedeno and J. Pingarron, *J. Electroanal. Chem.*, 2007, **603**, 1-7.
202. R. K. Mendes, P. Cervini and É. T. G. Cavalheiro, *Talanta*, 2006, **68**, 708-712.
203. D. Sun, L. Zhu and G. Zhu, *Anal. Chim. Acta*, 2006, **564**, 243-247.
204. F. Marken, M. L. Gerrard, I. M. Mellor, R. J. Mortimer, C. E. Madden, S. Fletcher, K. Holt, J. S. Foord, R. H. Dahm and F. Page, *Electrochem. Commun.*, 2001, **3**, 177-180.
205. D. O'Hare, J. V. Macpherson and A. Willows, *Electrochem. Commun.*, 2002, **4**, 245-250.
206. Ü. A. Kırgöz, D. Odacı, S. Timur, A. Merkoçi, N. Pazarlıoğlu, A. Telefoncu and S. Alegret, *Bioelectrochemistry*, 2006, **69**, 128-131.
207. A. M. Bond, P. J. Mahon, J. Schiewe and V. V. Beckett, *Anal. Chim. Acta*, 1997, **345**, 67-74.
208. D. Demetriades, A. Economou and A. Voulgaropoulos, *Anal. Chim. Acta*, 2004, **519**, 167-172.
209. J. J. Sun, L. Guo, D. F. Zhang, W. H. Yin and G. N. Chen, *Electrochem. Commun.*, 2007, **9**, 283-288.
210. N. Y. Stozhko, N. A. Malakhova, M. V. Fyodorov and K. Z. Brainina, *J. Solid State Electrochem.*, 2008, **12**, 1219-1230.
211. Z. Hu, C. J. Seliskar and W. R. Heineman, *Anal. Chim. Acta*, 1998, **369**, 93-101.
212. J. Liu, X. Wang, G. Chen, N. Gan and S. Bi, *Analyst*, 2001, **126**, 1404-1408.
213. Q. Yin, N. Brandon and G. Kelsall, *J. Appl. Electrochem.*, 2000, **30**, 1109-1117.
214. I. Viter, A. Kamenev and A. Sidakov, *Zh. Anal. Khim.*, 1994, **49**, 1295-1298.
215. A. Kamenev and M. Kovalenko, *J. Anal. Chem.*, 2000, **55**, 594-597.
216. C. Brett, L. Angnes and H. D. Liess, *Electroanalysis*, 2001, **13**, 765-769.
217. R. Pauliukaitė and C. Brett, *Electroanalysis*, 2005, **17**, 1354-1359.

218. M. Huang, M. J. Huang, P. W. Faguy and W. P. Pan, *Electroanalysis*, 1997, **9**, 1201-1204.
219. C. Gouveia-Caridade, R. Pauliukaite and C. Brett, *Electroanalysis*, 2006, **18**, 854-861.
220. Z. Liu, S. Huan, J. Jiang, G. Shen and R. Yu, *Talanta*, 2006, **68**, 1120-1125.
221. R. Adams, *Anal. Chem.*, 1958, **30**, 1576-1576.
222. J. Lu, X. He, X. Zeng, Q. Wan and Z. Zhang, *Talanta*, 2003, **59**, 553-560.
223. J. Zima, I. Švancara, J. Barek and K. Vytřas, *Crit. Rev. Anal. Chem.*, 2009, **39**, 204-227.
224. K. C. Honeychurch, J. P. Hart, D. C. Cowell and D. W. Arrigan, *Electroanalysis*, 2002, **14**, 177-185.
225. F. Wang, X. Wei, C. Wang, S. Zhang and B. Ye, *Talanta*, 2010, **80**, 1198-1204.
226. E. Ç. Canpolat, E. Şar, N. Y. Coşkun and H. Cankurtaran, *Electroanalysis*, 2007, **19**, 1109-1115.
227. H. Cong, Z. J. Li, Q. X. Geng, Z. Tao and G. Wei, *J. Inclusion Phenom. Macrocyclic Chem.*, 2015, **81**, 493-498.
228. R. M. Kotkar, P. B. Desai and A. K. Srivastava, *Sens. Actuators B*, 2007, **124**, 90-98.
229. R. M. Kotkar and A. K. Srivastava, *Sens. Actuators B*, 2006, **119**, 524-530.
230. V. S. Ijeri, P. V. Jaiswal and A. K. Srivastava, *Anal. Chim. Acta*, 2001, **439**, 291-297.
231. R. M. Kotkar and A. K. Srivastava, *J. Inclusion Phenom. Macrocyclic Chem.*, 2008, **60**, 271-279.
232. Spartan 10, Wavefunction, Inc., Irvine, CA, USA.
233. C. F. Macrae, P. R. Edgington, P. McCabe, E. Pidcock, G. P. Shields, R. Taylor, M. Towler and J. V. D. Streek, *J. Appl. Cryst.* , 2006, **39**, 453-457.
234. R. Sheehan and P. J. Cragg, in *Supramolecular Chemistry: From Molecules to Nanomaterials*, eds. P. A. Gale and J. W. Steed, John Wiley & Sons Ltd., Chichester, 2012, pp. 689-708.
235. R. Sheehan and P. J. Cragg, *Supramol. Chem.*, 2008, **20**, 443-451.
236. J. P. Stewart, *J. Comput. Chem.*, **10**, 209-220.
237. O. Lawal, K. S. J. Iqbal, A. Mohamadi, P. Razavi, H. T. Dodd, M. C. Allen, S. Siddiqui, F. Fucassi and P. J. Cragg, *Supramol. Chem.*, 2009, **21**, 55-60.
238. G. W. Gokel and M. M. Daschbach, *Coord. Chem. Rev.*, 2008, **252**, 886-902.
239. A. Ulman, in *An Introduction to Ultrathin Organic Films: From Langmuir--Blodgett to Self--Assembly*, Academic press, London, U.K.,2013, pp. 237-301.

240. J. Sagiv, *J. Am. Chem. Soc.*, 1980, **102**, 92-98.
241. P. E. Laibinis, G. M. Whitesides, D. L. Allara, Y. T. Tao, A. N. Parikh and R. G. Nuzzo, *J. Am. Chem. Soc.*, 1991, **113**, 7152-7167.
242. F. Song, S. Zhang, D. Bonifazi, O. Enger, F. Diederich and L. Echegoyen, *Langmuir*, 2005, **21**, 9246-9250.
243. D. L. Allara and R. G. Nuzzo, *Langmuir*, 1985, **1**, 45-52.
244. L. M. Goldenberg, M. R. Bryce and M. C. Petty, *J. Mater. Chem.*, 1999, **9**, 1957-1974.
245. R. M. Crooks and A. J. Ricco, *Acc. Chem. Res.*, 1998, **31**, 219-227.
246. K. B. Blodgett and I. Langmuir, *Phys. Rev.* , 1937, **51**, 964.
247. K. B. Blodgett, *J. Am. Chem. Soc.*, 1935, **57**, 1007-1022.
248. I. Langmuir, *J. Am. Chem. Soc.*, 1917, **39**, 1848-1906.
249. W. Bigelow, D. Pickett and W. Zisman, *J. Colloid Sci.* , 1946, **1**, 513-538.
250. H. Finklea, S. Avery, M. Lynch and T. Furtsch, *Langmuir*, 1987, **3**, 409-413.
251. H. O. Finklea, D. A. Snider, J. Fedyk, E. Sabatani, Y. Gafni and I. Rubinstein, *Langmuir*, 1993, **9**, 3660-3667.
252. L. H. Dubois and R. G. Nuzzo, *Ann. Rev. Phys. Chem.*, 1992, **43**, 437-463.
253. A. Ulman, *Chem. Rev.*, 1996, **96**, 1533-1554.
254. F. Schreiber, *J. Phys.: Condens. Matter*, 2004, **16**, R881.
255. C. D. Bain, E. B. Troughton, Y. T. Tao, J. Evall, G. M. Whitesides and R. G. Nuzzo, *J. Am. Chem. Soc.*, 1989, **111**, 321-335.
256. A. Ulman, J. E. Eilers and N. Tillman, *Langmuir*, 1989, **5**, 1147-1152.
257. M. D. Porter, T. B. Bright, D. L. Allara and C. E. Chidsey, *J. Am. Chem. Soc.*, 1987, **109**, 3559-3568.
258. R. A. Marcus and N. Sutin, *Biochim. Biophys. Acta.*, 1985, **811**, 265-322.
259. M. A. Rampi and G. M. Whitesides, *Chem. Phys.*, 2002, **281**, 373-391.
260. R. G. Nuzzo, F. A. Fusco and D. L. Allara, *J. Am. Chem. Soc.*, 1987, **109**, 2358-2368.
261. T. Kawaguchi, Y. Yamauchi, H. Maeda and H. Ohmor1, *Anal. Sci.*, 1994, **10**, 963-965.
262. J. Zhang, A. M. Kuznetsov, I. G. Medvedev, Q. Chi, T. Albrecht, P. S. Jensen and J. Ulstrup, *Chem. Rev.*, 2008, **108**, 2737-2791.
263. M. Fibbioli, K. Bandyopadhyay, S. G. Liu, L. Echegoyen, O. Enger, F. Diederich, P. Bühlmann and E. Pretsch, *Chem. Commun.*, 2000, 339-340.
264. T. D. Chung, J. Park, J. Kim, H. Lim, M. J. Choi, J. R. Kim, S. K. Chang and H. Kim, *Anal. Chem.*, 2001, **73**, 3975-3980.

265. A. Ikeda, T. Tsudera and S. Shinkai, *J. Org. Chem.*, 1997, **62**, 3568-3574.
266. G. Eisenman, *Biophys. J.*, 1962, **2**, 259-323.
267. G. J. Higby, *Gold bulletin*, 1982, **15**, 130-140.
268. J. Turkevich, P. C. Stevenson and J. Hillier, *Discuss. Faraday Soc.*, 1951, **11**, 55-75.
269. G. Frens, *Kolloid-Z. Z. Polym.*, 1972, **250**, 736-741.
270. G. Frens, *Nature*, 1973, **241**, 20-22.
271. M. Brust, M. Walker, D. Bethell, D. J. Schiffrin and R. Whyman, *J. Chem. Soc., Chem. Commun.*, 1994, 801-802.
272. Y. Cheng and D. J. Schiffrin, *J. Chem. Soc., Faraday Trans.*, 1996, **92**, 3865-3871.
273. C. A. Foss Jr, G. L. Hornyak, J. A. Stockert and C. R. Martin, *J. Phys. Chem.*, 1994, **98**, 2963-2971.
274. J. C. Hulteen, C. J. Patrissi, D. L. Miner, E. R. Crosthwait, E. B. Oberhauser and C. R. Martin, *J. Phys. Chem. B*, 1997, **101**, 7727-7731.
275. P. Calandra, G. Calogero, A. Sinopoli and P. G. Gucciardi, *Int. J. Photoenergy*,, 2010, **2010**, 109495-109499.
276. J. Yguerabide and E. E. Yguerabide, *Anal. Biochem.* , 1998, **262**, 137-156.
277. S. Link and M. A. El-Sayed, *Ann. Rev. Phys. Chem.*, 2003, **54**, 331-366.
278. H. Jans and Q. Huo, *Chem. Soc. Rev.*, 2012, **41**, 2849-2866.
279. X. Huang and M. A. EI-Sayed, *J. Adv. Res.*, 2010, **1**, 13-28.
280. Cytodiagnostics, http://www.cytodiagnostics.com/store/pc/Gold-Nanoparticle-Properties-d2.htm, (Accessed 25 June, 2016).
281. R. Jin, G. Wu, Z. Li, C. A. Mirkin and G. C. Schatz, *J. Am. Chem. Soc.*, 2003, **125**, 1643-1654.
282. J. S. Lee, P. A. Ulmann, M. S. Han and C. A. Mirkin, *Nano lett.*, 2008, **8**, 529-533.
283. A. K. Boal, F. Ilhan, J. E. Derouchey, T. A. Thomas, T. P. Russell and V. M. Rotello, *Nature*, 2000, **404**, 746-748.
284. J. Jin, T. Iyoda, C. Cao, Y. Song, L. Jiang, T. J. Li and D. B. Zhu, *Angew. Chem., Int. Ed.*, 2001, **113**, 2193-2196.
285. J. Liu, S. Mendoza, E. Román, M. J. Lynn, R. Xu and A. E. Kaifer, *J. Am. Chem. Soc.*, 1999, **121**, 4304-4305.
286. V. Patil, K. Mayya, S. Pradhan and M. Sastry, *J. Am. Chem. Soc.*, 1997, **119**, 9281-9282.
287. C. O. Mellet, J. M. G. Fernández and J. M. Benito, *Chem. Soc. Rev.*, 2011, **40**, 1586-1608.
288. G. W. Gokel, W. M. Leevy and M. E. Weber, *Chem. Rev.*, 2004, **104**, 2723-2750.

289. K. Kim, N. Selvapalam, Y. H. Ko, K. M. Park, D. Kim and J. Kim, *Chem. Soc. Rev.*, 2007, **36**, 267-279.
290. A. Acharya, K. Samanta and C. P. Rao, *Coordin. Chem. Rev.*, 2012, **256**, 2096-2125.
291. H. Li, D. Xiong, Y. Chen, P. Xie and J. Wan, *J. Inclusion Phenom. Macrocyclic Chem.*, 2008, **60**, 169-172.
292. A. Arduini, D. Demuru, A. Pochini and A. Secchi, *Chem. Commun.*, 2005, 645-647.
293. C. Han, L. Zeng, H. Li and G. Xie, *Sens. Actuators B*, 2009, **137**, 704-709.
294. S. W. Oh, J. D. Moon, H. J. Lim, S. Y. Park, T. Kim, J. Park, M. H. Han, M. Snyder and E. Y. Choi, *FASEB J.*, 2005, **19**, 1335-1340.
295. Y. Chen, J. Zhang, Y. Gao, J. Lee, H. Chen and Y. Yin, *Bio-sens. Bioelectron.*, 2015, **72**, 306-312.
296. S. Y. Lin, S. W. Liu, C. M. Lin and C. H. Chen, *Anal. Chem.*, 2002, **74**, 330-335.
297. S. O. Obare, R. E. Hollowell and C. J. Murphy, *Langmuir*, 2002, **18**, 10407-10410.
298. Y. Kim, R. C. Johnson and J. T. Hupp, *Nano Lett.*, 2001, **1**, 165-167.
299. Y. Yao, M. Xue, J. Chen, M. Zhang and F. Huang, *J. Am. Chem. Soc.*, 2012, **134**, 15712-15715.
300. Y. Yao, K. Jie, Y. Zhou and M. Xue, *Tetrahedron Lett.*, 2014, **55**, 3195-3199.
301. H. Li and Y. W. Yang, *Chin. Chem. Lett.*, 2013, **24**, 545-552.
302. J. Zhou, M. Chen, J. Xie and G. Diao, *ACS Appl. Mater. Interfaces*, 2013, **5**, 11218-11224.
303. M. M. Tian, D. X. Chen, Y. L. Sun, Y. W. Yang and Q. Jia, *RSC Adv.*, 2013, **3**, 22111-22119.
304. Y. Yao, Y. Zhou, J. Dai, S. Yue and M. Xue, *Chem. Commun.*, 2014, **50**, 869-871.
305. X. Liao, L. Guo, J. Chang, S. Liu, M. Xie and G. Chen, *Macromol. Rapid Commun.*, 2015, **36**, 1492-1497.
306. C. Park, E. S. Jeong, K. J. Lee, H. R. Moon and K. T. Kim, *Chem. Asian J.*, 2014, **9**, 2761-2764.
307. Y. Yao, Y. Wang and F. Huang, *Chem. Sci.*, 2014, **5**, 4312-4316.
308. V. Montes-Garcia, C. Fernandez-Lopez, B. Gomez, I. Perez-Juste, L. Garcia-Rio, L. M. Liz-Marzan, J. Perez-Juste and I. Pastoriza-Santos, *Chem. Eur. J.*, 2014, **20**, 8404-8409.
309. K. Smith and C. Oatley, *Br. J. Appl. Phys.*, 1955, **6**, 391.
310. W. Zhou, R. Apkarian, Z. L. Wang and D. Joy, in *Scanning Microscopy for Nanotechnology*, eds. W. Zhou and Z. L. Wang, Springer, New York, 2006, pp. 1-40.

311. M. R. Lee, *Mineral. Mag.*, 2010, **74**, 1-27.
312. R. Egerton, in *Electron Energy-Loss Spectroscopy in the Electron Microscope*, Springer, 2011, pp. 29-109.
313. D. J. Smith, *Mater. Today*, 2008, **11**, 30-38.
314. M. Brust, M. Walker, D. Bethell, D. J. Schiffrin and R. Whyman, *J. Chem. Soc., Chem. Commun.*, 1994, 801-802.
315. J. M. Ha, A. Katz, A. B. Drapailo and V. I. Kalchenko, *J. Phys. Chem. C*, 2009, **113**, 1137-1142.
316. R. L. McCreery, *Chem. Rev.*, 2008, **108**, 311-345.

8.1 Publications

1. **Raghuram Reddy Kothur** and Peter J. Cragg, Recent Developments in Pillar[5]arene Chemistry, *Sci. Adv. Today*, 2 (2**016)**, 25247.

2. **Raghuram Reddy Kothur**, Flavia Fucassi, Gennaro Dichello, Ludovic Doudet, Wafa Abdalaziz, Bhavik Anil Patel, Gareth WV Cave, Ian A Gass, Dipak K Sarker, Sergey V Mikhalovsky, and Peter J. Cragg, 'Synthesis and Applications of Copillar[5]arene Dithiols', *Supramol. Chem.*, 28 (**2016**), 436-443.

3. **Raghuram Reddy Kothur**, B. A. Patel, and P. J. Cragg, 'Pillar[*n*]arene-Based Chemical Sensors', *Sci. Lett. J.*, 4, (**2015**), 1-8.

4. **Raghuram Reddy Kothur**, Jessica Hall, Bhavik Anil Patel, Chi Leng Leong, Martyn G. Boutelle, and Peter J. Cragg, 'A Low pH Sensor from an Esterified Pillar[5]arene', *Chem. Commun.*, 50 (**2014**), 852-854.

5. Lorraine E Dube, Bhavik A Patel, Aidan Fagan-Murphy, **Raghu R Kothur**, and Peter J Cragg, 'Detection of Clinically Important Cations by a Pillar[5]arene-Modified Electrochemical Sensor', *Chem. Sens.*, 3 (**2013**), 1-6.

APPENDIX

9.1 Additional information of Chapter – 2

1. ^{1}H NMR spectrum of 1 in $CDCl_3$

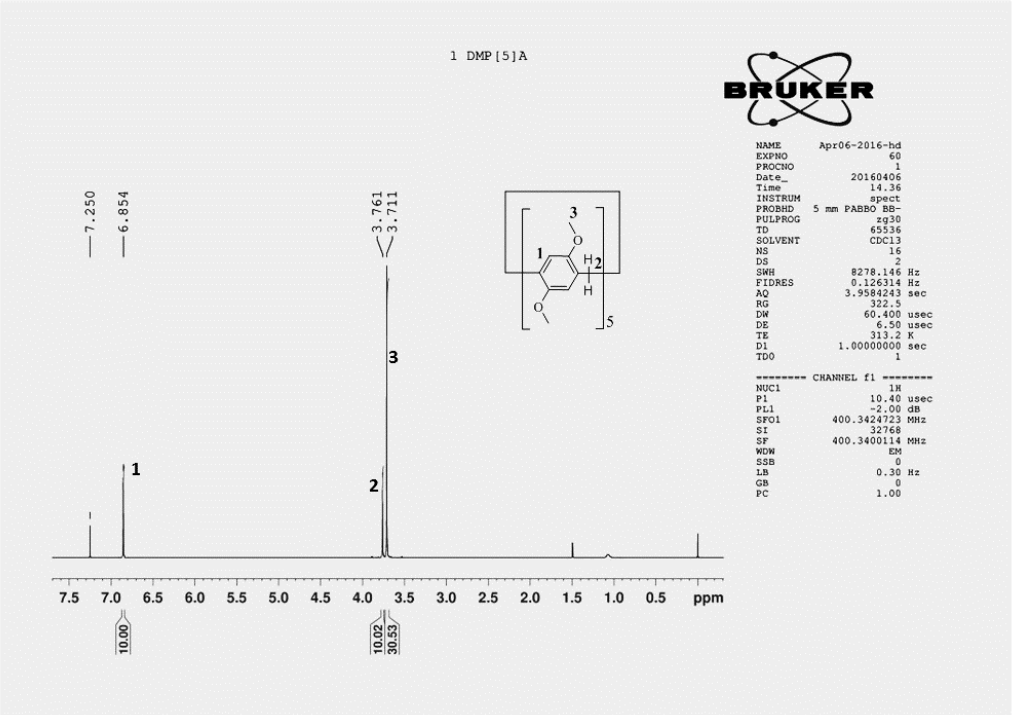

2. ^{13}C NMR spectrum of 1 in $CDCl_3$

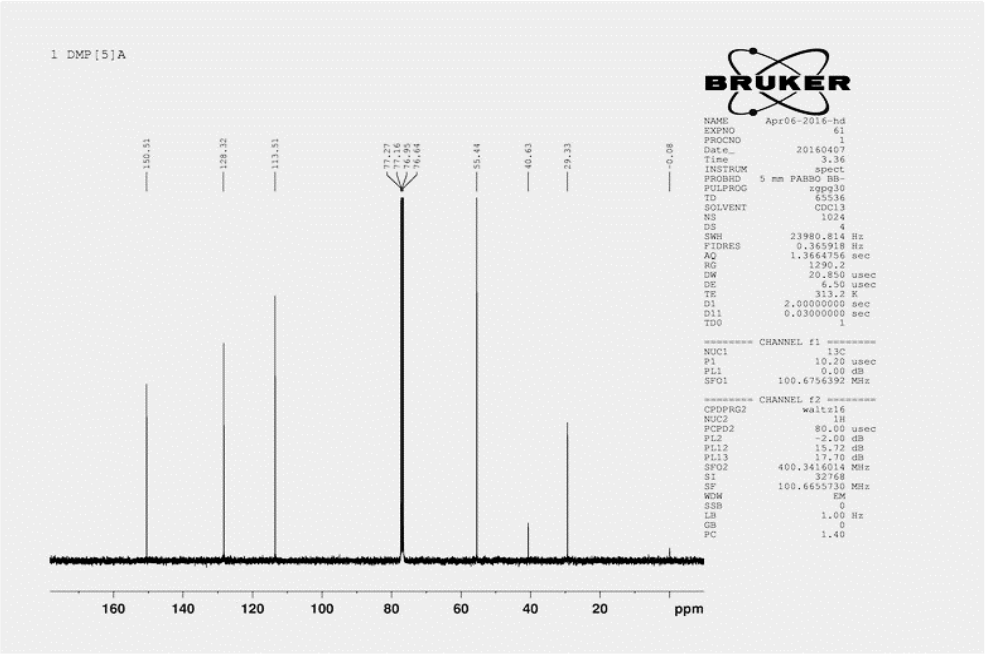

3. ESI mass spectrum of 1

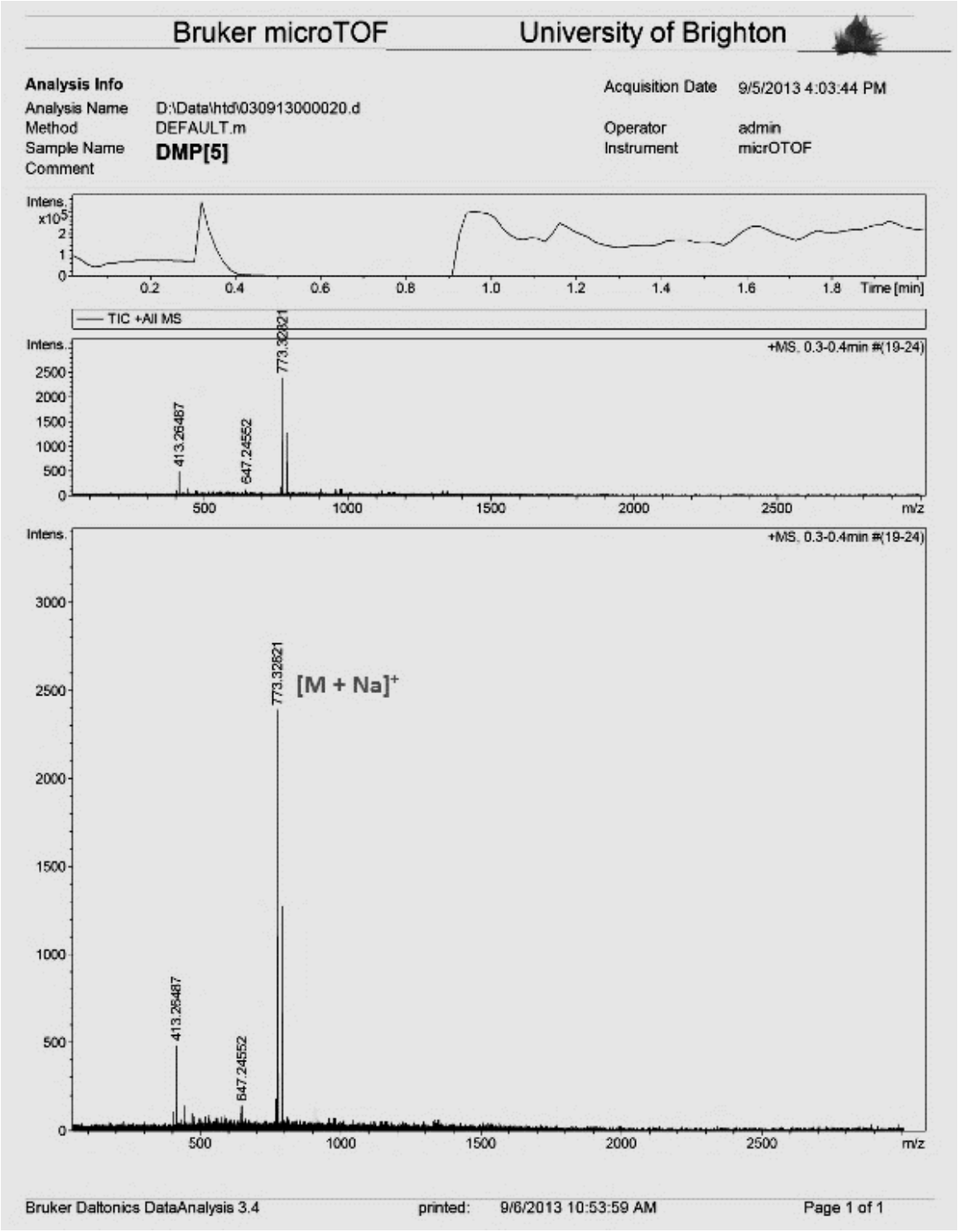

4. ^{1}H NMR spectrum of 3 in $CDCl_3$

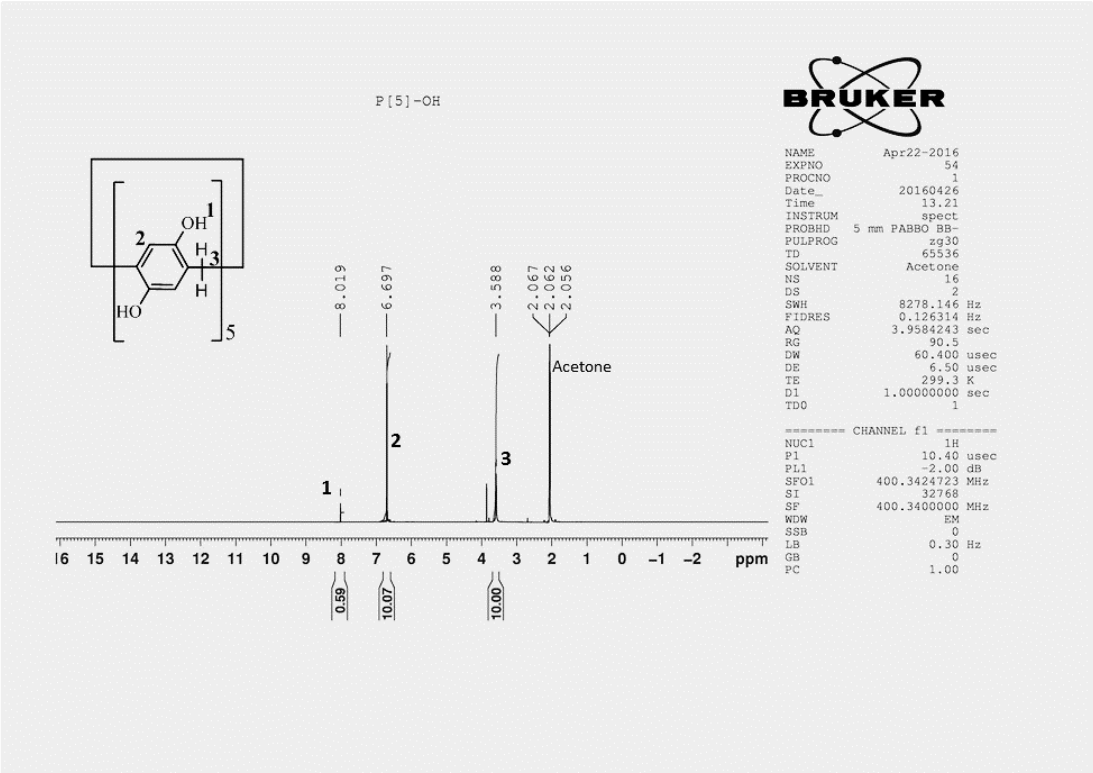

5. ^{13}C NMR spectrum of 3 in $CDCl_3$

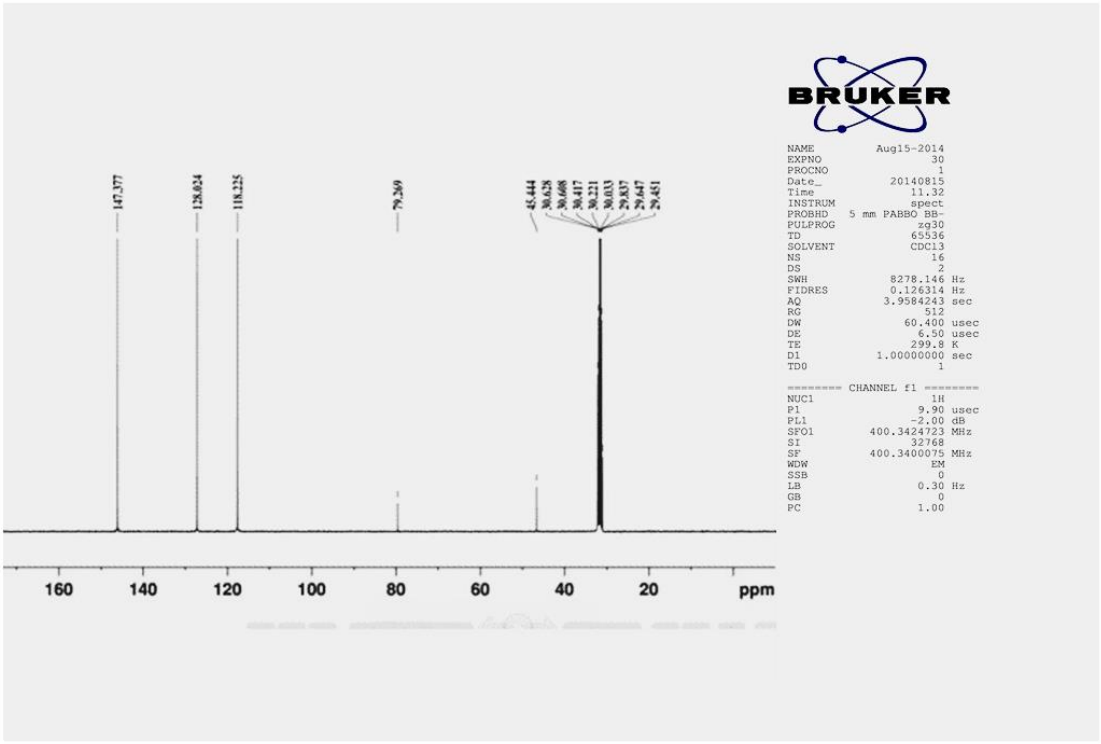

6. ESI mass spectrum of 3

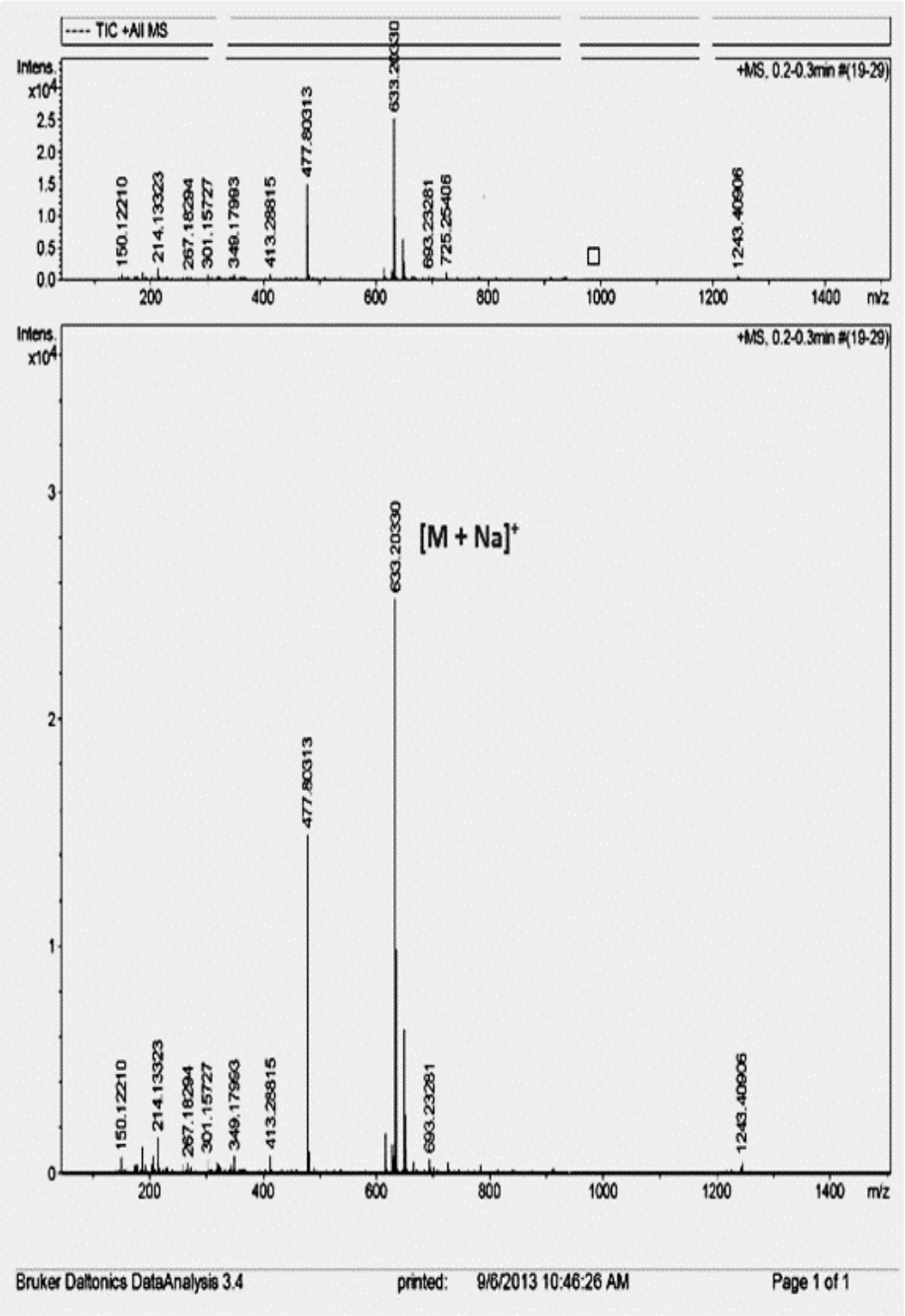

7. ^{1}H NMR spectrum of 21 in $CDCl_3$

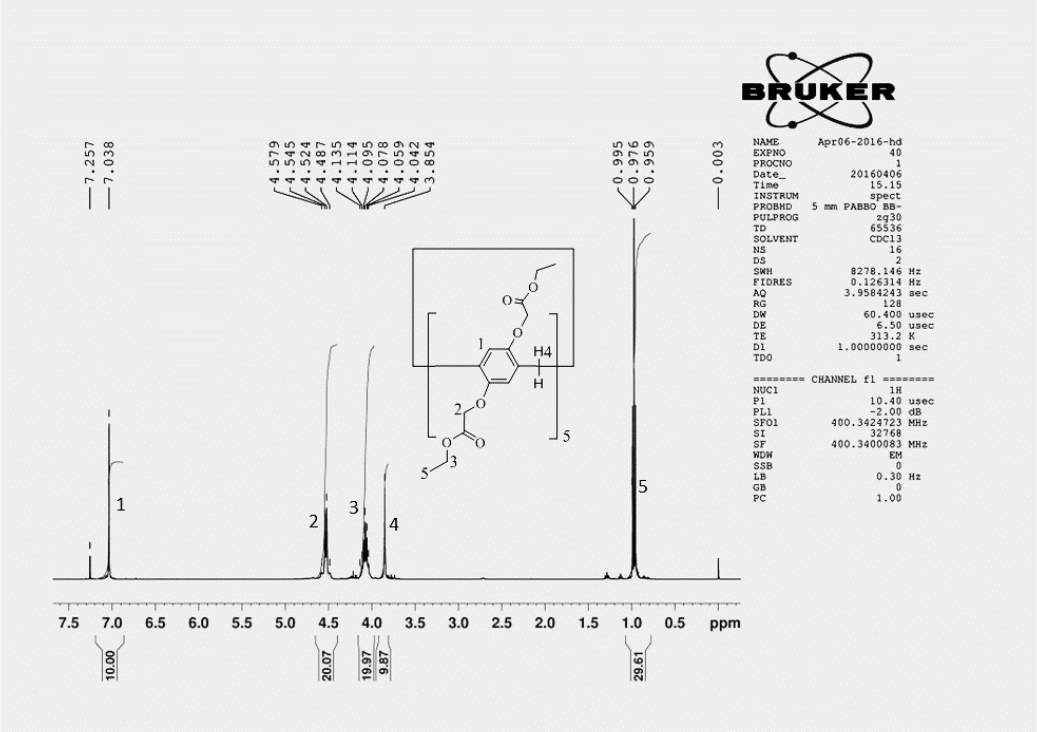

8. ^{13}C NMR spectrum of 21 in $CDCl_3$

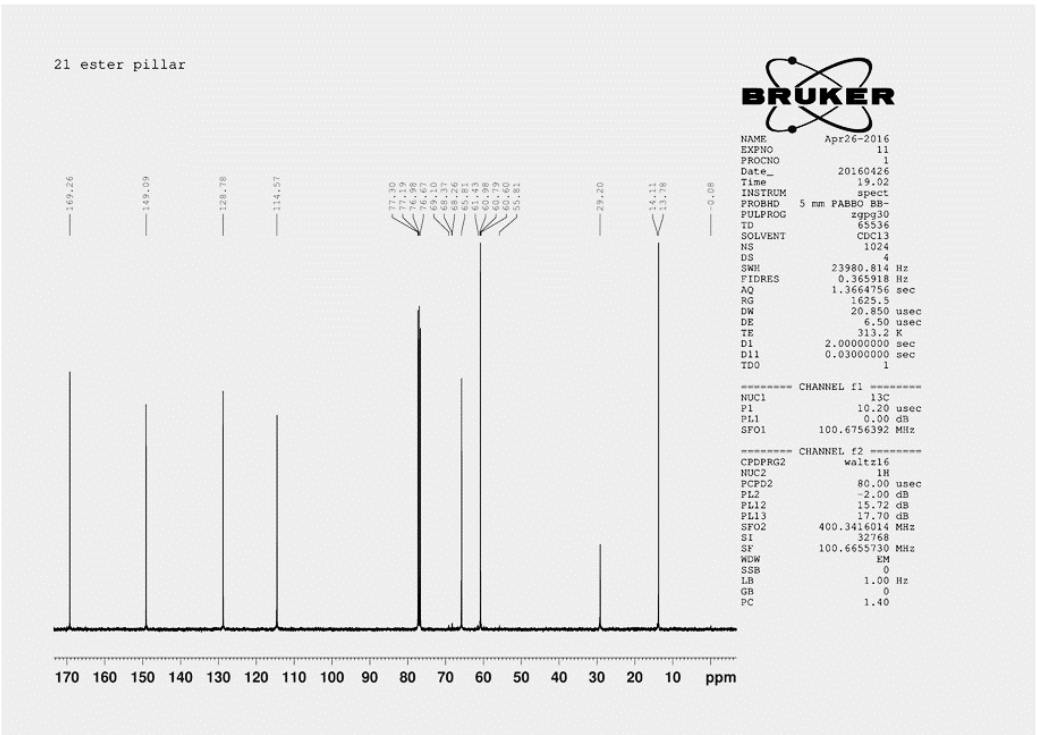

9. ESI mass spectrum of 21

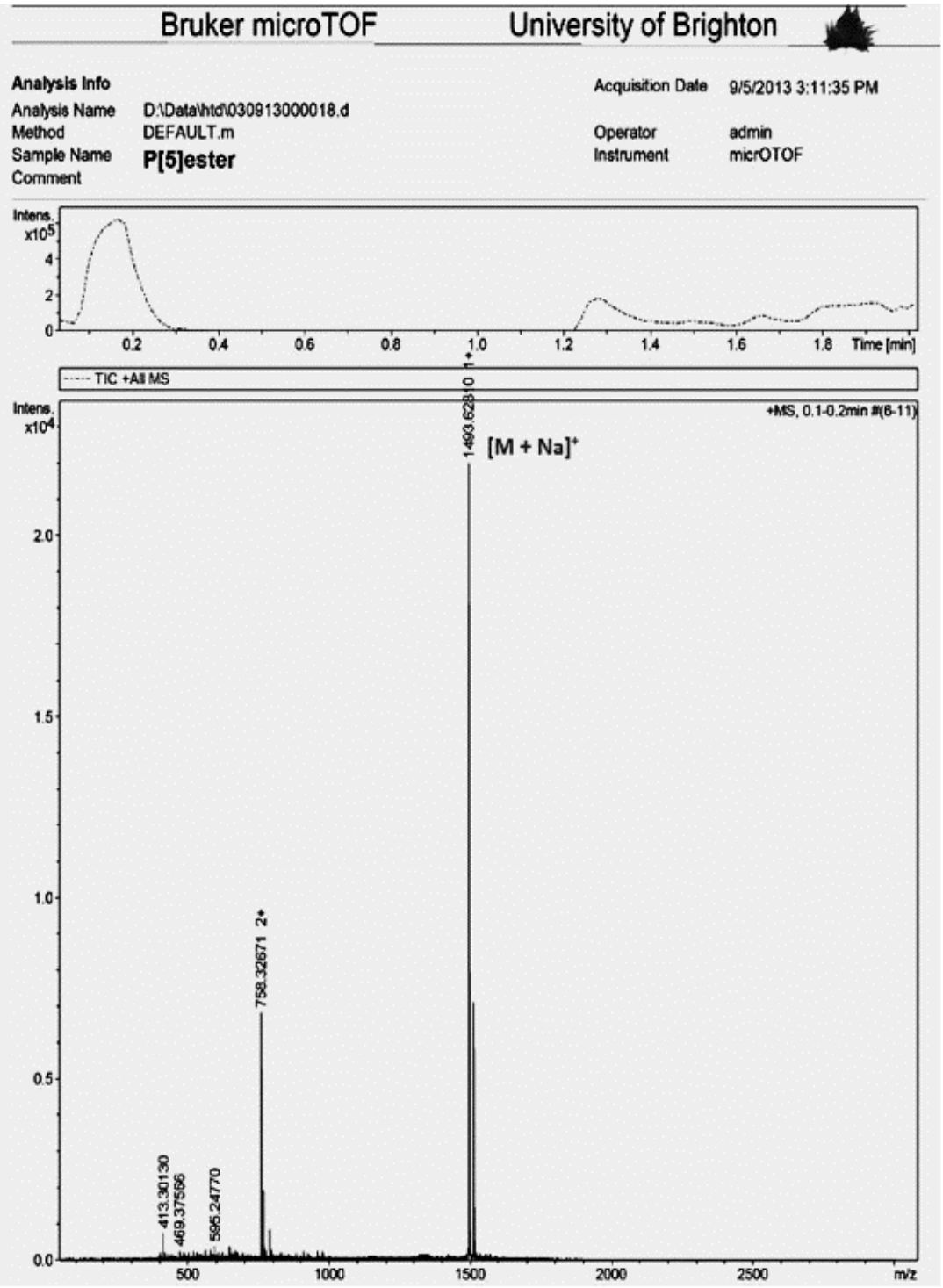

10. ^{1}H NMR spectrum of 40 in $CDCl_3$

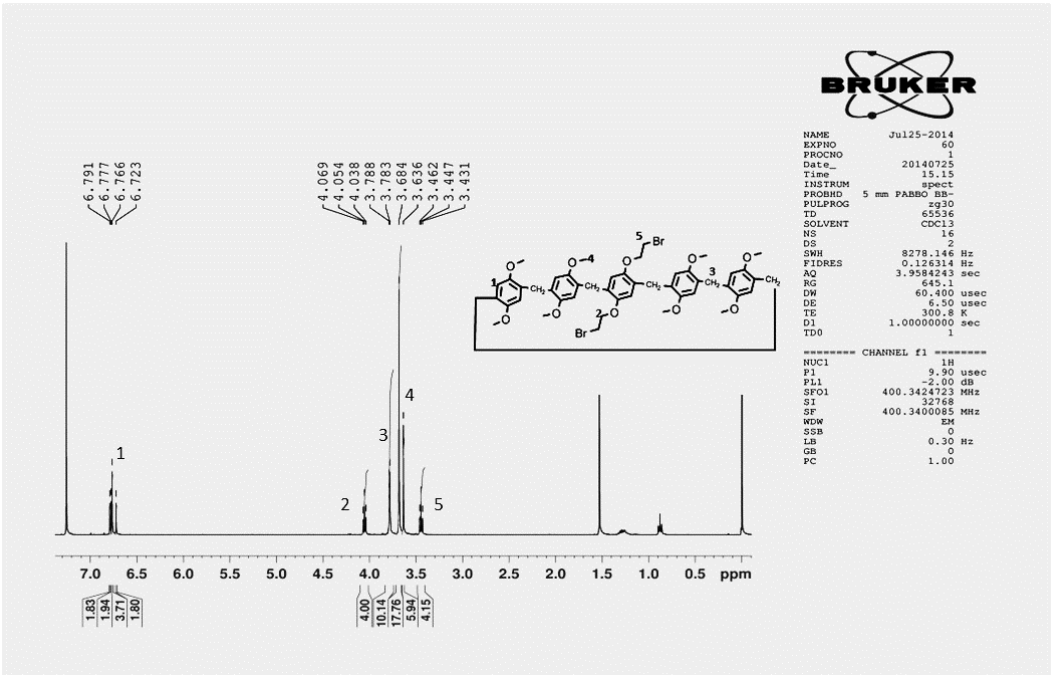

11. ^{13}C NMR spectrum of 40 in $CDCl_3$

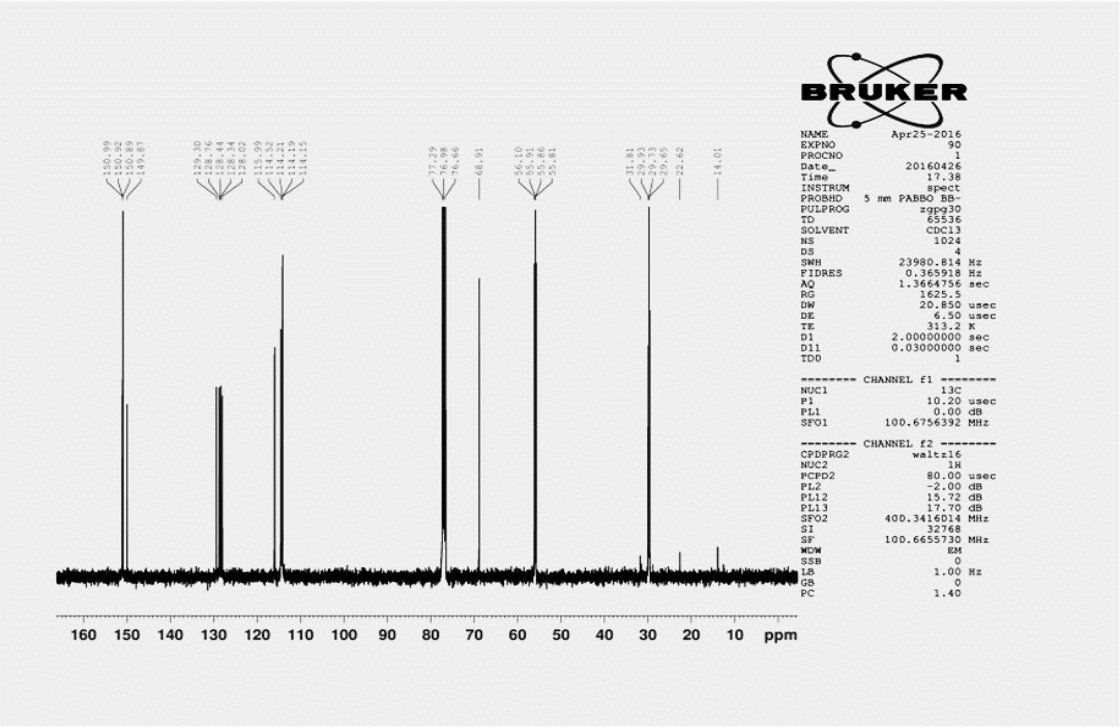

12. ESI mass spectrum of 40

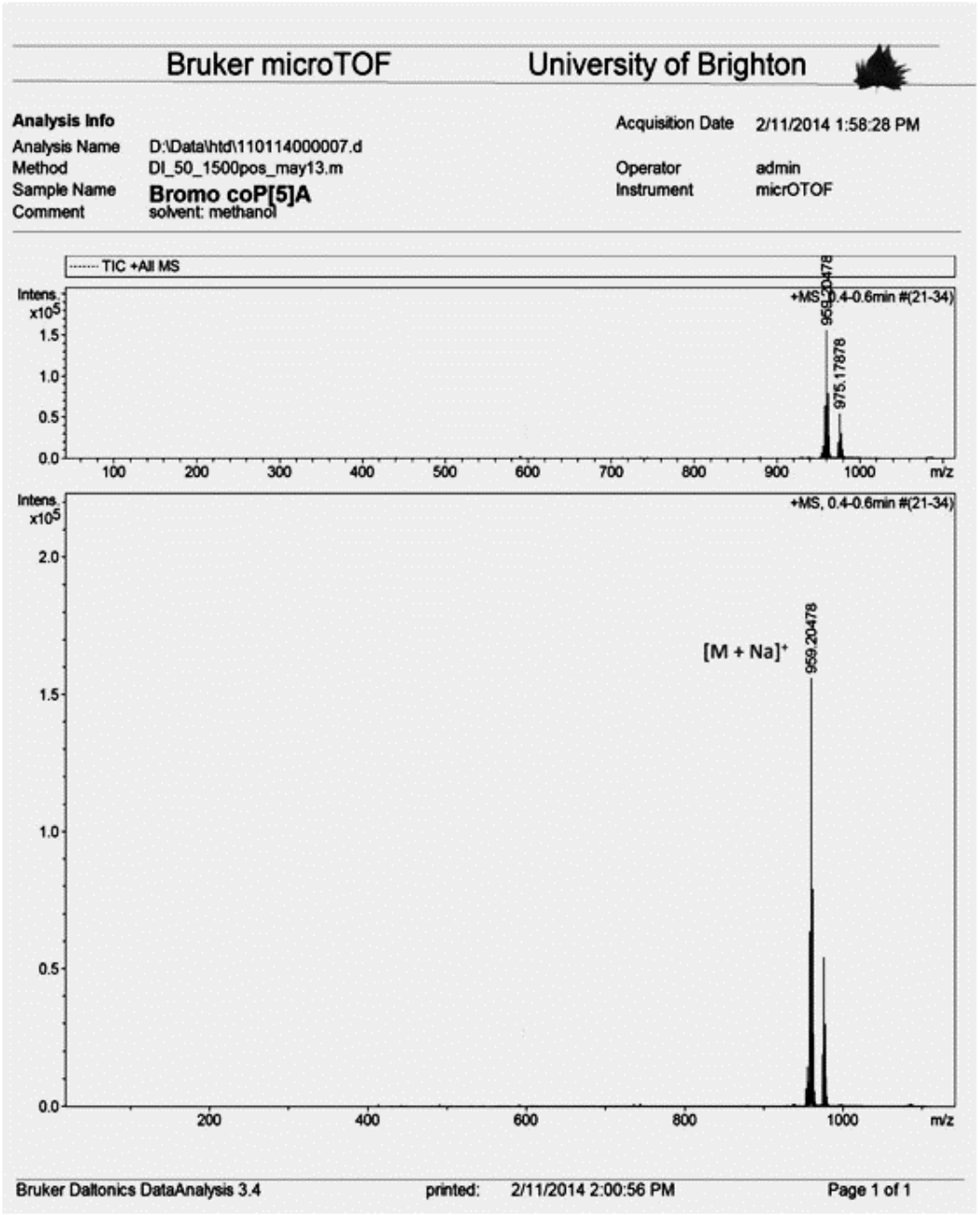

13. ^{1}H NMR spectrum 41 in $CDCl_3$

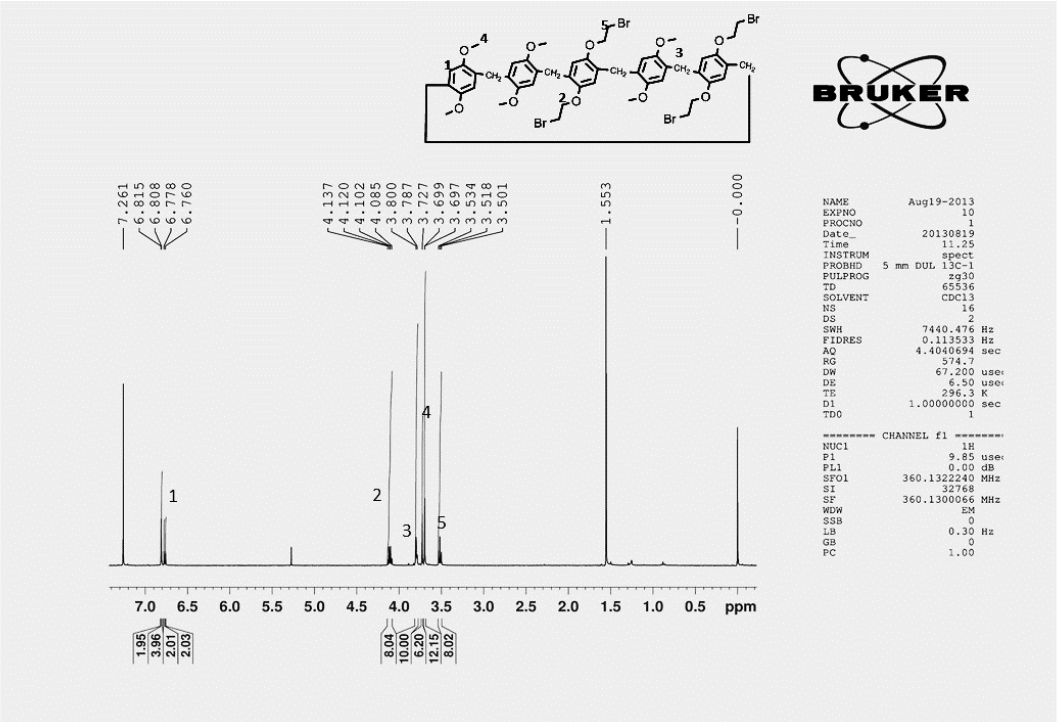

14. ^{13}C NMR spectrum of 41 in $CDCl_3$

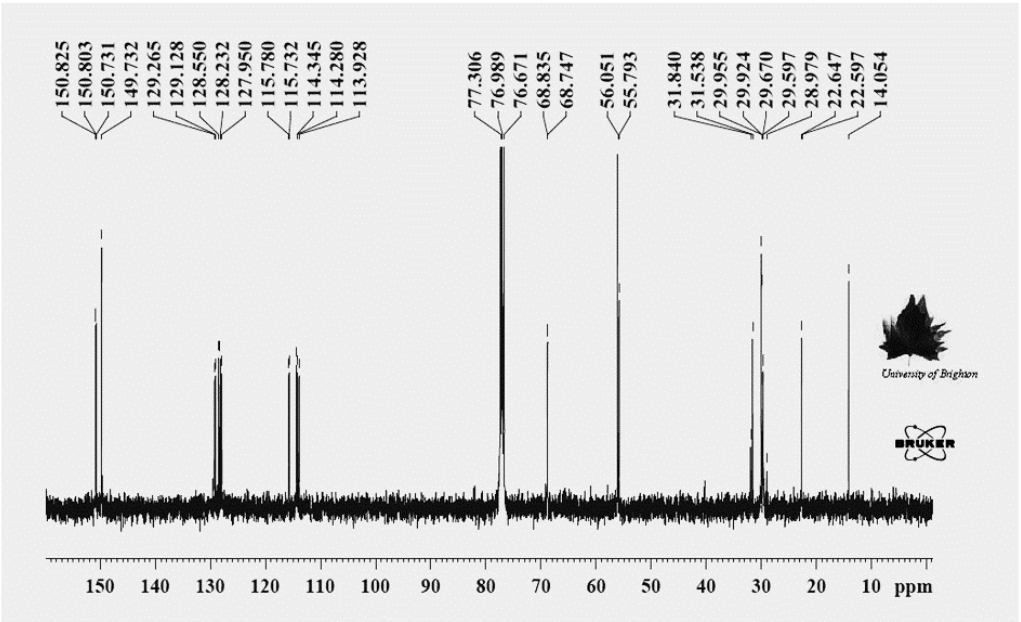

15. ESI mass spectrum of 41

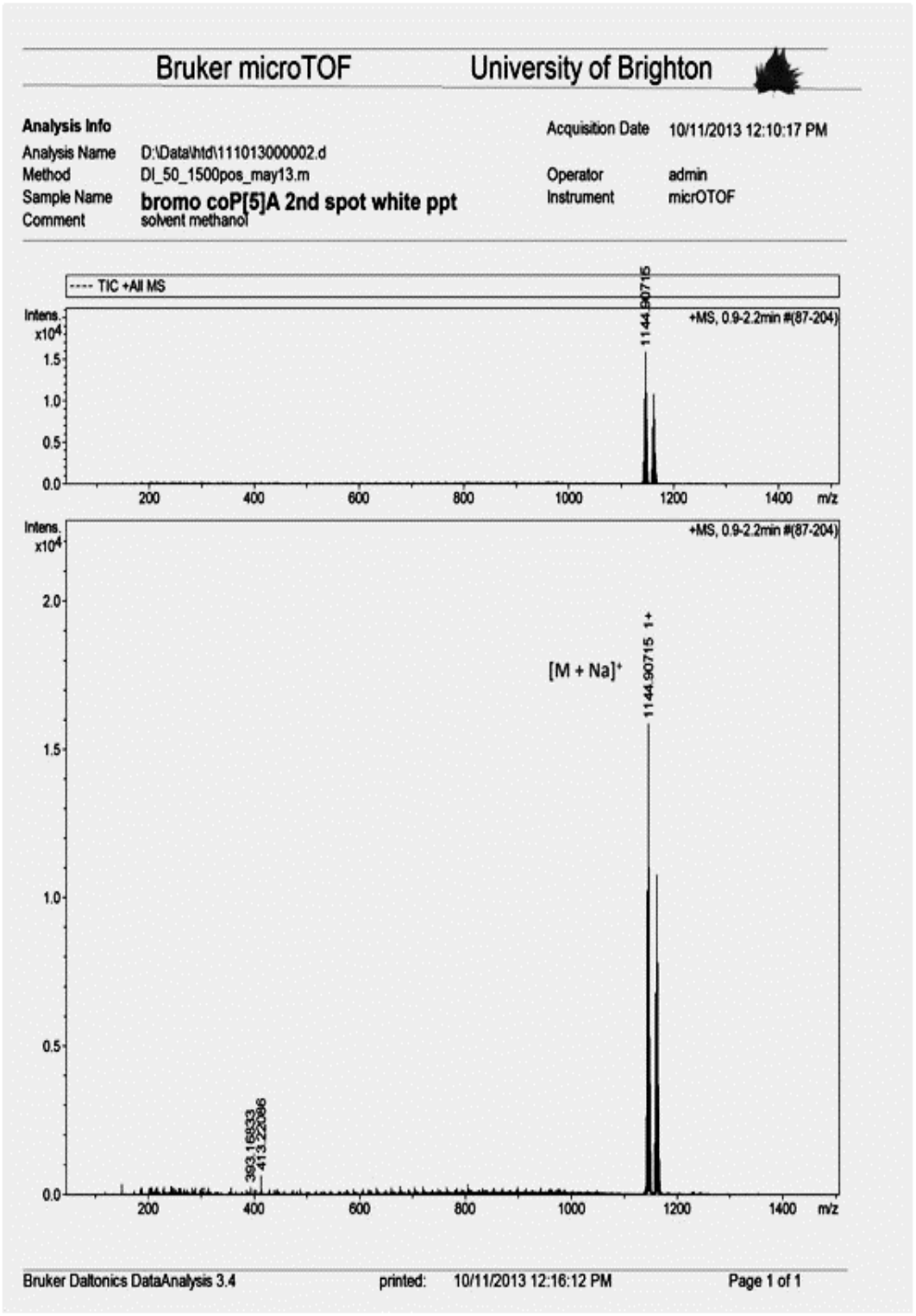

16. ^{1}H NMR spectrum of 42 in $CDCl_3$

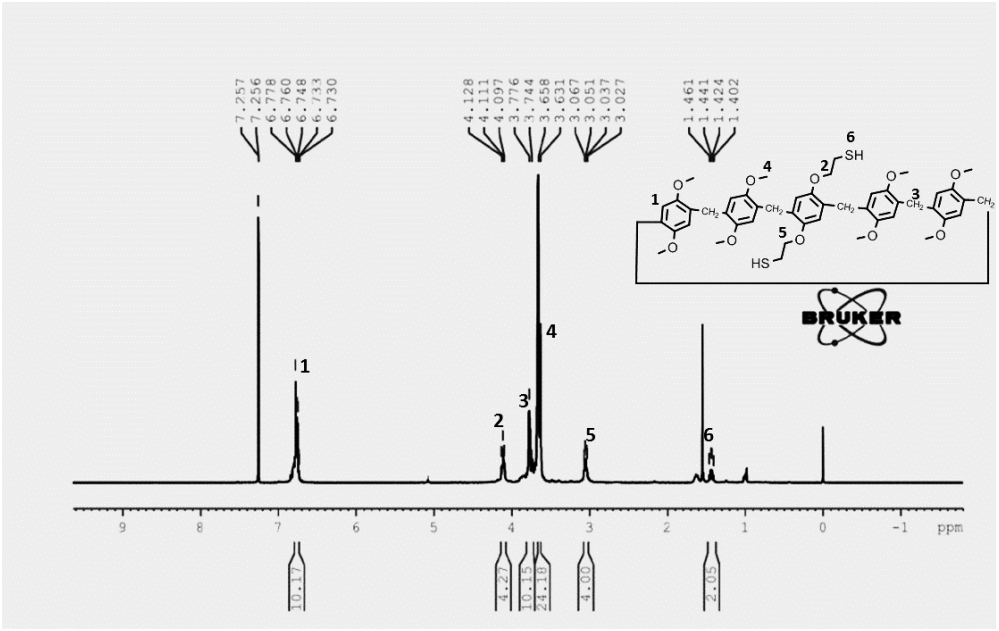

.

17. ^{13}C NMR spectrum of 42 in $CDCl_3$

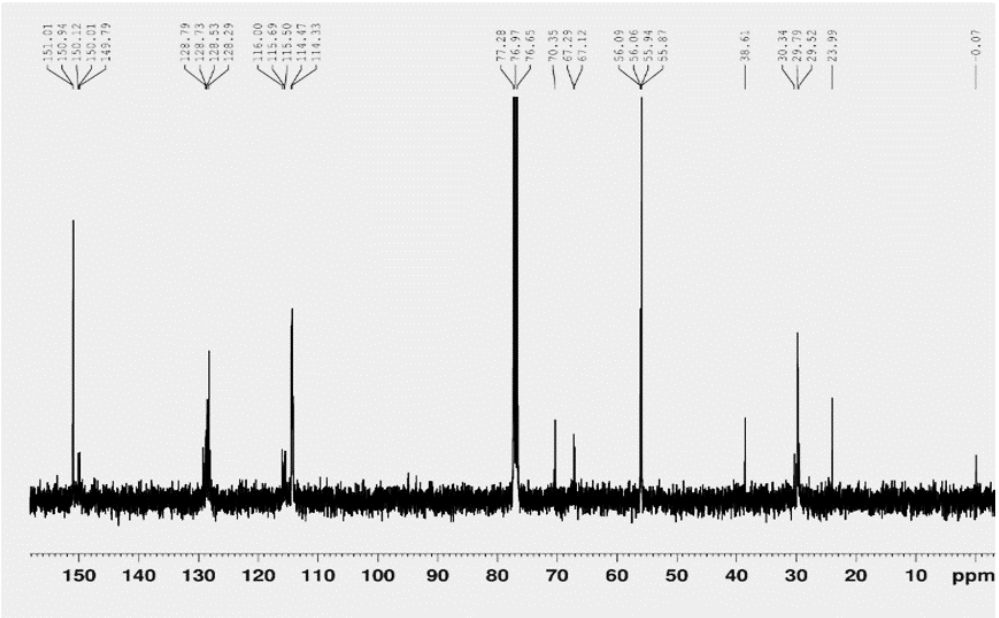

18. ESI mass spectrum of 42

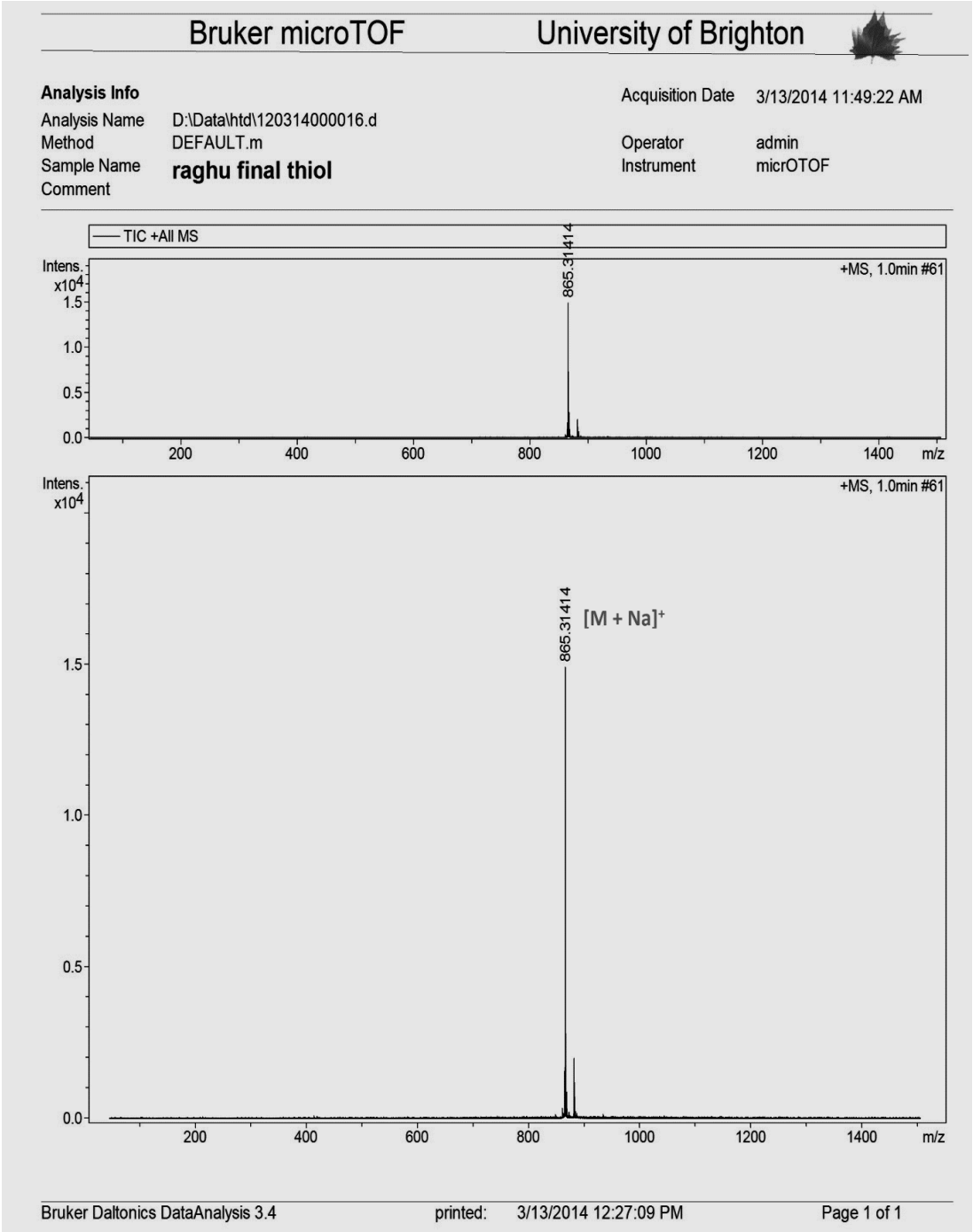

19. ^{1}H NMR spectrum of 6 in $CDCl_3$

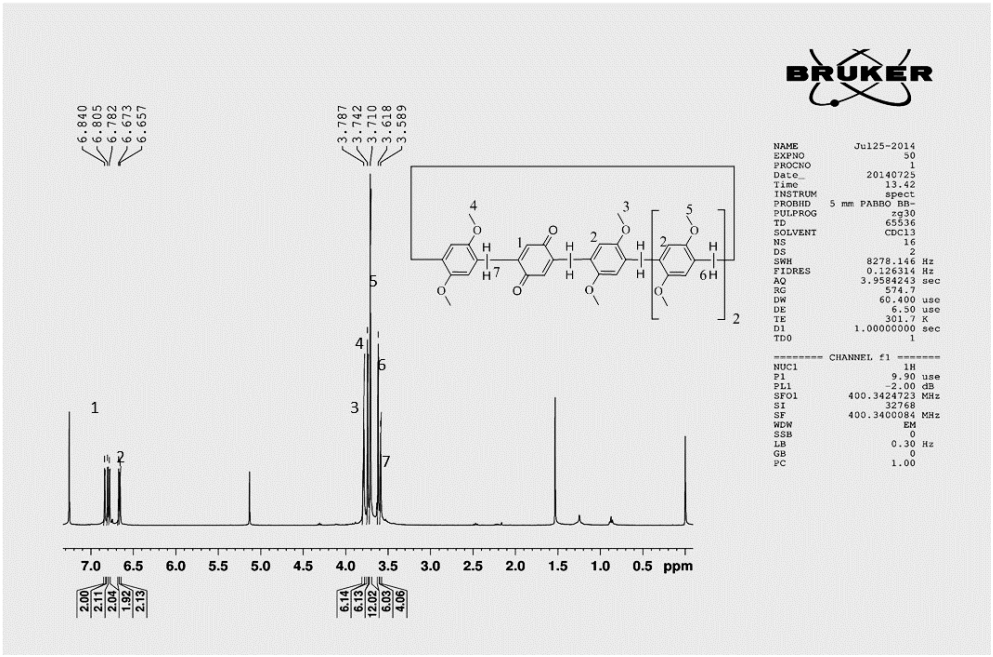

20. ^{1}H NMR spectrum of 7 in $CDCl_3$

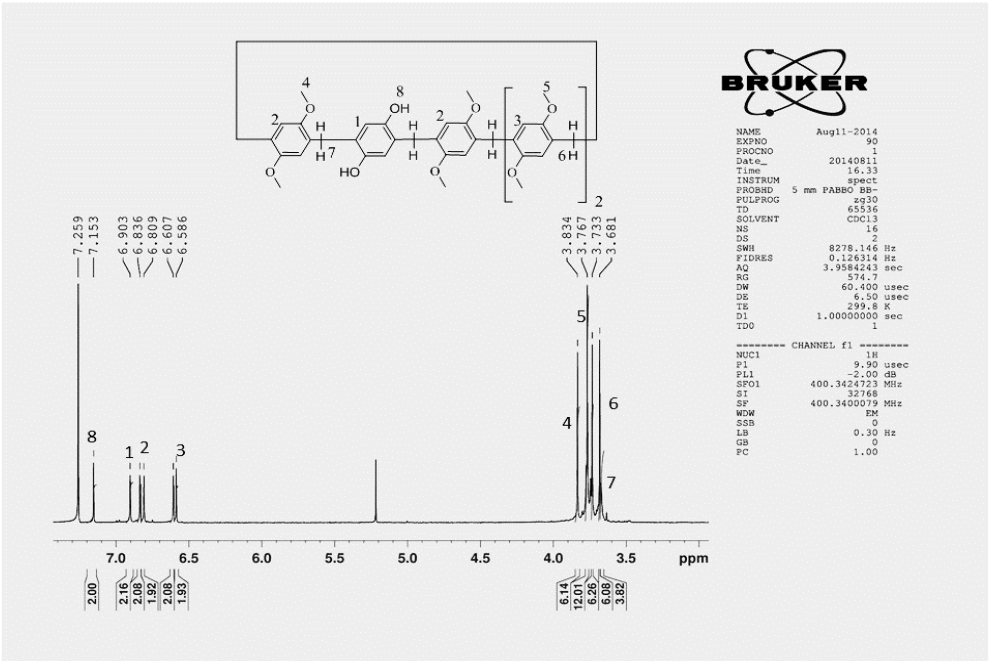

21. ^{13}C NMR spectrum of 7 in $CDCl_3$

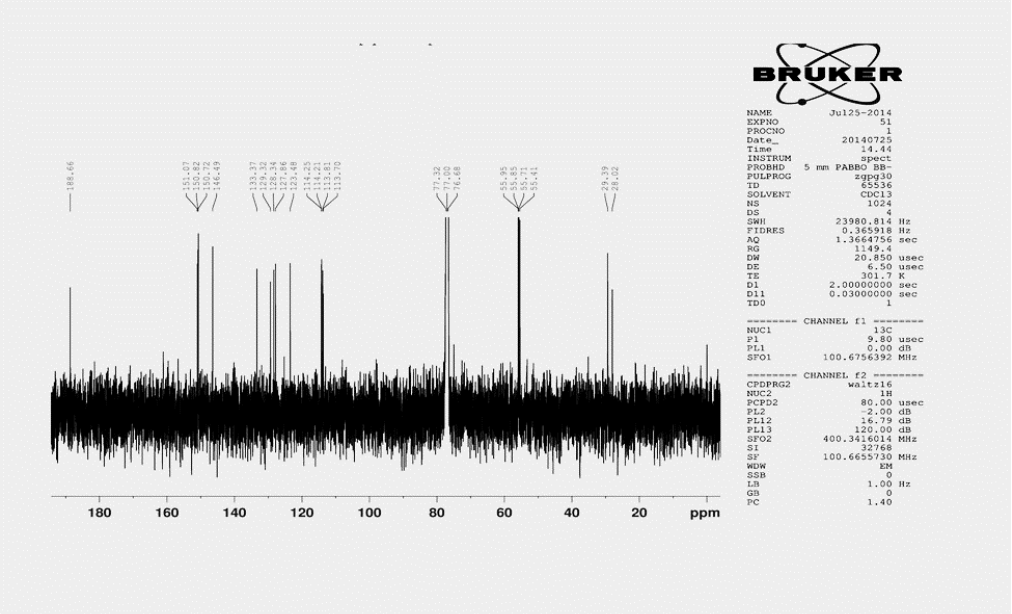

22. ^{1}H NMR spectrum of 44 in $CDCl_3$

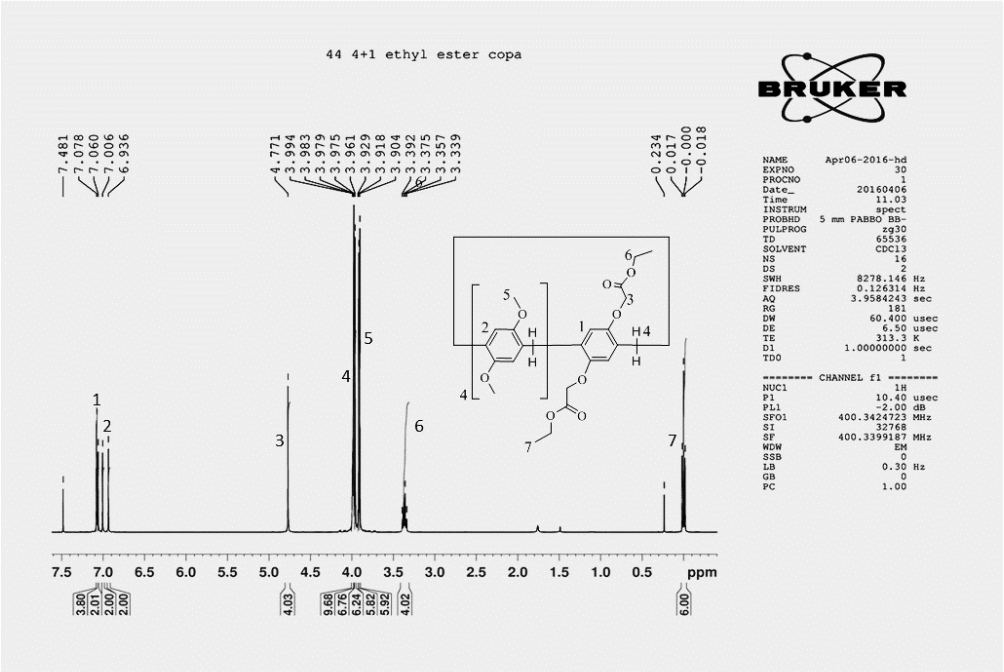

23. ^{13}C NMR spectrum of 44 in $CDCl_3$

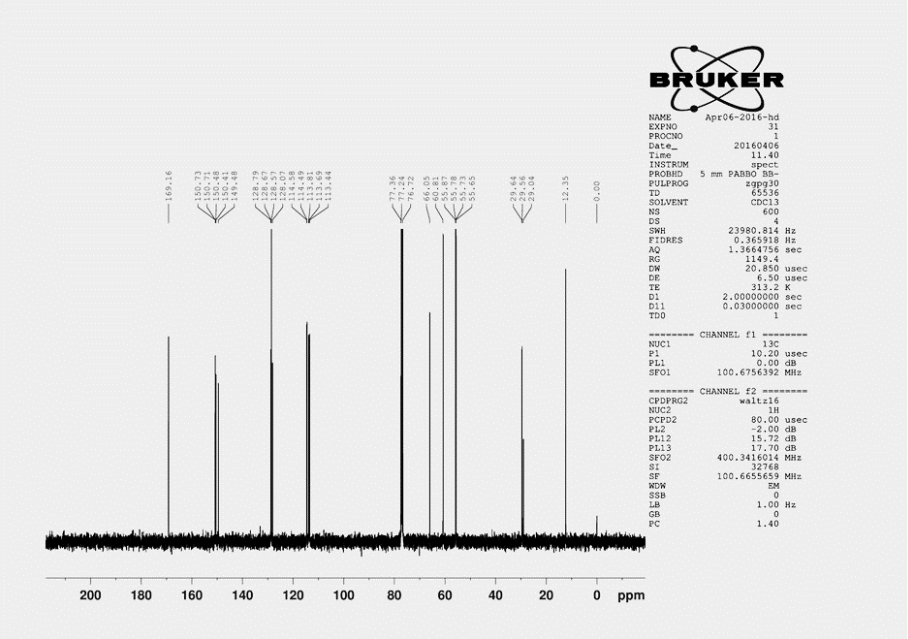

24. H^1 NMR spectrum of 35 in $CDCl_3$

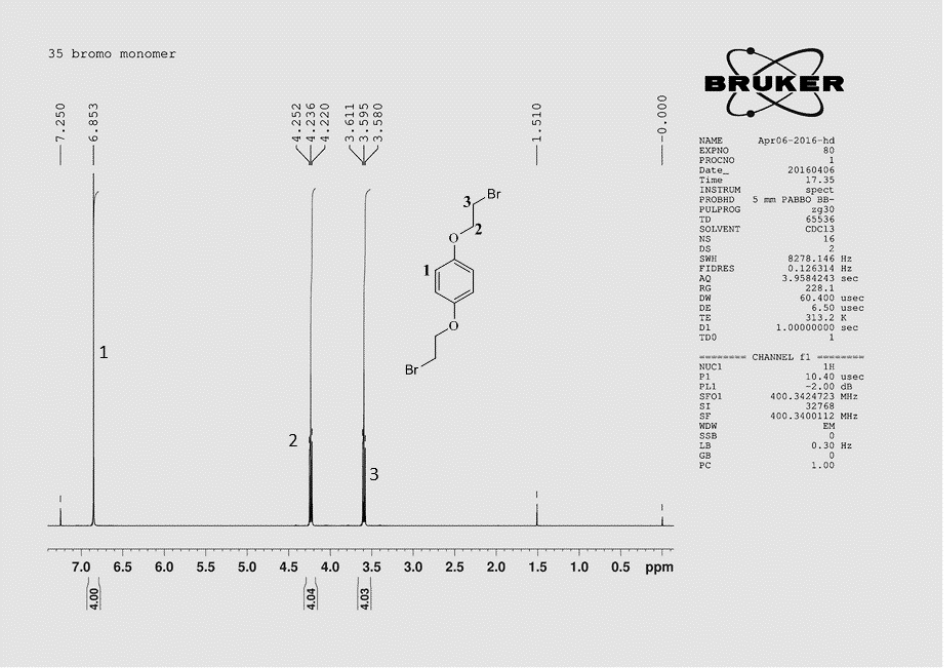

25. ^{13}C NMR spectrum of 35 in $CDCl_3$

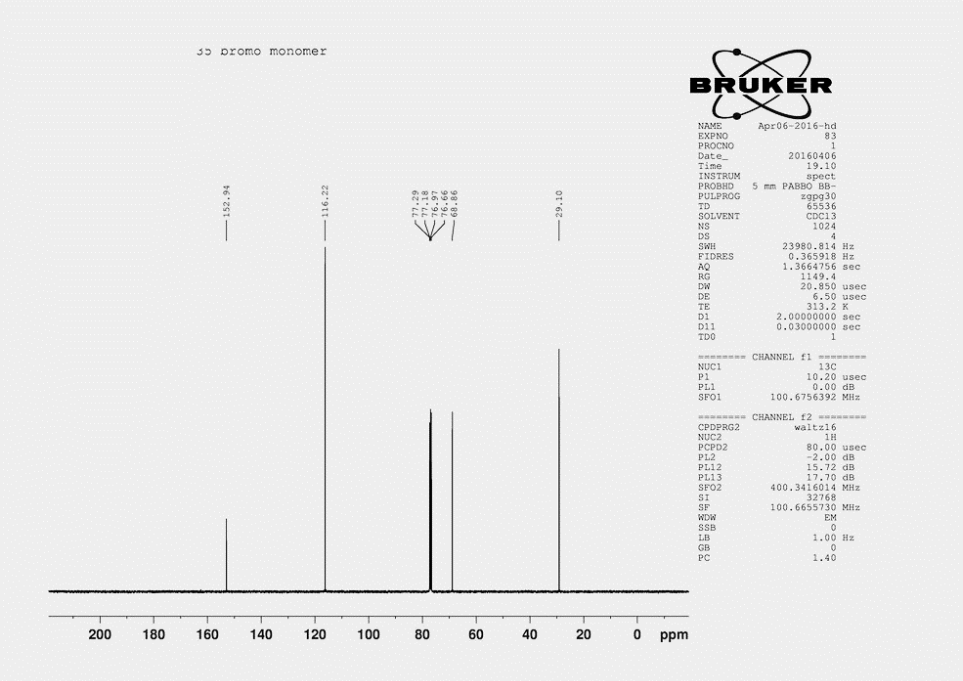

26. ^{1}H NMR spectrum of 38 in $CDCl_3$

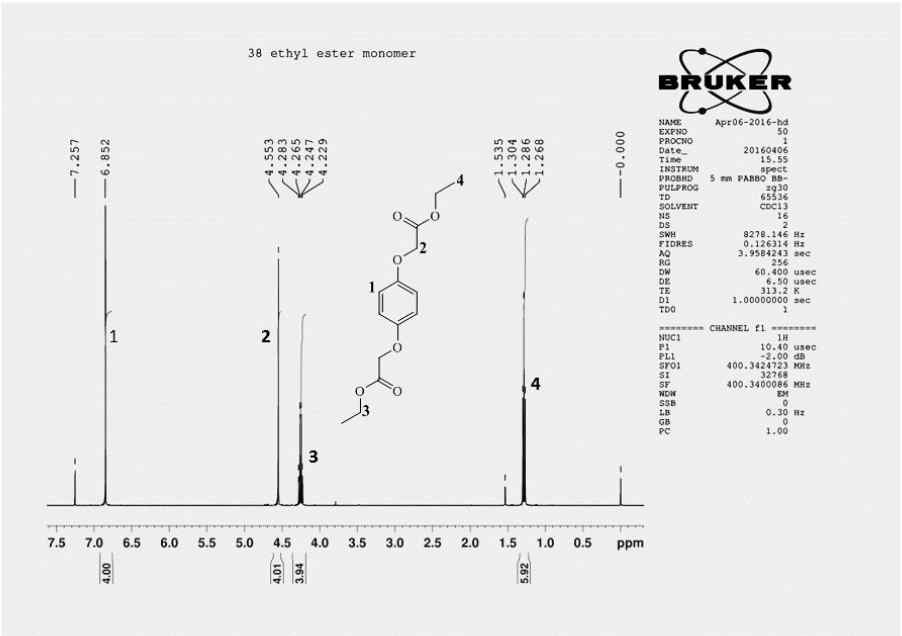

27. ^{13}C NMR spectrum of 38 in $CDCl_3$

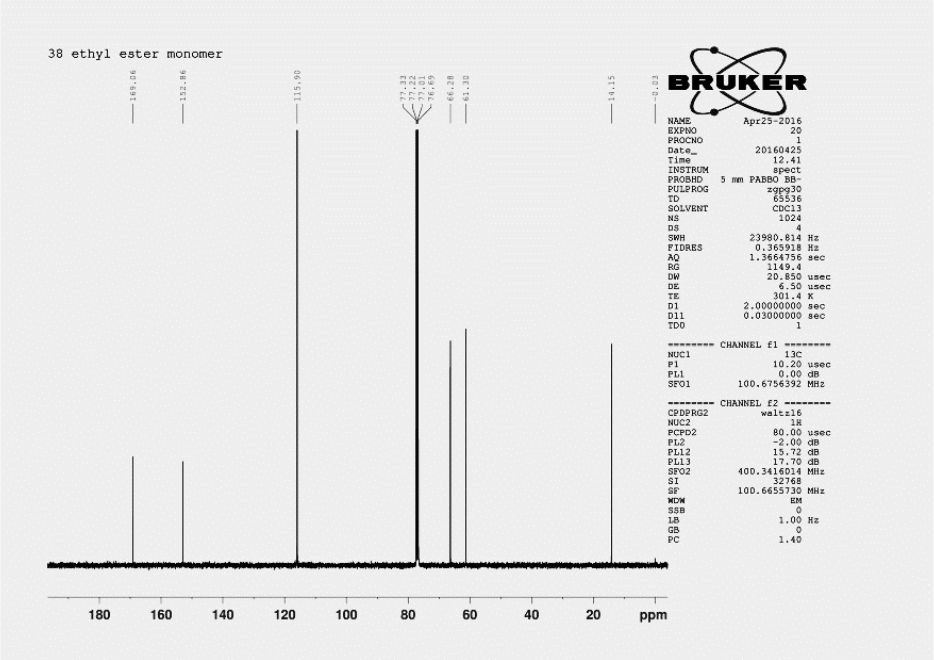

28. ^{13}C NMR spectrum of 37 in $CDCl_3$

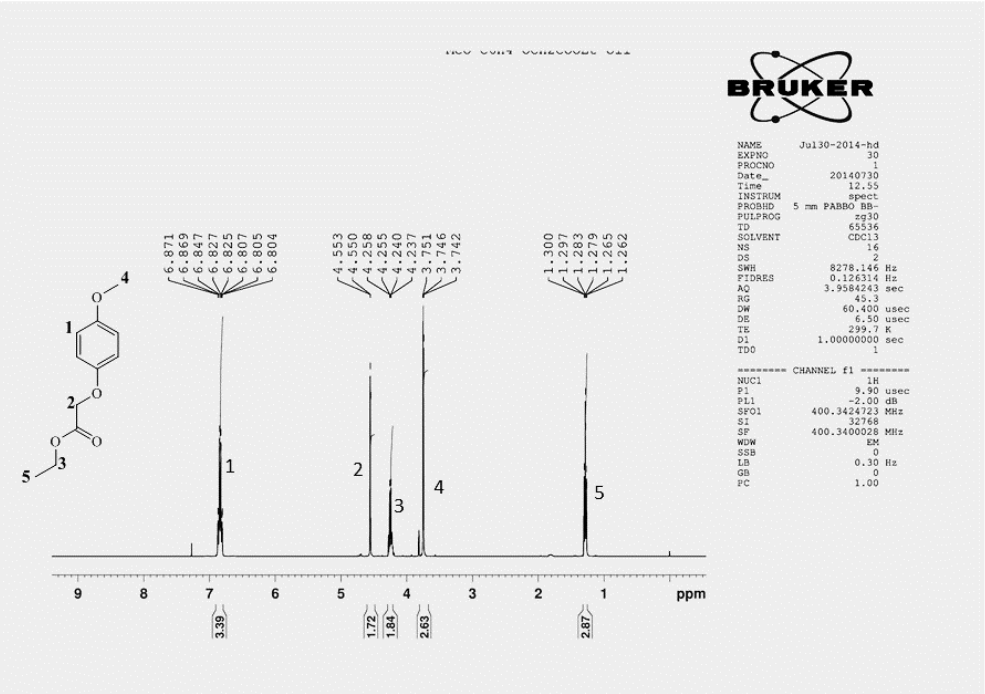

29. ^{1}H NMR spectrum of 37 in $CDCl_3$

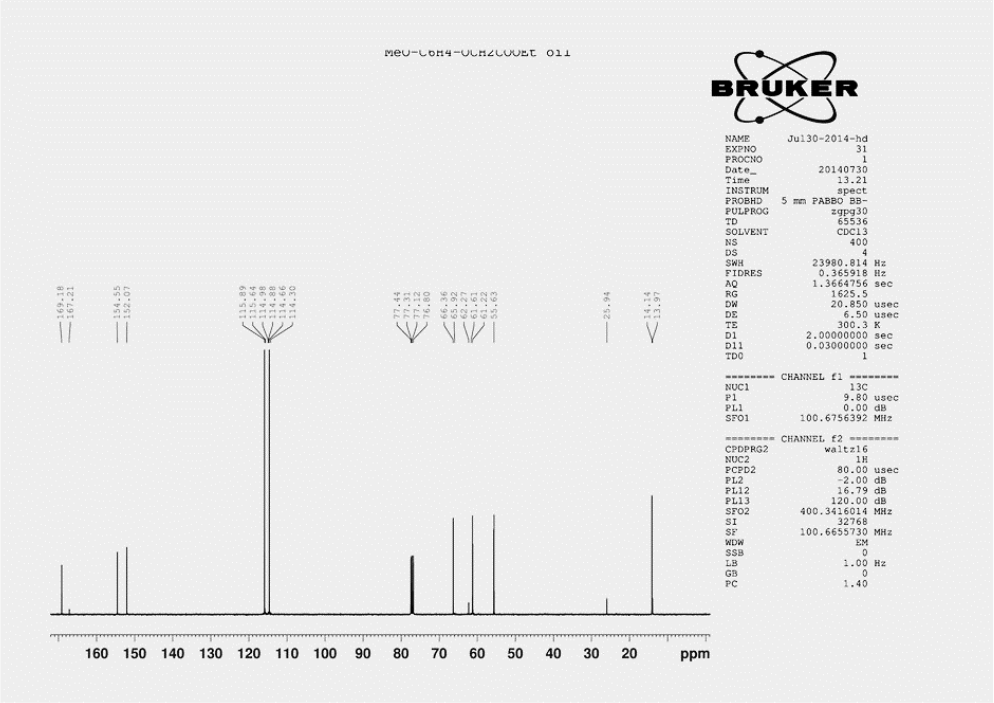

9.2 Permission for figure reproduction

In the present thesis several figures were reproduced with the permission from publishers through Rights-link**.**

RightsLink — Copyright Clearance Center

Figure Number	License Number	Licensed Content Title	Licensed Content Publication	Licensed Content Publisher
12	3741611366067	Self-assembly and proton conductance of organic nanotubes from pillar[5]arenes	Tetrahedron Letters	Elsevier
13	3741611091767	Synthesis, conformational and host–guest properties of water soluble pillar[5]arene	Chemical Communications (Cambridge)	Royal Society of Chemistry
15	3741610829219	A nonsymmetric pillar[5]arenebased selective anion receptor for fluoride	Chemical Communications (Cambridge)	Royal Society of Chemistry
17	Copyright © 2012	Pillar[6]arene Based Photoresponsive Host–Guest Complexation	Journal of the American Chemical Society	American Chemical Society
18	Copyright © 2014	Proton Transfer in Host–Guest Complexation between a Difunctional Pillar[5]arene and Alkyldiamines	Organic Letters	American Chemical Society
20	3741600118223	A new water soluble pillar[5]arene: synthesis and application in the preparation of gold nanoparticles	Chemical Communications (Cambridge)	Royal Society of Chemistry
21	3741590604570	Gold nanoparticles stabilized by an amphiphilic pillar[5]arene: preparation, self-assembly into composite microtubes in water and application in green catalysis	Chemical Science	Royal Society of Chemistry
22	Copyright © 2012	Viologen-mediated assembly of and sensing with carboxylatopillar [5] arene-modified gold nanoparticles	Journal of the American Chemical Society	American Chemical Society
23	3741600554210	Supramolecular self-assembly and photophysical properties of pillar[5]arene stabilized CdTe quantum dots mediated by viologens	RSC Advances	Royal Society of Chemistry
24	3741601478456	Host–guest recognition induced color change of water soluble pillar[5]arene modified silver nanoparticles for visual detection of spermine analogues	Chemical Communications (Cambridge)	Royal Society of Chemistry
25	3741610363300	Water soluble pillar[6]arene stabilized silver nanoparticles: preparation and application in amino acid detection	Tetrahedron Letters	Elsevier
29	3741580688371	Fundamentals of Electrochemical Theory	Wiley Books	John Wiley and Sons
45	3741620188195	A low pH sensor from an esterified pillar[5]arene	Chemical Communications (Cambridge)	Royal Society of Chemistry